FNT/T 97/19

Precision Physics at LEP

G. Montagna([1]), O. Nicrosini([1]) and F. Piccinini([1])

([1]) *Dipartimento di Fisica Nucleare e Teorica - Università di Pavia, and Istituto Nazionale di Fisica Nucleare - Sezione di Pavia, Italy*

To appear in the RIVISTA DEL NUOVO CIMENTO

Contents

1 – Introduction **2**

2 – Small-Angle Bhabha Scattering and the Luminosity Measurement **6**
2˙1 *Luminosity Monitoring.* – 7
2˙2 *Sensitivity of Observables to Luminosity.* – 10
2˙3 *Radiative Corrections to Small-Angle Bhabha Scattering.* – 11
2˙4 *Computational Tools.* – 14
2˙5 *The Total Theoretical Error.* – 17
2˙6 *Recent Developments and Perspectives.* – 22

3 – Z^0 Physics **24**
3˙1 *Realistic Observables and Z^0 Parameters.* – 25
3˙2 *Electroweak Corrections.* – 28
3˙2.1 One-loop Feynman diagrams. 29
3˙2.2 Calculational schemes. 33
3˙2.3 Transition amplitudes and effective couplings. 38
3˙2.4 Higher-order electroweak corrections. 39
3˙3 *QCD Corrections.* – 41
3˙3.1 Mixed electroweak-QCD corrections. 41
3˙3.2 Final-state QCD corrections. 42
3˙4 *QED Corrections.* – 46
3˙4.1 Initial-state radiation. 47
3˙4.2 Final-state radiation. 52
3˙4.3 Initial-final state interference. 55
3˙5 *Computational Tools.* – 55
3˙6 *Theoretical Uncertainties.* – 58

4 – Fits to Precision Data **63**
4˙1 *Determination of the Electroweak Parameters.* – 64
4˙2 *Standard Model Fits.* – 69
4˙2.1 Determination of the *top*-quark mass. 72
4˙2.2 Determination of the Higgs-boson mass. 75
4˙2.3 Determination of α_s. 78
4˙3 *Model Independent Approaches and Physics Beyond the Standard Model.* – 81
4˙3.1 S-matrix approach. 81
4˙3.2 Model-independent analysis of precision data. 82
4˙3.3 Physics beyond the Standard Model. 85

5 – Physics at LEP2 **89**
5˙1 *Two-Fermion Processes.* – 89
5˙1.1 Weak corrections. 91
5˙1.2 QED corrections. 92
5˙1.3 Radiative events. 96
5˙2 *Four-Fermion Processes.* – 99
5˙2.1 Tree-level calculations. 101
5˙2.2 Gauge invariance. 102
5˙2.3 Radiative corrections. 105
5˙2.4 Computational tools. 112
5˙3 *The W-boson Mass and Anomalous Couplings.* – 115
5˙3.1 The W-boson mass. 115
5˙3.2 Anomalous couplings. 118
5˙4 *Higgs-boson Searches.* – 120

6 – Conclusions **126**

A – Universal Photonic Corrections **128**
A˙1 *The Structure Function Method.* – 129
A˙2 *The Parton Shower Method.* – 133
A˙3 *YFS Exponentiation.* – 134

B – Vacuum Polarization Corrections **138**

C – One-loop Integrals and Dimensional Regularization **142**

1. – Introduction

According to the present understanding of particle physics, the fundamental interactions among elementary particles are described by the so-called Standard Model (SM) of the electroweak and strong interactions. It is a non abelian gauge theory based on the group $SU(2) \otimes U(1)$ for the description of the electromagnetic and weak forces in unified form (the so-called standard electroweak theory) [1] and the group $SU(3)$ colour for the strong interactions (the so-called Quantum Chromodynamics or QCD) [2].

In the SM the fundamental constituents of matter are quarks and leptons (matter fields), while the quanta mediating the interactions among the matter particles are the photon, the $W^{\pm}$ and Z^0 bosons and the gluons (gauge fields). Both quarks and leptons interact *via* the electroweak force, while quarks in addition do participate also in strong interactions. In the electroweak sector of the SM, the fundamental fermions are grouped into three different generations. Each generation contains a charged lepton (e, μ, τ), an associated neutrino $(\nu_e, \nu_\mu, \nu_\tau)$, an "up" quark (u, c, t) and a "down" quark (d, s, b). Fermions belonging to different generations have identical couplings but are distinguishable by their masses. Although the SM does not predict the number of sequential generations, the present precision measurements at LEP/SLC rule out the existence of a fourth generation with a neutrino of mass up to 45 GeV (see Sect. **4**˙1). All the matter particles assumed by the SM have been experimentally discovered. In fact, the long-awaited *top* quark has been recently observed by the CDF and D0 Collaborations at the TEVATRON, and the value obtained for its mass ($m_t = 175.6 \pm 5.5$ GeV) is in good agreement with the mass range indirectly obtained from LEP/SLC precision measurements (see Sect. **4**˙2.1).

In order to realize the unification of electromagnetic and weak interactions, the standard electroweak theory predicts the existence of four vector bosons as carriers of the electroweak force: $\gamma, W^{\pm}, Z^0$. The electromagnetic interaction is described in terms of the massless photon γ. Both charged and neutral current weak interactions are predicted by the theory and described by the exchange of heavy $W^{\pm}$ and Z^0 bosons. The intermediate vector bosons $W^{\pm}$ and Z^0, and all the fermions, acquire mass by the mechanism of spontaneous symmetry breaking of the $SU(2) \otimes U(1)$ gauge symmetry, the so-called Higgs mechanism [3]. Strictly speaking, no mass value is predicted by the theory; on the other hand, by making use of low-energy experimental data, it is possible to determine the vector boson masses and the masses of all the fermions with the exception of the *top* quark, for which high-energy data are necessary. As a consequence of the Higgs mechanism, the existence of a neutral scalar boson, the Higgs boson, is predicted by the theory. However, also the mass of this particle is a free parameter that has to be determined experimentally. At present, the Higgs boson has not been yet experimentally observed, and its discovery would certainly represent one of the most important tests of the SM. Present negative searches at LEP provide the mass limit $m_H > 77$ GeV at 95% CL (see Sect. **4**˙2.2).

The first experimental confirmation of the electroweak theory was the observation of the neutral currents in neutrino-electron scattering experiments [4]. Since then, important experimental results, such as the discovery of the $W^{\pm}$ and Z^0 bosons by the UA1/UA2 Collaborations in proton-antiproton collisions [5] and the evidence for the γ-Z interference in $e^+e^- \to f\bar{f}$ processes at PEP/PETRA [6], provided further support to the SM. With the advent of the electron-positron accelerators LEP (Large Electron Positron collider at CERN) and SLC (Stanford Linear Collider at SLAC), the modern era of *precision tests* of the SM was started. At LEP in its first phase (LEP1) and SLC the Z^0 bosons are copiously produced in a very clean experimental environment, enabling the determination of the electroweak observables with impressive precision and offering the possibility to test the predictive power of the SM at the level of its quantum structure.

LEP1 and SLC colliders began their operation in the fall 1989. The energies of the electron (e^-) and positron (e^+) beams were chosen to be approximately equal to 45 GeV, in such a way that the available centre of mass energy was centered around the mass of the neutral vector boson of the weak interaction, the Z^0 boson ($E_{cm} \simeq 91$ GeV). LEP1

was terminated in the fall 1995 in order to allow a second phase in the LEP experimental program (LEP2) at energies above the Z^0 peak, while SLC will continue in data taking close to the Z^0 resonance still for a few years. The high-energy reactions studied at LEP1 by the four experiments ALEPH, DELPHI, L3 and OPAL and at SLC by the SLD Collaboration are two-fermion production processes in e^+e^- collision, *i.e.*

$$e^+e^- \to \gamma, Z \to f\bar{f}\,,$$

with

$$\begin{aligned} f\bar{f} = \; & \nu\bar{\nu}(\nu_e\bar{\nu}_e, \nu_\mu\bar{\nu}_\mu, \nu_\tau\bar{\nu}_\tau) && \text{(invisible final states)}, \\ & l^+l^-(e^+e^-, \mu^+\mu^-, \tau^+\tau^-) && \text{(charged leptons final states)}, \\ & q\bar{q}(u\bar{u}, d\bar{d}, s\bar{s}, c\bar{c}, b\bar{b}) && \text{(hadron final states)}\,. \end{aligned}$$

About 16 millions of Z^0 events have been detected at LEP and about 100 thousands at SLC, using in the latter polarized electron beams. Thanks to the very large data sample, a remarkable precision has been reached in the measurements of the Z-boson properties and observables, such as mass, total and partial decay widths, production cross sections and forward-backward asymmetries. For example, the mass of the Z^0 boson is at present known with a relative error of 2×10^{-5}, $M_Z = 91186.7\pm2.0$ MeV; the total Z^0 decay width has been measured with a relative error of 1×10^{-3}, *i.e.*$\Gamma_Z = 2494.8\pm2.5$ MeV [7,8]. The evolution with time of the experimental uncertainties on M_Z and Γ_Z during the years 1989-1997 is shown in Fig. 1. Three years of data taking at LEP1 (1991, 1993 and 1995) were devoted to a precision scan around the resonance, doing measurements also off-peak in the range 88-95 GeV; the rest of data taking was performed exclusively on the Z^0 peak. Several technological ingredients contributed to reach the fantastic performances of the LEP1 program summarized in Fig. 1. For instance, the method of resonant spin depolarization adopted in the LEP beam energy measurement allowed to reach a very precise calibration, of the order of 1 MeV. Quite curiously, many important unexpected phenomena affected LEP energy calibration during operation: tide effects and field rise due to the passage of the TGV on the nearby railway are probably the two most famous examples. The installation of precision luminometers also contributed significantly to the success of the LEP program, allowing a luminosity measurement at the level of 0.1% or better, that is unavoidable to make optimal use of the high statistics collected at LEP. In parallel with the technological and experimental progress, a large effort was undertaken by hundreds of theorists in the calculation of radiative corrections. The excellent performance of the machine, associated with the above theoretical effort, allowed to test the fine structure of the Standard Model of electroweak interactions with an unprecedented level of precision (*precision physics at LEP*). In this sense, precision tests at the Z^0 peak can be compared with classical tests of Quantum Electrodynamics (QED), like $g-2$ and Lamb shift experiments. Besides a highly nontrivial test of the standard theory at the level of quantum loops, the availability of both accurate measurements and calculations provided the opportunity of putting limitations on models predicting physics beyond the standard model.

After the long data taking at the Z^0 pole and a short run at intermediate energy in the 1995 fall (LEP1.5 phase), the second phase of LEP (LEP2) started operating in 1996. The main reason for the energy upgrade of the LEP machine was the precise measurement of the properties of the charged vector bosons of the weak interaction, the $W^\pm$ bosons, through the study of the reaction

$$e^+e^- \to W^+W^- \to f_1\bar{f}_2f_3\bar{f}_4\,,$$

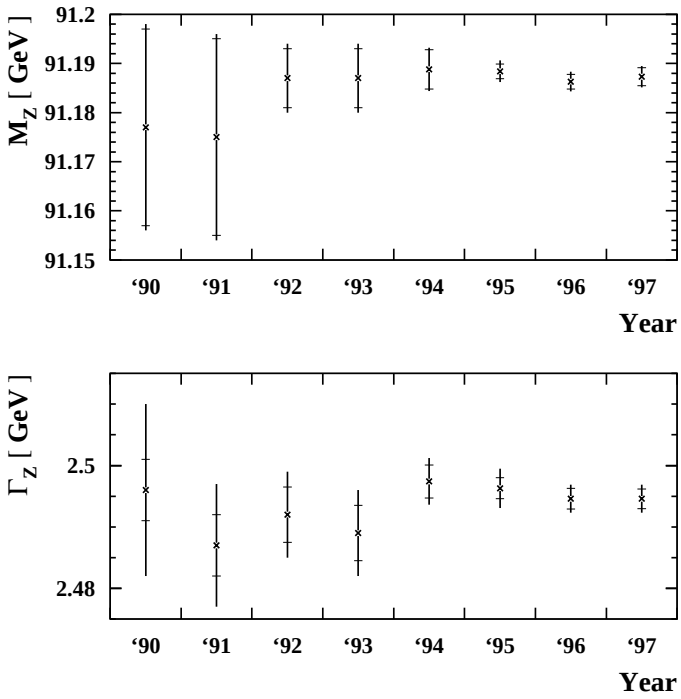

Fig. 1. – The time evolution of the errors on M_Z and Γ_Z (from [7]).

with the following possible four-fermion final-states

$$
\begin{aligned}
& l\bar{\nu}_l \bar{l}' \nu_{l'} (l = e, \mu, \tau) && \text{(leptonic final states)}, \\
& l\bar{\nu}_l q_1 \bar{q}_2 (l = e, \mu, \tau; q = u, d, c, s) && \text{(semi-leptonic final states)}, \\
& q_1 \bar{q}_2 q_3 \bar{q}_4 (q = u, d, c, s) && \text{(hadronic final states)}\,.
\end{aligned}
$$

The 1996 LEP2 run was split into two parts. The first run was at the centre of mass energy $\sqrt{s} = 161.3$ GeV, *i.e.* 0.5 GeV above the nominal WW production threshold, while the second one at $\sqrt{s} = 172$ GeV. The current LEP2 schedule foresees running during the years 1997-1999 with centre of mass energies from 184 GeV in 1997 to 194 GeV in 1998-1999. Compared to LEP1, the LEP2 physics potential will be characterized by a statistical error of the order of 1%, instead of 0.1% at LEP1. Nonetheless, also LEP2 has to be considered as a machine for precision physics, since it will allow to measure the mass of the W boson with an envisaged precision of 40-50 MeV, that is better than the current best determination of M_W at hadron machines, and to study in detail the couplings of the W's with the other gauge bosons γ and Z^0, thus directly probing the non-abelian nature of the electroweak theory. Therefore, the LEP2 experimental program does constitute a nice completion of the precision studies at LEP1 and SLC. Needless to say, besides the precision measurement of the properties of the charged vector bosons, LEP2 could also provide important pieces of information on the Higgs boson and physics beyond the SM.

In the recent few years, several reviews on the status of precision measurements at LEP1/SLC and of the calculation of radiative corrections in the SM have been published in the literature. From an experimental point of view, the main aspects of precision tests at LEP1/SLC have been summarized for instance in ref. [9]. The concepts and results of the calculation of radiative corrections have been reviewed for instance in ref. [10]. Before the start of the LEP1/SLC operations, the status of theoretical calculations and computational tools was described in refs. [11–13]. In view of the final analysis of the precision data, the status of precision calculations was critically reviewed in ref. [14], with special emphasis on the uncertainty inherent to the theoretical predictions. The theoretical results and related software necessary for the experiments at LEP2 were summarized in ref. [15].

The LEP/SLC physics program is a very wide one, ranging from precision measurements of vector boson properties, to QCD studies, searches of new particles, determination of dynamical properties of heavy flavours, and so on. The main goal of the present review is to give a comprehensive account of *precision physics at LEP*, meant as the whole of precision tests of the electroweak sector of the SM and its implications for new physics. More precisely, the theoretical apparatus needed for precision calculations at LEP/SLC will be described and its link with data analysis pointed out, aiming at emphasizing the intimate and fruitful connection between theoretical ideas and experimental results. Too technical details are inevitably omitted; however, particular care has been devoted to compiling an as complete as possible bibliography, where the interested reader can find additional information. The experimental data considered throughout the paper are the ones presented at the 1997 Summer Conferences [7, 8, 16].

The review is organized as follows. Section **2** is dedicated to small-angle Bhabha scattering and its relevance for the luminosity measurement. In Sect. **3** the large-angle processes at the Z^0 resonance, relevant for the study of the Z-boson properties, are considered, reviewing the theoretical ingredients necessary for high-precision calculations of the Z-boson observables. It is then shown how the theoretical tools developed are used to fit the experimental data, in order to determine the *top*-quark and Higgs-boson masses and the strong coupling constant α_s, and eventually establish the existence of new physics beyond the SM (Sect. **4**). The most important issues of electroweak physics at LEP2 are covered in Sect. **5**, where two-fermion processes far from the resonance (Sect. **5**˙1) and four-fermion processes at and above the W-boson pair production threshold (Sect. **5**˙2) are discussed. At last, the conclusions are drawn in Sect. **6**. Three technical appendices are dedicated to relevant theoretical subjects common to various items of LEP physics, namely the universal photonic corrections (Appendix A), the vacuum polarization correction (Appendix B) and the scalar integrals and dimensional regularization (Appendix C).

2. – Small-Angle Bhabha Scattering and the Luminosity Measurement

The process $e^+e^- \to e^+e^-$ (Bhabha scattering) is a peculiar one. Actually, at a difference from all the other two-fermion production processes, that occur as e^+e^- annihilation, *i.e.* are s-channel processes, the amplitude for $e^+e^- \to e^+e^-$ receives contributions both from s- and t-channel diagrams (see Fig. 2). In the energy region typical of LEP1/SLC ($\sqrt{s} \simeq M_Z$, M_Z being the Z-boson mass) the Bhabha scattering process exhibits completely different features, depending on the fact that the final state electrons are detected at large or small scattering angles. In the first case, the amplitude is dominated by s-channel subprocesses, and in particular by the $e^+e^- \to Z^0$ annihilation,

in such a way that the process is sensitive to the Z-boson properties. In the second one, the smaller is the scattering angle the larger is the contribution of the t-channel photon-exchange diagram, in such a way that for sufficiently small scattering angles Bhabha scattering is essentially a pure QED process, substantially independent of the Z^0 physics. These dynamical features of Bhabha scattering allow to use it both as a tool for studying Z^0 physics (large-angle cross sections and forward-backward asymmetries) and as a tool for the high precision luminosity monitoring (small-angle cross section). The first case will be examined in Sect. **3**, while the second one will be addressed in the following. Before starting the discussion on small-angle Bhabha scattering, it is worth noticing that a large amount of work has been dedicated to Bhabha scattering in general. The interested reader is referred for instance to refs. [17] and [18] for a detailed account and a comprehensive compilation of the relevant literature.

2˙1. *Luminosity Monitoring.* – The luminosity $\mathcal{L}$ of a collider is the proportionality constant between the event rate dN/dt and the corresponding cross section σ for any given process, according to the relation

$$\frac{dN}{dt} = \mathcal{L}\sigma, \qquad N = \sigma \int dt\mathcal{L} = \sigma L. \tag{1}$$

In the practice, an experiment measures the number of events for a given process and, by making use of the inverse of eq. (1), quotes the experimental cross sections as

$$\sigma = \frac{1}{L}N. \tag{2}$$

From eq. (2) it is clear that, in order to fully exploit the experimental information contained in N, the error affecting the luminosity L must be smaller than the experimental error affecting N. The luminosity of a collider depends in a highly non-trivial way on machine and beam parameters. It is of course possible to compute it given these parameters, but, in particular for LEP, such a determination is affected by an intrinsic uncertainty which is completely unsatisfactory in view of the extremely high experimental accuracy. This is why the luminosity is monitored adopting a different strategy, namely by identifying a process which is in principle not affected (or only slightly affected) by *unknown* physics, so that its cross section can be computed within a firmly established theory, and determining the luminosity *via* the relation

$$L = \frac{1}{\sigma_{known}}N. \tag{3}$$

The luminosity determined by eq. (3) is then used for the determination of all the experimental cross sections *via* eq. (2) (for a review on the precision determinations of the accelerator luminosity in LEP experiments, the interested reader is referred to [19] and references therein).

Such a process does exist, and is the Bhabha scattering $e^+e^- \to e^+e^-$ at small scattering angle. The main reasons why the small-angle Bhabha scattering (SABH) fulfils the requirements just described are the following:

- the SABH process is substantially a QED process, dominated by photon exchange in the t-channel; this, in turn, implies that
  - its theoretical cross section is dominated by a contribution that is in principle calculable by means of perturbative QED at arbitrary precision;

– the Z-boson exchange contribution to its cross section, *via* Z-boson annihilation in the s channel, Z-boson exchange in the t channel and Z-γ interferences, is very small; hence a detailed knowledge of the Z-boson properties, like the precise value of its mass and decay width, to be determined in large-angle processes, has a negligible influence on the luminosity monitoring;

- the SABH cross section is large, and can be rendered much larger than the typical Z-boson annihilation peak cross sections provided the detection angular region for the SABH events is sufficiently close to the beam pipe, so that the statistical uncertainty of N in the r.h.s. of eq. (3) can be kept small.

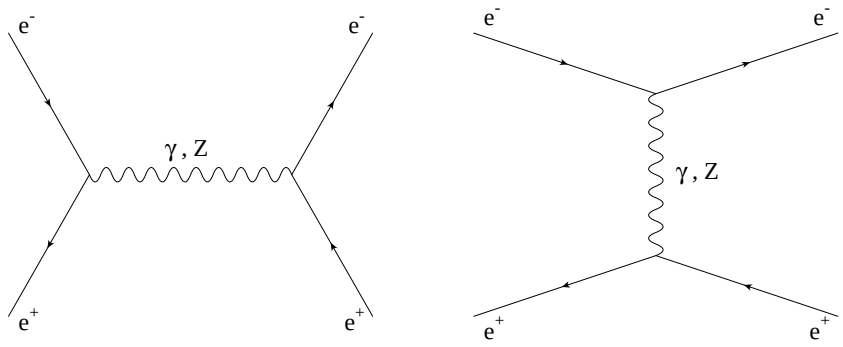

Fig. 2. – The Feynman diagrams for the tree-level Bhabha scattering cross section.

The tree-level differential cross section corresponding to t-channel photon exchange is given by (see for instance ref. [17] and references therein)

$$\frac{d\sigma_0}{d\Omega} = \frac{\alpha^2}{4s}\frac{2}{(1-\cos\vartheta)^2}\left[4+(1+\cos\vartheta)^2\right], \tag{4}$$

where ϑ is the electron scattering angle, $\sqrt{s}$ is the total centre of mass (c.m.) energy and α is the QED coupling constant.

The calculation of the theoretical SABH cross section to be inserted into eq. (3) will involve in general the calculation of radiative corrections. These are numerically dominated by photonic corrections, *i.e.* by those corrections obtained by adding real or virtual photon lines to the tree-level amplitudes, which in turn depend very critically on the phase space integration region. Hence, in order to exploit eq. (3) for the high precision luminosity monitoring, the theoretical cross section must be computed by taking into account carefully the experimental definition of a SABH event. Skimming over the details of the various SABH Event Selections (ES's), which vary from experiment to experiment, the general features of SABH event are the following:

- the forward and backward luminometers cover an angular region of few degrees, starting from, say, 1°;

- a SABH event is detected as a signal coincidence of the forward luminometer with the backward luminometer;

- for technical reasons, asymmetric angular acceptances are adopted; for instance, a narrower (N) acceptance on the e^+ side and a wider (W) acceptance on the e^- side; the results of the NW and WN ES's are averaged;

- for technical reasons, a calorimetric measurement on the final-state electrons is performed; this means that experimentally a final-state electron cannot be distinguished by a final-state electron accompanied by collinear photons;

- very mild energy/acollinearity cuts are imposed on the scattered electrons, compatible with the previous items.

From the general features of a SABH event, and taking into account that photonic radiation is mostly soft and/or collinear to the charged lines, the following picture can be drawn:

- events with the final-state electrons inside the luminometers, accompanied by soft photons or initial-state photons lost in the beam pipe are detected as good SABH events;

- since initial-state radiation (ISR) causes a boost of the c.m. of the reaction, and since the final-state electrons cannot be too acollinear, there is a natural cut-off on the amount of ISR allowed;

- events with the final-state electrons inside the luminometers accompanied by collinear photons are detected as good SABH events; this means that final-state radiation (FSR) must be integrated over a finite region surrounding the final-state electron; this in turn implies, for a sort of Kinoshita-Lee-Nauenberg (KLN) mechanism [20], that for FSR the so-called "logarithmically enhanced" corrections are greatly suppressed (more on this in Sect. **2**˙3);

- initial- or final-state photons can convert into additional fermionic pairs, which for most of the events are lost in the beam pipe or collinear to the final-state electrons;

- events accompanied by the radiation of virtual photons are degenerate with the elastic event;

- since in general there is no particle identification in the luminometers, it can happen that, for instance, a final-state electron radiates a hard photon in such a way that the photon hits the luminometer, while the electron is lost; also such an event is in general registered as a good SABH event.

Given the above picture, it is clear that in order to perform the phase space integration over all the configurations that correspond to a good SABH event the most versatile tool, *i.e.* a Monte Carlo (MC) integrator and/or event generator, is mandatory. Nonetheless, as a matter of fact the calculations necessary to compute the theoretical SABH cross section are so sophisticated that all kind of information, even analytical or semi-analytical, are precious. A detailed account of the status of all the theoretical calculations available at present will be given in Sect. **2**˙4. It is worth noting that the total error affecting the determination of the luminosity by means of eq. (3) receives contributions both from the experimental error of the number of events N and from the

theoretical error of the SABH process cross section. Actually, by performing the standard propagation of errors on eq. (3) one obtains

$$\frac{\delta L}{L} = \frac{\delta N}{N} \oplus \frac{\delta \sigma}{\sigma}, \tag{5}$$

where the first term in the r.h.s. is the experimental error, the last one is the relative error on the theoretical cross section and $\oplus$ means the sum in quadrature.

2˙2. *Sensitivity of Observables to Luminosity.* – The LEP experiments determine the Z-boson parameters by means of combined fits to the measured hadronic and leptonic cross sections and leptonic forward-backward asymmetries (see Sects. **3** and **4** for more details). In particular, in order to facilitate the comparison and the combination of the results, the LEP Collaborations quote, besides other choices, the following set of nine parameters:

$$M_Z, \quad \Gamma_Z, \quad \sigma_h^0, \quad R_{e,\mu,\tau}, \quad A_{FB}^{e,\mu,\tau}, \tag{6}$$

where M_Z and Γ_Z are the Z-boson mass and total width, respectively, σ_h^0 is the hadronic peak cross section for Z-boson exchange only, R_i are the ratios of the hadronic width to the i-th leptonic width and A_{FB}^i are the leptonic forward-backward asymmetries at $\sqrt{s} = M_Z$ for Z-boson exchange only. These parameters are quoted after having been corrected for the effect of ISR, final-state QED and QCD corrections, as well as for t-channel and s-t interference for e^+e^- final states. By assuming lepton universality, the three values of R_i and A_{FB}^i are combined into a single R_l and A_{FB}^l, and the corresponding fit is a 5-parameter fit. In both cases, the so called derived parameters, such as for instance the leptonic width and the number of light neutrinos, are computed by expressing them as functions of the fundamental parameters.

TABLE I. – Line shape and asymmetry parameters from 5-parameter fits to the data of the four LEP1 experiments, made with a theoretical luminosity error of 0.16%, 0.11% and 0.06%. In the lower part of the Table also derived parameters are listed (from ref. [18]).

theoretical luminosity error	0.16%	0.11%	0.06%
M_Z [GeV]	91.1884 ± 0.0022	91.1884 ± 0.0022	91.1884 ± 0.0022
Γ_Z [GeV]	2.4962 ± 0.0032	2.4962 ± 0.0032	2.4961 ± 0.0032
σ_h^0 [nb]	41.487 ± 0.075	41.487 ± 0.057	41.487 ± 0.044
R_l	20.788 ± 0.032	20.787 ± 0.032	20.786 ± 0.032
A_{FB}^l	0.0173 ± 0.0012	0.0173 ± 0.0012	0.0173 ± 0012
Γ_h [GeV]	1.7447 ± 0.0030	1.7447 ± 0.0028	1.7446 ± 0.0027
Γ_l [MeV]	83.93 ± 0.13	83.93 ± 0.13	83.93 ± 0.12
σ_l^0 [nb]	1.9957 ± 0.0044	1.9958 ± 0.0038	1.9959 ± 0.0034
Γ_h/Γ_Z [%]	69.90 ± 0.089	69.90 ± 0.079	69.89 ± 0.072
Γ_l/Γ_Z [%]	3.362 ± 0.0037	3.362 ± 0.0032	3.362 ± 0.0028
Γ_{inv} [MeV]	499.9 ± 2.4	499.9 ± 2.1	499.9 ± 1.9
Γ_{inv}/Γ_l [%]	5.956 ± 0.030	5.956 ± 0.024	5.956 ± 0.020
N_ν	2.990 ± 0.015	2.990 ± 0.013	2.990 ± 0.011

In order to understand the effect of the luminosity error on the physical observables, one can assume, as a first approximation, that the luminosity error affects, among the

fundamental parameters, the hadronic peak cross section only, in a way that is determined from eq. (2) by performing the standard propagation of errors:

$$\delta\sigma_h^0 = (\delta\sigma_h^0)_{exp} \oplus \sigma_h^0 \frac{\delta L}{L}. \tag{7}$$

In eq. (7) the first term in the r.h.s. is the experimental error on the hadronic peak cross section, while the second term is the error on the cross section as due to the luminosity uncertainty. The influence of the luminosity error on the derived parameters is then determined by their dependence on σ_h^0.

Actually, in the practice the LEP Collaborations combine their results, propagating both the systematic and statistical uncertainties, and taking into account all the correlations between the parameters by means of the full covariance matrix. Table I shows an example of the results of such a procedure, by assuming a relative luminosity error of 0.16%, 0.11% and 0.06%, respectively. As can be noticed, the luminosity error affects, besides the hadronic peak cross section σ_h^0, almost all the derived parameters.

2˙3. *Radiative Corrections to Small-Angle Bhabha Scattering.* – The radiative corrections to the SABH process are dominated by photonic corrections, *i.e.* by those corrections coming from graphs obtained from the tree-level ones by adding real and/or virtual photon lines, and by the vacuum polarization correction. This last effect is taken into account by simply using the running QED coupling constant $\alpha(-t)$, where t is the squared four-momentum transfer of the reaction, as shown in Appendix B. In the present section, some generalities on photonic corrections are reviewed.

Once the infra-red (IR) divergence present in real and virtual corrections separately has been canceled by properly summing over all the degenerate states, the n-th order QED correction takes on the following form

$$\sigma^{(n)} = \left(\frac{\alpha}{\pi}\right)^n \sum_{k=0}^{n} a_k^{(n)} \mathcal{L}^k(Q^2), \tag{8}$$

where $\sigma^{(n)}$ is the n-th order contribution to the corrected cross section, $\mathcal{L}(Q^2) = L_{Q^2} - 1$ and $L_{Q^2} = \ln(|Q^2|/m_e^2)$ is the so called *collinear logarithm*, Q^2 being a typical scale involved in the process. The collinear logarithm L_{Q^2} originates from the phase space integration of the emitted photon, and in particular from those configurations in which the emitted photon is almost collinear to the radiating charged fermion line. In the SABH process, the relevant scale entering the collinear logarithm is $Q^2 = -t$, t being the squared four-momentum transfer of the reaction. It is worth noticing that, due to the smallness of the electron mass m_e, L_t is of the order of 15 for $-t \simeq 1$ GeV^2, *i.e.* for values of the four-momentum transfer typical of small-angle processes at LEP. This is the reason why QED radiative corrections are numerically very relevant.

The coefficients $a_k^{(n)}$ in eq. (8) are in turn given by the following general expression

$$a_k^{(n)} = \sum_{j=0}^{k} b_{kj}^{(n)} l^j, \tag{9}$$

where l is the so called IR logarithm, $l \simeq \ln(E/E_\gamma^{max})$, E being the beam energy and E_γ^{max} being some cutoff on the maximum photon energy, respectively. As a property of QED corrections, the IR logarithm l can become huge when shrinking the photon phase

space. In general, however, such corrections depend critically on the details of the ES considered.

The purpose of the present discussion is to derive a sort of *rule of thumb* able to provide the order of magnitude of the various QED corrections. To this aim, an approximate calculation is a useful guideline. As a general warning, however, it is worth noting that the coefficients a_k, due to the presence of the IR logarithm, are IR sensitive, so that they can become very large in *pathological* situations, *i.e.* when very tight cuts on the emitted photons are imposed. After this *caveat*, the corrected cross section σ for the SABH process in the leading logarithmic (LL) approximation, obtained for instance by means of the Structure Function method, taking into account initial- and final-state radiation but neglecting convolution effects (see Appendix A for more details) can be written as [17]

$$\sigma \simeq \sigma_0 \varepsilon^{\beta}. \tag{10}$$

The symbols in eq. (10) have the following meaning: σ_0 is the tree-level cross section, β is given by

$$\beta = 2\frac{\alpha}{\pi}\mathcal{L}(Q^2) \tag{11}$$

and $\varepsilon = \varepsilon_i \varepsilon_f$ is the product of two, in principle different, cutoffs for ISR and FSR.

The series expansion of eq. (10) up to third order in α reads:

$$\sigma \simeq \sigma_0 \left(1 + \beta \ln \varepsilon + \frac{1}{2!}\beta^2 \ln^2 \varepsilon + \frac{1}{3!}\beta^3 \ln^3 \varepsilon\right) + \mathcal{O}(\beta^4). \tag{12}$$

It is worth noting that in the LL approximation the coefficients a_n are proportional to the n-th power of the IR logarithm l.

TABLE II. – The canonical coefficients indicating the generic magnitude of various leading and subleading contributions up to third-order, for a non-calorimetric ES. The collinear logarithm $L_t = L = \ln(|t|/m_e^2)$ is calculated for $\vartheta_{min} = 30$ mrad and $\vartheta_{min} = 60$ mrad and for two values of the c.m. energy: at LEP1 ($\sqrt{s} = M_Z$), where the corresponding $|t| = (s/4)\vartheta_{min}^2$ are 1.86 and 7.53 GeV^2, and at LEP2 energy ($\sqrt{s} = 200$ GeV), where the corresponding $|t|$ are 9 and 36 GeV^2, respectively (from ref. [18]).

		$\vartheta_{min} = 30$ mrad		$\vartheta_{min} = 60$ mrad	
		LEP1	LEP2	LEP1	LEP2
$\mathcal{O}(\alpha L)$	$4\frac{\alpha}{\pi}L$	137×10^{-3}	152×10^{-3}	150×10^{-3}	165×10^{-3}
$\mathcal{O}(\alpha)$	$\frac{\alpha}{\pi}$	2.3×10^{-3}	2.3×10^{-3}	2.3×10^{-3}	2.3×10^{-3}
$\mathcal{O}(\alpha^2L^2)$	$\frac{1}{2}\left(4\frac{\alpha}{\pi}L\right)^2$	9.4×10^{-3}	11×10^{-3}	11×10^{-3}	14×10^{-3}
$\mathcal{O}(\alpha^2L)$	$\frac{\alpha}{\pi}\left(4\frac{\alpha}{\pi}L\right)$	0.31×10^{-3}	0.35×10^{-3}	0.35×10^{-3}	0.38×10^{-3}
$\mathcal{O}(\alpha^3L^3)$	$\frac{1}{3!}\left(4\frac{\alpha}{\pi}L\right)^3$	0.42×10^{-3}	0.58×10^{-3}	0.57×10^{-3}	0.74×10^{-3}

In order to exploit the information contained in eq. (12), it is necessary to specify the main features of the ES one is considering. Let us begin with a non-calorimetric ES. It is not a realistic case; nonetheless, it can be considered as a very useful benching situation. Such an ES is characterized by the fact that in principle it is possible to

separate final-state fermions from the photon(s) radiated by them, in such a way that a maximum photon energy cutoff, irrespective of the fact that the photon comes from initial- or final-state particles, is meaningful. For such an ES, one can take in eq. (12)

$$\varepsilon \simeq \varepsilon_i^2 \simeq \varepsilon_f^2 \simeq \varepsilon_{nc}^2, \tag{13}$$

in such a way that eq. (12) becomes

$$\sigma \simeq \sigma_0 \left(1 + 2\beta \ln \varepsilon_{nc} + \frac{1}{2!}(2\beta)^2 \ln^2 \varepsilon_{nc} + \frac{1}{3!}(2\beta)^3 \ln^3 \varepsilon_{nc}\right) + \mathcal{O}(\beta^4). \tag{14}$$

By defining now as *canonical coefficients* the coefficients appearing in front of the IR sensitive terms, the canonical coefficients of the $\mathcal{O}(\alpha^n L^n)$ corrections, with $1 \leq n \leq 3$, can be directly read off eq. (14), and are 2β, $(2\beta)^2/2$ and $(2\beta)^3/3!$, respectively. The algorithms described in Appendix A allow to take these corrections into account naturally. Going beyond the LL approximation, eq. (14) does not provide information any more. Actually, the non-leading corrections are typically process dependent, and can be computed only by means of a full diagrammatic calculation. On the other hand, a non-collinear photon is known to produce a correction whose typical size is α/π, which sets the size of the non-leading $\mathcal{O}(\alpha)$ correction. Moreover, the $\mathcal{O}(\alpha^2 L)$ corrections come from configurations for which there is one collinear and one non-collinear photon, so that their typical size is $2\beta\alpha/\pi$. The situation is summarized in Tab. II, where also a numerical estimate of the canonical coefficients for a non-calorimetric measurement is given. It is worth noticing that both these non-leading corrections are relevant for obtaining a theoretical error of the order of 0.1%.

Let us now consider the more realistic case of a calorimetric ES (see Sect. **2**˙1). For such an ES, it is not possible in principle to separate a final-state fermion from its accompanying radiation. This means that one is effectively almost inclusive on FSR, *i.e.* that $\varepsilon_f \simeq 1$ and $\varepsilon \simeq \varepsilon_i = \varepsilon_c$. Equation (14) is then modified as follows:

$$\sigma \simeq \sigma_0 \left(1 + \beta \ln \varepsilon_c + \frac{1}{2!}\beta^2 \ln^2 \varepsilon_c + \frac{1}{3!}\beta^3 \ln^3 \varepsilon_c\right) + \mathcal{O}(\beta^4). \tag{15}$$

By comparing eq. (15) with eq. (14), one obtains the relation between the canonical coefficients for a non-calorimetric ES and those of a calorimetric ES. In particular, the $\mathcal{O}(\alpha^n L^n)$ coefficients are reduced by factor of 2, 4 and 8 for $n = 1, 2, 3$, respectively. One can not expect *a priori* a reduction in the coefficient of the $\mathcal{O}(\alpha)$ correction. Hence, there is a reduction of a factor of 2 in the coefficient of the $\mathcal{O}(\alpha^2 L)$ correction. The situation is summarized in Tab. III.

At present, there is complete control of the $\mathcal{O}(\alpha L, \alpha, \alpha^2 L^2, \alpha^3 L^3)$ corrections, for an arbitrary ES. ([1]) The $\mathcal{O}(\alpha^2 L)$ corrections are not fully under control, in the sense that are either analytically known for non-realistic (non-calorimetric) ES's or only approximated for realistic (calorimetric) ES's (see Sect. **2**˙4 for more details). As it will be seen in the following, the approximate knowledge of the $\mathcal{O}(\alpha^2 L)$ corrections is the main source of theoretical error on the SABH cross section. An illustrative plot concerning photonic radiative corrections to the SABH process can be found in Fig. 3. The tree-level cross section corresponding to the ES adopted is $\sigma_0 = 140.02$ nb. As can be seen in the first

([1]) Actually, at present a theoretical error of technical origin is attributed to the $\mathcal{O}(\alpha^3 L^3)$ corrections, that however is negligible with respect to the one due to missing $\mathcal{O}(\alpha^2 L)$ corrections (see Sect. **2**˙5).

TABLE III. – The relation between the canonical coefficients for a non-calorimetric ES (see Tab. II) and a calorimetric ES.

	non-cal. ES	reduction factor	cal. ES
$\mathcal{O}(\alpha L)$	$4\frac{\alpha}{\pi}L$	1/2	$2\frac{\alpha}{\pi}L$
$\mathcal{O}(\alpha)$	$\frac{\alpha}{\pi}$	1	$\frac{\alpha}{\pi}$
$\mathcal{O}(\alpha^2 L^2)$	$\frac{1}{2}\left(4\frac{\alpha}{\pi}L\right)^2$	1/4	$\frac{1}{2}\left(2\frac{\alpha}{\pi}L\right)^2$
$\mathcal{O}(\alpha^2 L)$	$\frac{\alpha}{\pi}\left(4\frac{\alpha}{\pi}L\right)$	1/2	$\frac{\alpha}{\pi}\left(2\frac{\alpha}{\pi}L\right)$
$\mathcal{O}(\alpha^3 L^3)$	$\frac{1}{3!}\left(4\frac{\alpha}{\pi}L\right)^3$	1/8	$\frac{1}{3!}\left(2\frac{\alpha}{\pi}L\right)^3$

plot, the photonic corrections reduce the cross section by an amount ranging from around 6% to around 16%, depending on the z_{min} cut (see the Figure for the definition of z_{min}). In the second plot, one can see that the non-leading $\mathcal{O}(\alpha)$ corrections reduce the cross section by around 1.5%, the higher-order LL corrections increase it by about 0.5%, and the non-leading $\mathcal{O}(\alpha^2 L)$ corrections introduce a further increase of about $0.1 \div 0.2\%$. All these corrections are relevant for a theoretical prediction at the 0.1% level.

There are also other radiative corrections to the SABH process, which however are much smaller than the photonic ones. They are the following:

- *light pairs*: these corrections arise from photons converting into $f\bar{f}$ pairs, and are dominated by e^+e^- pairs; they give typically a contribution of the order of few 10^{-4} with respect to the tree-level cross section (see [24] and references therein);

- *QED radiative corrections to Z-γ interference*: they alter sizably the tree-level Z-γ interference contribution, since it changes sign when crossing the resonance; they are under control (see [25], [26] and references therein).

Non-QED corrections other than vacuum polarization are absolutely negligible.

2˙4. *Computational Tools.* – In the present section the basic features of the computer codes available for the calculation of the SABH process cross section are briefly summarized. The aim of this discussion is to make an inventory of the theoretical approaches to the problem, and of their realizations in the form of `FORTRAN` codes, rather than to give an exhaustive description of the programs, which can be found in the literature.

`BHAGEN95` [27] — It is a MC integrator for both small- and large-angle Bhabha scattering. It is a structure function based program (see Appendix A˙1) for all-orders resummation, including complete photonic $\mathcal{O}(\alpha)$ and leading logarithmic $\mathcal{O}(\alpha^2 L^2)$ corrections in all the channels (long writeup in [18]).

`BHLUMI` [28, 29] — It is a MC event generator for small-angle Bhabha scattering. It includes multi-photon radiation in the framework of YFS exclusive exponentiation (see Appendix A˙3). Its matrix element includes complete $\mathcal{O}(\alpha)$ and leading logarithmic $\mathcal{O}(\alpha^2 L^2)$ corrections. Some non-leading $\mathcal{O}(\alpha^2 L)$ corrections are also taken into account. The program provides the full event in terms of particle flavors and four-momenta with an arbitrary number of additional radiative photons. It is the standard package used by the LEP Collaborations for the calculation of the theoretical SABH cross section.

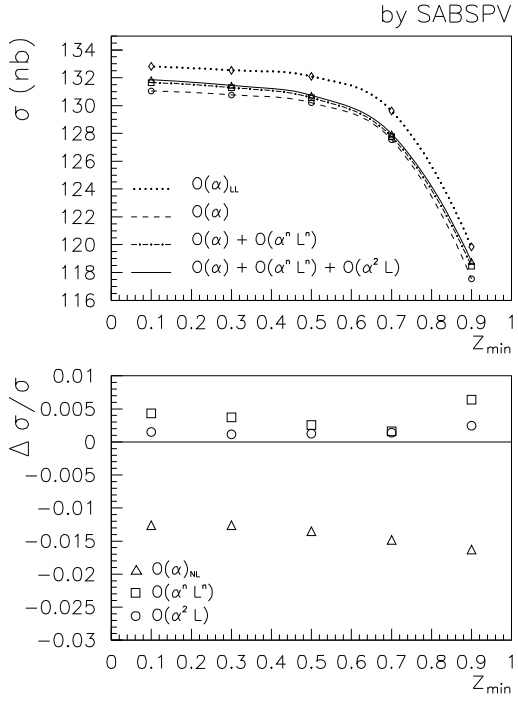

Fig. 3. – The effect of photonic corrections to the SABH process at different perturbative order/accuracy as a function of $z_{min} = E_+E_-/E^2_{beam}$, at $\sqrt{s} = 92.3$ GeV. $E_{+,-}$ are the energies deposited in the positron and electron clusters, respectively. The ES adopted is CALO2 (see ref. [18]). The tree-level cross section for this ES is $\sigma_0 = 140.02$ nb. The first plot shows the cross section including LL $\mathcal{O}(\alpha)$, exact $\mathcal{O}(\alpha)$, exact $\mathcal{O}(\alpha)$ plus higher-order LL and the same plus non-leading $\mathcal{O}(\alpha^2)$ corrections. In the second plot, $\Delta\sigma/\sigma$ means the effect of non-leading $\mathcal{O}(\alpha)$ corrections (triangles), of higher-order LL corrections (squares), and an estimate af the effect of non-leading $\mathcal{O}(\alpha^2 L)$ corrections (circles). The numerical results have been obtained by `SABSPV` [21–23].

LUMLOG — It is a MC event generator for the SABH process (part of `BHLUMI`, see [28]). Photonic corrections are treated at the leading logarithmic level, in the strictly collinear approximation, and in inclusive way. Structure functions exponentiated up to $\mathcal{O}(\alpha^3 L^3)$ are included. At the $\mathcal{O}(\alpha^2)$ it includes the leading corrections of the kind $\mathcal{O}(\alpha^2 L^2)$. It is used to improve `OLDBIS` (more on this later) in the sector of higher-order photonic corrections.

NLLBHA [30] — It is the `FORTRAN` translation of the only available fully analytical non-leading second-order calculation. At the $\mathcal{O}(\alpha^2)$ it includes all the next-to-leading corrections $\mathcal{O}(\alpha^2 L)$. It is also able to provide $\mathcal{O}(\alpha^3 L^3)$ photonic corrections and light pair corrections, including the simultaneous emission of photon and light pair. It is a semi-analytical result, at present available for a bare ES.

OLDBIS [31] — It is a classical MC event generator for the Bhabha process (the modernized version is part of `BHLUMI`, see [28]). It includes exact $\mathcal{O}(\alpha)$ photonic corrections. It

is used to improve LUMLOG in the sector of $\mathcal{O}(\alpha)$ photonic corrections.
OLDBIS+LUMLOG — It is the "tandem" developed in parallel with BHLUMI in order to take into account higher-order corrections (LUMLOG) on top of the exact $\mathcal{O}(\alpha)$ result (OLDBIS). The matching between $\mathcal{O}(\alpha)$ and higher-order corrections is performed in *additive* form. This means that no $\mathcal{O}(\alpha^2 L)$ corrections are present.
SABSPV [21, 22] — It is a MC integrator, designed for small-angle Bhabha scattering. It is based on a proper matching of the exact $\mathcal{O}(\alpha)$ cross section for t-channel photon exchange [17, 32] and of the leading logarithmic results for the full Bhabha scattering cross section in the structure function approach [33]. The matching is performed both in *additive* and *factorized* forms, the first form being used for comparisons only. In its default mode (factorized cross section) it includes the bulk of the $\mathcal{O}(\alpha^2 L)$ corrections.

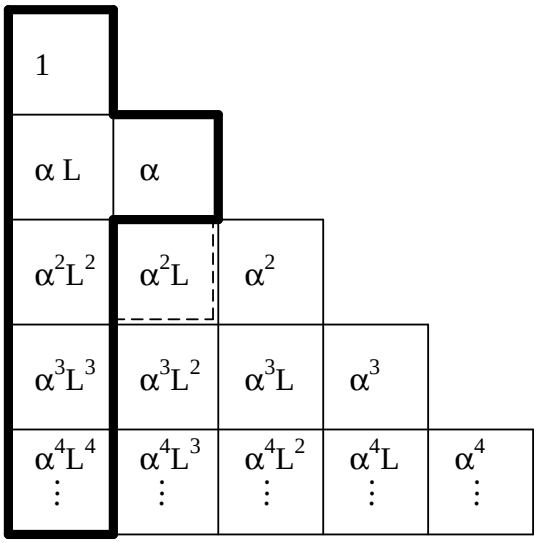

Fig. 4. – The general structure and the present situation concerning QED corrections to the SABH process. The thick line isolates the corrections exactly known for every ES. The dashed line points out the $\mathcal{O}(\alpha^2 L)$ corrections. They are at present the main source of theoretical error, since they are either approximately known for realistic ES's or exactly known for unrealistic ES's.

The situation of the computer codes available for the SABH process can be summarized as follows:

- with the exception of LUMLOG, all the other codes implement exact $\mathcal{O}(\alpha)$ photonic corrections for the SABH process; with the exception of OLDBIS, all the other codes implement some form of higher-order photonic corrections;
- BHAGEN95, OLDBIS+LUMLOG and SABSPV in the additive form include higher-order corrections in the leading logarithmic approximation;
- BHLUMI and SABSPV in its default form include also the bulk of the $\mathcal{O}(\alpha^2 L)$ corrections, for every ES;
- NLLBHA includes the full set of the $\mathcal{O}(\alpha^2 L)$ corrections, but limited to a bare ES.

The situation concerning the QED corrections at present under control for every ES is described in Fig. 4.

2˙5. *The Total Theoretical Error.* – Any theoretical prediction performed by means of a perturbative theory is affected by an intrinsic uncertainty because the perturbative series must be truncated at some finite order (with the possible exception of those corrections that can be resummed to all the perturbative orders, such as, for instance, the universal photonic corrections). Hence the theoretical error of a perturbative prediction is dominated by the largest unknown corrections, *i.e.* by the lowest order corrections not under control. When applying the above definition to the SABH process, it turns out that there are several sources of theoretical error, namely the ones quoted in Tab. IV. Up to date, the most important one is due to the missing photonic $\mathcal{O}(\alpha^2 L)$ corrections, which at present are not fully under control as shown in Fig. 4.

TABLE IV. – Summary of the total (physical+technical) theoretical uncertainty for a typical calorimetric detector. For LEP1, the above estimate is valid for the angular range within $1^\circ - 3^\circ$, and for LEP2 it covers energies up to 176 GeV, and angular ranges within $1^\circ - 3^\circ$ and $3^\circ - 6^\circ$ (from ref. [34]).

	LEP1	LEP1	LEP2
Type of correction/error	Past	Present	Present
(a) Missing photonic $\mathcal{O}(\alpha^2 L)$	0.15%	0.10%	0.20%
(b) Missing photonic $\mathcal{O}(\alpha^3 L^3)$	0.008%	0.015%	0.03%
(c) Vacuum polarization	0.05%	0.04%	0.10%
(d) Light pairs	0.01%	0.03%	0.05%
(e) Z-boson exchange	0.03%	0.015%	0.0%
Total	0.16%	0.11%	0.25%

Moreover, when considering the calculation of a cross section for a realistic ES, one has to implement the theoretical formulation of the problem in a computational tool, typically a `FORTRAN` code performing all the numerical integrations. In so doing, other sources of uncertainty are added, that are of technical origin, such as, for instance, approximations in the formulae, numerical algorithms performing the phase space integrations and so on. On the whole, also the actual implementation in itself of a given theoretical formulation gives rise to a finite contribution to the total theoretical error.

From now on, the precision reached in principle by means of a given theoretical formulation will be referred to as the "physical precision" of the approach, as distinct from the precision reached in its actual implementation, which will be referred to as the "technical precision".

As a matter of fact, the LEP Collaborations use the MC `BHLUMI` to compute the SABH theoretical cross section. Hence, a key issue is determining the theoretical error of the prediction by `BHLUMI`. Since the codes described in the previous Section differ from one another in the treatment of higher-order next-to-leading corrections, a careful comparison of their predictions together with a deep understanding of their differences can be used to infer an estimate of the total theoretical error on the SABH cross section.

The most extensive work in this directions has been performed in the context of the Workshop *Physics at LEP2*, held at CERN, Geneva, during 1995, and in particular

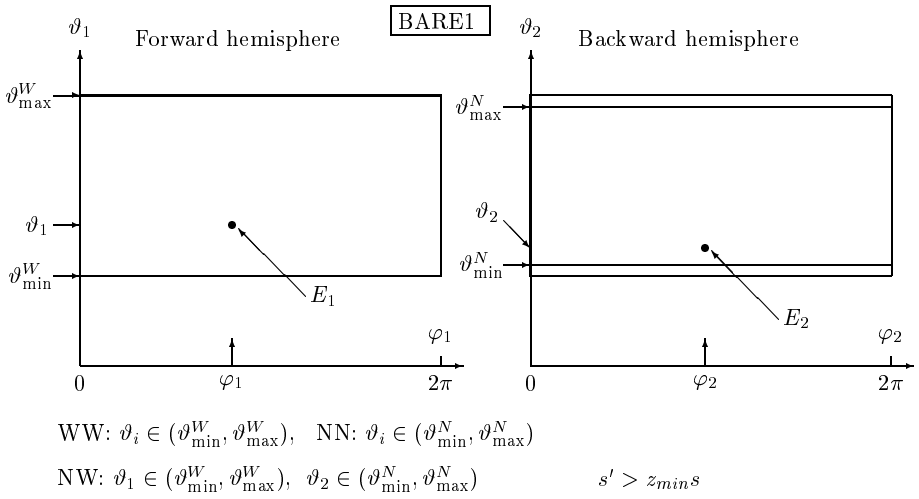

Fig. 5. – Geometry and acceptance of the simple (non-calorimetric) ES BARE1. This ES restricts the polar angles ϑ_i in the forward/backward hemispheres and requires a certain minimum energy to be detected simultaneously in both hemispheres. Photon momentum is not constrained at all. The entire "fiducial" ϑ-range, *i.e.* the wide (W) range, is $(\vartheta^W_{\min}, \vartheta^W_{\max}) = (0.024, 0.058)$ rad and the narrow (N) range is $(\vartheta^N_{\min}, \vartheta^N_{\max})$, where $\vartheta^N_{\min} = \vartheta^W_{\min} + \delta_\vartheta$, $\vartheta^N_{\max} = \vartheta^W_{\max} - \delta_\vartheta$ and $\delta_\vartheta = (\vartheta^W_{\max} - \vartheta^W_{\min})/16$. This ES can be symmetric WW or NN, or asymmetric NW (see the description in the figure). The energy cut $s' > z_{min}s$ involves the momenta of the outgoing $e^\pm$ ($s' = (q^+ + q^-)^2$) only (from ref. [18]).

within the Working Group "Event Generators for Bhabha scattering" [18], whose main tasks were

- to make an inventory of all the available MC event generators, developed by independent collaborations, for Bhabha processes at LEP1 and LEP2, both at small and large scattering angles;
- to improve the understanding of their theoretical uncertainties by means of systematic comparisons of MC's between themselves and with non-MC approaches.

The main emphasis was put on SABH processes, because of the pressing need to match the theoretical precision of the calculations with the much improved experimental accuracy ($\leq 0.1\%$) of the luminosity measurement. In particular, the main achievement of the Working Group, which is the result of a combined effort by several collaborations addressing several theoretical and experimental issues, was the reduction of the theoretical error on the SABH cross section from 0.16% to 0.11% for typical ES's at LEP1, and a first estimate of the theoretical error on the SABH cross section at LEP2 [34].

The various components of the theoretical error on the SABH cross section are quoted in Tab. IV (see ref. [34]), where a summary of the past and present situation at LEP1 together with the present estimate valid for LEP2 is given. The errors in the Table are understood to be attributed to the cross section for any typical (asymmetric) ES, for a LEP1 experiment in the angular range $1^\circ - 3^\circ$, calculated by `BHLUMI 4.03` [28]. In the case of LEP2, the estimate extends to the angular range $3^\circ - 6^\circ$, and also to a possible narrower angular range (say $4^\circ - 6^\circ$) that may be necessary due to the effect of

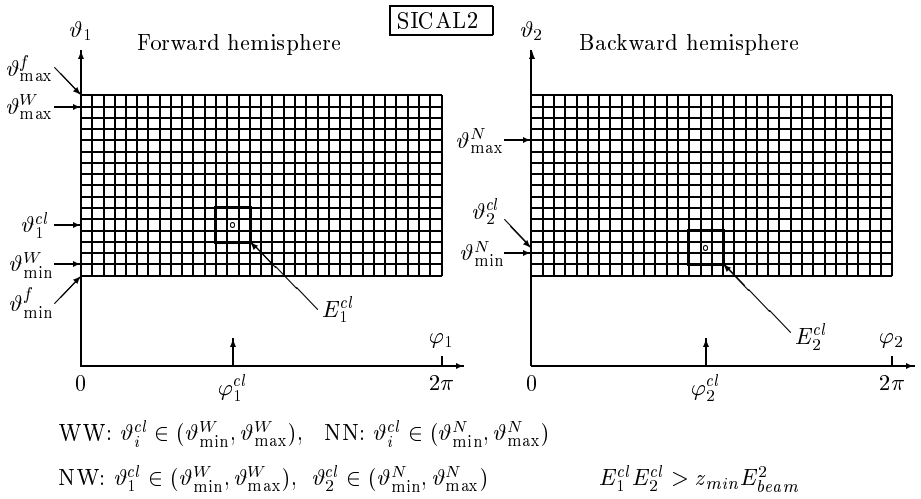

Fig. 6. – Geometry and acceptance of the calorimetric ES SICAL2. This ES restricts the polar angles ϑ_i in the forward/backward hemispheres and requires a certain minimum energy to be detected simultaneously in both hemispheres. No restrictions on azimuthal angles φ_i are there. The entire "fiducial" ϑ-range, $(\vartheta^f_{\min}, \vartheta^f_{\max}) = (0.024, 0.058)$ rad, includes the wide (W) range $(\vartheta^W_{\min}, \vartheta^W_{\max})$ and the narrow (N) range $(\vartheta^N_{\min}, \vartheta^N_{\max})$ exactly as depicted in the figure. This ES can be symmetric WW or NN, or asymmetric NW. The energy cut and the ϑ-cuts involve the definition of the *cluster*. Each side detector consists of 16×32 equal *plaquettes*. A single plaquette registers the total energy of electrons and photons. The plaquette with the maximum energy, together with its 3×3 neighborhood, is called cluster. The total energy registered in the cluster is E^{cl}_i and its angular position is $(\vartheta^{cl}_i, \varphi^{cl}_i)$, $i = 1, 2$. More precisely the angular position of a cluster is the average position of the *centers* of all 3×3 plaquettes, weighted by their energies (the definitions of φ's are adjusted in such a way that $\varphi_1 = \varphi_2$ for back-to-back configuration). The plaquettes of the cluster which spill over the angular range (outside thick lines) are also used to determine the total energy and the average position of the cluster, as in the backward hemisphere (from ref. [18]).

synchrotron radiation masks in the experiments. The entries include combined technical and physical precision.

As can be seen in the Table, at the present stage the theoretical error is still dominated by the error on photonic corrections, quoted in entries (a) and (b), and in particular by the one due to missing $\mathcal{O}(\alpha^2 L)$ corrections of entry (a). Since the error of entry (a) is by far dominant with respect to all the other ones, it is worth devoting some space to describe how it has been estimated, namely by adopting the following procedure:

- only the photonic corrections to the dominant part of the SABH cross section, namely the one due to t-channel photon exchange, have been considered as a first step;

- four families of ES's have been defined (for the details concerning the definitions of the ES's the reader is referred to [18]); the simplest one, BARE1 (see Fig. 5), is an ES in which cuts are applied only to the "bare" final-state fermions; the other ones, CALO1, CALO2 and SICAL2, are calorimetric ES's, implementing more and more complex clustering algorithms; in particular, SICAL2 (see Fig. 6) is very similar

to a "real" experimental ES; since photonic corrections are very sensitive to the details of the ES, defining these four ES's allows to span in detail the photonic phase space; even if the ES BARE1 is far from realistic, the presently available analytical calculation including the complete set of $\mathcal{O}(\alpha^2 L)$ corrections refers to such an ES, and so provides a very important cross-check of the MC programs;

- all the available codes have been run for all the ES's, varying inside any ES the threshold requirements for the final-state fermions/clusters;

- a test concerning the technical precision has been performed, namely comparing the exact up to $\mathcal{O}(\alpha)$ cross sections provided by the various codes; agreement at the level of a few 10^{-4} relative deviation has been achieved;

- finally, the results of the codes including the full higher-order photonic corrections have been compared, for all the situations explored (see Fig. 7).

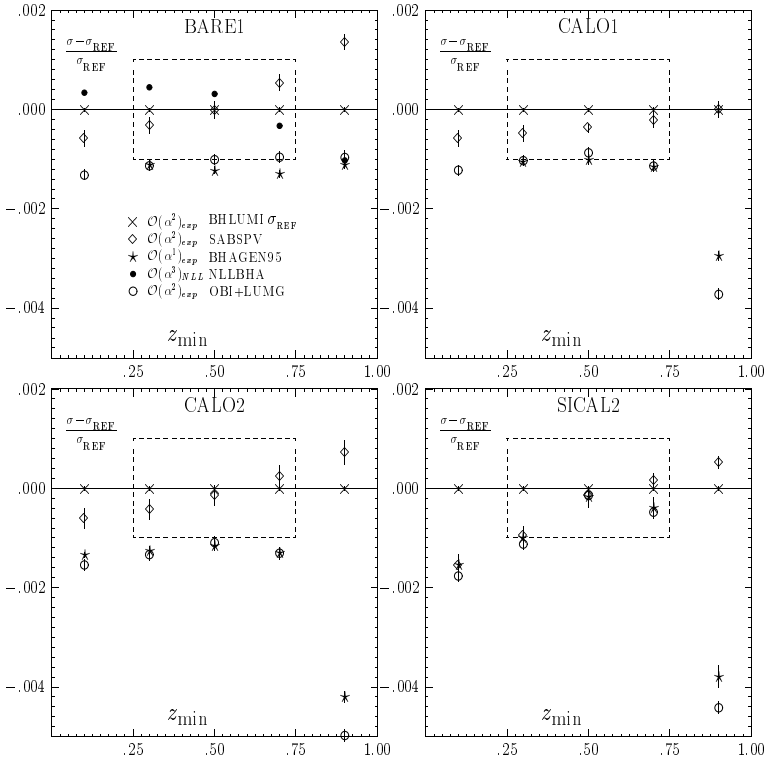

Fig. 7. – Monte Carlo results for the symmetric Wide-Wide ES's BARE1, CALO1, CALO2 and SICAL2, for matrix elements beyond first order. Z-boson exchange, up-down interference and vacuum polarization are switched off. The c.m. energy is $\sqrt{s} = 92.3$ GeV. z_{min} is the cut condition on the final-state energies, defined as $E_+E_-/E^2 \geq z_{min}$, $E_{-,+}$ being the final-state energy of the bare electron and positron, respectively. The *fiducial* angular range is 0.024-0.058 rad (for more details on the ES, the reader is referred to [18]). In the plot, the $\mathcal{O}(\alpha^2)^{YFS}_{exp}$ cross section from `BHLUMI 4.03` is used as a reference cross section (from refs. [18, 34]).

The result of this procedure allowed the definition of "one-per-mill regions", referring to realistic threshold cuts, within which most of the predictions lie. Moreover, for those cases for which the predictions do not lie within the "one-per-mill regions", the reasons for the deviations involved have been carefully investigated and eventually understood.

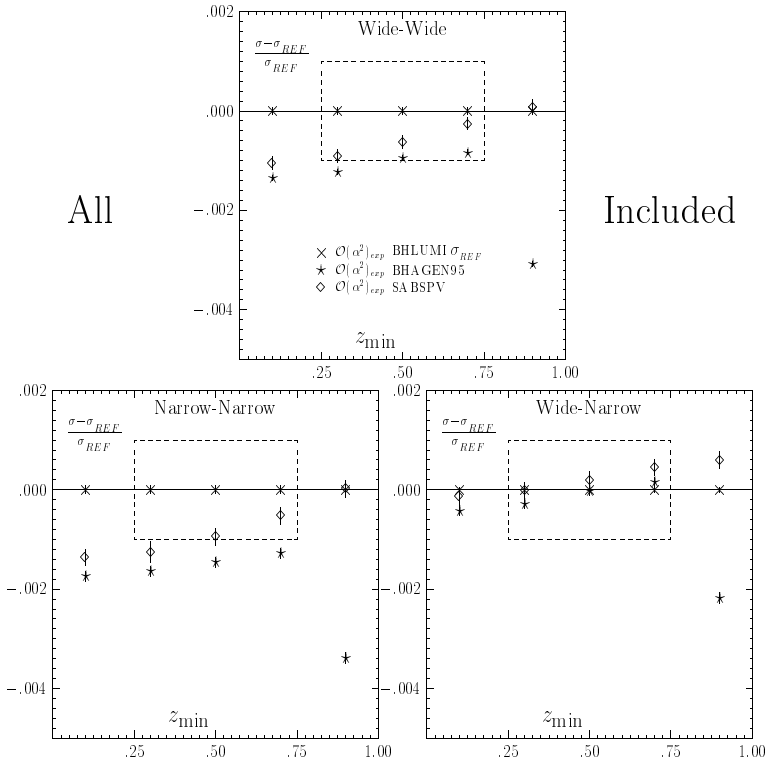

Fig. 8. – Monte Carlo results for various symmetric/asymmetric versions of the CALO2 ES, for matrix elements beyond first order. Z-boson exchange, up-down interference and vacuum polarization are switched ON. The c.m. energy is $\sqrt{s} = 92.3$ GeV. z_{min} is the cut condition on the final-state energies, defined as $E_+E_-/E^2 \geq z_{min}$, $E_{-,+}$ being the final-state energy of the electron and positron clusters, respectively. The *fiducial* angular range is 0.024-0.058 rad (for more details on the ES, the reader is referred to [18]). In the plot, the $\mathcal{O}(\alpha^2)^{YFS}_{exp}$ cross section from `BHLUMI 4.03` is used as a reference cross section (from refs. [18, 34]).

An analogous procedure has been followed after the inclusion of all the relevant radiative corrections (vacuum polarization, Z-boson exchange contributions and so on), and extending the comparisons also to asymmetric ES's, leading to the results shown as an example in Fig. 8. A similar analysis has also been performed for the first time in situations which are typical at the LEP2 experiments. The conclusion drawn at the end of all these comparisons is that now the theoretical uncertainty due to uncontrolled $\mathcal{O}(\alpha^2 L)$ corrections is reduced from 0.15% to 0.10% for the LEP1 situation, and estimated to be 0.20% at LEP2. As far as entry (b), the "missing photonic $\mathcal{O}(\alpha^3 L^3)$" uncertainty, is concerned, new estimates of the effect have resulted in a more conservative theoretical error, namely 0.015% to be compared with the old estimate of 0.008%.

As far as all the other entries in Tab. IV are concerned, namely entries (c), the

"vacuum polarization" uncertainty, (d), the "light pairs" uncertainty, and (e), the "Z-boson exchange" uncertainty, two of them, (c) and (e), are reduced with respect to the previous situation thanks to several new fits of the hadronic contribution to the vacuum polarization, and some additional original work on the Z-boson exchange contribution done during the workshop. New estimates, both MC and analytical, of the light pairs contribution, (d), featuring more complete calculations done during the workshop, have resulted in a more conservative estimate of the pairs effect uncertainty of 0.03%.

In conclusion, the total (physical + technical) theoretical uncertainty on the SABH cross section for a typical calorimetric detector is at present 0.11% at LEP1 and 0.25% at LEP2. While the theoretical precision reached in the LEP2 case is sufficient, further improvements in the LEP1 case are desirable.

2˙6. *Recent Developments and Perspectives.* – After the completion of the Working Group "Event Generators for Bhabha scattering" [18], some additional work, relevant for a further reduction of the theoretical uncertainty on the SABH cross section, has been done by the `BHLUMI` [35–39] and `SABSPV` [23] groups.

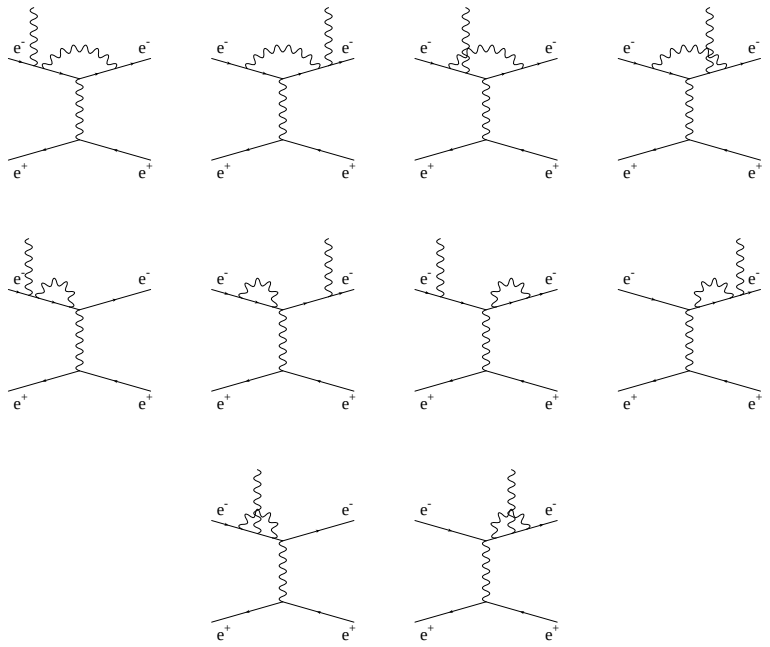

Fig. 9. – Examples of virtual corrections to single bremsstrahlung in the SABH process (see ref. [35, 37]). Only graphs concerning the real emission by the electron line are shown.

Concerning the `BHLUMI` group, the exact virtual one-loop corrections to the hard bremsstrahlung process in the SABH scattering (see Fig. 9) have been computed [35, 37]. These results are needed to complete the exact treatment of the $\mathcal{O}(\alpha^2 L)$ photonic corrections, since the contributions from double bremsstrahlung [40] and the two-loop electron form factor [41] are known. None of these corrections is at present implemented in `BHLUMI` [35]. It has to be noticed that this is the first exact, completely differential, result for the virtual one-loop corrections to the hard bremsstrahlung process in the

SABH scattering. Thanks to this result, the authors are able to estimate the size of the missing $\mathcal{O}(\alpha^2)L$ part in `BHLUMI`, for a realistic NW ALEPH SICAL luminometer, finding it below 2×10^{-4} of the Born cross section in the massless limit. Work is in progress in order to generalize the result to the massive case, and in order to compare its effect with the semi-analytical calculation of the `NLLBHA` group [30].

Concerning the `SABSPV` group, the theoretical formulation has been refined in order to eliminate a phase-space approximation in the $\mathcal{O}(\alpha^2 L)$ sector and the result has been analytically checked against the available complete $\mathcal{O}(\alpha^2 L)$ results already present in the literature for an academic ES (namely a BARE ES) in the soft-photon approximation, both for the annihilation and scattering channels [23]. For the annihilation channel, the results have been compared in particular with the ones shown in ref. [42], finding that

- the $\mathcal{O}(\alpha)$ perturbative result is exactly recovered, by construction;
- all the IR-singular terms, namely the ones containing $\ln^2 \varepsilon$ and $\ln \varepsilon$, where $\varepsilon = \Delta E/E$, are exactly recovered at the level of $\mathcal{O}(\alpha^2 L_s^2)$, $\mathcal{O}(\alpha^2 L_s)$ and $\mathcal{O}(\alpha^2)$, where $L_s = \ln(s/m^2)$;
- the difference between the two results starts at the level of $(\alpha/\pi)^2 L_s$ times a constant;

in particular, such a difference reads

$$\left.\frac{\delta\sigma}{\sigma_0}\right|_{(\alpha^2 L_s)} = \left(\frac{\alpha}{\pi}\right)^2 L_s \left[3\zeta(3) - \frac{3}{2}\zeta(2) + \frac{3}{16}\right], \tag{16}$$

where $\delta\sigma$ is the difference between the cross section of [42] and the cross section of ref. [23]. The difference numerically amounts to a relative deviation of about 1.7×10^{-4}. The residual difference is at $\mathcal{O}(\alpha^2)$ times a constant and is numerically irrelevant. For the scattering channel, the results have been compared with the ones of ref. [30]. The results of the comparison are the same as in the annihilation case up to the $\mathcal{O}(\alpha^2 L_t)$ corrections, namely the difference appears at the level of $(\alpha/\pi)^2 L_t$ times a constant and reads

$$\left.\frac{\delta\sigma}{\sigma_0}\right|_{(\alpha^2 L_t)} = 2\left(\frac{\alpha}{\pi}\right)^2 L_t \left[3\zeta(3) - \frac{3}{2}\zeta(2) + \frac{3}{16}\right], \tag{17}$$

where $\delta\sigma$ is the difference between the cross section of [30] in soft approximation and the cross section of ref. [23]. This difference numerically amounts to a relative deviation of about 2.2×10^{-4}, since the overall factor of two is compensated by the fact that $L_t \simeq 2/3 L_s$. In this case, also an additional difference appears, namely at the level of the IR-sensitive truly $\mathcal{O}(\alpha^2)$ terms, which reads

$$\left.\frac{\delta\sigma}{\sigma_0}\right|_{(\alpha^2)} = -\left(\frac{\alpha}{\pi}\right)^2 \left[4\ln^2 \varepsilon + 8\ln \varepsilon\right], \tag{18}$$

and is numerically irrelevant for a realistic situation. Therefore, the $\mathcal{O}(\alpha^2 L)$ corrections taken into account by the method of ref. [23] represent the bulk of the complete set. By taking now into account that the canonical coefficient of the $\mathcal{O}(\alpha^2 L)$ corrections for a calorimetric (realistic) ES is one half of the corresponding one for the BARE ES (see Tab. III), and considering a safety factor of three, the authors of [23] estimate that the

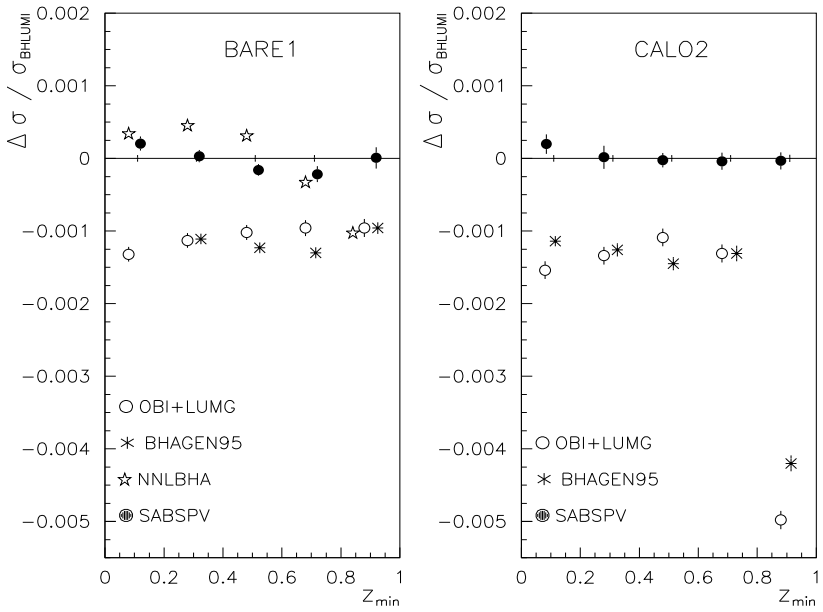

Fig. 10. – Comparison of Monte Carlo's. The relative differences between the codes involved in the comparison and the cross section by `BHLUMI 4.03` taken as a reference cross section are shown as functions of the cut $z_{min} = E_+E_-/E^2_{beam}$. $E_{+,-}$ are the energies deposited in the positron and electron clusters, respectively. The details of the clustering algorithms (BARE1 and CALO2) are given in [18]. The c.m. energy is $\sqrt{s} = 92.3$ GeV. For more details see ref. [23].

overall theoretical error of the approach, as far as QED corrections are concerned, is $\delta\sigma/\sigma \simeq 3 \times 10^{-4}$.

The situation is described in Fig. 10, where two ES's have been considered, namely a bare and a calorimetric ES. As can be seen, `BHAGEN95` and `OLDBIS+LUMLOG`, which do not take into account $\mathcal{O}(\alpha^2 L)$ corrections, differ from `BHLUMI`, which is taken as the reference cross section, by about 0.1%. `NLLBHA` shows differences which are contained within 0.1%; since the `NLLBHA` formulae coincide with the `SABSPV` ones up to the $\mathcal{O}(\alpha^2 L)$ corrections in the soft-photon region, such differences in the soft-photon region are presumably due to lack of exponentiation in `NLLBHA`. `BHLUMI` and `SABSPV` differ at most by 0.025%, consistently with the independent estimates of accuracies provided by their authors, respectively.

The results shown pave the way to a definite reduction of the theoretical luminosity error at the level of 0.05%. This is anyway not far from the smallest possible theoretical error, since the vacuum polarization uncertainty is 0.04% in its own (see Tab. IV).

3. – Z^0 Physics

The most important processes at the Z^0 resonance are represented by two-fermion production. In the case in which there are no electrons in the final state, the tree-level

Feynman diagrams for the s-channel annihilation $e^+e^- \to \gamma, Z \to f\bar{f}$ $(f \neq e)$ are depicted in Fig. 11. In the presence of electrons in the final state, there are additional t-channel amplitudes, which at large scattering angles are essentially backgrounds to the dominant s-channel annihilation (see Fig. 2 in Sect. **2**). The high degree of precision (at

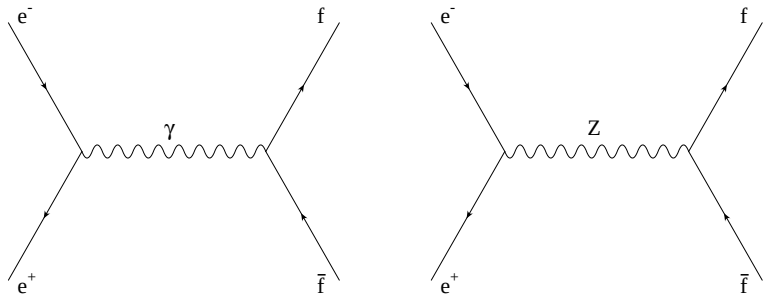

Fig. 11. – The tree-level Feynman diagrams for the process $e^+e^- \to \gamma, Z \to f\bar{f}$ $(f \neq e)$.

the level of 0.1% or better) reached in the measurement of the electroweak parameters at the Z^0 pole requires the inclusion in the theoretical predictions of radiative corrections beyond the Born approximation, in order to perform a meaningful comparison between theory and experiment. Radiative corrections to $e^+e^- \to \gamma, Z \to f\bar{f}$ processes are due to electroweak and strong forces as described by the Standard Model (SM) of the fundamental interactions, based on the gauge group $SU(2) \otimes U(1) \otimes SU(3)$. At a difference from the small-angle Bhabha process, where the calculation of QED radiative corrections only is enough to reach the aimed 0.1% theoretical precision, the two-fermion production in e^+e^- neutral current processes receives important contributions also from the electroweak and strong sector of the theory. Therefore, the fine structure of the SM can be probed by precision physics at LEP/SLC in a highly non trivial way at the level of quantum loops. The issue of radiative corrections has been studied at length in the past. For instance, the situation before the starting of LEP operations is reviewed in refs. [12], [13] and [43]. More recently, in view of the final analysis of LEP1 data, the theoretical studies have been updated in ref. [14].

In the present section, the basic aspects concerning the theoretical treatment of radiative corrections in precision calculations for the Z^0 resonance are reviewed, through the analysis of the main ingredients of pure weak, QCD and QED corrections to two-fermion production amplitudes. It is also discussed how the theoretical formulae are realized in the form of computational tools used for data analysis. The uncertainties associated to the theoretical predictions and their impact on the precision calculation of the Z-boson observables are finally analyzed.

3˙1. *Realistic Observables and Z^0 Parameters.* – The data published by the LEP Collaborations and used to extract information on the SM and its possible extensions refer to two main classes of observables:

- realistic observables;
- the Z^0 parameters or *pseudo-observables*.

The cross sections $\sigma(s)$ and the forward-backward asymmetries $A_{FB}(s)$ of the two-fermion production processes

$$e^+e^- \to (\gamma, Z) \to f\bar{f}(n\gamma), \tag{19}$$

quoted as functions of the centre of mass (c.m.) energy and including real and virtual photonic corrections (*i.e.* "dressed by QED") are collectively referred to as realistic observables. They are defined as

$$\sigma = \sigma_F + \sigma_B, \tag{20}$$

$$A_{FB} = \frac{\sigma_F - \sigma_B}{\sigma_F + \sigma_B}, \tag{21}$$

where $\sigma_{F,B}$ are the cross sections in the forward and backward hemisphere, respectively, *i.e.*

$$\sigma_F = 2\pi \int_0^1 d\cos\vartheta \, \frac{d\sigma}{d\Omega}, \qquad \sigma_B = 2\pi \int_{-1}^0 d\cos\vartheta \, \frac{d\sigma}{d\Omega}. \tag{22}$$

In the tree-level approximation, for unpolarized initial- and final-state fermions, the differential cross section $d\sigma_0/d\Omega$, as obtained from the calculation of the Feynman diagrams shown in Fig. 11, is given by

$$\frac{d\sigma_0}{d\Omega} = \frac{d\sigma_0^\gamma}{d\Omega} + \frac{d\sigma_0^{\gamma Z}}{d\Omega} + \frac{d\sigma_0^Z}{d\Omega}, \tag{23}$$

where the γ, γZ and Z contributions read

$$\begin{aligned}
\frac{d\sigma_0^\gamma}{d\Omega} &= \frac{\alpha^2 Q_f^2 N_c}{4s} \left(1 + \cos^2\vartheta\right), \\
\frac{d\sigma_0^{\gamma Z}}{d\Omega} &= -\frac{\alpha G_\mu M_Z^2 Q_f N_c}{4\sqrt{2}\pi s} \mathrm{Re}\big(\chi(s)\big) \left[g_v^e g_v^f \left(1 + \cos^2\vartheta\right) + 2 g_a^e g_a^f \cos\vartheta\right], \\
\frac{d\sigma_0^Z}{d\Omega} &= \frac{G_\mu^2 M_Z^4 N_c}{32\pi^2 s} |\chi(s)|^2 \left[\big((g_v^e)^2 + (g_a^e)^2\big)\big((g_v^f)^2 + (g_a^f)^2\big)\left(1 + \cos^2\vartheta\right)\right. \\
&\quad \left. + 8 g_v^e g_a^e g_v^f g_a^f \cos\vartheta\right].
\end{aligned} \tag{24}$$

In eq. (24) the symbols are defined as follows. ϑ is the fermion scattering angle. G_μ is the muon decay constant, α is the QED coupling constant and M_Z is the Z-boson mass. Q_f is the final-state fermion charge, in units of the positron charge. N_c is the colour factor, $N_c = 1, 3$ for leptons and quarks respectively. g_v^i and g_a^i are the tree-level vector and axial-vector couplings of the ith fermion to the Z^0 boson, given by

$$g_v^i = I_3^i - 2Q_i \sin^2\vartheta_W, \qquad g_a^i = I_3^i, \tag{25}$$

I_i^3 being the third weak-isospin component of the ith fermion and $\sin^2\vartheta_W$ the squared sine of the weak mixing angle. At last, $\chi(s)$ is the resonating factor

$$\chi(s) = \frac{s}{(s - M_Z^2) + i\Gamma_Z M_Z}, \tag{26}$$

Γ_Z being the total Z-boson width.

From the explicit expression of the differential cross section given in eqs. (23) and (24) it is straightforward to derive the expressions for the total cross section and forward-backward asymmetry. Concerning the total cross section, at $\sqrt{s} = M_Z$ the Z-boson contribution can be written in terms of total and partial Z-boson widths (see eq. (31) below), while the γZ term is exactly vanishing and the γ contribution gives an effect contained below 1%. As far as the forward-backward asymmetry is concerned, still at $\sqrt{s} = M_Z$, it takes the form shown in eq. (32) below.

The data presented by the LEP Collaborations for the realistic observables concern typically two different experimental configurations:

- extrapolated set-up: a cut on the invariant mass of the final-state fermions or on the invariant mass of the event after initial-state radiation (ISR) alone is imposed; the data corresponding to this inclusive situation are also said *perfect data*;
- "realistic" set-up: simple kinematical cuts, such as cuts on the energies or the invariant mass of the final-state products, angular acceptance and acollinearity angle of the outgoing fermions, are imposed.

Owing to the critical dependence of the QED corrections on the applied cuts, the comparison of the theory with the data for both the above set-up necessarily requires the availability of formulations (and relative computational tools) as complete as possible in the treatment of QED effects. Moreover, when aiming to fit "realistic" observables, a special effort must be devoted to the development of compact analytical and semi-analytical formulae for QED corrections.

The Z^0 parameters, or *pseudo-observables*, are extracted from the measured cross sections and asymmetries after some deconvolution or unfolding procedure. Basically, these quantities are determined by the LEP experiments by means of combined fits to the hadronic and leptonic cross sections and leptonic asymmetries, after corrections for the effect of ISR. Besides ISR, other radiative corrections or specific uninteresting effects can be depurated from the measurements in the unfolding procedure. For example, the deconvoluted forward-backward asymmetry includes the Z-boson exchange only (*i.e.* after subtraction of the γ and γZ contributions) and also final-state QED and eventually QCD corrections are subtracted from the experimental data. For the quantities relative to the e^+e^- final state, the t and s-t interference contributions are subtracted as well. More details about the fitting procedure adopted by the LEP Collaborations for the extraction of the Z^0 parameters are given in Sect. **4**. Therefore, the Z^0 parameters are secondary quantities or, in this sense, *pseudo-observables*. They are anyway of utmost importance for the precision tests of the SM, since they depend on the details of the internal structure of the electroweak theory. The Z^0 parameters considered in the literature are given in Tab. V. The *effective sine* is defined as

$$4\,|Q_f|\sin^2\vartheta^f_{eff} \;=\; 1 - \frac{g^f_V}{g^f_A}, \tag{27}$$

where Q_f is the electric charge of the fermion f in units of the positron charge, g^f_V and g^f_A are the *effective* neutral current vector and axial-vector couplings of the Z^0 to a fermion pair $f\bar{f}$, respectively. By definition, the total and partial widths of the Z^0 include final-state QED and QCD radiation. The invisible Z-boson width Γ_{inv}, the ratios R and the hadronic peak cross section are defined as

$$\Gamma_{inv} \;=\; \Gamma_Z - \Gamma_e - \Gamma_\mu - \Gamma_\tau - \Gamma_h, \tag{28}$$

TABLE V. – The most relevant Z^0 parameters.

Observable	Symbol
hadronic peak cross-section	σ_h
partial leptonic and hadronic widths	Γ_l $(l = e, \mu, \tau)$, Γ_c, Γ_b
total width	Γ_Z
hadronic width	Γ_h
invisible width	Γ_{inv}
ratios	R_l, R_b, R_c
forward-backward asymmetries	A^l_{FB}, A^b_{FB}, A^c_{FB}
polarization asymmetries	P^τ, P^b
left-right asymmetry (SLC)	A^e_{LR}
effective sine	$\sin^2\vartheta^l_{eff}$, $\sin^2\vartheta^b_{eff}$

$$R_l = \frac{\Gamma_h}{\Gamma_l}, \tag{29}$$

$$R_{b,c} = \frac{\Gamma_{b,c}}{\Gamma_h}, \tag{30}$$

$$\sigma^0_{had} = 12\pi \frac{\Gamma_e \Gamma_h}{M_Z^2 \Gamma_Z^2}. \tag{31}$$

By definition, σ^0_{had} includes only the Z-boson exchange. Forward-backward, left-right and polarization asymmetries, unlike the widths, are depurated, as said above, of the effects of QED and QCD corrections and, like σ^0_{had}, refer to pure Z-boson exchange. This allows to express them as simple combinations of the effective Z^0 couplings as follows:

$$A^f_{FB} = \frac{3}{4} A_e A_f, \tag{32}$$

$$A^e_{LR} = A_e, \tag{33}$$

$$P^f = -A_f, \tag{34}$$

where

$$A_f = \frac{2 g^f_V g^f_A}{(g^f_V)^2 + (g^f_A)^2}. \tag{35}$$

Analogously, the decay width of the Z^0 boson into a $f\bar{f}$ pair is given by the following expression:

$$\Gamma_f = 4 N_c \Gamma_0 [(g^f_V)^2 R^f_V + (g^f_A)^2 R^f_A], \tag{36}$$

where Γ_0 is given by $\Gamma_0 = G_\mu M_Z^3 / 24\sqrt{2}\pi$, and R^f_V and R^f_A are factors taking into account QED and QCD final-state radiation (FSR) and mass effects.

3˙2. *Electroweak Corrections.* – The high precision reached in the measurements at LEP and SLC allows to test the SM at the level of its radiative corrections. This can be done by virtue of the renormalizability of the theory [44]. The one-loop radiative corrections to $e^+e^- \to f\bar{f}$ can be divided into two classes, separately gauge invariant: the pure QED corrections and the electroweak ones. The former are obtained by adding

a virtual or real photon line to the lowest order Feynman diagrams, while the latter consist of all the remaining diagrams at one-loop order. As will be seen in the following the two classes of corrections are very different in many aspects and therefore different methods of calculation are required in order to reach the necessary theoretical accuracy. Contrary to the pure QED corrections, the electroweak corrections amount numerically to a few percent so that a one-loop approximation is already almost satisfactory. On the other hand, they depend on the fundamental parameters of the theory, so that particular attention must be devoted to the inclusion of potentially large higher-order effects in order to fully exploit the experimental accuracy to get information on the still unknown parameters. In the present Section the fundamental ingredients of electroweak corrections are illustrated and discussed.

3˙2.1. One-loop Feynman diagrams. The calculation of the electroweak corrections involve the evaluation of diagrams with closed loops, where an integration over the loop momentum is present which diverges for large momenta (ultraviolet divergences). For this reason a regularization procedure is needed in order to deal with finite and mathematically well defined integrals, before implementing a renormalization program. The most used method in the case of gauge theories is the dimensional regularization [45–47] because it allows to maintain Lorentz and gauge invariance at any step of the calculation. Some details about this procedure are given in Appendix C.

The electroweak one-loop corrections to $e^+e^- \to f\bar{f}$ can be classified in vector boson self-energies, fermion self-energies, vertex and box corrections. The fermion self-energies are commonly accounted as part of the vertex corrections. The vector boson self-energies, also referred to as *oblique corrections*, include the following transitions: γ-γ, γ-Z, Z-γ, Z-Z and W-W.

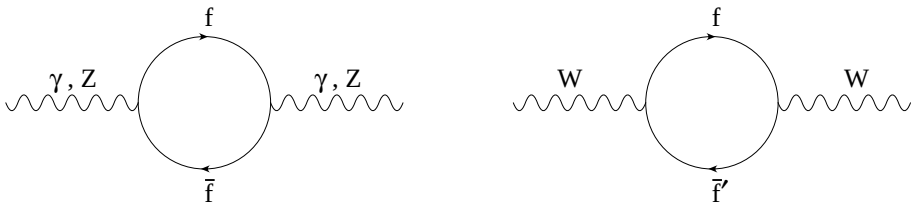

Fig. 12. – One-loop fermionic contributions to vector-boson self-energies.

All the above classes of corrections can be written in terms of general two-, three- and four-point functions introduced in ref. [48], which in turn can be reduced to certain combinations of the basic scalar one-, two-, three- and four-point integrals introduced in ref. [49]. Some simple examples of the procedure are given in Appendix C. The general expressions of the scalar form factors for arbitrary momentum and masses are not simple functions of their arguments and have to be computed numerically by means of the relations given in refs. [48–50].

Within the set of the vector boson self-energies two different kinds of corrections can be distinguished for their different numerical relevance: the fermion-loop contribution which is the leading one (see Fig. 12) and the bosonic contribution (see Fig. 13). Being gauge invariant by themselves, the fermion-loop corrections can be resummed with some procedure in order to take into account of reducible higher-order effects. The complete expressions for the vector boson self-energies in terms of two-point functions can be found

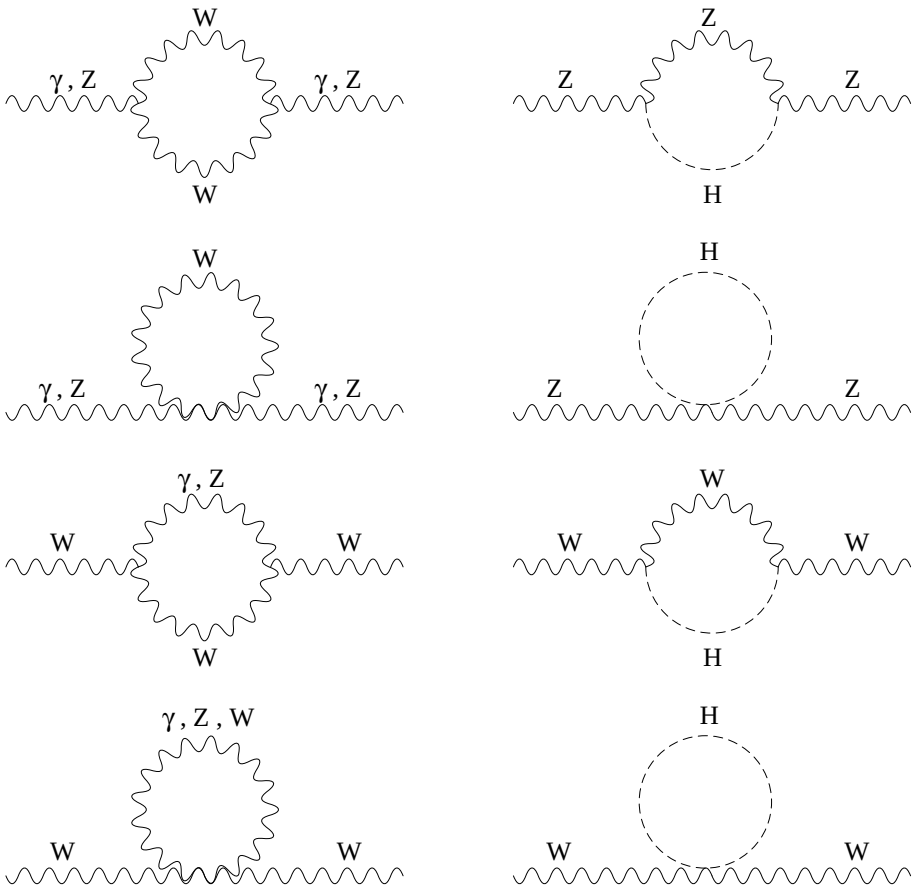

Fig. 13. – One-loop bosonic contributions to vector-boson self-energies.

in refs. [48,50,51]. Here only the fermion contributions are recalled because they deserve some important comments. The γ-γ transition is given by [50]

$$S_\gamma(p^2) = \frac{e^2}{16\pi^2} p^2 \sum_f Q_f^2 N_c \{8B_{21}(p^2, m, m) - 4B_0(p^2, m, m)\}, \tag{37}$$

where B are two-point functions and the sum is extended to all charged fermions. This expression is the same as obtained in QED, since the SM coupling between photon and fermions recovers the QED case. The quantity

$$\Pi^{\gamma\gamma}(p^2) = \frac{S_\gamma(p^2)}{p^2} \tag{38}$$

is known as the photon vacuum polarization. It is interesting to work out the two-point functions for the following asymptotic cases, for a fermion of given flavour:
• light fermions ($|p^2| >> m^2$)

$$\Pi^{\gamma\gamma}(p^2) = \frac{e^2}{12\pi^2} Q_f^2 \left(-\Delta + \ln m^2 - \frac{5}{3} + \ln \frac{|p^2|}{m^2} - i\pi \right), \tag{39}$$

• heavy fermions ($|p^2| << m^2$)

$$\Pi^{\gamma\gamma}(p^2) = \frac{e^2}{12\pi^2} Q_f^2 \left(-\Delta + \ln m^2 - \frac{p^2}{5m^2} \right). \tag{40}$$

Apart from the terms $\Delta - \ln m^2$, which are related to the ultraviolet divergences and are removed by the renormalization procedure, it is worth noticing the term proportional to $\ln(|p^2|/m^2)$ in the light fermions limit. At energies of the order of 100 GeV, as is the case at LEP, this terms is the origin of large corrections coming from the light fermion spectrum of the theory. While the leptonic contribution can be unambiguously calculated, the hadronic one is affected by a large uncertainty, because the light-quark masses can not be unambiguously defined. For this reason the hadronic contribution to the photon vacuum polarization is calculated by means of a dispersion relation as described in Appendix B. As far as the *top*-quark contribution to the vacuum polarization is concerned, taking into account the *top*-quark mass value of about $170 \div 180$ GeV, the heavy fermion limit of $\Pi^{\gamma\gamma}$ can be taken, resulting in a small effect. This happens because the $U(1)_{e.m.}$ group of the SM is not spontaneously broken so that the decoupling theorem [52] can be applied.

The combination of two-point form factors present in the fermionic contribution to the γ-Z transition is the same as the $\gamma\gamma$ case apart from the couplings. It is at this point worth noticing that, contrary to the case of the photon self-energy, the bosonic contribution to the mixed γ-Z transition is not proportional to p^2 so that it is different from zero for $p^2 = 0$.

The massive vector boson self-energies have the following expressions:

$$\begin{aligned} S_+(p^2) = \frac{g^2}{16\pi^2} N_c \sum_d \Big[\; & 2\; p^2 \{ B_{21}(p^2, m_d, m_u) + B_1(p^2, m_d, m_u) \} \\ & + (m_u^2 - m_d^2) B_1(p^2, m_d, m_u) - m_d^2 B_0(p^2, m_d, m_u) \Big], \end{aligned} \tag{41}$$

where g is the $SU(2)$ coupling constant and the sum is extended over the fermionic doublets;

$$\begin{aligned} S_0(p^2) = \frac{g^2}{16\pi^2} N_c \sum_f \Big[\; & p^2 \; \frac{(g_v^f)^2 + (g_a^f)^2}{4c_\vartheta^2} \{ 8B_{21}(p^2, m, m) - 4B_0(p^2, m, m) \} \\ & - \; \frac{m^2}{2c_\vartheta^2} B_0(p^2, m, m) \Big], \end{aligned} \tag{42}$$

where the sum is extended to all fermions. As before it is interesting to consider the two limits of light and heavy fermions:

• light fermions

$$S_+(p^2) = \frac{g^2}{12\pi^2} \frac{p^2}{4} N_c (-\Delta + \ln |p^2| - i\pi), \tag{43}$$

$$S_0(p^2) = \frac{g^2}{12\pi^2} \frac{(g_v^f)^2 + (g_a^f)^2}{4c_\vartheta^2} p^2 (-\Delta + \ln |p^2| - i\pi); \tag{44}$$

• heavy fermions

$$S_+(p^2) = \frac{g^2}{12\pi^2} N_c \Big[-\frac{p^2}{4}(\Delta - \ln m_u^2) - \frac{3m_u^2}{8}(\Delta - \ln m_u^2 + \frac{1}{2}) \Big], \tag{45}$$

$$S_0(p^2) = \frac{g^2}{12\pi^2} N_c \Big[-\frac{(g_v^f)^2 + (g_a^f)^2}{4c_\vartheta^2} p^2 - \frac{3m_u^2}{8c_\vartheta^2} \Big] (\Delta - \ln m_u^2), \tag{46}$$

where the contribution of a single doublet in the charged vector boson case has been written. Some comments are in order here. The ultraviolet divergences are associated only with the real parts of the self-energies, as the imaginary parts are directly related to the widths of the gauge bosons. Furthermore it appears in the heavy fermions limit a term proportional to m_u^2, that becomes numerically relevant in the case of the *top* quark.

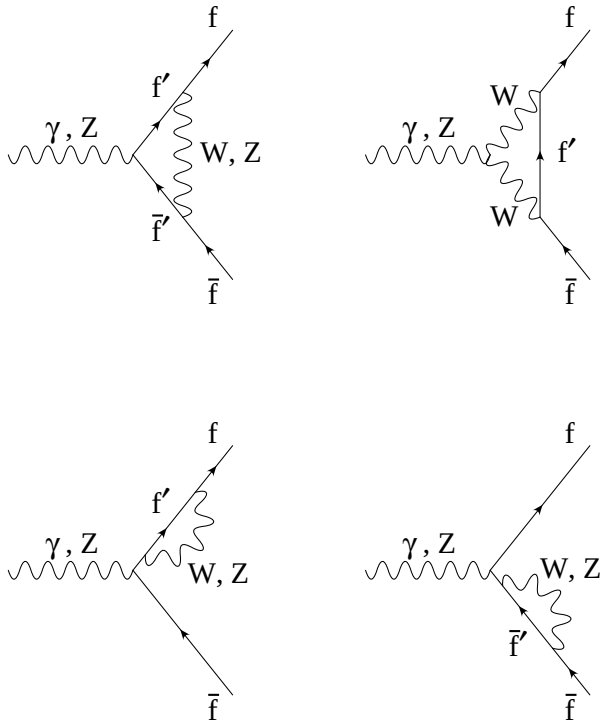

Fig. 14. – One-loop vertex corrections.

As far as the vertex corrections are concerned (see Fig. 14), neglecting the external fermion masses only two combinations of three-point functions $C(p^2, m_f, M_V, m_f)$ are present in the calculations [48, 51]:

$$\begin{aligned} C_{ff}^V(p^2) = &- 2C_{24}(p^2, m_f, M_V, m_f) - \big[C_{11}(p^2, m_f, M_V, m_f) \\ &+ C_{23}(p^2, m_f, M_v, m_f)\big] p^2 + 1, \end{aligned} \tag{47}$$

when only one gauge boson is present in the loop, and

$$\begin{aligned} C_f^{VV}(p^2) = &\ 6\ C_{24}(p^2, M_V, m_f, M_V) + \big[C_0(p^2, M_V, m_f, M_V) \\ &+ C_{11}(p^2, M_V, m_f, M_V) + C_{23}(p^2, M_V, m_f, M_V)\big] p^2 - 1, \end{aligned} \tag{48}$$

when two gauge bosons circulate in the loop. In the case of the $b\bar{b}$ final state, due to the effect of internal *top*-quark lines, five different combinations of three-point functions are needed, whose explicit expression can be found in [51]. As for the massive vector boson self-energies, terms of order m_t^2 originate from the vertex corrections to the $b\bar{b}$ final state [53]. In order to complete the vertex corrections, the wave function factors of the external fermions have to be added, which can be obtained from the fermion self-energy diagrams [50].

Last, the contribution of box diagrams for the process $e^+e^- \to f\bar{f}$ (see Fig. 15) can be written in terms of two combinations of four-point functions. They are ultraviolet finite, apart from the unitary gauge, and since they are not resonating at the Z^0 peak, their effect is numerically very small, so that generally they are neglected for LEP1 physics, although their inclusion is necessary for the gauge invariance of the calculation. As will be discussed in Sect. **5**˙1.1, the box corrections become relevant far away from the Z^0 peak.

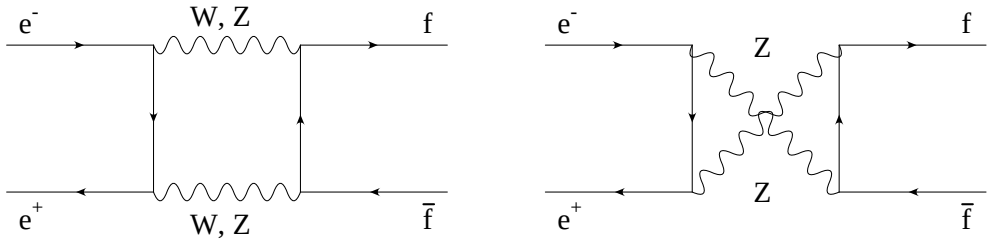

Fig. 15. – One-loop box corrections.

It is worth noticing that, from the point of view of the determination of unknown SM parameters, the bosonic corrections involving the insertion of internal Higgs-boson lines are particularly interesting, since they introduce a dependence of the theoretical predictions on the unknown Higgs-boson mass m_H.

3˙2.2. Calculational schemes. The tree-level Lagrangian of the SM contains in its electroweak part a certain number of free parameters which need to be fixed by comparison with experimental data. The choice of the lagrangian parameters and their relations with a set of experimental data is the content of a renormalization scheme.

The gauge sector of the minimal SM is characterized by three free parameters fixed by three input data points, which have to be known with high experimental accuracy, as they are the input for precision calculations. At present the three most precise experimental quantities are the fine structure constant α, measured by means of one the methods quoted in Appendix B, the muon decay constant G_μ, measured through the muon lifetime, and the Z-boson mass measured at LEP1. Their precision makes them the most widely used experimental input data for the calculation of radiative corrections. Having defined the parameters, the calculation of any other physical quantity can be used as a test of the theory by direct comparison of the theoretical prediction for the observable with its experimental value.

The relations between the lagrangian parameters and the measurable quantities depend on the order at which perturbation theory is carried on. In particular, going beyond the tree-level approximation, the situation is complicated by the appearance of ultraviolet divergences which make the differences between the tree-level parameters and the radia-

tively corrected ones infinitely large. Because of this, a commonly adopted procedure is the introduction of counter-terms: each bare parameter is split into the renormalized parameter and a counter-term which absorbs the ultraviolet divergences plus finite terms. The values of this finite parts depend on the renormalization prescriptions. Due to the renormalization group invariance, all renormalization schemes are equivalent. However, since the radiative corrections are obtained from a finite order perturbative expansion (eventually supplemented by resummation to all orders of some class of gauge invariant contributions), the predictions for physical quantities are scheme dependent. The differences between two calculations, performed at a fixed perturbative order in two different schemes, appear in higher-order terms. This fact allows to estimate the size of missing higher-order effects by comparing the results obtained with calculations based on different renormalization schemes (see Sect. **3**˙6). Given the high precision of the experiments at the Z^0 peak, it is very important to keep under control these higher-order effects. In the literature several schemes have been adopted for the calculation of radiative corrections. With the exception of the low energy scheme [50, 54–56], which has been used before the advent of LEP, it is worth mentioning the following calculational schemes adopted for various formulations of radiative corrections to observables at the Z^0 resonance:

- the on-shell scheme [57];
- the $\overline{MS}$ scheme [58];
- the G_μ scheme [59];
- the * scheme [60].

In the following a brief review of the various schemes is given.

The basic idea of the on-shell scheme is the observation that Thomson scattering and the particle masses set natural scales where the parameters e, M_Z, M_W, m_H and m_f can be defined. The finite parts of the mass counter-terms are fixed by the renormalization conditions that the particle propagators have poles at their physical masses. In the case of unstable particles like the $W^\pm$ and Z^0 bosons the mass is not uniquely defined. For LEP1 physics the vector boson mass is commonly defined as the zero of the real part of the inverse propagator. At one-loop order, after a Dyson resummation of the self-energy diagrams and neglecting external fermion masses, the propagator is given by the expression

$$\frac{1}{p^2 + {M_V^0}^2 - S_V(p^2)}, \tag{49}$$

where the Lorentz structure has been neglected for simplicity and M_V^0 is the bare mass. In the case of the Z-boson propagator, due to γZ mixing eq. (49) is modified by reducible higher-order terms, which for simplicity are not considered here. Introducing the mass counter-term means the following relation between the bare mass M_V^0 and the physical mass M_V:

$${M_V^0}^2 = M_V^2 + \delta M_V^2. \tag{50}$$

Inserting the above expression for the bare mass in the propagator of eq. (49), the expression of the counter-term can be easily identified as

$$\delta M_V^2 = \mathrm{Re} S_V(M_V^2). \tag{51}$$

The charge counter-term is fixed by the condition that e equals the $ee\gamma$ coupling constant in the Thomson limit of Compton scattering. At one-loop order, the $ee\gamma$ coupling receives contributions only from the photon self-energy and the mixed γ-Z transition, because the corrections related to the external particles cancel each other as a consequence of a generalization of the QED Ward identity. The expression for the charge counter-term reads

$$\frac{\delta e}{e} = \frac{1}{2}\Pi_{\gamma\gamma}(0) - \frac{s_W}{c_W}\frac{\Sigma_{\gamma Z}(0)}{M_Z^2}, \tag{52}$$

where s_W and c_W are the sine and cosine of the weak mixing angle defined in the SM by

$$\sin^2\vartheta_W = 1 - \frac{M_W^2}{M_Z^2}. \tag{53}$$

According to ref. [61], the above definition of $\sin^2\vartheta_W$ is assumed to be valid to all orders of perturbation theory.

As a matter of fact, the precision of the W-boson mass measurement is not adequate for precision physics at the Z^0 resonance. For this reason the input W-boson mass is replaced by the more accurate value of G_μ obtained from the μ-lifetime τ_μ:

$$\frac{1}{\tau_\mu} = \frac{G_\mu^2 m_\mu^5}{192\pi^3}\left(1 - \frac{8m_e^2}{m_\mu^2}\right)\left[1 + \frac{\alpha}{2\pi}\left(1 + \frac{2\alpha}{3\pi}\ln\frac{m_\mu}{m_e}\right)\left(\frac{25}{4} - \pi^2\right)\right]. \tag{54}$$

This equation, obtained within the effective four-fermion Fermi interaction with the inclusion of QED radiative corrections up to $\mathcal{O}(\alpha^2)$, is used as the definition of G_μ in terms of the experimental μ lifetime. Calculating the last one within the SM at one-loop order, the following relation can be established between G_μ and M_W:

$$\frac{G_\mu}{\sqrt{2}} = \frac{e^2}{8s_W^2 M_W^2}(1 + \Delta r), \tag{55}$$

where Δr is a ultraviolet finite combination of counter-terms and loop diagrams. Since Δr is a function of e, M_W, M_Z, m_H and m_t, eq. (55) can be solved iteratively for M_W. By inspection of the various contributions, Δr can be written in the following form:

$$\Delta r = \Delta\alpha - \frac{c_W^2}{s_W^2}\Delta\rho + (\Delta r)_{rem}, \tag{56}$$

where $\Delta\alpha$ is the fermionic contribution to the photonic vacuum polarization, and $\Delta\rho$ is the following ultraviolet finite combination [62, 63]:

$$\Delta\rho = \frac{\Sigma_Z(0)}{M_Z^2} - \frac{\Sigma_W(0)}{M_W^2}, \tag{57}$$

which is quadratic in the *top*-quark mass

$$\Delta\rho = N_c\frac{G_\mu m_t^2}{8\pi^2\sqrt{2}}. \tag{58}$$

$\Delta\rho$ is the corrections to the ρ parameter, defined as $\rho = M_W^2/M_Z^2\cos^2\vartheta_W$, which is equal to one in the minimal SM at the tree level [62–64]. $(\Delta r)_{rem}$ takes into account non-leading corrections, among which the most interesting ones, from the phenomenological

point of view, are due to Higgs-boson loops, yielding as leading contribution the following asymptotic logarithmic term ($m_H \gg M_W$) [65–67]

$$(\Delta r)^{Higgs}_{rem} \simeq \frac{\sqrt{2}G_\mu M_W^2}{16\pi^2}\left\{\frac{11}{3}\left(\ln\frac{m_H^2}{M_W^2}-\frac{5}{6}\right)\right\}, \tag{59}$$

and to *top*-quark loops, yielding a logarithmic term given by

$$(\Delta r)^{top}_{rem} = \frac{\sqrt{2}G_\mu M_W^2}{16\pi^2}2\left(\frac{c_W^2}{s_W^2}-\frac{1}{3}\right)\ln\frac{m_t^2}{M_W^2}+\dots \tag{60}$$

At the one-loop order, no quadratic Higgs-boson mass corrections appear as a consequence of the so-called *custodial* symmetry of the Higgs-boson sector of the minimal SM.

Due to the presence of large contributions to Δr of the kind $\alpha\ln(M_Z/m_f)$, these terms are resummed to all orders by writing eq. (55) in the following form [68]:

$$\frac{G_\mu}{\sqrt{2}} = \frac{e^2}{8s_W^2 M_W^2(1-\Delta r)}. \tag{61}$$

This form takes into account to a good approximation also the terms of the order of $\alpha^2\ln(m_f/M_Z)$ [68]. More details on higher-order terms are given in Sect. **3**˙2.4.

The method outlined above of parameter renormalization is sufficient to obtain finite S-matrix elements. However propagators and vertices by themselves are not finite. To this aim also field renormalization has to be carried out. This allows to fulfill further renormalization conditions, in particular the vanishing of the mixed γ-Z transition for real photons. The different ways of implementing field renormalization and the different gauges in which the calculations are performed are the main differences among the various realizations of the on-shell scheme present in the literature.

In the $\overline{MS}$ scheme, the counter-terms are defined only through the divergent parts proportional to $\Delta - \ln m^2$ of the radiative corrections to the bare parameters, as these are fixed only by the bare Lagrangian, and do not depend on particular renormalization conditions as is the case for the on-shell scheme. The $\overline{MS}$ expressions of the parameters can be directly obtained replacing the bare parameters with the $\overline{MS}$ ones, and replacing at the same time the quantity Δ in the radiative corrections to the bare parameters with $\ln\mu^2$, μ being the renormalization scale. In so doing, the $\overline{MS}$ parameters depend on the arbitrary scale μ, which can be naturally chosen to be M_Z for electroweak calculations. The $\overline{MS}$ electroweak mixing angle can be defined as

$$\hat{s}^2 = 1 - \frac{\hat{M}_W^2}{\hat{M}_Z^2}, \tag{62}$$

where $\hat{M}_{W,Z}$ are the $\overline{MS}$ vector boson masses.

According to refs. [69] and [70], a way to link directly $\hat{s}^2$ to the experimental inputs α, G_μ, and M_Z is to calculate the radiative corrections to μ decay within the $\overline{MS}$ framework introducing the correction $\Delta\hat{r}_W$ together with a generalized relation between the W- and Z-boson physical masses:

$$\hat{s}^2(1-\Delta\hat{r}_W) = \frac{\pi\alpha}{\sqrt{2}G_\mu M_Z^2}, \tag{63}$$

$$M_W^2 = \hat{c}^2\hat{\rho}M_Z^2, \tag{64}$$

where $\hat{\rho}^{-1} = 1 - \Delta\hat{\rho}$.

Within the $\overline{MS}$ scheme the relation giving the M_W-M_Z interdependence can be expressed as

$$\frac{M_W^2}{M_Z^2} = \frac{\hat{\rho}}{2}\left\{1 + \left[1 - \frac{4A^2}{M_Z^2\hat{\rho}(1-\Delta\hat{r}_W)}\right]^{\frac{1}{2}}\right\}, \tag{65}$$

with $A = \left(\pi\alpha/\sqrt{2}G_\mu\right)^{\frac{1}{2}}$.

The advantage of adopting the $\overline{MS}$ scheme is twofold [71]. First, this calculational framework leads to effective couplings which absorb the largest part of the *top*-quark and Higgs-boson mass dependence of the radiative corrections. Secondly, the knowledge of the gauge coupling constants at the Z-boson mass can be naturally extrapolated to higher energies in order to test scenarios of Grand Unification.

The idea of the G_μ scheme is to directly relate the bare parameters to the input data α, G_μ and M_Z. This can be realized according to different methods, for example by assuming on-shell parameters [72] or $\overline{MS}$ parameters [51,73]. Here a brief account of the second realization is given, where the bare parameters are chosen to be the $SU(2)$ coupling constant g, the W-boson mass M_W and the squared sine of the weak mixing angle s_ϑ^2. Starting from the observation that there is no one to one correspondence between lagrangian parameters and experimental data, in this scheme no attempt is made to define renormalized parameters (in particular s_ϑ^2) beyond lowest order. A set of three fitting equations [51,63] for the bare parameters is introduced, corresponding to the definition of α from Thomson scattering, G_μ from the μ lifetime and M_Z from the zero of the real part of the inverse Z^0 propagator:

$$d_i^{exp} = d_i^{th}(g, M_W, s_\vartheta, \Delta), \qquad (i = 1, 2, 3). \tag{66}$$

In eq. (66), d_i^{th} are the theoretical expressions of α, G_μ and M_Z in terms of g, M_W, s_ϑ^2 and Δ, whereas d_i^{exp} are the corresponding experimental values. The equations can be solved to first order in perturbation theory with respect to the bare parameters which contain ultraviolet divergences represented by the quantity Δ. They can be properly modified to account for resummation of relevant gauge invariant higher-order effects [51]. In the calculation of any physical quantity by means of one-loop diagrams calculated with tree-level parameters and tree diagrams calculated with up to one-loop order parameters the ultraviolet divergences cancel. This procedure is suitable for an order by order numerical renormalization. In the numerical calculation, the quantity Δ enters as an arbitrary parameter which can assume any numerical value without changing the final result.

The condition $\Sigma_{Z\gamma} = 0$ is fulfilled through a proper redefinition of the bare coupling g^0, which automatically guaranties that the sum of all $Zf\bar{f}$ vertices is ultraviolet finite [51].

It is worth noticing that in the G_μ scheme the W-boson mass plays the same rôle as any other physical observable, contrary to the on-shell scheme where at the same time it appears as a prediction and as an intermediate parameter for the calculation of other observables.

In the $*$ scheme, an effective lagrangian to one loop is introduced, and the universal effects of oblique corrections resummed to all orders are absorbed in the following three running parameters (free of ultraviolet divergences): $e_*^2(q^2)$, $s_*^2(q^2)$ and $G_{\mu*}^2(q^2)$. The values of these three starred functions have to be fixed at a certain set of q^2's and then can be calculated at any other scale by means of a set of evolution equation. The choice

of ref. [74] is to fix e_*^2 and $G_{\mu *}^2$ at $q^2 = 0$ by means of α and G_μ, and s_*^2 at the Z-boson mass scale by means of the pole of the Z^0 propagator. In order to cure the problem $\Sigma_{\gamma Z}(0) \neq 0$ in the bosonic sector, a rediagonalization of the neutral current sector in the one-loop lagrangian is performed including in the self-energies the contribution of the universal and gauge dependent parts of the vertex corrections.

Besides the calculational schemes described above, one should also mention the *Z-peak subtracted* representation of $e^+e^- \to f\bar{f}$ processes at one loop, recently suggested in [75]. In this approach, the input parameter G_μ is replaced by quantities measured on top of the Z^0 resonance. For instance, for leptonic final states the new input parameters are the leptonic Z-boson width Γ_l and the effective sine $\sin^2 \vartheta^l_{eff}$, that reabsorb the bulk of loop effects, while the residual one-loop corrections are contained in quantities subtracted at $Q^2 = M_Z^2$. This approach has been proved to be particularly powerful for the description of e^+e^- annihilations above the Z^0 peak, especially if an investigation of models of new physics is the final goal.

3˙2.3. Transition amplitudes and effective couplings. The basic ingredients of loop calculations described in the previous subsections can be used to evaluate transition amplitudes for the physical process $e^+e^- \to f\bar{f}$. Before discussing the radiative corrected amplitude, it is worth recalling the general structure of the tree-level amplitude which, excluding for simplicity the case of Bhabha scattering, reads [76]:

$$\mathcal{M} \sim \frac{1}{s}\left[Q_e Q_f \gamma_\alpha \otimes \gamma^\alpha + \chi \gamma_\alpha (g_v^e - g_a^e \gamma_5) \otimes \gamma^\alpha (g_v^f - g_a^f \gamma_5))\right], \tag{67}$$

where χ is the propagator ratio

$$\chi = \frac{s}{s - M_Z^2 + i\Gamma_Z(s) M_Z}, \tag{68}$$

and the symbol $\Gamma_\alpha \otimes \Gamma^\alpha$ means product of spinorial currents. The s-dependent width $\Gamma_Z(s) \simeq s\Gamma_Z/M_Z^2$ appearing in eq. (68) is due to the imaginary part of the Z self energy. In eq. (67), the photon and the Z-boson exchange diagrams are well separated and moreover the Z^0 contribution is written in a factorized form. By virtue of these two properties, simple relations between the pseudo-observables defined in Sect. **3**˙1 and the measured quantities can be established.

However the two features are lost when the electroweak non-photonic corrections (self-energy diagrams, $Zf\bar{f}$ vertex insertions and weak boxes) are considered. In this case the matrix element can be written in the following way:

$$\begin{aligned}\mathcal{M} \sim \frac{1}{s}\big[&\alpha(s)\gamma_\alpha \otimes \gamma^\alpha + \chi\left(F_{vv}^{ef}(s,t)\gamma_\alpha \otimes \gamma^\alpha - F_{va}^{ef}(s,t)\gamma_\alpha \otimes \gamma^\alpha \gamma_5\right.\\ &\left. - F_{av}^{ef}(s,t)\gamma_\alpha\gamma_5 \otimes \gamma^\alpha + F_{aa}^{ef}(s,t)\gamma_\alpha\gamma_5 \otimes \gamma^\alpha\gamma_5\right)\big],\end{aligned} \tag{69}$$

where $\alpha(s)$ is the QED running coupling constant with only fermionic contributions (in order to have a gauge invariant term) and the form factors F_{ij}^{ef} are complex valued functions of the input parameters and of the kinematical variables s and t. Usually the self-energies contributions are resummed in their fermionic component to take into account large higher-order reducible diagrams. The bosonic parts are instead expanded at $\mathcal{O}(\alpha)$, in order to preserve gauge invariance. The dependence of the form factors on t is only due to the presence of box diagrams. Being non-resonant at the Z^0 peak, their numerical effects are very small and can be neglected, even if from a theoretical point

of view the gauge invariance is no more respected. Other non-resonating contributions, such as the bosonic insertions to the photon propagator and photon-fermion vertex corrections, can be safely neglected. Another commonly used approximation is the Z^0 pole approximation, which means to fix the scale in the form factors at the value M_Z^2, since the weak corrections depend very mildly on the scale around the Z^0 peak. After these approximations the factorization of the Z^0 contribution is re-established and the form factors take on the form:

$$F_{ij}^{ef}(M_Z^2) = G_i^e(M_Z^2)G_j^f(M_Z^2). \tag{70}$$

This means that the Z-boson part of the corrected amplitude can be obtained from the tree-level expression by replacing the vector and axial vector couplings with the corrected versions defined above by eq. (70). The imaginary parts of the couplings $G_i^f(M_Z^2)$ are generally small with respect to the real parts, so that the following effective couplings are commonly introduced:

$$g_{V,A}^f = \mathrm{Re}G_{v,a}^f(M_Z^2). \tag{71}$$

As already noticed in Sect. **3**˙1, the decay width of the Z^0 boson into a $f\bar{f}$ pair is given by the following expression in terms of the effective couplings:

$$\Gamma_f = 4N_c\Gamma_0[(g_V^f)^2R_V^f + (g_A^f)^2R_A^f]. \tag{72}$$

In the literature other sets of parameters replacing the effective couplings are present. For example according to ref. [66] the parameters ρ_f and k_f are introduced related to g_V^f and g_A^f by the following relations:

$$\rho_f = 4(g_A^f)^2 \tag{73}$$

$$\frac{g_V^f}{g_A^f} = 1 - 4|Q_f|s_W^2k_f, \tag{74}$$

with

$$\rho_f = 1 + \delta\rho_f, \tag{75}$$

$$k_f = 1 + \delta k_f. \tag{76}$$

By means of these parameters, the Z^0 partial widths can be written in the following way (neglecting for simplicity final-state QED and QCD interactions and mass effects):

$$\Gamma_f = \Gamma_0 N_c^f \rho_f[4(I_f^3 - 2Q_f s_W^2 k_f)^2 + 1]. \tag{77}$$

The above described procedure of step-by-step approximations, leading from the exact one-loop amplitude to an approximate amplitude formally identical, or very similar, to the Born-approximation one, but written in terms of form factors evaluated at the Z^0 peak, is known as Improved Born Approximation (IBA). Some different realizations of IBA's are available in the literature, and can be found for instance in [66, 77, 78].

3˙2.4. Higher-order electroweak corrections. Given the high precision reached in the experimental measurements, particular attention must be paid to include in the electroweak corrections potentially large higher-order effects. These generally originate

from terms containing logarithms of the type $\ln(M_Z/m_f)$, where m_f stand for a generic fermion mass, or from contributions proportional to the *top*-quark mass. In Sect. **3**·2.2 the prescription based on renormalization group arguments [68, 79]

$$1 + \Delta r \to \frac{1}{1 - \Delta r} \tag{78}$$

has been introduced to include to all orders the leading logarithms of $\mathcal{O}(\alpha^n \ln^n(M_Z/m_f))$, contained in $\Delta\alpha$ of eq. (55), giving the interdependence between M_W, M_Z and G_μ. However, with this prescription the powers $(\Delta\rho)^n$ are not correctly resummed. In ref. [80] it has been shown how to take into account in the on-shell scheme the leading two-loop contributions proportional to m_t^4 by means of the replacement

$$\frac{1}{1 - \Delta r} \to \frac{1}{1 - \Delta\alpha} \cdot \frac{1}{1 + \frac{c_W^2}{s_W^2}\Delta\bar{\rho}} + \Delta r_{rem}, \tag{79}$$

where $\Delta\bar{\rho}$ includes the contribution of two-loop one particle irreducible diagrams:

$$\Delta\bar{\rho} = 3x_t \left[1 + x_t \rho^{(2)} \left(\frac{m_H}{m_t}\right)\right], \quad x_t = \frac{G_\mu m_t^2}{8\pi^2\sqrt{2}}. \tag{80}$$

The two-loop correction $\rho^{(2)}$ was first calculated in ref. [81] in the limit of light Higgs-boson mass $m_H << m_t$, yielding $\rho^{(2)} = 19 - 2\pi^2$. More recently the calculation has been carried out by several groups [82–84] for arbitrary values of the ratio m_H/m_t in the limit of vanishing gauge coupling constants. In ref. [68] it has been shown that the fermionic mass singularities of $\mathcal{O}(\alpha^2 \ln(M_Z/m_f))$ are correctly taken into account by keeping Δr_{rem} in the denominator, *i.e.*

$$\frac{1}{1 - \Delta r} \to \frac{1}{(1 - \Delta\alpha)\left(1 + \frac{c_W^2}{s_W^2}\Delta\bar{\rho}\right) - \Delta r_{rem}}. \tag{81}$$

The effects of two-loop heavy Higgs-boson contributions have been investigated in refs. [85] and [86].

Very recently the two-loop sub-leading corrections of $\mathcal{O}(\alpha^2 m_t^2/M_W^2)$ have been calculated for the vector-boson masses correlation [87–89], and found to be potentially of the order of the leading m_t^4 contributions, depending on the Higgs-boson mass. Moreover, the exact two-loop Higgs-boson mass dependence has also become available [90], introducing a shift in the W-boson mass contained within 4 MeV [91] with respect to the calculation of ref. [88, 89].

Another place where higher-order electroweak effects play an important rôle is the partial width $Z \to f\bar{f}$. The effective couplings contain leading universal parts, arising from self-energies and counter-terms, and flavour-dependent parts coming from vertex corrections. The leading universal contributions are given by [76]

$$(\delta\rho_f)_{univ} = \Delta\rho + \ldots, \tag{82}$$

$$(\delta k_f)_{univ} = \frac{c_W^2}{s_W^2}\Delta\rho + \ldots. \tag{83}$$

The higher-order terms can be incorporated by means of the following replacements:

$$\rho_f \to \frac{1}{1 - \Delta\bar{\rho}} + \ldots \tag{84}$$

$$k_f \to 1 + \frac{c_W^2}{s_W^2}\Delta\bar{\rho} + \ldots, \tag{85}$$

with $\Delta\bar{\rho}$ given by eq. (80).

The partial decay width $Z \to b\bar{b}$ contains an additional m_t dependence due to vertex diagrams with virtual *top*-quark lines, resulting in additional leading terms of the order $G_\mu m_t^2$ for the effective couplings ρ_b and k_b. The additional leading two-loop electroweak effects of the order $G_\mu^2 m_t^4$ have been computed in refs. [82] and [83], and amount to the following redefinition of the effective couplings:

$$\rho_b \to \rho_b(1+\tau_b)^2, \tag{86}$$

$$k_b \to \frac{k_b}{1+\tau_b}, \tag{87}$$

where τ_b is given by

$$\tau_b = -2x_t\left[1 + x_t\tau^2\left(\frac{m_t^2}{m_H^2}\right)\right], \tag{88}$$

where $\tau^2(m_t^2/m_H^2)$ can be found in [82, 83].

At the level of two-loop or higher-order corrections, other phenomenologically relevant contributions come from the mixed electroweak-QCD corrections, discussed in the next Section.

3˙3. *QCD Corrections.* – QCD corrections play a significant rôle as higher-order corrections due to virtual gluon insertions in electroweak loops (mixed electroweak-QCD corrections) and as final-state corrections in the hadronic decay channels. With the exception of very recent improvements, an account of perturbative QCD calculations for the Z-boson observables can be found in [14] and [92].

3˙3.1. Mixed electroweak-QCD corrections. The need of very accurate predictions demanded by the high precision of the measurements on the Z^0 peak, motivated various authors to perform calculations of higher-order effects beyond the one-loop and higher-order electroweak corrections already discussed in Sect. **3**˙2. Great effort was spent in the calculation of corrections due to the insertion of virtual gluons in the electroweak quark loops, known as *mixed electroweak-QCD corrections*, giving rise to contributions simultaneously depending on the weak coupling G_μ and the coupling of the strong interaction α_s. Higher-order corrections of this kind have been calculated both for W- and Z-boson self-energies, thus affecting all $Z \to f\bar{f}$ decay channels, and specifically for the peculiar $Z \to b\bar{b}$ vertex.

QCD corrections to the gauge-bosons self-energies have been computed in the SM considering the insertion of one and two gluons into the internal quark loops. Typical Feynman diagrams contributing to these corrections are depicted in Fig. 16.

Fig. 16. – Example of Feynman diagrams for QCD corrections to gauge-bosons self-energies.

The diagrams involving the exchange of a single gluon, described for instance by the first graph in Fig. 16, give rise to two-loop corrections of the order of $\alpha\alpha_s$, that are now

exactly known [93] and are dominated by terms of order $G_\mu \alpha_s m_t^2$. The insertion of two virtual gluons, of the kind depicted in the second graph of Fig. 16, generates a three-loop contribution of the order of $\alpha\alpha_s^2$, that is partially under control and introduces effects of the form $G_\mu \alpha_s^2 m_t^2$ [94]. In formulae, the effect of such corrections to the $\Delta\rho$ factor introduced in Sect. **3**˙2 can be cast, in the heavy *top*-quark limit, as follows

$$\Delta\rho \to \Delta\rho \cdot (1 + \delta\rho_{QCD}) \tag{89}$$

where $\delta\rho_{QCD}$ is the QCD correction to the leading $G_\mu m_t^2$ term

$$\delta\rho_{QCD} \;=\; -2.86 a_s - 14.6 a_s^2, \qquad a_s = \frac{\alpha_s(m_t)}{\pi}\,, \tag{90}$$

the running coupling constant α_s being evaluated at the energy scale given by the *top*-quark mass. It is worth noticing that the QCD correction to the ρ parameter is negative, and tends to screen the electroweak contribution.([2])

A second source of higher-order mixed effects comes from QCD corrections to the $Z \to b\bar{b}$ electroweak vertex once corrected by the one-loop contributions depicted in Fig. 14 (see Sect. **3**˙2). Due to the presence of virtual *top*-quark lines in the one-loop $b\bar{b}$ vertex, significant non-universal mixed corrections, depending on α_s and m_t, are additionally present for the $b\bar{b}$ final state. The effects induced by $\mathcal{O}(\alpha_s)$ gluon radiation introduce two-loop corrections to the leading electroweak term of the order of $G_\mu \alpha_s m_t^2$ [96] and to the $\ln(m_t/M_W)$ term of the order of $G_\mu \alpha_s \ln(m_t/M_W)$, the latter with a very small numerical coefficient [97]. The missing next-to-leading corrections of $\mathcal{O}(\alpha\alpha_s)$ to the partial width Γ_b have been very recently calculated [98], thus improving the SM prediction for the $Z \to b\bar{b}$ vertex.

Finally, final-state mixed corrections to the $Z \to q\bar{q}$ decay channels, due to the interplay between QED and QCD radiation off final-state quarks, are exactly available [99] and taken into account in the theoretical predictions. For example, the Z^0 decay width into $q\bar{q}$ final states receives a contribution from these mixed corrections given by the factor

$$\delta^{fs}_{\alpha\alpha_s} \;=\; Q_f^2 \frac{3}{4} \frac{\alpha(s)}{\pi} \left[1 - \frac{1}{3}\frac{\alpha_s(s)}{\pi}\right] \quad \text{with } s = M_Z^2\,, \tag{91}$$

that can be easily deduced from the QCD results for the $Z \to q\bar{q}$ decay width, discussed in the next Section.

3˙3.2. Final-state QCD corrections. In addition to the classes of radiative corrections discussed in the two previous Sections, an adequate theoretical description of the processes explored at LEP requires, as a further basic ingredient, the inclusion of the QCD corrections to the $Z \to q\bar{q}$ decay channels, arising from the emission of real and virtual gluons off the final-state quarks (see Fig. 17). Among the observables measured at the Z^0 peak, these corrections affect the total hadronic cross section $\sigma_{\rm had}$, the FB asymmetry of heavy-quark ($q = c, b$) production $A_{FB}^{c,b}$, as well as the total hadronic width Γ_h and the partial widths into c and b quarks $\Gamma_{c,b}$. When discussing final-state QCD effects in hadronic Z-boson decays, it is necessary to distinguish between corrections to the production of light, or massless, quarks and corrections to the heavy-quark production.

([2]) The SUSY-QCD corrections to $\Delta\rho$ have been recently computed; they could introduce a shift of the order of 10 MeV on the W-boson mass [95].

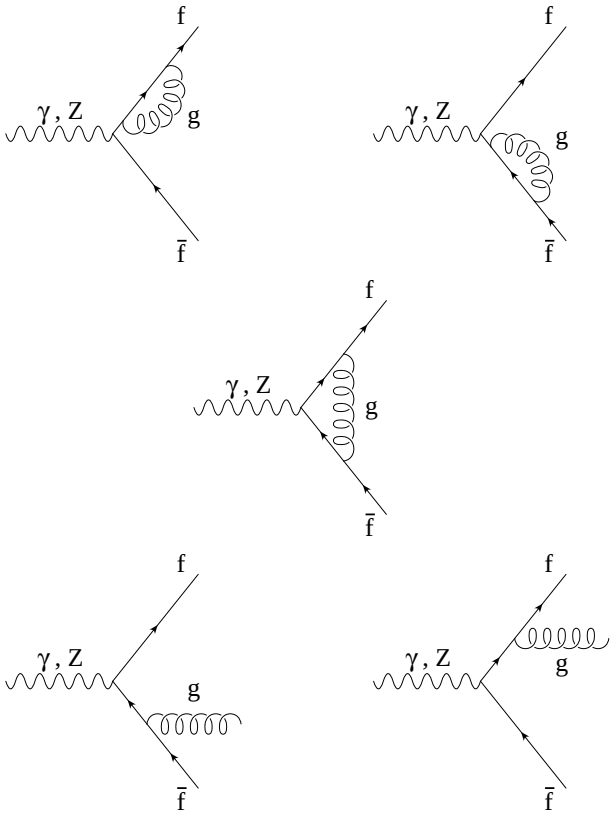

Fig. 17. – Feynman diagrams for final-state $\mathcal{O}(\alpha_s)$ QCD corrections.

In the case of light quarks ($q = u, d, s$) with $m_q \simeq 0$, the QCD final-state correction to the cross section (or, equivalently, to the partial decay width) is completely known up to $\mathcal{O}(\alpha_s^3)$. This high perturbative accuracy is of course of the utmost importance in view of a precise determination of the strong coupling constant in Z-boson decays, as it will be shown in the following. The result for the Z^0 partial widths into massless quarks can be written as

$$\Gamma = \Gamma_0 \left[(g_V^f)^2 + (g_A^f)^2 \right] K_{QCD} \tag{92}$$

with

$$\Gamma_0 = N_C^f \frac{G_\mu M_Z^3 \sqrt{2}}{12\pi} \quad (N_C^f = \text{colour factor}) , \tag{93}$$

g_V^f and g_A^f being the *effective* electroweak couplings. K_{QCD} is the up to three-loop correction factor for massless quarks given by [100, 101]

$$K_{QCD} = 1 + \frac{\alpha_s}{\pi} + 1.41 \left(\frac{\alpha_s}{\pi}\right)^2 - 12.8 \left(\frac{\alpha_s}{\pi}\right)^3 . \tag{94}$$

Actually, leading and next-to-leading second-order *top*-quark mass corrections to the $q\bar{q}$ decay width in the massless limit are also available in the literature [102] and are taken

into account in the more refined (but too lengthy to be shown here) QCD radiation factors usually implemented in standard computational tools for LEP1 physics. The complete expressions, together with a discussion of the numerical effects of the various contributions, can be found in the recent review paper of ref. [92].

For massive quarks the situation is different, due to the presence of finite mass terms. In such a case, the vector and axial-vector contribution to the Z-boson decay width receive different corrections, known at different perturbative orders. Actually, the calculation of the axial-vector part of the hadronic Z-boson decay rate is more involved than that of the vector part. This is because the heavy quark does not decouple in the axial-vector part and hence one cannot avoid calculating massive diagrams. In particular, the $b\bar{b}$ final state receives peculiar contributions from *top*-quark dependent two-loop diagrams in the axial-vector part. Consequently, the formula of eq. (92) in the massless limit needs to be integrated with additional correction factors for massive quarks, of the form

$$\Gamma = \Gamma_0 \left[(g_V^{c,b})^2 R_V + (g_A^{c,b})^2 R_A \right]. \tag{95}$$

The coefficients in the perturbative expansions

$$R_V = c_V^1 \frac{\alpha_s}{\pi} + c_V^2 \left(\frac{\alpha_s}{\pi}\right)^2 + c_V^3 \left(\frac{\alpha_s}{\pi}\right)^3 + \ldots, \tag{96}$$

$$R_A = c_A^1 \frac{\alpha_s}{\pi} + c_A^2 \left(\frac{\alpha_s}{\pi}\right)^2 + \ldots, \tag{97}$$

depending on the heavy-quark masses and m_t, are calculated up to third order in the vector part and up to second order in the axial-vector part [92, 103–105]. Given the above formulae for the quark partial widths in the massless limit and massive case, the total hadronic width and cross section can be obtained as the sum over the partial contributions of each $q\bar{q}$ channel.

Recently, the non-factorizable part of the two-loop $\mathcal{O}(\alpha\alpha_s)$ correction to the hadronic Z-boson width has been calculated, introducing an extra negative contribution of about -0.6 MeV [106].

Concerning the forward-backward asymmetry for heavy quarks, the QCD corrections to A_{FB} are available in the literature [107]. At the order α_s, they yield a correction of the kind

$$A_{FB} \to A_{FB} \left(1 - k\frac{\alpha_s}{\pi}\right) \tag{98}$$

where k depends on the mass of the heavy quark, and its explicit expression can be found in [108].

Last, a few comments are in order. First, since the above QCD factors depend on the perturbative expansion parameter α_s and the latter depends on the energy scale according to the renormalization group equation for the β function, a formula for the *running* of α_s needs to be specified. Indicating with μ the renormalization scale and with n_f the number of active quark flavours of mass $m_q \ll \mu$, the solution for $\alpha_s^{(n_f)}(\mu)$ typically used reads [92, 104]

$$\alpha_s(\mu) = \frac{\pi}{\beta_0 L} \left\{ 1 - \frac{1}{\beta_0 L} \frac{\beta_1 \ln L}{\beta_0} + \frac{1}{\beta_0^2 L^2} \left[\frac{\beta_1^2}{\beta_0^2} \left(\ln^2 L - \ln L - 1 \right) + \frac{\beta_2}{\beta_0} \right] \right\}, \tag{99}$$

with

$$\beta_0 = \left(11 - \frac{2}{3}n_f\right)/4\,, \qquad \beta_1 = \left(102 - \frac{38}{3}n_f\right)/16\,,$$
$$\beta_2 = \left(\frac{2857}{2} - \frac{5033}{18}n_f + \frac{325}{54}n_f^2\right)/64\,. \tag{100}$$

In the above formulae $L = \ln(\mu^2/\Lambda^2_{\overline{MS}})$. Actually eq. (99), together with the coefficients of eq. (100), is valid in the modified minimal subtraction ($\overline{MS}$) scheme and corresponds to the three-loop expansion of the QCD β function. It is used with $n_f = 5$ for the number of active flavours and it is technically called next-next-to-leading solution of $\alpha_s(\mu)$. At present, also the four-loop coefficient in the $\overline{MS}$ scheme is available [109], thanks to the recent calculation of the coefficient β_3 of the QCD β function [110]. A second comment concerns the mass correction terms entering the QCD factors for heavy-quarks. Analogously to the coupling constant, the quark masses are running parameters in QCD and obey the renormalization group equation controlled by the anomalous dimension γ_m, that is known up to three-loop accuracy. The masses appearing in the formulae for c- and b-quark production have thus to be understood as running (μ dependent) quark masses. The relations used to account for such effect read as follows [14]:

$$\overline{m}(\mu) = \overline{m}(m^2)\exp\left\{-\int_{\alpha_s(m^2)}^{\alpha_s(\mu)} dx\frac{\gamma_m(x)}{\beta(x)}\right\},$$
$$m_q = \overline{m}_q(m_q^2)\left\{1 + \frac{4}{3}\frac{\alpha_s(m_q)}{\pi} + K_q\frac{\alpha_s^2(m_q)}{\pi} + \mathcal{O}(\alpha_s^3)\right\}, \tag{101}$$

where m_q is the so-called *pole* mass (defined in quantum field theory as the position of pole of a renormalized quark propagator), $\overline{m_q}$ is the $\overline{MS}$ running mass and $K_{c,b} = 13.3, 12.4$. Notice that the running mass depends on α_s. Using, for instance, for the b-quark pole mass $m_b = (4.7 \pm 0.2)$ GeV and $\alpha_s(M_Z) = 0.12$, one obtains a running mass at the Z^0 peak of $\overline{m}_b(M_Z) \simeq 2.8$ GeV, leaving non-negligible mass effects. The running c-quark mass $\overline{m}_c$ is about a factor of five smaller than $\overline{m}_b$, thus making c-quark mass corrections almost invisible in the Z-boson decays [92].

Before turning to QED corrections, it is worth quantifying the effect of the electroweak and QCD corrections discussed up to now. To this aim, Fig. 18 shows the comparison between the total cross section and the forward-backward asymmetry for the process $e^+e^- \to \mu^+\mu^-$ at the tree level (dashed line) and the full prediction including all the one-loop and the relevant higher-order electroweak and QCD corrections (solid line). In Fig. 19 relative deviations for the cross section and absolute deviations for the asymmetry are shown. The dotted lines represent the difference between strictly tree-level predictions and "tree-level like" results, obtained by running the QED coupling constant (and hence $\sin^2\vartheta_W$) and including final-state QED and QCD corrections in the total Z-boson width in the propagator. The dashed lines represent the deviations of the last prediction from a full electroweak/QCD calculation. The full electroweak/QCD results have been produced by means of `TOPAZ0` in its default mode, neglecting theoretical uncertainties (see Sect. **3**·6). As can be seen from the figures, the bulk of the corrections is due to the running of the QED coupling constant and to final-state QCD corrections to the Z-boson width. However, there is an effect of $0.5 \div 1\%$ on the cross section and up to 0.002 on the asymmetry due to non-trivial corrections as computed by means of a full electroweak/QCD calculation.

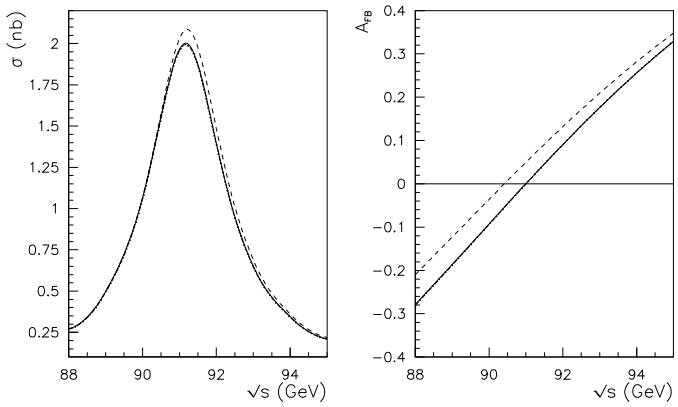

Fig. 18. – Comparison between the cross section and the forward-backward asymmetry for $e^+e^- \to \mu^+\mu^-$, as computed in the Born approximation (dashed line) and including all the one-loop and the relevant higher-order electroweak and QCD corrections (solid line). Numerical results for this last case by `TOPAZ0` [111].

3˙4. *QED Corrections.* – As already said in Sect. **2**˙3, QED corrections originate from those diagrams with extra real and/or virtual photons added to the tree-level graphs (see Figs. 22, 23 and 24 below). Although these corrections are not particularly interesting with respect to the underlying theory, they need a special attention at LEP, as at any other e^+e^- collider, because the size of their effects strongly depends on the experimental cuts, and therefore their proper treatment constitutes the unavoidable link between the data taking and the physics analysis [43]. In fact, they are large corrections at high energies because, as already explained in Sect. **2**˙3, they are dominated by logarithmic contributions of the kind $(\alpha/\pi)L$, $L = \ln(s/m_e^2)$ being the so-called *collinear logarithm*. At LEP1, where $s \simeq M_Z^2$, L is of the order of 25, and the *effective* expansion parameter in perturbation theory is $\beta = 2\alpha(L-1)/\pi \simeq 0.1$ rather than α. The Breit-Wigner line-shape of the Z^0 resonance in Born approximation is sensibly modified by the QED corrections for the following typical effects [112, 113]:

- the peak height is lowered by around 25%;
- the peak position is shifted towards higher energies by around 100 MeV;
- a hard radiative tail, that increases the lowest-order cross section, appears above, say, 93 GeV.

The significant distortion introduced by the QED corrections on the Z^0 line-shape of the process $e^+e^- \to$ hadrons can be clearly seen in Fig. 20.

Also the forward-backward asymmetry, A_{FB}, which crosses the zero in the proximity of M_Z, is significantly affected by the QED corrections, that shift the position of its zero and globally change its shape [114, 115]. The QED effects on A_{FB} for the reaction $e^+e^- \to \mu^+\mu^-$ are illustrated in Fig. 21.

The whole set of QED corrections to s-channel e^+e^- annihilations can be divided into three subsets, each separately gauge-invariant:

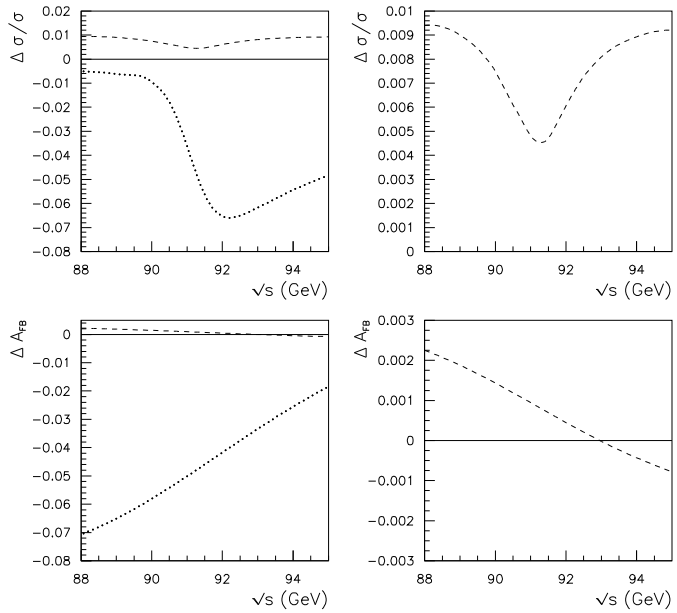

Fig. 19. – The left windows show the bulk of electroweak/QCD corrections as obtained by means of a "tree-level like" calculation (dotted line) and the residual effect of a complete electroweak/QCD calculation (dashed line). The right windows show a blow-up of this last difference. Numerical results for the full electroweak/QCD prediction by TOPAZ0 [111].

- initial-state corrections;
- final-state corrections;
- initial-final state interference.

The initial-state corrections are by far the dominant ones, because, at a difference from final-state and initial-final state interference contributions, they are responsible for a reduction of the c.m. energy available for the hard-scattering reaction.

3˙4.1. Initial-state radiation. The Feynman diagrams for $\mathcal{O}(\alpha)$ initial-state QED corrections to a generic s-channel process $e^+e^- \to \gamma, Z^0 \to f\bar{f}$ are depicted in Fig. 22.

Since at LEP1 energies the electron-positron collision takes place at energies very close to the Z-boson mass, M_Z, the radiation emitted by the initial-state (ISR) is essentially radiation of soft photons. This remarkable property is a direct consequence of the fact that the maximum energy of the photons emitted by the initial-state can not exceed the ratio $\varepsilon_{max} = \Gamma_Z/M_Z$, with $\varepsilon_{max} \simeq 0.03$. In fact, the finite Z-boson width, Γ_Z, acts as a natural cut-off that strongly inhibits the emission of those hard photons, of energy fraction larger than ε_{max}, that would prevent the formation of the Z^0 resonance. This soft-photon dominance at the Z^0 peak is a very useful guideline when facing the

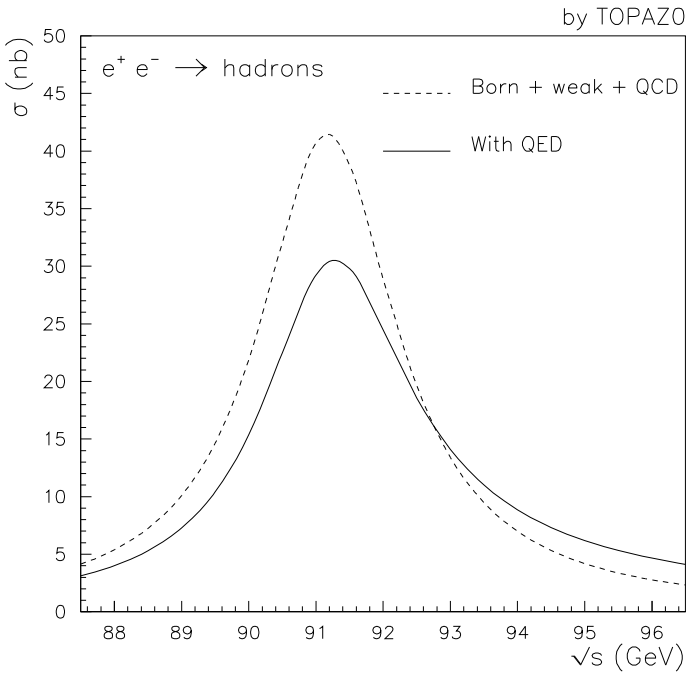

Fig. 20. – The effect of QED corrections on the Z^0 line-shape of $e^+e^- \to$ hadrons. The dashed line is the QED-deconvoluted cross section, the solid line is the QED corrected one. Numerical results by `TOPAZ0` [111].

problem of including finite order perturbative corrections, beyond the leading logarithmic (LL) approximation, that are actually demanded by the high-precision level of the LEP1 measurements.

As recalled in Sect. **2**˙3, the n-th order contribution to a QED corrected cross section $\sigma^{(n)}$ can be cast in the form

$$\sigma^{(n)} = \left(\frac{\alpha}{\pi}\right)^n \sum_{k=0}^{n} a_k^{(n)} \mathcal{L}^k, \tag{102}$$

where $\mathcal{L} = \mathcal{L}(s) = L - 1$. The coefficients $a_k^{(n)}$ in eq. (102) are given by the following expression

$$a_k^{(n)} = \sum_{j=0}^{k} b_{kj} l^j, \tag{103}$$

where l is the so called IR logarithm given by $l = \ln(E/\Delta E)$, ΔE being the maximum energy of the emitted photons. This general expansion obviously applies to the IS QED corrected cross section. For example, the up to $\mathcal{O}(\alpha)$ cross section in the soft-photon

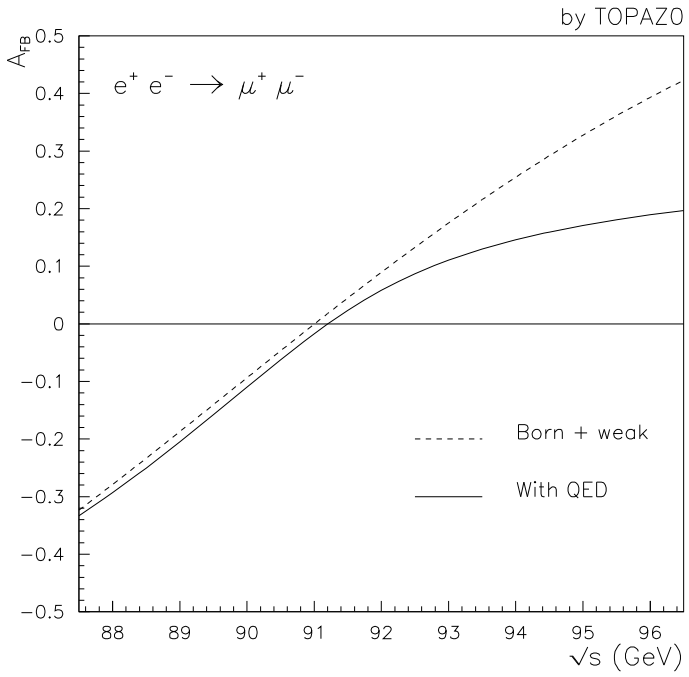

Fig. 21. – The effect of QED corrections on the forward-backward asymmetry A_{FB} of $e^+e^- \to \mu^+\mu^-$ around the Z^0 peak. The dashed line is the QED-deconvoluted asymmetry, the solid line is the QED corrected one. Numerical results by `TOPAZ0` [111].

approximation, as obtained by standard diagrammatic techniques, reads

$$\sigma^{(\alpha)}(s) = \sigma_0(s)\left\{1 + \frac{\alpha}{\pi}\left[-2l(L-1) + \frac{3}{2}L + \frac{\pi^2}{3} - 2\right]\right\}, \tag{104}$$

which shows a large $\mathcal{O}(\alpha)$ negative correction, clearly indicating that higher-order QED corrections are required for a high-precision reconstruction of the Z^0 line-shape. These higher-order effects are kept under control at all orders by employing one of the approaches described in Appendix A. For instance, in the structure function (SF) approach the LL-corrected cross section, in the extrapolated set-up, can be written as

$$\sigma(s) = \int_0^{\Delta E/E} dx H(x,s)\sigma_0\left((1-x)s\right), \tag{105}$$

$H(x,s)$ being the QED *radiator* of eq. (186), and $\sigma_0(s)$ being the lowest order cross section, possibly including all the short-distance process dependent corrections, as the electroweak and QCD ones previously discussed. This allows to exactly reproduce the LL content of eq. (102) at any order and, in particular, that of eq. (104) at $\mathcal{O}(\alpha)$ (see the series expansion in the LL approximation given by eq. (12) in Sect. **2**˙3). The sub-leading terms present in eq. (104) are not naturally reproduced by the perturbative expansion

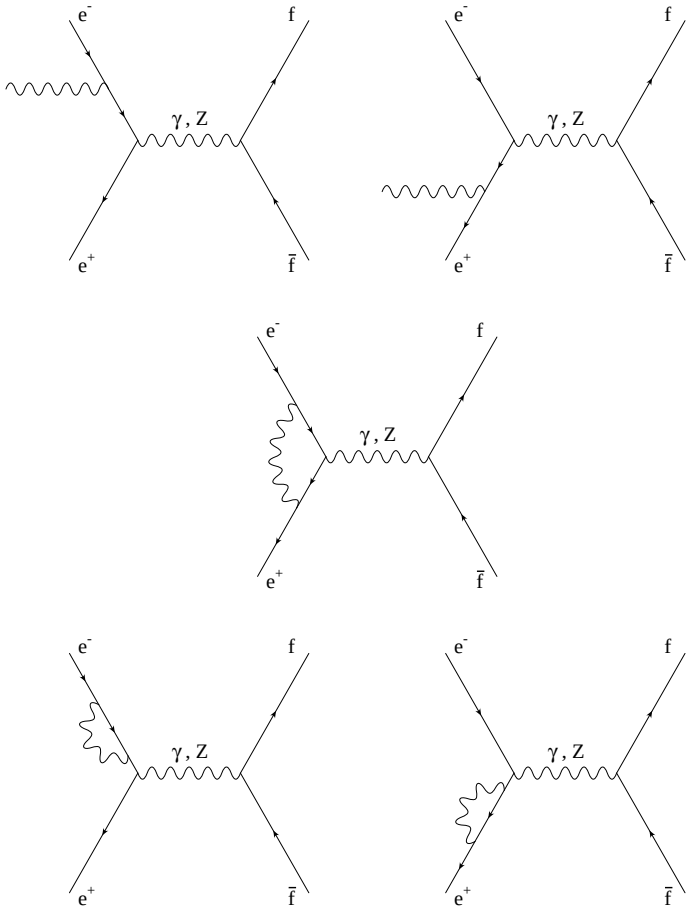

Fig. 22. – The Feynman diagrams for $\mathcal{O}(\alpha)$ initial-state QED corrections to s-channel process $e^+e^- \to \gamma, Z^0 \to f\bar{f}$.

of the cross section obtained via the algorithms for the calculation of universal photonic corrections. It is worth noting that they are numerically important for a description of the Z^0 line-shape with a theoretical accuracy at the 0.1% level. For this reason, they are usually incorporated in the algorithms for the resummation of LL corrections, by means of a proper matching with the perturbative diagrammatic results. For instance, in the SF approach, a standard procedure consists in replacing the Gribov-Lipatov form factor in front of the exponentiated term of the SF's $(\beta/2)\,(1-x)^{\frac{\beta}{2}-1}$ by means of a soft+virtual K-factor Δ'_{S+V} given, up to the first order in α, by

$$\Delta'_{S+V}(s) = 1 + \frac{\alpha}{2\pi}\left[\frac{3}{2}L + \frac{\pi^2}{3} - 2\right], \tag{106}$$

in such a way that the up to $\mathcal{O}(\alpha)$ cross section of eq. (104) is exactly reproduced. By virtue of the soft-photon dominance in the ISR mechanism previously discussed, the hard-photon non-leading contributions, left-over in the above derivation, turn out

to be numerically unimportant at LEP1. For the applications to precision physics at the Z^0 peak, the inclusion of sub-leading terms in the SF approach is pushed up to $\mathcal{O}(\alpha^2)$ [112], relying upon the exact second-order calculation of initial-state QED corrections to s-channel processes available in the literature [41,116,117]. By exploiting again the soft-photon dominance, one can extract from the second-order complete calculation the soft+virtual contributions only, so that the up to $\mathcal{O}(\alpha^2)$ K-factor, to be placed in front of the electron SF, can be cast in the form

$$\Delta'_{S+V}(s) = 1 + \Delta^{'(\alpha)}_{S+V}(s) + \Delta^{'(\alpha^2)}_{S+V}(s) \tag{107}$$

and is calculable through the relation

$$\Delta_{S+V}(s) = \left(\Delta'_{S+V}(s)\right)^2 - \frac{\pi^2}{24}\beta^2. \tag{108}$$

The quantity $\Delta_{S+V}(s)$ contains the non-leading non-IR sensitive diagrammatic corrections to the cross section corrected by the inclusion of soft+virtual photons up to $\mathcal{O}(\alpha^2)$, analogous to the one shown in eq. (104). Equation (108), that relates $\Delta_{S+V}(s)$ and $\Delta'_{S+V}(s)$, can be derived from the explicit integration of eq. (172) in Appendix A in the soft-photon approximation. By inspection, $\Delta_{S+V}(s)$ is given by

$$\Delta_{S+V}(s) = 1 + \left(\frac{\alpha}{\pi}\right)\Delta^{(\alpha)}_{S+V}(s) + \left(\frac{\alpha}{\pi}\right)^2\Delta^{(\alpha^2)}_{S+V}(s), \tag{109}$$

where the perturbative corrections $\Delta^{(\alpha)}_{S+V}(s)$ and $\Delta^{(\alpha^2)}_{S+V}(s)$ are explicitly given by

$$\begin{aligned}
\Delta^{(\alpha)}_{S+V}(s) &= \frac{3}{2}L + \frac{\pi^2}{3} - 2, \\
\Delta^{(\alpha^2)}_{S+V}(s) &= \left(\frac{9}{8} - \frac{\pi^2}{3}\right)L^2 + \left[-\frac{45}{16} + \frac{11}{12}\pi^2 + 3\,\zeta(3)\right]L + \text{constant terms}.
\end{aligned} \tag{110}$$

In eq. (110) ζ is the Riemann function, with $\zeta(3) \simeq 1.202$. With respect to the exact second-order calculation, $\mathcal{O}(\alpha^2)$ sub-leading non-soft corrections are neglected, but they are negligible in the resonance region, their contribution to the cross section being at the level of 0.01% [113, 118–120]. The above described procedure for matching LL results with exact finite-order calculations is valid in the soft-photon approximation. It is worth noticing, however, that a general prescription is also known, valid for any ES, *i.e.* taking into account also hard-photon contributions, as can be found in [23].

A complete treatment of IS $\mathcal{O}(\alpha^2)$ QED effects to the Z^0 line-shape requires, as a last ingredient, the inclusion of the corrections arising from the conversion of a photon into leptonic pairs and/or hadrons (pair corrections). These contributions, which are dominated by e^+e^- pairs, can be included using the $\mathcal{O}(\alpha^2)$ formulae available in the literature [121]. Their main effect is a reduction of the peak cross section of around 0.3%, hence significant in the light of the remarkable experimental precision of the LEP1 data.

Equation (105) allows to understand the main effects of ISR on the Z^0 line shape. Actually, since $\Delta E/E$ is of the order of Γ_Z/M_Z around the resonance, the explicit calculation of the integral appearing in eq. (105) in the soft-photon limit leads to the following reduction of the peak height:

$$\frac{\sigma}{\sigma_0} \simeq \left(\frac{\Gamma_Z}{M_Z}\right)^{\beta} \simeq 0.75. \tag{111}$$

On the other hand, eq. (105) is nothing but a weighted average of the lowest-order cross section for c.m. energies smaller than the nominal one, the weight being the radiator H itself. This leads to a shift of the corrected peak position towards higher energies by about 100 MeV, and to the raising of a radiative tail above the resonance (see Fig. 20). It is worth noticing, in particular, that the contribution of soft-photon exponentiation to the shift of the peak position is of the order of 15 MeV, and thus phenomenologically relevant in view of the experimental precision of the determination of the Z-boson mass.

Before concluding the discussion on ISR, it is worth noticing that the analogue of eq. (105) for the corrected forward-backward asymmetry in principle does not apply. Indeed, since A_{FB} is a less inclusive quantity than the total cross section, kinematical effects can show up, thus introducing the need for improving eq. (105). However, at the resonance these effects are negligible due to soft-photon dominance, and anyway they can be naturally taken into account in a more appropriate SF formulation, as described in [122].

3˙4.2. Final-state radiation. The final-state QED corrections, although numerically smaller than the IS ones under many typical experimental conditions, are an essential ingredient for a high-precision phenomenology of the LEP1 processes. They must be included in any formulation of Z^0 physics that aims at a theoretical precision at the level of 0.1%. The Feynman diagrams for $\mathcal{O}(\alpha)$ final-state QED corrections to a generic s-channel process $e^+e^- \to \gamma, Z^0 \to f\bar{f}$ are depicted in Fig. 23.

With respect to the emission of photons by the initial state, the mechanism of bremsstrahlung by the final-state particles is no more characterized by the soft-photon dominance discussed above, simply because the radiation process occurs after the formation of the Z^0 resonance. This implies that the control on final-state QED corrections at the level of sub-leading and constant terms necessarily requires a full perturbative calculation, including hard photon bremsstrahlung. A treatment of FSR completely flexible with respect to *any* kind of ES requires the usage of numerical (Monte Carlo) techniques in order to perform the phase space integrations in the presence of arbitrary cuts. However, when considering particular experimental selection criteria actually adopted by the LEP Collaborations, it is possible to obtain the final-state $\mathcal{O}(\alpha)$ QED correction according to a completely analytical procedure [123,124]. In this case, the final-state corrected cross section can be obtained by calculating the exact matrix element associated to the gauge-invariant set of Feynman diagrams describing final-state real photon radiation in e^+e^- annihilation (see Fig. 23), integrating it over the phase space allowed by cuts and matching the obtained result with the soft+virtual correction. For example, if one assumes that only an invariant mass cut of the type $M^2(f\bar{f}) \geq s_0$ is present, then the above strategy leads to the following analytical correction factors [78,122,124,125]

$$
\begin{aligned}
\delta^{fs}_{F+B} &= \frac{\alpha}{\pi} Q_f^2 \left\{ \left[x + \frac{1}{2} x^2 + 2 \ln(1-x) \right] L_f \right. \\
&\quad + x \left(1 + \frac{1}{2} x \right) \ln x + 2 \ln(1-x) (\ln x - 1) \\
&\quad \left. + 2 \, \mathrm{Li}_2(x) \right\}, \qquad (112) \\
\delta^{fs}_{F-B} &= \frac{\alpha}{\pi} Q_f^2 \left\{ \left[x + \frac{1}{2} x^2 + 2 \ln(1-x) \right] L_f \right. \\
&\quad + 2 \ln(1-x) (\ln x - 1) - 2 x
\end{aligned}
$$

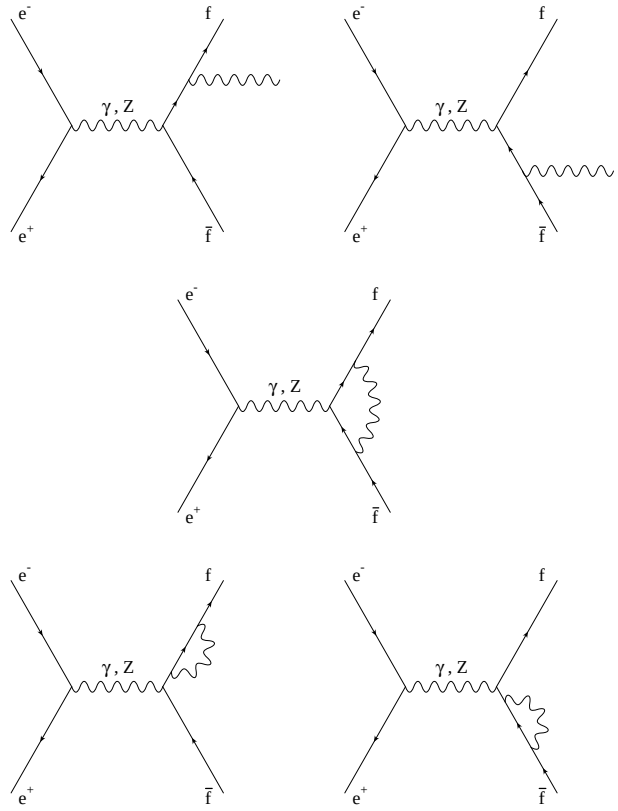

Fig. 23. – The Feynman diagrams for $\mathcal{O}(\alpha)$ final-state QED corrections to s-channel process $e^+e^- \to \gamma, Z^0 \to f\bar{f}$.

$$+ 2\,\mathrm{Li}_2(x)\Big\}, \tag{113}$$

where $L_f = \ln(s/m_f^2)$, $x = s_0/s$ and $(F \pm B)$ denotes the forward $\pm$ backward cross sections defined in eq. (22). In eq. (112) and (113), $\mathrm{Li}_2(x)$ is the dilogarithm function. It is worth observing that when no cuts are applied (*i.e.* in the limit $x \to 0$ in the latter equations) the final-state correction factor for the total cross section reduces to $3\alpha Q_f^2/4\pi$, that is the well-known inclusive final-state correction, while the asymmetry does not get any effect. The very small value (0.17% for fermions with unit charge) of the final-state correction to the fully inclusive cross section is a consequence of the cancellation of mass and collinear singularities established by the Kinoshita-Lee-Nauenberg theorem [20]. Besides an invariant mass cut, also the effect of acollinearity and/or energy threshold cuts can be treated analytically, and the expressions for the corresponding $\mathcal{O}(\alpha)$ correction factors can be found in the literature [124]. The availability of such results in analytical form is of utility for Z^0 physics at LEP1 in order to test Monte Carlo programs and to develop fast computational tools for fitting realistic observables.

Whenever particularly tight cuts are imposed, the treatment of FSR at the $\mathcal{O}(\alpha)$ can become inadequate and a procedure of resummation of the LL contributions needs to be advocated [126]. The leading terms can be quite easily identified either analyzing

the explicit perturbative results or invoking one of the algorithms for the universal photonic corrections described in Appendix A. This allows to see that final-state leading contributions are of the form

$$2\,\frac{\alpha}{\pi}\,Q_f^2\,\ln(1-s_0/s)\,(L_f-1)\,, \tag{114}$$

so that they can be extracted from the finite order correction and summed up to all orders according to the preferred resummation technique. By using, for instance, a "naive" exponentiation procedure, the final-state correction factor, including higher-order leading contributions and exact sub-leading terms at $\mathcal{O}(\alpha)$, can be cast in the form

$$\delta^{fs} \;=\; \Delta^{'(\alpha)}_{V+S}(s)\,\exp\left\{2\,\frac{\alpha}{\pi}\,Q_f^2\,\ln(1-s_0/s)\,(L_f-1)\right\} \;+\; \delta^{fs,r}, \tag{115}$$

where $\Delta^{'(\alpha)}_{V+S}(s)$ is the soft+virtual K-factor of eq. (106) (provided that the substitution $m_e \to m_f$ is performed in the collinear logarithm) and $\delta^{fs,r}$ is the residual correction factor including sub-leading terms as obtained after depuration of leading logarithms from the complete $\mathcal{O}(\alpha)$ results.

All the above discussion and formulae concerning FSR are valid for a non-calorimetric ES (see Sect. **2**˙3 for more details) according to which the energy of the final-state fermions measured by the experimental apparatus coincides with the energy of the "bare" particles, regardless of the emission of collinear final-state photons. However, when considering the process of large-angle Bhabha scattering, this assumption turns out to be unrealistic. Actually, what is detected in the real environment is an *electromagnetic jet* of half-opening angle δ_c, where δ_c is an experimental parameter describing the resolution power of the calorimeter. This electromagnetic effect can be analytically accounted for by adding to the $\mathcal{O}(\alpha)$ final-state correction for "bare" electrons the contribution due to a hard photon of energy fraction greater than $1-x$, where x is s_0/s for an invariant mass cut and $2E_0/\sqrt{s}$ for an energy threshold cut, and collinear with the final fermion within an angle $0 \le \vartheta_\gamma \le \delta_c$. For electrons in the energy regime of LEP the contribution reads [127]

$$\begin{aligned} F_{coll} \;&=\; 2\,\frac{\alpha}{\pi}\,C, \\ C \;&=\; -\ln(1-x)\Big[\ln\left(1+r^2x^2\right)-1\Big] \\ &\quad+\Big[\frac{1}{4}-\Big(1-\frac{1}{2}(1-x)\Big)^2\Big]\ln\left(1+r^2x^2\right) \\ &\quad+\frac{\pi^2}{3}+\frac{9}{4}-\frac{5}{2}(1-x)+\frac{1}{4}(1-x)^2 \\ &\quad+2\ln x\ln(1-x)+\,2\mathrm{Li}_2(1-x), \end{aligned} \tag{116}$$

where

$$r=\frac{\delta_c\sqrt{s}}{2m_e}, \tag{117}$$

m_e being the electron mass. Equation (116) holds under the conditions $\delta_c \ll 1$ rad and $r \gg 1$, that are both very well satisfied at LEP, where δ_c is of the order of a few degrees. It is worth stressing that the effect of the calorimetric measurement, superimposed over the correction for "bare" final-state particles, depends very critically on the energy or invariant mass threshold, being at the level of 0.1% for low energy thresholds (around 1 GeV) but raising to order 1 per cent at, say, 10 GeV.

3˙4.3. Initial-final state interference. While the initial- and final-state QED corrections are functions of s only, the initial-final state interference correction depends also on the fermion scattering angle ϑ and therefore induces a modification of the ϑ dependence of the Born differential cross section. It receives contributions from the interferences between the real radiation diagrams of Figs. 22 and 23 and from the interference between the tree-level amplitudes and the QED box diagrams shown in Fig. 24. The leading angular

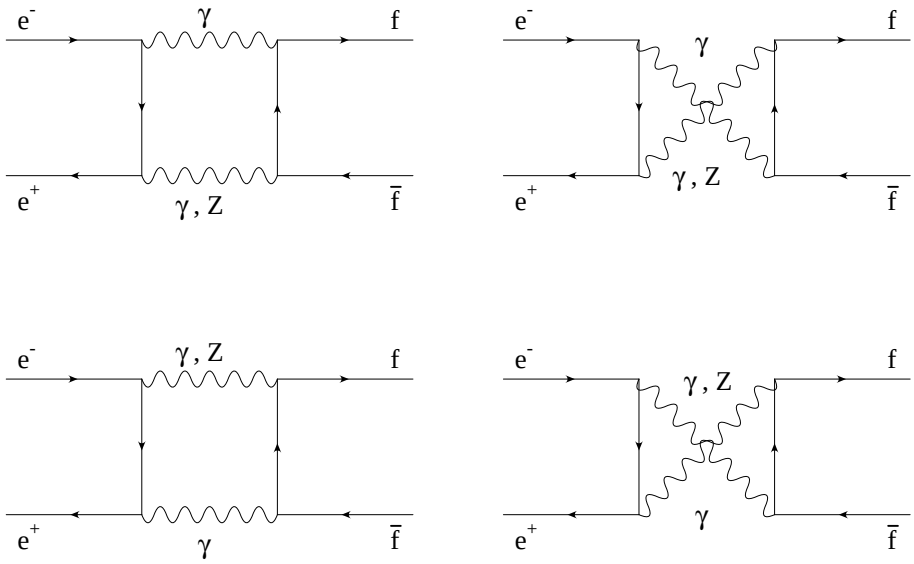

Fig. 24. – The Feynman diagrams for $\mathcal{O}(\alpha)$ QED box corrections to s-channel process $e^+e^- \to \gamma, Z^0 \to f\bar{f}$.

dependent terms that enter the result are of the form $\ln(t/u) = \ln(\tan(\vartheta/2))$ [128, 129]. This explains why the initial-final state interference is numerically small under many realistic experimental conditions, even if its actual magnitude crucially depends on the applied cuts. A physical argument can also be advocated to understand the rôle of the initial-final state interference in the region of the Z^0 resonance. In fact, when the Z^0 is produced close to its mass shell, the wave functions for initial- and final-state radiation are separated in space-time due to the finite Z^0 lifetime, so that their overlap is small. This implies that for loose cuts the interference effect is typically at the level of 10^{-3} or even smaller. Only when particularly tight cuts are imposed or one moves away from the peak, the above argument is invalidated and the interference can become more sizeable. In order to keep under control all the situations, the correction due to the initial-final state interference is included in the theoretical predictions, generally using the existing exact $\mathcal{O}(\alpha)$ calculations (including hard bremsstrahlung), that are sufficient for the realistic ES. For very tight, unrealistic, photon energy cuts, a proper exponentiation procedure can be introduced.

3˙5. *Computational Tools.* – In order to perform actual precision tests of the electroweak theory in e^+e^- collisions at the Z^0 pole, very precise measurements of cross sections and asymmetries are required, that in turn imply, together with a high statistics, a deep knowledge of systematics effects, such as the acceptance, selection efficiency

and backgrounds for a given reaction. The tools used by LEP Collaborations to determine experimental acceptances and efficiencies are unavoidably Monte Carlo event generators since they allow to simulate experimental cuts with the maximum flexibility. Just to give some examples, the LEP experiments commonly use the generators `HERWIG` [130] and `PITHYA/JETSET` [131] to simulate the process $e^+e^- \to$ hadrons, `KORALZ` [132] for the production of μ and τ pairs, `BHAGENE3` [133], `BHWIDE` [134] and `UNIBAB` [135] for the large-angle Bhabha scattering. `HERWIG` and `PITHYA/JETSET` are generators for the study of hadronic final states in e^+e^-, ep and pp collisions, describing the phase of parton cascade in the framework of perturbative QCD and the hadronization mechanism by using independent theoretical models. `KORALZ` is a Monte Carlo program developed for s-channel $e^+e^- \to f\bar{f}$ processes, including electroweak loops and using YFS exponentiation (see Appendix A) for the treatment of photonic radiation. Large-angle Bhabha generators will be described in the following.

However, in addition to Monte Carlo Generators, fast analytical and semi-analytical programs are of utmost importance for Z^0 precision physics, because, although they can account for simple kinematical cuts only, they are necessary tools in order to extract the electroweak parameters from the measurements according to an iterative fitting procedure. These fitting programs are also said *electroweak libraries*. As a matter of fact, the fitting programs mostly used by the LEP Collaborations are `BHM` [136], `MIZA` [137], `TOPAZ0` [111] and `ZFITTER` [138]. However, the extreme complexity in the calculation of radiative corrections and the relevance of improvements and cross-checks for precision physics at LEP, motivated a number of theoretical groups to develop completely independent and original electroweak libraries. The availability of various independent electroweak libraries turned out to be particularly useful in the context of the job of the Electroweak Working Group at CERN [76]. The aim of such a collaboration work was the estimate of the theoretical error inherent to the SM predictions for $e^+e^- \to f\bar{f}$ processes, in view of the final analysis of LEP precision data (see Sect. **3**·6 for more details). The basic features of the codes that contributed to reach the above task are shortly described in the following, with particular emphasis on their main physics input as well as their numerical output. However, for more details on technical aspects of these programs and their underlying formulation, the reader is referred to the original literature and to ref. [76].

`BHM` [136] — It is a semi-analytical program for the calculations of the Z^0 parameters and realistic observables for an extrapolated set-up only. It relies upon the on-shell renormalization scheme for the formulation of weak loops and the QED radiator for the treatment of ISR (see Appendix A).

`LEPTOP` [139] — It is an analytical code, developed by the ITEP Moscow group, giving predictions for the the Z^0 parameters in the so-called $\overline{\alpha}$-Born approximation. It consists in taking as "tree-level approximation" the one obtained by using $\alpha(M_Z)$ overall, and computing $\sin^2\vartheta_W$ from $\alpha(M_Z)$, G_μ and M_Z, with the residual electroweak corrections on top of this.

`TOPAZ0` [111] — It is a semi-analytical program, developed by the Pavia and Torino groups, that can be used to calculate both *pseudo-observables* and realistic observables, the latter over both an extrapolated and a more realistic set-up. It is additionally able to calculate the full Bhabha scattering cross section at large angles. It employes the $\overline{MS}$ scheme for the treatment of the electroweak corrections. QED corrections are exactly included at $\mathcal{O}(\alpha)$ for s-channel processes, at the LL level for t and s-t contributions to the large-angle Bhabha scattering. On top of that, higher-order QED corrections are implemented using the SF approach (see Appendix A).

WOH [140] — It is an analytical code for the calculation of the *pseudo-observables* only. It is based on the on-shell renormalization scheme and, basically, it leads back to the same approach of BHM, so that BHM/WOH are not completely independent of one another.
ZFITTER [138] — It is a semi-analytical program, of the Dubna-Zeuthen group, that, as TOPAZ0, allows to obtain predictions for both the *pseudo-observables* and the realistic ones, but excluding large-angle Bhabha scattering. The on-shell renormalization scheme is used for electroweak loops; QED corrections are exactly treated at $\mathcal{O}(\alpha)$, together with soft-photon exponentiation for ISR and FSR.

To summarize, all the above codes can provide predictions for the Z^0 parameters and therefore can all be used as fitting tools to these de-convoluted quantities. BHM, TOPAZ0 and ZFITTER can also calculate realistic observables and fit data for such observables. TOPAZ0 is also additionally able to calculate the full Bhabha scattering observables. Concerning the treatment of electroweak loops, the codes employ completely independent calculational schemes, with the exception of BHM/WOH that essentially are based on the same approach. QED corrections in the three QED dressers are treated according to different theoretical methods, whereas QCD corrections are common to a large extent in all the codes. How these codes were used as *tools* to estimate the intrinsic theoretical uncertainties in precision calculations for the Z^0 resonance is explained in Sect. **3**˙6.

The special rôle played by large-angle Bhabha (LABH) scattering in Z^0 precision physics led the to development of dedicated semi-analytical and Monte Carlo programs for such a process. Two of them, BHAGEN95 and TOPAZ0, have been previously described, the former in Sect. **2**˙4 and the latter here in the present Section. The other programs used by the LEP experiments for the study of $e^+e^- \to e^+e^-$ at large angles are briefly described in the following. It is worth pointing out that the Bhabha process, when considering large scattering angles and the energy region around the Z^0 peak, is basically a s-channel resonant process with "small" non-resonant contributions, so that its dynamics is completely different from that of the same process at small scattering angles, that has been already discussed in details in Sect. **2**. In particular, whereas non-QED effects other than vacuum polarization are absolutely negligible in the SABH case, an accurate treatment of the electroweak loops is a necessary ingredient for a precision calculation of the LABH reaction [78, 141, 142]. As a consequence, the computational tools (and their underlying formulations) for the LABH process are very different with respect to the ones used for the luminosity monitoring and already described in Sect. **2**˙4.
ALIBABA [142] — It is a semi-analytical program, implementing exact $\mathcal{O}(\alpha)$ weak and QED corrections to all Bhabha channels. The higher-order QED effects consist of LL $\mathcal{O}(\alpha^2)$ plus soft-photon exponentiation.
BHAGENE3 [133] — It is a Monte Carlo event generator, including one-loop and the most relevant two-loop electroweak corrections. The $\mathcal{O}(\alpha)$ QED corrections uses the exact matrix element and are supplemented with higher-order soft-photon effects.
BHWIDE [134] — It is a recent Monte Carlo event generator, based on the electroweak library of ALIBABA for the treatment of $\mathcal{O}(\alpha)$ weak and QED corrections. It includes multiphoton radiation in the framework of Yennie-Frautschi-Suura (YFS) exponentiation (see Appendix A) and can be considered as the extension of the code BHLUMI (see Sect. **2**˙4) to large angles.
UNIBAB [135] — It is a Monte Carlo event generator, relying upon an updated version of the ALIBABA electroweak library. The QED corrections are implemented assuming s-channel dominance and using photon shower algorithms for ISR and FSR (see Appendix A).

A more extensive description of the LABH programs, together with global compar-

isons between the semi-analytical and Monte Carlo programs, can be found in the recent work of ref. [18]. At LEP1, when analyzing LABH data, the common procedure employed is the so-called t-channel subtraction, where t and s-t contributions are subtracted from the data. As a matter of fact, the two programs commonly used to perform this unfolding are `ALIBABA` and `TOPAZ0`. Furthermore, besides the programs described above, one should also mention the codes `ALISTAR` and `MIZA`, that are basically rearrangements of `ALIBABA` developed for fitting purposes and specific experimental needs.

3˙6. *Theoretical Uncertainties.* – The very high experimental precision reached by the LEP Collaborations in the measurement of the Z^0 parameters and realistic observables (of the order of 0.1% or even below), necessarily requires a careful estimate of the intrinsic uncertainties associated to the SM theoretical predictions for these observables. In fact, as already discussed in Sect. **2**˙5 when addressing the problem of the total theoretical error in the luminosity measurement, any prediction obtained *via* a perturbative expansion is intrinsically affected by an uncertainty that is mainly due to neglecting higher-order contributions. The evaluation of such an uncertainty turns out to be a particularly severe problem whenever considering precision calculations for the Z^0 resonance, since the higher-order contributions depend in a highly non-trivial way on the whole stuff of radiative corrections in the SM (weak, QCD, mixed ew/QCD, QED). For this reason, a combined effort by different groups of theorists is in principle the best strategy to address this delicate subject. Such an effort was pursued by the collaboration work of the Electroweak Working Group, held at CERN, Geneva, during 1994 and concluded at the beginning of 1995. The composition of the Electroweak Working Group consisted of the authors of those formulations and relative computational programs containing at that time the state-of-the-art of the radiative corrections to the electroweak Z^0 observables: `BHM`, `LEPTOP`, `TOPAZ0`, `WOH` and `ZFITTER`. They have been already described in some detail in the previous Section. Because all these codes basically include the same content in the perturbative expansion (*i.e.* exact $\mathcal{O}(\alpha)$ electroweak corrections plus higher-order leading contributions), but differ in the choice of the renormalization scheme and in the treatment of higher-order sub-leading effects, they are ideal *tools* to provide an *estimate* of the theoretical uncertainties. The latter can be classified as follows:

- *Parametric uncertainties:* are related to the experimental precision of the input parameters. Among them, the largest uncertainty comes from $\alpha(M_Z)$: $|\Delta\alpha^{-1}(M_Z)|$ = 0.09; other sources are the errors on $\alpha_s(M_Z)$ and on the heavy-quark masses. These uncertainties can be estimated comparing the effects of variations in the input parameters within their errors [76].

- *Scheme-dependence uncertainties:* are associated to the choice of the calculational scheme. In fact, in a given renormalization framework the truncation of the perturbative series is realized in some specific way. An estimate of these uncertainties can be obtained by comparing the predictions for a given observable obtained with two codes based on different renormalization schemes. This is possible since, as discussed in Sect. **3**˙5, `BHM/WOH` and `ZFITTER` employ the on-shell scheme, `TOPAZ0` makes use of the $\overline{MS}$ scheme and an original approach is implemented in `LEPTOP` .

- *Intrinsic uncertainties:* are inherent in a given renormalization framework. They are a consequence of the still missing higher-order terms, reflecting in a certain degree of arbitrariness on how to combine the various theoretical ingredients in order to get the final expressions for the observables. This arbitrariness can be

quantified using the concept of *option*, *i.e.* a set of alternative but equally plausible implementations of the building blocks of the radiative corrections within a given calculational scheme [143].

To better illustrate the meaning of *intrinsic uncertainties*, it is worth presenting and discussing a few examples of *option*. A first one [144] refers to different possible implementations of QCD and QED final-state corrections to a given Z^0 partial width $\Gamma_f = \Gamma(Z \to f\bar{f})$. Let us suppose that $\mathcal{O}(\alpha)$ QED and $\mathcal{O}(\alpha_s^2)$ QCD corrections to the above width are known but that the mixed $\mathcal{O}(\alpha\alpha_s)$ corrections have not yet been calculated. Therefore, one can combine the two above final-state corrections either according to a *factorized* representation

$$\Gamma_f = \Gamma_f^{EW} \left(1 + \frac{3}{4} Q_f^2 \frac{\alpha}{\pi}\right) \left[1 + \frac{\alpha_s}{\pi} + c_2 \frac{\alpha_s^2}{\pi^2}\right], \tag{118}$$

or an *expanded* one

$$\Gamma_f = \Gamma_f^{EW} \left[1 + \frac{3}{4} Q_f^2 \frac{\alpha}{\pi} + \frac{\alpha_s}{\pi} + c_2 \frac{\alpha_s^2}{\pi^2}\right]. \tag{119}$$

In the latter equations, Γ_f^{EW} denotes the electroweakly-corrected partial width. Owing to the lack of knowledge of the exact $\mathcal{O}(\alpha\alpha_s)$ corrections, the two realizations are of course equally correct and could be both implemented into a program as two different *options*. They differ by a term of the order of $3\alpha\alpha_s Q_f^2/4\pi^2$, that can be seen as a naive estimate of the unknown mixed corrections. The explicit calculation of such corrections should reduce the uncertainty moving it to $\mathcal{O}(\alpha\alpha_s^2)$. Indeed, this correction is today available, giving the result

$$\Gamma_f = \Gamma_f^{EW} \left[1 + \frac{3}{4} Q_f^2 \frac{\alpha}{\pi} - \frac{1}{4} Q_f^2 \frac{\alpha}{\pi}\frac{\alpha_s}{\pi} + \frac{\alpha_s}{\pi} + c_2 \frac{\alpha_s^2}{\pi^2}\right], \tag{120}$$

so that the two above realizations can not be longer seen as options.

Another theoretical uncertainty, which is related to the pure weak corrections to the pseudo-observables, is the leading-remainder splitting in the effective couplings discussed in Sect. **3**˙2.3. These generally contain a leading universal part, which is usually resummed, and a non leading (remainder) part. The way of performing the separation between leading and remainder part and the way of treating the last are not uniquely defined, so that they are a source of theoretical uncertainty. A typical example is provided by Δr (the same reasoning, as the one shown in the following, also holds for the quantities $\delta\rho_f$ and δk_f) introduced in eq. (55) and split into a leading and a remainder part according to eq. (56), where the leading term contains the light fermion mass singularities and the terms proportional to m_t^2. In this separation the remainder contains, among others, logarithmic contributions in the *top*-quark and Higgs-boson masses, which can be numerically important. In resumming Δr as in eq. (61), to take into account of the leading terms to all orders, different ways of treating Δr_{rem} are in principle possible, *i.e.* they are different options which give an estimate of the associated theoretical uncertainty [76]:

$$\frac{1}{1 - \Delta r_L - \Delta r_{rem}},$$
$$\frac{1}{1 - \Delta r_L}\left(1 + \frac{\Delta r_{rem}}{1 - \Delta r_L}\right),$$

$$\frac{1+\Delta r_{rem}}{1-\Delta r_L},$$
$$\frac{1}{1-\Delta r_L}+\Delta r_{rem}.$$

In the specific case of Δr, the last two expansions are not valid according to the arguments given in ref. [68].

The two examples given above should clarify the meaning of intrinsic theoretical error and how to estimate it by considering proper options. Actually, apart from the factorization of QCD and EW corrections and the leading-remainder splitting, other options have been carefully examined by the Electroweak Working Group, such as the choice of the scale of α in the non-leading corrections (in particular the vertex corrections), the linearization of the radiatively corrected quantities like $\sin^2\vartheta^l_{eff}$, different choices of implementing the resummation of the vector-bosons self-energies, in particular the terms related to the Higgs-boson contribution, and the choice of the scale of α_s in the mixed electroweak-QCD corrections. The results obtained by the work of the Electroweak Working Group, based on a careful analysis of both the pseudo-observables and realistic ones, allowed to draw at that time (beginning of 1995) the following conclusions on the theoretical accuracy of the precision calculations for the Z^0 resonance [76]:

- the differences between the predictions of different computational tools are small compared to the experimental errors;
- the parametric uncertainty due to $\Delta\alpha_{had}$ is the dominant source of error and the real "bottleneck" to improve the theoretical accuracy; only new accurate measurements of the cross section of $e^+e^-\to$ hadrons at low energy could reduce it;
- complete one-loop calculations, supplemented with higher-order leading effects are adequate for Z^0 precision physics, but the control on two-loop electroweak sub-leading corrections would significantly reduce the still remaining uncertainty.

The first two conclusions still remain valid today. Concerning the third point, progress in the calculation of important two-loop electroweak sub-leading corrections has been achieved after the conclusion of the work of the Electroweak Working Group. In fact, the two-loop next-to-leading heavy *top*-quark contributions of the order of $G_\mu m_t^2 M_Z^2$ to the M_W-M_Z interdependence and to $\sin^2\vartheta^{lept}_{eff}$ have been completely calculated in the $\overline{MS}$ framework and for two different realizations of the on-shell scheme [88, 89] (see also [90, 91]). These newly calculated corrections give a nice reduction of the theoretical error of electroweak origin, especially for M_W and $\sin^2\vartheta^{lept}_{eff}$ [89, 145], even if it should be noticed that they have not yet been implemented, at the time of writing, in standard computational tools for LEP1 precision physics.([3])

Concerning the theoretical uncertainty associated to the treatment of QED corrections, of utmost importance for the study of the realistic distributions, the conclusions of the analysis performed by the Electroweak Working Group, as obtained through a critical comparison of QED dressers over both an extrapolated and realistic set-up, can be summarized as follows:

([3]) After the completion of this work, the two-loop electroweak sub-leading corrections of refs. [88, 89], together with the QCD calculation of ref. [106] and the QED effects studied in ref. [120], have been implemented in a new version of the code `TOPAZ0` [146].

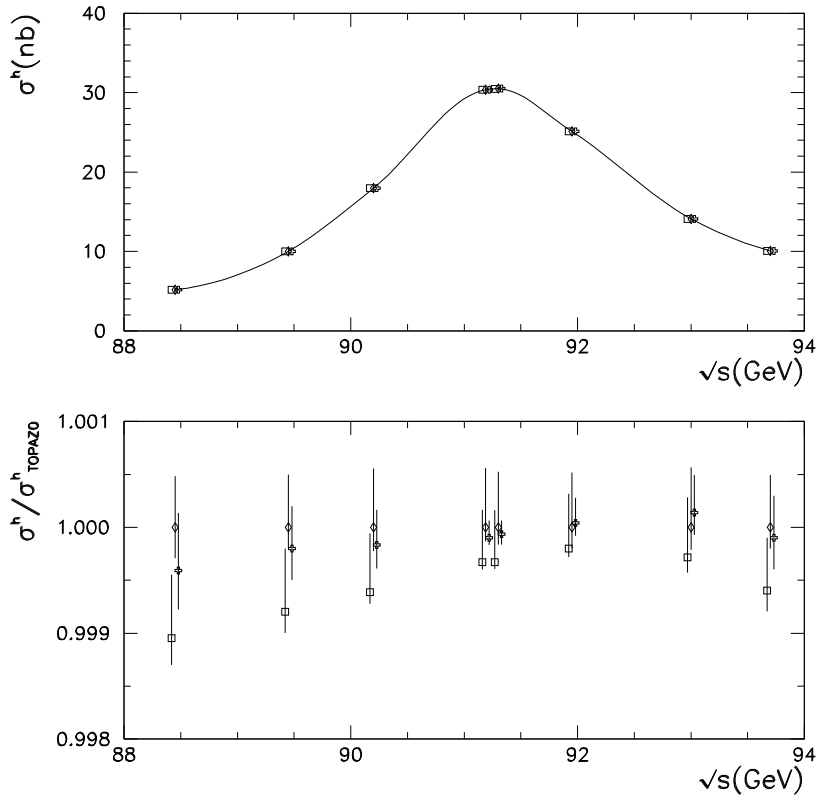

Fig. 25. – A comparison between theoretical predictions for the hadronic cross section. The squares, diamonds and crosses represent `BHM` [136], `TOPAZ0` [111] and `ZFITTER` [138], respectively (from ref. [76]). The lower window shows the predictions of the codes together with their estimate of the theoretical error.

- for s-channel annihilation processes, the theoretical error is of the order of 0.1%, almost independently of the considered c.m. energy (see Figs. 25 and 26);
- for full Bhabha scattering, the theoretical accuracy can be estimated, with due caution, to be at the level of 0.1-0.2% before and strictly around the peak, growing to about 1% (depending on the imposed experimental cuts) on the hard radiative tail.

It is worth pointing out that the above uncertainties associated to the photonic corrections actually match the statistics and systematics of the LEP1 data for the realistic distributions. In fact, whenever a somehow large theoretical error is present for full Bhabha scattering, this shows up in an energy regime (the hard radiative tail above the peak) where the experimental precision is much lower (*i.e.* around an order of magnitude larger) than the corresponding theoretical accuracy.

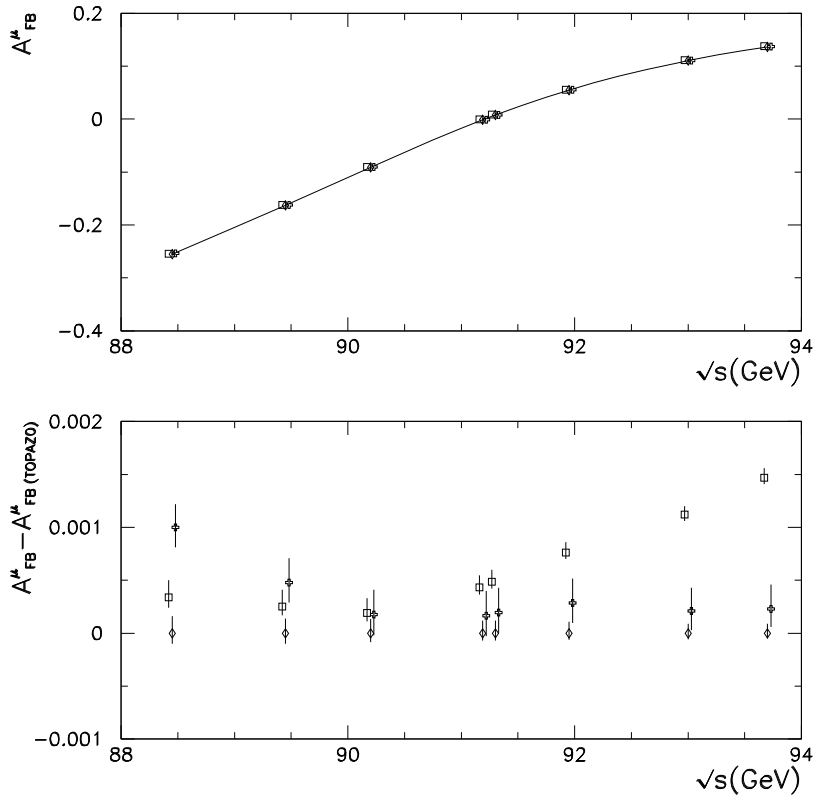

Fig. 26. – The same as in Fig. 25 for the μ forward-backward asymmetry (from ref. [76]).

As far as s-channel processes are considered, the estimate of the QED theoretical accuracy provided by the Electroweak Working Group has been recently reinforced by a novel investigation of the effects of LL $\mathcal{O}(\beta^3)$ photonic corrections to the QED radiator [120], usually neglected in standard computational tools and not taken into account in the analysis of the Electroweak Working Group. In fact, it has been shown that the $\mathcal{O}(\beta^3)$ corrections introduce, on an extrapolated cross section computed with a standard QED radiator with up to $\mathcal{O}(\beta^2)$ non-soft terms, a systematic shift of around -0.07%, that confirm *a posteriori* the estimate of the Electroweak Working Group. However, the size of the effect also indicates that these LL third-order QED corrections should be carefully taken into account in the theoretical predictions for the realistic observables of two-fermion production, in the light of the latest experimental data for some realistic observables, such as the cross section of $e^+e^- \to$ hadrons.

Concerning the estimate of the theoretical error in the large-angle Bhabha scattering, it substantially traces back to a certain disagreement between the predictions of `ALIBABA` and `TOPAZ0` far from the peak and due, as discussed in the literature [78], to

a different implementation of QED final-state corrections, yielding a difference in the treatment of $\mathcal{O}(\alpha^2)$ sub-leading contributions. In fact, in ALIBABA final-state corrections are implemented factorizing the leading terms only and summing up at $\mathcal{O}(\alpha)$ non-leading effects, whereas in TOPAZ0 a fully factorized prescription is followed, in order to preserve the so-called classical limit according to which the cross section of a real scattering process must vanish in the absence of electromagnetic radiation. This fundamental property is not guaranteed by an additive formulation. Furthermore, as shown and extensively discussed in [23], a fully factorized form allows to keep under control in an effective way the bulk of $\mathcal{O}(\alpha^2)$ next-to-leading QED corrections of the order of $\mathcal{O}(\alpha^2 L)$, that are on the contrary completely absent in the additive prescription (see also the discussion given in Sects. **2**˙3, **2**˙5 and **2**˙6 on the rôle of the $\mathcal{O}(\alpha^2 L)$ corrections in the present theoretical error to the SABH process). Therefore, with respect to an additive formulation, a factorized formulation is more accurate from the point of view of the perturbative content as well as more theoretically founded. However, after the completion of the work performed in ref. [76], a much more extensive analysis of the large-angle Bhabha process has been performed in ref. [18]. In this last analysis, several codes other than ALIBABA and TOPAZ0, noticeably BHWIDE, have been used for the comparisons. Moreover, also more realistic ES's have been adopted, namely calorimetric ES's in addition to the unrealistic BARE ES adopted in ref. [76], and this is a key point in order to obtain a reliable error estimate (see the discussion in Sect.**2** for more details). Thanks to these results, it may be concluded that the theoretical error of the large-angle Bhabha scattering is 0.3% on peak, and 0.5% off peak [18].

4. – Fits to Precision Data

The application of the theoretical results discussed in Sect. **3** to the analysis of precision data collected at LEP1/SLC leads to the indirect determination of the fundamental parameters of the Standard Model (SM). Actually, the high experimental accuracy makes the electroweak measurements on the Z^0 peak sensitive to the mass of the particles circulating in the loops, although they are not energetically accessible. Hence the precision data can be used to infer valuable constraints on the *top*-quark and the Higgs-boson masses, as well as on the value of the strong coupling constant α_s. The level of agreement between theory and experiment allows in addition to derive hints on possible new physics scenarios beyond the standard description of fundamental particles and interactions.

The present section is devoted to illustrate the procedure adopted by the experiments to extract the electroweak Z^0 parameters from the directly measured production cross sections and forward-backward asymmetries. The interpretation of the experimental results in terms of the SM parameters is discussed. The most recent indirect limits obtained for the *top*-quark and Higgs-boson masses *via* the virtual effects due to radiative corrections to the precision observables are presented, and compared with present information from direct searches. The determination of α_s from precision data at the Z^0 pole is compared with other measurements in different processes and at different energy scales. The issue of a more model-independent attitude towards the precision measurements is in conclusion addressed, discussing the S-matrix approach as a framework for a model-independent determination of the Z-boson parameters, and the ε parameterization of pure weak loops as a strategy for a model-independent analysis of the electroweak quantities. The implications of precision data for new physics beyond the SM are briefly examined.

4˙1. *Determination of the Electroweak Parameters.* – The "primary" observables measured by the LEP experiments are the cross sections and forward-backward asymmetries of the two-fermion processes $e^+e^- \to \gamma Z \to f\bar{f}$ quoted as a function of the centre of mass (c.m.) energy (see Sect. **3**˙1). The channels considered are the hadronic ($q\bar{q}$) and leptonic (l^+l^-, $l = e, \mu, \tau$) final states. The cross section data are determined by making use of the relation of eq. (2) in Sect. **2**˙1, once the number of events for a given channel has been determined and corrected for the trigger efficiency, the geometrical acceptance and the efficiency of the selection cuts. Analogously, the data for the forward-backward (FB) asymmetry A_{FB} are obtained exploiting the definition

$$A_{FB} = \frac{N_F - N_B}{N_F + N_B}, \tag{121}$$

where $N_F(N_B)$ is the number of events collected with a forward (backward) scattered fermion. This determination of the FB asymmetry is known as the *counting* method. Alternatively, the FB asymmetry is obtained from a maximum likelihood fit of an asymmetric differential cross section of the form

$$\frac{d\sigma}{d\cos\vartheta} \propto 1 + \cos^2\vartheta + \frac{8}{3} A_{FB} \cos\vartheta \tag{122}$$

to the experimental angular distribution. The expression given by eq. (122), where ϑ is the angle between the incoming electron and the outgoing fermion, is the form predicted by the electroweak theory in the lowest-order approximation and applies to s-channel annihilation only. For $e^+e^- \to e^+e^-$, due to the presence of t-channel contributions, a similar but more complicated expression is used. This second determination of the FB asymmetry is known as the *fitting* or *likelihood* method.

From the measured hadronic and leptonic cross sections and leptonic forward-backward asymmetries, the parameters of the Z^0 resonance are extracted by the LEP Collaborations by means of a combined fit to the data [147]. The Z^0 parameters are obtained using a χ^2 minimization procedure with the correlations among the data (common experimental errors, theoretical luminosity error, uncertainties from the LEP energy calibration, etc.) taken into account using a covariance matrix. Several sets of parameters can be (and actually are) introduced to parameterize the measurements. However, in order to make possible a combination of the results obtained by each of the four LEP Collaborations as well as for comparison purposes, the LEP experiments use a standard set containing *nine* free Z^0 parameters:

- the Z-boson mass, M_Z, and its total width Γ_Z;
- the hadronic pole cross section σ_h^0, defined by eq. (31) in Sect. **3**˙1;
- the ratios $R_{e,\mu,\tau} = \Gamma_h/\Gamma_{e,\mu,\tau}$;
- the pole asymmetries $A_{FB}^e, A_{FB}^\mu, A_{FB}^\tau$, that can be expressed in terms of the effective vector and axial-vector neutral current couplings of the fermions according to the relations given by eqs. (32) and (35) in Sect. **3**˙1.

These parameters are chosen because they are most directly related to the experimental quantities and are weakly correlated. If the assumption of lepton universality is additionally introduced, then the numbers of parameters reduces from nine to five, *i.e.*

$$M_Z, \quad \Gamma_Z, \quad \sigma_h^0, \quad R_l = \Gamma_h/\Gamma_l, \quad A_{FB}^l, \tag{123}$$

that actually is another standard set of parameters commonly used by the LEP Collaborations.

The extraction of the Z^0 parameters from a combined fit to the hadronic and leptonic cross sections and leptonic forward-backward asymmetries requires that an appropriate parameterization for these last realistic observables is introduced. By exploiting the relation between the effective couplings and the Z^0 partial width, the cross section can be written in terms of mass, total and partial widths of the Z boson, without relying upon any particular assumption on the validity of the Standard Model (SM) [113, 148, 149]:

$$\sigma(s) = \frac{12\pi\Gamma_e\Gamma_f}{|s - M_Z^2 + iM_Z\Gamma_Z(s)|^2}\left(\frac{s}{M_Z^2} + R_f\frac{s - M_Z^2}{M_Z^2} + I_f\frac{\Gamma_Z}{M_Z} + \ldots\right) + \sigma_\gamma, \tag{124}$$

where

$$\Gamma_Z(s) = \Gamma_Z\left(\frac{s}{M_Z^2} + \varepsilon\frac{s - M_Z^2}{M_Z^2} + \ldots\right), \tag{125}$$

and the partial widths are understood expressed in terms of the Z^0 parameters. The term σ_γ identifies the γ-exchange contribution known from QED, R_f and I_f describe the γ-Z interference and ε is the correction due to finite final-state fermion mass effects. This procedure justifies the typical Breit-Wigner ansatz for the Z^0 contribution adopted by the LEP Collaborations,

$$\sigma_Z^f = \frac{12\pi}{M_Z^2}\Gamma_e\Gamma_f\frac{s}{(s - M_Z^2)^2 + s^2\Gamma_Z^2/M_Z^2}, \tag{126}$$

for a given $f\bar{f}$ channel, although the forms actually used by each experiment may differ in some detail. The photon-exchange contribution is calculated from QED and the γ-Z electroweak interference is taken into account as well, usually computing it within the SM. Although the interference contribution is small around the Z^0 peak, it is important for the precise measurement of M_Z and therefore some more general fit, where the SM dependence of the γZ effect is somehow relaxed, are actually performed by the experiments (see Sect. **4**˙3.1 below).

It is worth pointing out that the above parameterization is introduced in order to describe just the short-distance behaviour of the cross section. Indeed, in the fit of the Z^0 parameters to the measured data, the QED radiative corrections enter as an unavoidable theoretical ingredient, and they are taken into account according to the algorithms described in Sect. **3**˙4 and in Appendix A. A complication in the fitting procedure arises when considering the Bhabha channel $e^+e^- \to e^+e^-$, because of the presence of t-channel contributions. To minimize this contamination the experiments adopt a selection with large polar angle acceptance (typically $45° < \vartheta < 135°$) where the s-channel Z-boson exchange largely dominates. The remaining t and s-t contributions are generally calculated by using the programs `ALIBABA` and `TOPAZ0`, in order to correct the cross section. The most recent LEP results for the Z-boson mass and width are shown in Figs. 27 and 28, respectively.

In addition to the above Z^0 parameters determined by means of a combined nine (five) parameters fit to the cross sections and asymmetries, other important electroweak observables are measured by the LEP experiments. Each of them is obtained according to a well-defined experimental strategy applied to a specific $f\bar{f}$ final-state. A first example is given by the τ polarization asymmetry P^τ that is defined as [150]

$$P^\tau = \frac{\sigma_R - \sigma_L}{\sigma_R + \sigma_L}, \tag{127}$$

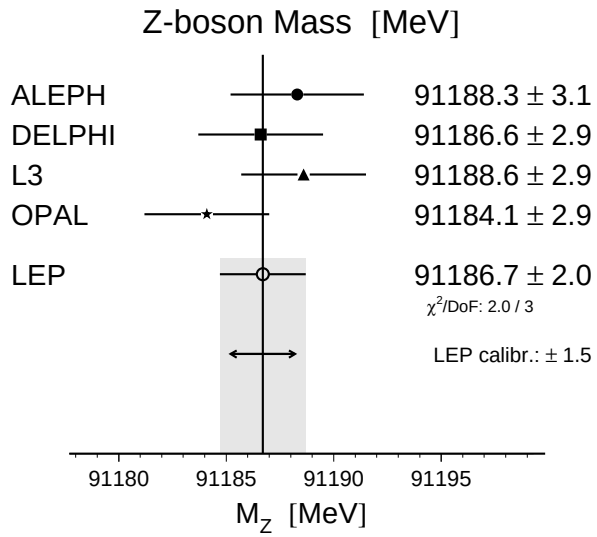

Fig. 27. – The Z-boson mass according to the most recent data analyses [7, 8].

where $\sigma_{R(L)}$ denotes the τ-pair cross section for the production of a right-handed (left-handed) τ^-. This quantity is experimentally determined by measuring the longitudinal polarization of τ pairs produced in Z^0 decays. The left-right asymmetry A_{LR} is another important manifestation of parity violation in weak interactions, that, however, requires longitudinal polarization of the initial-state electrons. Owing to the difficulties in achieving a high degree of polarization at LEP collider because of the presence of depolarizing effects, the left-right asymmetry has not been measured by the LEP experiments but by the SLD Collaboration at SLC, where the conditions for polarization measurements are much more favourable. In fact, an average degree of polarization of the incoming electrons $< P_e >$ reaching 77% has been obtained at SLC. The left-right asymmetry is determined by the SLD experiment exploiting the relation [151]

$$A_{LR} = \frac{1}{< P_e >} \frac{N_{e_l} - N_{e_r}}{N_{e_l} + N_{e_r}}, \tag{128}$$

where N_{e_l} and N_{e_r} are the observed numbers of hadronic events using left-handed and right-handed electron beams, respectively.

Further interesting electroweak observables in Z^0 decays are derived from the analysis of the final states containing c and b quarks (*heavy flavours*). These measurements require sophisticated tagging techniques of heavy flavours (such as mass or lifetime tagging), whose description is beyond the aim of the present review (see for instance ref. [152] for an overview of the tagging methods used at LEP). The Z^0 parameters that are determined from these studies are

$$R_b = \Gamma_b/\Gamma_h, \quad R_c = \Gamma_c/\Gamma_h, \quad A^b_{FB}, \quad A^c_{FB}, \tag{129}$$

where $\Gamma_{b(c)}$ is the Z^0 width for the decay into $b(c)$ quarks, A^b_{FB}, A^c_{FB} are the b- and c-quark pole forward-backward asymmetry. As already remarked in Sect. **3**˙1, the results

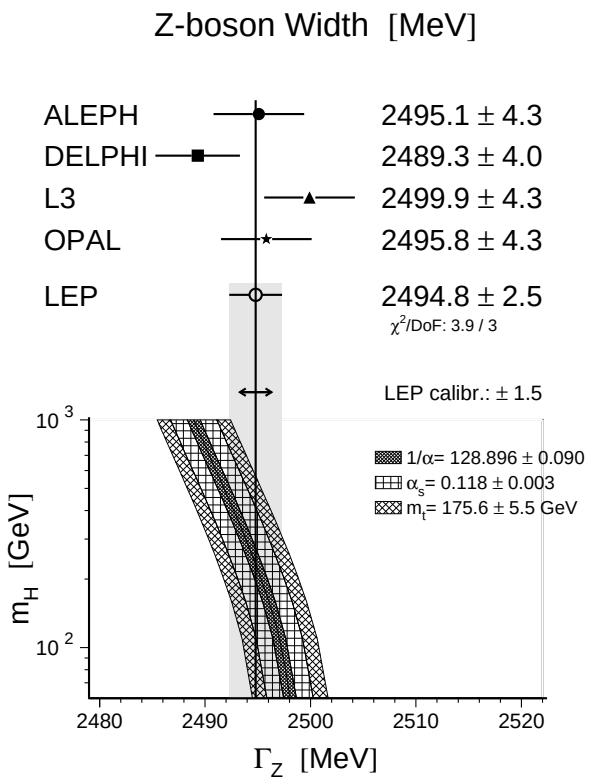

Fig. 28. – The Z-boson width according to the most recent data analyses [7,8].

for A_{FB}^b and A_{FB}^c are quoted after having subtracted from the data, besides the effect of initial-state radiation (ISR), also the effects of QCD corrections, in order to deal with a pure electroweak observable.

Once the above "primary" Z^0 parameters are extracted from the data, other important additional quantities, such as the Z^0 partial widths Γ_h, Γ_l and Γ_{inv}, are derived. Γ_{inv} denotes the Z-boson invisible width that can be obtained *via* the relation (assuming lepton universality)

$$\Gamma_{inv} = \Gamma_Z - \Gamma_h - 3\Gamma_l. \tag{130}$$

Its present experimental value is [7,8]

$$\Gamma_{inv} = 500.1 \pm 1.8 \text{ MeV}. \tag{131}$$

This quantity is of particular interest for the extraction of the number of light neutrino species N_ν. In order to get rid of the bulk of the non-negligible *top*-quark mass dependence of the partial widths, N_ν can be conveniently derived from the comparison of the experimental ratio Γ_{inv}/Γ_l with the corresponding SM prediction, yielding the result [7,8]

$$N_\nu = 2.993 \pm 0.011. \tag{132}$$

This determination, that firmly proves the existence of three standard light neutrino families, agrees well with the independent measurement obtained by means of the process $e^+e^- \to \nu\bar{\nu}\gamma$, known as *radiative neutrino counting* reaction. It gives rise to a signature where only a single bremsstrahlung photon and nothing else is seen in the detector. The Feynman diagrams contributing in the SM to this process are depicted in Fig. 29.

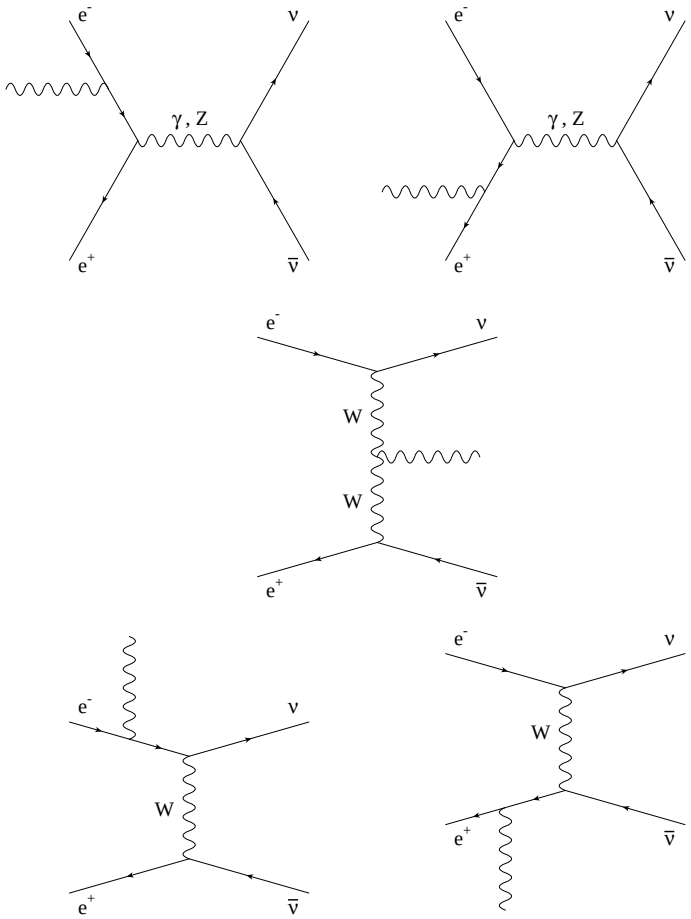

Fig. 29. – The tree-level Feynman diagrams for the process $e^+e^- \to \nu\bar{\nu}\gamma$.

The study of the *radiative neutrino counting* events offers the possibility to determine in a rather direct way the partial width of the Z^0 into invisible particles, since the Z-boson exchange contribution, largely dominating the $e^+e^- \to \nu\bar{\nu}\gamma$ cross section around the Z^0 peak, is proportional to the number of neutrinos. For that reason, this procedure is known as *direct determination of the invisible width*. In practice, the measured cross section as a function of the c.m. energy is compared with the SM calculation for different numbers of neutrino generations. A meaningful comparison between theory and experiments requires that electroweak radiative corrections, especially the large effects introduced by ISR, to $e^+e^- \to \nu\bar{\nu}\gamma$ are taken into account, although the statistical precision of the direct determination of the invisible width is smaller than the one achieved in

the measurements of the observables of two-fermion production processes (see ref. [153] and references therein). Yet, the study of *radiative neutrino counting* events clearly rules out the existence of a fourth family with light neutrinos in the SM.

In addition to the number of light neutrinos, there are other derived electroweak parameters that deserve mention for their rôle in precision tests of the electroweak theory. From the partial widths of the Z^0 into charged leptons, b and c quarks, the τ polarization asymmetry, the left-right asymmetry as well as the forward-backward asymmetry in leptonic and heavy-flavour channels, the LEP/SLC experiments determine the vector and axial-vector neutral current couplings of fermions. These results for the effective Z-boson couplings g_V^f and g_A^f make use of the relations between the Z^0 parameters and the couplings themselves given by eqs. (32)-(34) and (35) for the asymmetries and polarizations, and eq. (36) for the partial widths given in Sect. **3**˙1. In particular, the comparison between electron, muon and tau couplings is in good agreement with lepton universality, with a precision of about 0.2% for g_A and $5 \div 10\%$ for g_V [8]. Furthermore, since the forward-backward and polarization asymmetries depend only on the ratio g_V^f/g_A^f, it is possible to express the asymmetry measurements in terms of a single parameter given by the effective weak mixing angle, *i.e.*

$$4\,|Q_f|\sin^2\vartheta^f_{eff} \;=\; 1 - \frac{g_V^f}{g_A^f}. \tag{133}$$

The value of $\sin^2\vartheta^f_{eff}$ is flavor-dependent due to the effects of weak vertex corrections that are non-universal. However, since the most precise results are obtained for the charged leptons, the mostly quoted value for the effective weak mixing angle coincides with $\sin^2\vartheta^l_{eff}$, that allows to combine into a single electroweak parameter all the leptonic asymmetry measurements.

It is worth pointing out in conclusion that, as a result of the procedure described in the present Section, the Z^0 parameters that are extracted by the LEP experiments carry dependence on the whole stuff of electro-weak, mixed electroweak/QCD as well as, for the quantities referring to $q\bar{q}$ final states, QCD radiative corrections, reviewed in Sects. **3**˙2-**3**˙3. Therefore, these observables can be conveniently used to measure quantum effects of the electroweak interactions, *i.e.* to derive interesting constraints on the SM parameters that enter the predictions *via* radiative corrections only, noticeably the *top*-quark mass m_t, the Higgs-boson mass m_H and the value of the strong coupling constant at the Z^0 pole $\alpha_s(M_Z)$. Such an analysis assumes the validity of the SM *ab initio*. However, if an appropriate strategy is organized, a model-independent analysis of the Z^0 parameters can be also performed, exploiting the high level of precision of the data in order to constrain new physics predicted by possible extensions of the SM. The physical and theoretical implications of the precision measurements of the electroweak Z^0 parameters are discussed in more detail in the following.

4˙2. *Standard Model Fits.* – A summary of the most recent measurements of the Z^0 parameters obtained by the LEP and SLC experiments is given in Tab. VI. According to a standard presentation, the data are compared with the SM predictions (third column) corresponding to a fit of the electroweak data in terms of m_t, m_H and $\alpha_s(M_Z)$, that will be described in more detail in the following. In the fourth column one can also see the *pulls* derived from the fit, *i.e.* the difference between each theoretical result and the corresponding experimental measurement, in units of the measurement error. A few but important comments about Tab. VI are in order here.

The first remark concerns the precision level reached in the experimental measurements at LEP and SLC. The Z-boson mass M_Z is now known with a relative error of 2×10^{-5} (absolute error of ± 2 MeV). The total Z^0 width and the hadronic peak cross section are determined with a relative experimental uncertainty of the order of 1×10^{-3} (with an absolute error for Γ_Z of around ± 3 MeV). All the asymmetry measurements have an absolute error smaller than 0.01, generally at the level of a few 0.001, and the effective weak mixing angle is derived with a precision of around ± 0.0003. Therefore, in the light of these numbers, the LEP1/SLC experimental program can be considered as a great success, being the precision reached better than that expected at the beginning of operation.

TABLE VI. – Electroweak data according to the most recent determination (see refs. [7] and [8]).

Quantity	Data (Jerusalem '97)	Standard Model	Pull
M_Z [GeV]	91.1867(20)	91.1866	+0.04
Γ_Z [GeV]	2.4948(25)	2.4966	−0.73
σ_h^0 [nb]	41.486(53)	41.467	+0.36
R_l	20.775(27)	20.756	+0.71
R_b (LEP+SLC)	0.2170(9)	0.2158	+1.38
R_c (LEP+SLC)	0.1734(48)	0.1722	+0.24
A_{FB}^l	0.0171(10)	0.0162	+0.89
A_τ	0.1411(64)	0.1471	−0.93
A_e	0.1399(73)	0.1471	−0.98
A_{FB}^b	0.0984(24)	0.1031	−1.95
A_{FB}^c	0.0741(48)	0.0737	+0.09
A_b (SLC direct)	0.900(50)	0.935	−0.69
A_c (SLC direct)	0.650(58)	0.668	−0.31
$\sin^2\theta_{eff}$(LEP-combined)	0.23199(28)	0.23152	+1.68
$A_{LR} \to \sin^2\theta_{eff}$ (SLC)	0.23055(41)	0.23152	−2.37
M_W [GeV] (CDF/D0+LEP2)	80.43(8)	80.375	+0.69
$1 - \frac{M_W^2}{M_Z^2}$ (νN)	0.2254(37)	0.2231	+0.63
m_t [GeV] (CDF/D0)	175.6(5.5)	173.1	+0.45

A second comment regards the level of agreement between theory and experiment. No significant evidence for departures from the SM predictions is present. Close to the end of the LEP1/SLC experimental program, the data support the SM in a remarkable way. Looking at the data in more detail, one could point out that there is an around 2σ deviation of the measured value of A_{FB}^b with respect to the SM prediction, that R_b is 1.4σ away from the SM expectation, that the determination of the effective weak mixing angle from A_{LR} at SLC differs significantly from the LEP average. However, one should also emphasize that the observed pulls just follow the pattern that can be expected from a normal distribution of experimental measurements [8, 154]. Moreover, the disagreement between the measured values of R_b and R_c and their SM expectation, that received much attention in the past (see for instance ref. [155] and references therein), has now substantially disappeared. Presumably, future improved measurements of the Z^0 parameters, especially in the b-quark sector at LEP and A_{LR} at SLC, will clarify the above issues.

Last but not least, the electroweak data contained in Tab. VI, by virtue of their

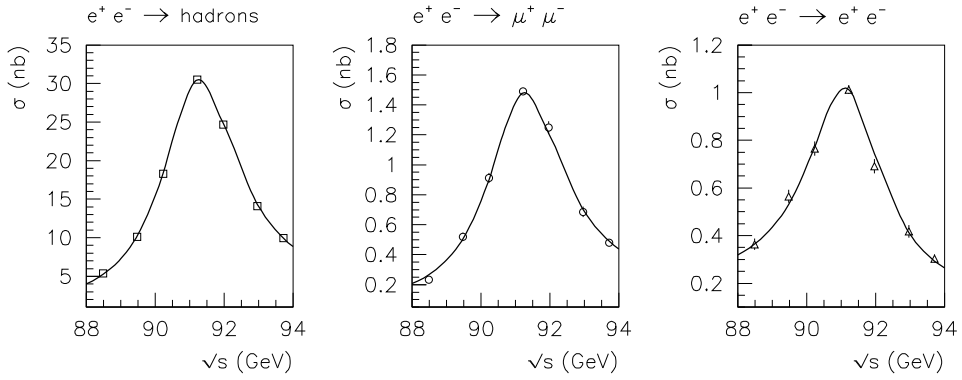

Fig. 30. – Data-theory comparison for realistic cross section data. Experimental data from ref. [156]. Theoretical predictions by TOPAZ0 [111].

high precision, can be used to derive constraints on the *top*-quark and the Higgs-boson masses, as well as on the value of $\alpha_s(M_Z)$, fully exploiting the predictive power of the SM, as a renormalizable quantum field theory, beyond the tree-level approximation (for instance, several fits performed by various authors, using older data sets, can be found in refs. [157–165]). Hence, the sensitivity of the electroweak data to quantum loops elevates the *precision physics* to the level of *discovery physics*. Moreover, the analysis can be generalized in order to constrain, disfavor or even rule out various extensions of the SM.

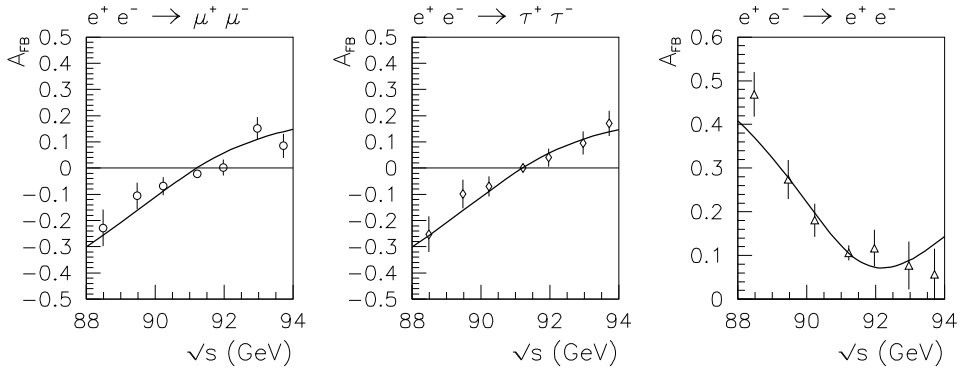

Fig. 31. – Data-theory comparison for realistic forward-backward asymmetry data. Experimental data from ref. [156]. Theoretical predictions by TOPAZ0 [111].

The procedure described above is the one that is commonly adopted by the LEP experiments. Its main advantage consists in the fact that it allows the extraction of

parameters (the Z^0 parameters) independent of the experimental details and hence easily comparable from experiment to experiment, both at different machines and energy scales. Moreover, and as a corollary, the procedure offers the possibility of fitting the unknown SM parameters by making use of a theoretical machinery which is completely independent of the experimental selection criteria. On the other hand, it is intrinsically a two-step procedure, requiring firstly the determination of the Z^0 parameters and secondly the fitting of the unknown SM parameters. It is worth noticing that an alternative but not antithetic procedure is possible, namely considering as fundamental experimental quantities the data for the realistic observables (see Sect. **3**˙1), and fitting the unknown SM parameters directly on them. This last procedure requires the use of theoretical tools that are able to provide predictions for the realistic observables, taking into account all the details of the experimental set-up. As a consequence, the required theoretical framework is sensibly more involved, but on the other hand the procedure is a single-step one. This last strategy has been used in the past by the LEP Collaborations and also by other authors [78, 166], yielding results compatible with the outcomes of the standard procedure. Figures 30 and 31 show the comparison between the experimental data for realistic cross sections and forward-backward asymmetries of ref. [156] and the theoretical prediction at best fit performed by `TOPAZ0` [111].

4˙2.1. Determination of the *top*-quark mass. One the most important recent achievements in particle physics has been the discovery of the *top* quark by the experiments CDF and D0 at the $p\bar{p}$ collider TEVATRON at FERMILAB in Chicago [167]. The present average of the mass values reported by the CDF and D0 Collaborations is $m_t = 175.6 \pm 5.5$ GeV [168], with a measured *top*-quark production cross section in fairly good agreement with the QCD prediction [169]. The main production mechanism for the *top* quark at the TEVATRON is the quark-antiquark annihilation into a gluon followed by the creation of a $t\bar{t}$ pair. Due to its short lifetime, the *top* quark can not be detected directly but only *via* its decay products, *i.e.* the weak decay $t \to W^+ b$, followed by the subsequent leptonic or hadronic W-boson decays $W \to l\bar{\nu}_l, u\bar{d}$. Hence, the production of the *top* quark at the hadron colliders gives rise to six-fermion final states $(b\bar{b}ud\bar{l}\bar{\nu}_l, b\bar{b}ud\bar{d}\bar{u})$, as depicted in Fig. 32.

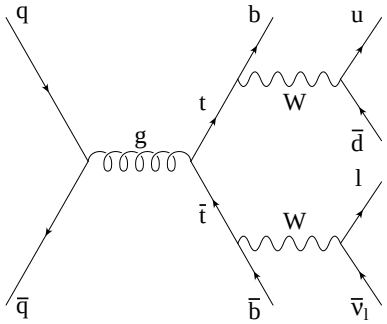

Fig. 32. – The main production mechanism for the *top* quark at the TEVATRON, yielding a six-fermion final state.

The *top*-quark mass is reconstructed by CDF and D0 measuring the energy and momenta of the final-state products in the dilepton (where both W decay leptonically) and lepton-plus-jets (where one W decays leptonically and the other one hadronically)

events.([4]) The large value obtained for m_t (the *top* quark is as heavy as a heavy nucleus) has as a direct consequence that the total width of this particle depends on the third power of the mass, reaching the value of about 1.5 GeV for $m_t \simeq 175$ GeV. As said above, this corresponds to an extremely short lifetime of about 10^{-24} s, so that the *top* quark decays immediately after its formation and $t\bar{t}$ bound states cannot be formed.

The direct evidence for the *top* quark in proton collisions and the measurement of its mass in a range around 170-180 GeV, in agreement with the indirect determination performed at LEP/SLC, constitutes a striking success for the SM at the quantum level and a remarkable confirmation of the precision tests of the electroweak interaction at LEP/SLC. Indeed, although the LEP energy is not sufficient to produce real *top* quarks, the effects of this particle and, in particular, of its high mass, can be felt in the precision measurements, *via* the radiative corrections induced by the loops containing the *top* quark as a virtual particle. In particular, thanks to the high statistics collected at the Z^0 resonance and the leading quadratic dependence of the theoretical predictions on m_t, the mass value of the *top* quark can be deduced from the virtual effects in electroweak observables with a precision comparable to the accuracy of the direct measurement.([5])

Since the mass of the *top* quark is at present known from CDF and D0 with a rather good precision, it is reasonable to adopt two different strategies in fitting the *top*-quark mass from the precision data, namely

- consider all the available electroweak data with the exclusion of the CDF/D0 measurement of m_t;
- consider the whole set of data, including m_t from CDF/D0.

The former procedure allows to establish whether the estimate of m_t from radiative corrections is in agreement with the direct measurement at the TEVATRON. The latter, being a more general type of fit, allows to test the overall consistency of the SM in a more complete way and to obtain the present best estimate of derived quantities such as the W-boson mass and $\sin^2\vartheta_{eff}$.

The results obtained according to the above strategies, when fitting the data with m_t, m_H and $\alpha_s(M_Z)$ as free parameters, are summarized in Tab. VII. As can be

TABLE VII. – Fits to α_s, m_t and m_H (from ref. [8]).

Parameter	LEP (incl. M_W)	All but M_W and m_t	All data
m_t [GeV]	158^{+14}_{-11}	157^{+10}_{-9}	173.1 ± 5.4
m_H [GeV]	83^{+168}_{-49}	41^{+64}_{-21}	115^{+116}_{-66}
$\alpha_s(M_Z)$	0.121 ± 0.003	0.120 ± 0.003	0.120 ± 0.003
χ^2/dof	8/9	14/12	17/15

seen from the table, the fitted mass of the *top* quark is somewhat lower than the direct measurement, even if in well agreement with it. This compatibility, as already remarked, is an impressive confirmation of the SM at the level of quantum effects and justifies combining the direct and indirect derivation of m_t. The 1σ errors returned by the fit

([4]) Recently CDF employed also the fully hadronic sample, that however gives a less precise determination of the *top*-quark mass.
([5]) The values quoted for m_t refer to the pole mass.

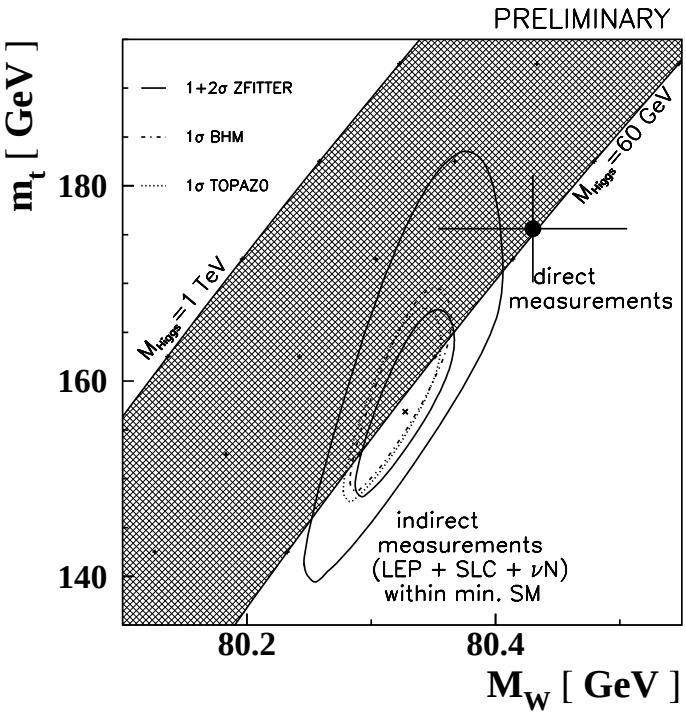

Fig. 33. – Contour plot showing the *top*-quark mass m_t versus the W-boson mass. The shaded area shows the SM prediction for the Higgs-boson mass (M_{Higgs} in the figure) between 60 GeV and 1 TeV. The theoretical predictions are performed by means of the codes `BHM` [136], `TOPAZ0` [111] and `ZFITTER` [138] (see ref. [7]).

include the uncertainties due to the error on $\alpha(M_Z)$ (inducing a m_t variation of about ± 4 GeV) and to missing higher-order electroweak corrections (affecting m_t by about ± 1 GeV).

By adopting the procedure of including the direct measurements of m_t among the input data, then typical results obtained are [7, 8]

$$\begin{aligned} & m_t = 173.1 \pm 5.4 \text{ GeV} , \\ & m_H = 115^{+116}_{-66} \text{ (or } m_H < 420 \text{ GeV at 95\% CL)}, \\ & \alpha_s(M_Z) = 0.120 \pm 0.003. \end{aligned} \tag{134}$$

From this fit, an indirect measurement of the W-boson mass M_W can be derived (see Fig. 33), *i.e.*

$$M_W = 80.375 \pm 0.030 \text{ GeV}. \tag{135}$$

This small error of 30 MeV on M_W from radiative corrections is clearly a challenge for future direct precision measurements of M_W at LEP2 and at the TEVATRON.

4˙2.2. Determination of the Higgs-boson mass. As already shown in Sect. **4**˙2.1, the electroweak precision data can be used to infer indirect limits on the mass of the yet elusive Higgs boson. As discussed in Sect. **3**˙2, the leading effect of the Higgs-boson mass on the observables is only logarithmic and correlated with m_t. These difficulties, associated with other problematic aspects that will be discussed later, naturally set the question how reliably the Higgs-boson mass m_H can be predicted from electroweak data. Clearly, the answer to this question is of utmost importance for planning the search for the Higgs boson at LEP2 and future accelerators.

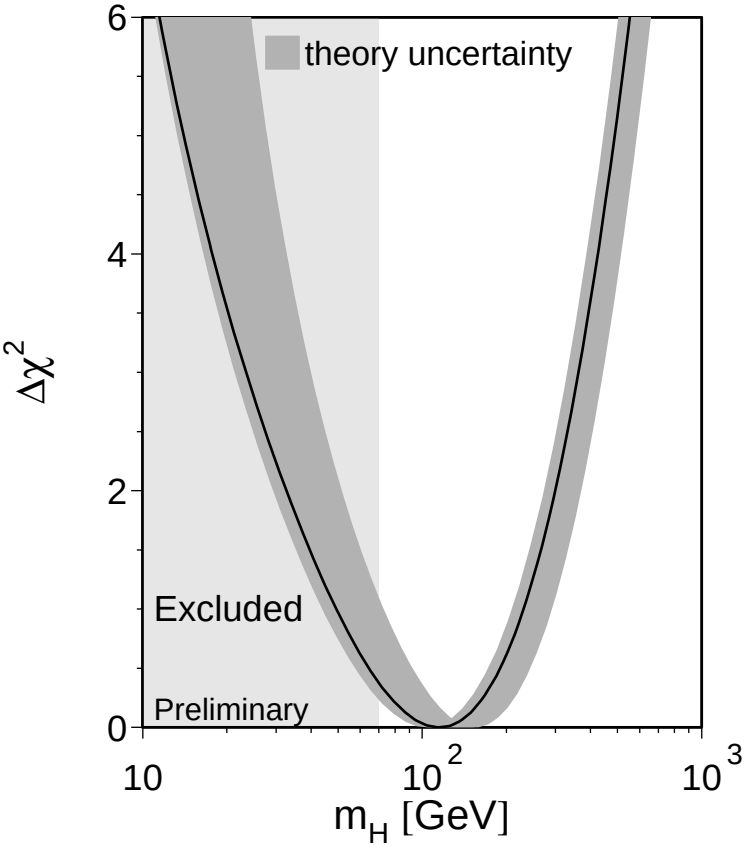

Fig. 34. – $\Delta\chi^2$ versus the Higgs-boson mass (see ref. [8]).

The indirect bounds that can be put on m_H from radiative corrections effects and their validity are matter of debate in the community of particle physicists and an unambiguous, unique answer to the above question can not be given, especially whenever one takes into account the large amount of investigations and detailed analyses present in the literature, many of which appeared after the discovery of the *top* quark at the TEVATRON [170–181]. Nonetheless, there are aspects concerning the constraints on m_H that are common to most of the analyses of precision data and therefore deserve special men-

tion. Before entering the details of the discussion, it is worth recalling that negative searches at LEP put the present lower limit on the Higgs-boson mass $m_H > 77$ GeV at 95% CL, derived assuming the validity of the minimal SM [182, 183].

The first common feature concerns the dependence of the fitted central value for m_H and of the 1σ errors on the set of input data considered. This rather strong dependence can be clearly seen, for example, from Tab. VII, looking at the variations of several tens of GeV on m_H, when considering the LEP data alone, all the available the data with the exception of M_W and m_t, and the whole set of data. It has been in particular emphasized by several authors that the exclusion of the SLD data for A_{LR} moves up m_H considerably, as a symptom of the clash between the $\sin^2\vartheta^l_{eff}$ determination from LEP and SLC. Actually, the SLD data alone leads to an unnatural bound on m_H at the 1σ level, in conflict with the limit from direct searches at LEP [161, 170, 184].

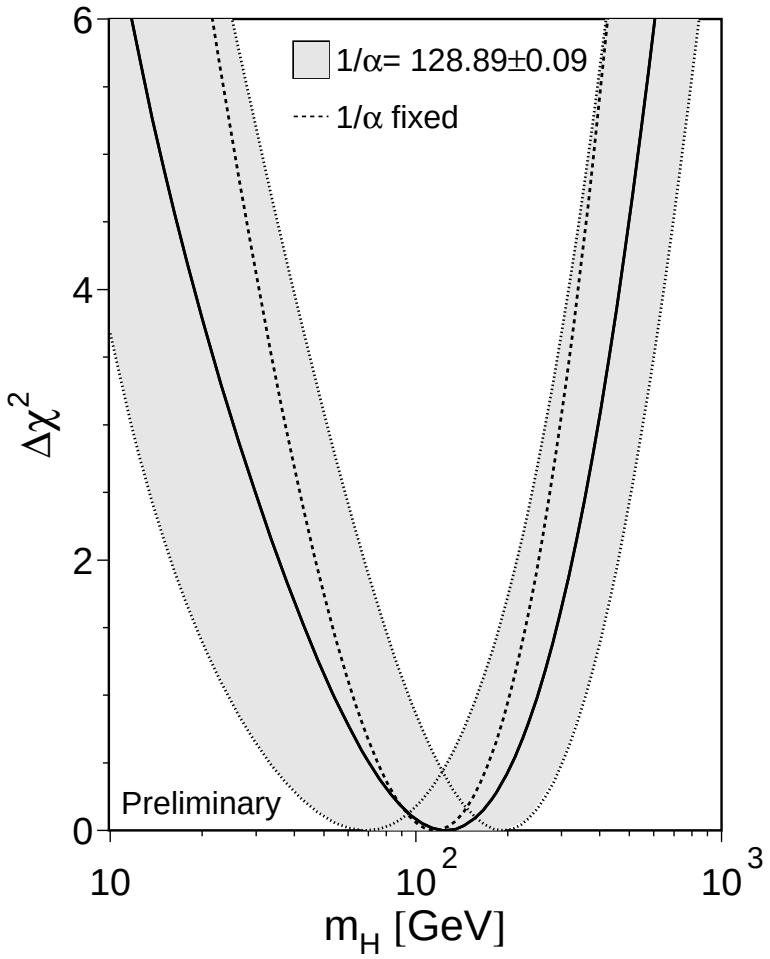

Fig. 35. – $\Delta\chi^2$ versus the Higgs-boson mass, taking into account the parametric uncertainty on $\alpha(M_Z)$ (from [185]).

A second common feature concerns the effect of including in the fit the theoretical

uncertainties, both *intrinsic* and *parametric*, of the SM calculations discussed in Sect. **3**·6. Contrary to m_t, that is marginally influenced by missing higher-order electroweak corrections and parametric uncertainties, the upper bounds on m_H are sensibly affected by parametric and intrinsic theoretical errors [179]. For example, the upper bound at 95% CL can vary by around 100 GeV as a result of different implementations of radiative corrections beyond the one-loop level, so that the χ^2 as a function of m_H appears as a band, representing the *intrinsic* theoretical error of the SM predictions, rather than a single curve (see Fig. 34).([6]) Similar considerations apply to the χ^2 distribution as a function of m_H when the input parameter of the fit $\alpha(M_Z)$ changes within its error. This parametric variation is actually larger than the one induced by different treatments of higher-order effects, pointing out the limitation imposed by the uncertainty on $\alpha(M_Z)$ in a sensible derivation of m_H from precision data (see Figs. 35 and 37).

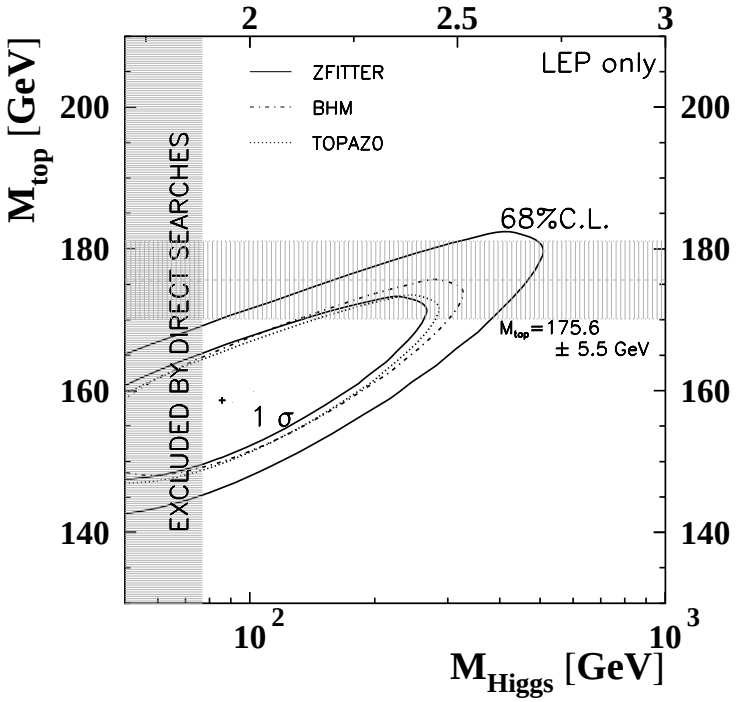

Fig. 36. – Contour plot showing the *top*-quark mass (M_{top} in the figure) versus the Higgs-boson mass (M_{Higgs} in the figure). The theoretical predictions are performed by means of the codes `BHM` [136], `TOPAZ0` [111] and `ZFITTER` [138] (see ref. [7]).

In the light of the above *caveat* in establishing a quite precise upper bound on m_H,

([6]) The recently calculated two-loop next-to-leading electroweak corrections of the order of $G_\mu^2 M_Z^2 m_t^2$ are expected to reduce this theoretical uncertainty, provided they are included in the standard electroweak libraries. Actually, after the completion of this work, the program `TOPAZ0` has been upgraded to include these corrections, together with the results of refs. [106] and [120] concerning QCD and QED corrections, respectively [146].

it turns out to be difficult going beyond the conclusion that the electroweak precision data, even when accounting for the direct measurement of m_t, imply an indirect upper bound at 95% CL of around 400-500 GeV, with a preference for a "light" Higgs boson of mass around $100 \div 150$ GeV (see Figs. 36 and 37).

4˙2.3. Determination of α_s. Besides the mass of the *top* quark and of the Higgs particle, the precision measurements of the electroweak parameters at the Z^0 pole provide the opportunity of an accurate determination of the coupling constant of the strong interactions α_s. Actually, e^+e^- machines are an ideal laboratory for QCD studies. Being the hadronic activity in e^+e^- collisions restricted to the final state, the measurement of α_s, as well as further tests of QCD, can be carried out in a particularly clean environment, where the experimental signatures of hadronic events are largely free of backgrounds (see ref. [186] for reviews on the subject).

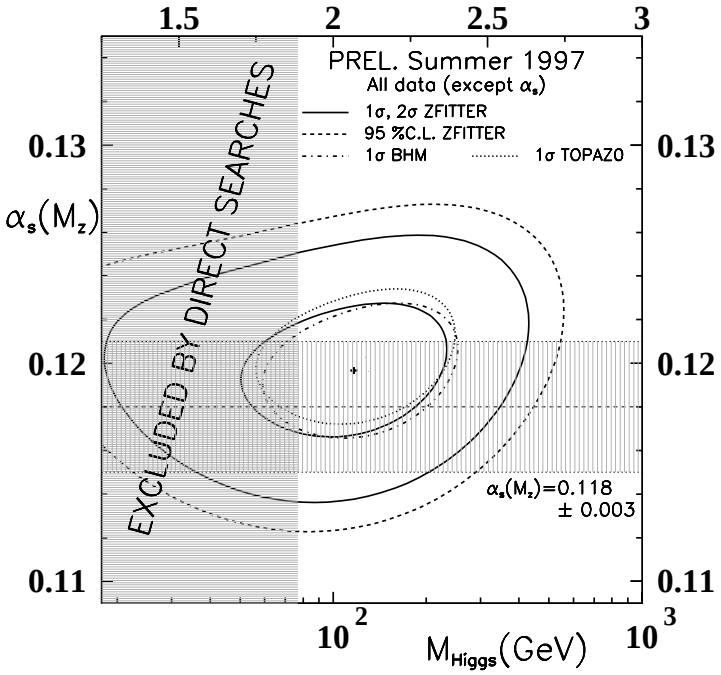

Fig. 37. – Contour plot showing $\alpha_s(M_Z)$ versus the Higgs-boson mass (M_{Higgs} in the figure). The theoretical predictions are performed by means of the codes `BHM` [136], `TOPAZ0` [111] and `ZFITTER` [138] (see ref. [7]).

Owing to the renormalization group dependence of the strong coupling constant on the hard energy scale Q (see the discussion in Sect. **3**˙3.2), a reference energy scale needs to be specified when quoting a value for α_s. Because of the large amount of data collected at LEP1 and SLC, it has become conventional to use $Q^2 = M_Z^2$, M_Z being the Z-boson mass, provided that the measured value of α_s is run from the scale at which the measurement takes place to M_Z (from now on, α_s will be used as a short-hand notation

for $\alpha_s(M_Z)$). This is in turn a great advantage since it allows to compare independent determinations of α_s in different reactions (e^+e^- annihilation, hadron-hadron collisions and deep-inelastic lepton-hadron scattering) at different energy scales, covering a range of Q^2 from roughly a few to 10^5 GeV^2. In particular, "low-Q^2" and "high-Q^2" results can be compared, thus providing a non-trivial check of the running of α_s as predicted by QCD, and a world-average value of α_s, as obtained by averaging all the available measurements once extrapolated to the Z-boson mass, can be derived.

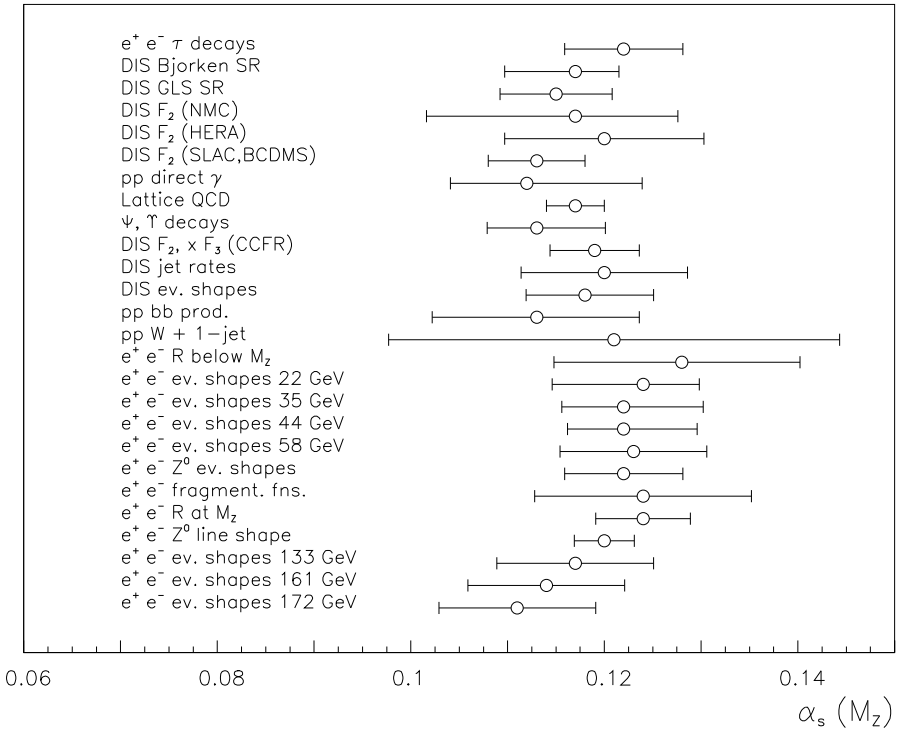

Fig. 38. – The $\alpha_s(M_Z)$ values and total errors from measurements at e^+e^-, lepton-hadron and hadron-hadron machines, and calculations from lattice QCD. The results are ordered vertically in $\sqrt{Q^2}$.

The data for the electroweak parameters can be used to measure α_s according to two different procedures, *i.e.*

- performing a fit, with α_s as a free parameter, to the single observable given by the ratio of hadronic to leptonic width R_l;
- performing a global fit to the whole set of the electroweak data (usually including the direct measurement of m_t), by allowing the three parameters m_t, m_H and α_s or the two parameters m_H and α_s to vary.

For the inclusive ratio R_l, the QCD corrections are known up to $\mathcal{O}(\alpha_s^3)$ for massless

TABLE VIII. – World averages of $\alpha_s(M_Z)$

Value	Error	Reference
0.118	0.003	ref. [187]
0.118	0.005	ref. [188]
0.118	0.004	ref. [189]
0.119	0.006	ref. [190]
0.119	0.004	ref. [154]
0.119	0.005	ref. [191]
0.119	0.004	ref. [8]

quarks, as discussed in Sect. **3**˙3.2, and the electroweak contributions are well under control since the main part of the weak radiative corrections, being common to the leptonic and hadronic Z^0 decay channels, cancel in the ratio of partial widths. From the experimental point of view, R_l, being a ratio, is known with a precision higher than that of single partial widths and is slightly affected by the luminosity uncertainty. Using the combined LEP result for R_l the fitted value of α_s is [7]

$$\alpha_s = 0.124 \pm 0.004(\text{exp.}) \pm 0.002(m_H), \tag{136}$$

where the experimental error is essentially due to the limited data sample and the theoretical error (m_H) derives from the residual dependence on m_H. It is worth noticing that the extraction of α_s from R_l doesn't require any specific knowledge about the hadronization mechanism. This α_s determination at the Z^0 peak is exactly analogous to the procedure followed when considering the published measurements for the ratio $R = \sigma(e^+e^- \to \text{hadrons})/\sigma(e^+e^- \to \mu^+\mu^-)$ at energies below the Z^0 resonance. The value obtained in such a case when fitting α_s to R as measured in the energy range $5 \leq \sqrt{s} \leq 65$ GeV is [188, 192]

$$\alpha_s = 0.128^{+0.012}_{-0.013} \pm 0.002(m_H), \tag{137}$$

where the second theoretical error is due to the variation of m_H in the range 60-1000 GeV.

An example of the second kind of determination of α_s from the Z^0 line-shape data is given by the three-parameter fit discussed at the end of Sect. **4**˙2.1, yielding the result [7,8]

$$\alpha_s = 0.120 \pm 0.003(\text{exp.}). \tag{138}$$

Detailed analyses of the theoretical uncertainties underlying the above determinations suggest that they can be estimated to contribute about ± 0.002 [193]. Actually, for all the input observables the non-perturbative effects are expected to be of the order of $1/M_Z$ and are hence usually neglected.

It should be kept in mind that the results for α_s from Z^0 data are obtained under the assumption that the hadronic width Γ_h is given by the SM. Therefore, a possible anomaly in Γ_b is a potential source of bias in the α_s derivation.

Besides the above quoted determinations of α_s, other measurements performed at e^+e^-, lepton-hadron and hadron-hadron machines need to be mentioned for their relevance, together with the calculations from lattice QCD. The interested reader is referred to the detailed compilations that can be found in refs. [188], [189], [190] and [8], together with references to the original literature.

A compilation of $\alpha_s(M_Z)$ determinations is given in Fig. 38, together with the corresponding total error. It is worth noticing that the most precise determination of α_s is obtained from a global fit to the whole set of precision data (Z^0 line-shape determination). By inspection of Fig. 38 it can be seen that there is agreement, within the errors, between "low-Q^2" and "high-Q^2" measurements. Contrary to a few years ago, where a discrepancy between low- and high-energy determinations was observed, the present status of α_s measurements is quite satisfactory, basically as a consequence of the fact that, while the α_s determination from deep-inelastic scattering and lattice QCD increased, the precise α_s measurement from fitting the electroweak data decreased. The problem of determining a world average of α_s has been considered by several authors. In Tab. VIII the most recent central values and corresponding errors are quoted, together with reference to the original literature.

4˙3. *Model Independent Approaches and Physics Beyond the Standard Model.* – The possibility of extracting predictions for the mass of the *top* quark and of the Higgs boson, as well as for $\alpha_s(M_Z)$, *via* the analysis of the electroweak precision data, as described in the previous sections, relies upon the assumption of the validity of the SM. In spite of the great success of such a strategy, it is of course important to exploit the high precision of LEP1/SLC measurements in order to test the validity of the SM in a way as independent as possible of the details of the underlying theory and, possibly, to derive also constraints on models of new physics beyond the SM. In order to achieve these goals, a model independent strategy for the analysis of precision data has to be organized. In the following, a model independent way of extracting Z^0 parameters (the S-matrix approach) is shortly described. Next, the ε parameterization as a tool for a model independent analysis of the Z^0 parameters is considered. At last, the implications of precision data for physics beyond the SM are briefly discussed.

4˙3.1. S-matrix approach. The original idea behind the parameterization of the Z^0 line shape introduced in ref. [113,148,149] was to allow a model independent extraction of the fundamental parameters of the Z^0 resonance, such as its mass, width and decay rates. In the following years this procedure has been posed on a firmer ground by appealing to the S-matrix theory [194–197]. Within this framework, the scattering amplitude can be cast into the form of a Laurent expansion around the Z^0 resonance as follows [198–200]:

$$A(s) = \frac{R}{s - s_p} + \sum_{n=0}^{\infty} B_n (s - s_p)^n = \frac{R}{s - s_p} + B_0 + \mathcal{O}(\Gamma_Z^2/M_Z^2), \tag{139}$$

where the quantities R, s_p and B_0 are complex numbers. Taking into account that an overall phase in the amplitude is unobservable, the cross section depends on five real parameters, which are separately gauge invariant, because the amplitude is an analytical function of s. The position of the complex pole defines the mass M and the width Γ in a gauge invariant and process independent way [201–203] through the relation

$$s_p = M^2 - iM\Gamma. \tag{140}$$

In the expansion given by eq. (139), the photonic contribution to the amplitude is part of the background denoted by B_0. Another approach followed in the literature [204] is to introduce explicitly the photon exchange contribution according to the parameterization

$$A(s) = \frac{R_Z}{s - s_p} + \frac{R_\gamma}{s} + B(s), \tag{141}$$

which has been implemented in the computer code SMATASY. In principle the parameterization of eq. (141) may lead to some difficulties related to the fact that the coefficients R_γ and B_i are not independent quantities [200, 204], but they disappear if a truncated version is employed. Neglecting terms of the order of Γ^2/M^2, the cross section for a given final state can be written in the following form [205]:

$$\sigma(s) = \frac{4}{3}\pi\alpha^2 \left[\frac{r_T^\gamma}{s} + \frac{s r_T + (s-M^2) j_T}{(s-M^2)^2 + M^2\Gamma^2}\right], \tag{142}$$

where r_T^γ is the photon exchange term and the parameters r_T and j_T are related to the Z-boson exchange residuum and to the γ-Z interference, respectively. On the same grounds as for the total cross sections, the asymmetries can be characterized around the Z^0 resonance by two parameters [206]:

$$A(s) = A_0 + A_1\left(\frac{s}{M^2} - 1\right) + \mathcal{O}\left(\frac{s}{M^2} - 1\right)^2, \tag{143}$$

with

$$A_0 = \frac{r_A}{r_T} + \mathcal{O}(\Gamma^2/M^2), \tag{144}$$

$$A_1 = \left[\frac{j_A}{r_A} - \frac{j_T}{r_T}\right], \tag{145}$$

where r_A and j_A are the analogues of r_T and j_T for the numerators of the asymmetries. In order to allow for a realistic data analysis, the universal effects of ISR need also to be taken into account, following the procedures described in Sect. **3**˙4 and in Appendix A.

The Z-boson mass and width parameters extracted with the S-matrix approach described above differ from the commonly defined on-shell Z-boson mass and running width by two-loop and higher order corrections, resulting in a shift of 34 MeV and 1 Mev respectively, according to the following expressions [198, 207–209]:

$$M = M_Z - \frac{\Gamma_Z^2}{2M_Z} \simeq M_Z - 34\text{MeV}, \tag{146}$$

$$\Gamma = \Gamma_Z - \frac{\Gamma_Z^3}{2M_Z^2} \simeq \Gamma_Z - 1\text{MeV}. \tag{147}$$

Taking into account of the proper definitions, the Z-boson mass and width obtained by fitting the data with the S-matrix formalism are in agreement with those obtained within the SM, showing its internal consistency, even if the error on the Z-boson mass is larger in the S-matrix approach, because the γ-Z interference is a free parameter. The fact that the γ-Z interference is sizeable off peak can be used to reduce the error on the parameter j_T^{had}. Actually, by adding to the peak results also data above and below the resonance, the values obtained from such an analysis are $M_Z = 91.1882 \pm 0.0029$ GeV and $j_T^{had} = 0.14 \pm 0.12$ [8]. These values are to be compared with $M_Z = 91.1867 \pm 0.0020$ from the standard analysis, and $j_T^{had} = 0.22$ as the SM expectation.

4˙3.2. Model-independent analysis of precision data. Since new physics effects can be more easily disentangled in the analysis of the Z^0 parameters if not obscured by our ignorance of SM parameters, it is convenient to introduce variables that are as free as possible from large m_t effects and hence sensitive to new physics. This attitude is followed in the model independent approach proposed and further developed in ref. [210],

where the validity of the SM is not assumed *ab initio* and appropriate variables (the ε parameters) are defined in order to provide an efficient parameterization of the most important electroweak data with respect to the sensitivity to new physics. More specifically, four independent quantities, indicated as $\varepsilon_1, \varepsilon_2, \varepsilon_3$ and ε_b, are introduced in one to one correspondence with the observables $M_W/M_Z, \Gamma_l, A_{FB}^l$ (assuming lepton universality) and Γ_b, that are chosen as primary defining measurements of the ε parameters. From these input data, the strategy consists in isolating the key quantities $\Delta\rho, \Delta r_W, \Delta k, \varepsilon_b$, that, as discussed in Sect. **3**˙2, are the dominant effects in weak radiative corrections due to gauge bosons self-energies and vertex corrections to the $Zf\bar{f}$ coupling. Indeed, the four quantities $\Delta\rho, \Delta r_W, \Delta k, \varepsilon_b$, whenever calculated in the SM, are dominated, for sufficiently large *top*-quark mass values, by quadratic terms in m_t of the order of $G_\mu m_t^2$. In particular, Δr_W is connected to Δr defined by eq. (56) in Sect. **3**˙2 according to the definition $(1-\Delta r) = (1-\Delta\alpha)(1-\Delta r_W)$, in such a way that the running of α ($\alpha(M_Z) = \alpha/(1-\Delta\alpha)$) due to known physics is extracted from Δr. Furthermore, ε_b is introduced in order to take care of the important non-oblique corrections to the $Z \to b\bar{b}$ vertex discussed in Sect. **3**˙2. The explicit relations between the primary defining observables and the $\Delta\rho, \Delta r_W, \Delta k, \varepsilon_b$ factors can be found in the original literature [210, 211]. Since the aim, as already stressed, is to provide a parameterization unaffected as much as possible by the relative ignorance of m_t, it is convenient to keep $\Delta\rho$ ($\varepsilon_1 = \Delta\rho$) and ε_b and introduce, in place of Δr_W and Δk, the two following linear combinations

$$\begin{aligned} \varepsilon_2 &= c_0^2\Delta\rho + \frac{s_0^2\Delta r_W}{c_0^2 - s_0^2 - 2s_0^2\Delta k}, \\ \varepsilon_3 &= c_0^2\Delta\rho + \left(c_0^2 - s_0^2\right)^2 \Delta k, \end{aligned} \tag{148}$$

where s_0^2 is an effective weak mixing angle containing only photon vacuum polarization effects, given by

$$s_0^2 c_0^2 = \frac{\pi\alpha(M_Z)}{\sqrt{2}G_\mu M_Z^2}, \qquad c_0^2 = 1 - s_0^2. \tag{149}$$

In this way, contributions of the order of $G_\mu m_t^2$ do not enter ε_2 and ε_3, that contain only logarithmic terms in m_t. Quadratic *top*-quark mass effects are confined in ε_1 and ε_b. Furthermore, the leading logarithmic terms for large Higgs-boson mass are contained in ε_1 and ε_3. For instance, the leading expressions for the ε parameters within the SM can be written as [210, 211]

$$\begin{aligned} \varepsilon_1 &= \frac{3G_\mu m_t^2}{8\pi^2\sqrt{2}} - \frac{3G_\mu M_W^2}{4\pi^2\sqrt{2}} \tan^2\vartheta_W \ln\left(\frac{m_H}{M_Z}\right) + \dots \\ \varepsilon_2 &= -\frac{G_\mu M_W^2}{2\pi^2\sqrt{2}} \ln\left(\frac{m_t}{M_Z}\right) + \dots \\ \varepsilon_3 &= \frac{G_\mu M_W^2}{12\pi^2\sqrt{2}} \ln\left(\frac{m_H}{M_Z}\right) - \frac{G_\mu M_W^2}{6\pi^2\sqrt{2}} \ln\left(\frac{m_t}{M_Z}\right) + \dots \\ \varepsilon_b &= -\frac{G_\mu m_t^2}{4\pi^2\sqrt{2}} + \dots \end{aligned} \tag{150}$$

Finally, the relations between the defining observables and the ε_i can be inverted in order to get the formulae for the ε_i in terms of the data. The explicit formulae read as follows

$$\varepsilon_1 = -0.9882 + 0.011963\,\Gamma_l/\mathrm{MeV} - 0.1511\,x,$$

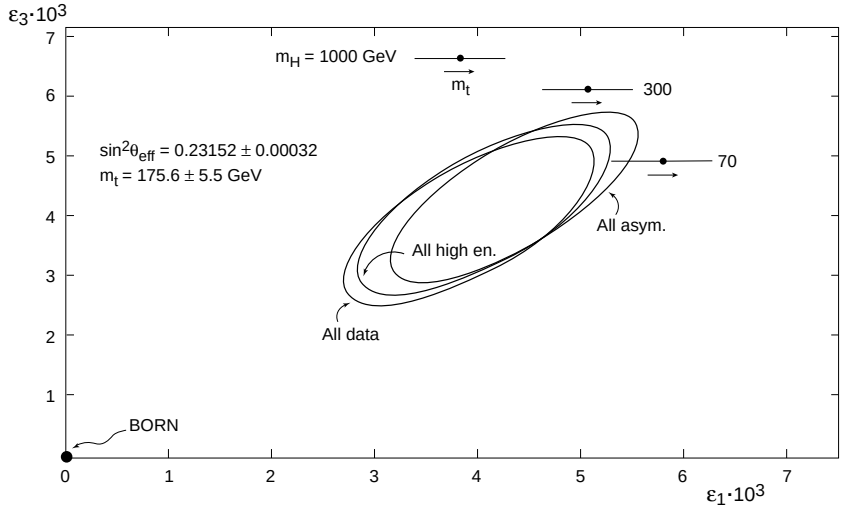

Fig. 39. – Electroweak precision data versus theory in the ε_1-ε_3 plane (from ref. [154]; see also refs. [210, 211]).

$$
\begin{aligned}
\varepsilon_3 &= -0.7146 + 0.009181\,\Gamma_l/\mathrm{MeV} - 0.69735\,x, \\
\varepsilon_b &= -0.62\,\varepsilon_1 + 0.24\,\varepsilon_3 + 0.436\;(\Gamma_b/\Gamma_{b0} - 1)\,, \\
\varepsilon_2 &= 1.43\,\varepsilon_1 - 0.86\,\varepsilon_3 + 0.43\,\Delta r_W, \qquad (151)
\end{aligned}
$$

where $x = g_V/g_A = 1 - 4(1 + \Delta k)s_0^2$ and Γ_{b0} is the value of Γ_b in the limit when all the ε's are neglected.

The parameters ε_1, ε_2 and ε_3 can be directly related to the variables S, T and U, that are other quantities proposed in the literature in order to parameterize the oblique corrections [212] and widely employed for model-independent studies of electroweak data [213]. However, while S, T and U are defined as deviations with respect to the SM predictions for specified values of m_t and m_H, the ε parameters are defined with respect to a reference approximation that is independent of m_t, in such a way that they are exactly zero in the SM in the limit of neglecting all pure weak loops [210]. Moreover, it is worth noticing that the definitions for the ε parameters are quite general because they do not refer to any particular model. Therefore, they are useful since they allow to perform a model-independent analysis of the electroweak precision data.

As a first step of such an analysis, it is possible to derive 1σ contours for the ε parameters by using the minimal set of data given by M_W/M_Z, Γ_l, A_{FB}^l and Γ_b. To include additional observables in the ε's analysis, further assumptions are required in order to maintain a consistent definition of the parameters. However, under appropriate hypotheses, the analysis can be generalized to include all the observables measured on the Z^0 peak, supplemented with low-energy electroweak measurements. The results obtained from the data can be then compared with the SM predictions, as a function of m_t and m_H, obtained by using computational tools that contain the state-of-the-art of radiative corrections. Examples of such a procedure are given by Figs. 39-40. From the comparison between theory and experiment in a given $\varepsilon_i - \varepsilon_j$ plane, it is possible with the present data to draw a number of significant conclusions. First, a preferred range for

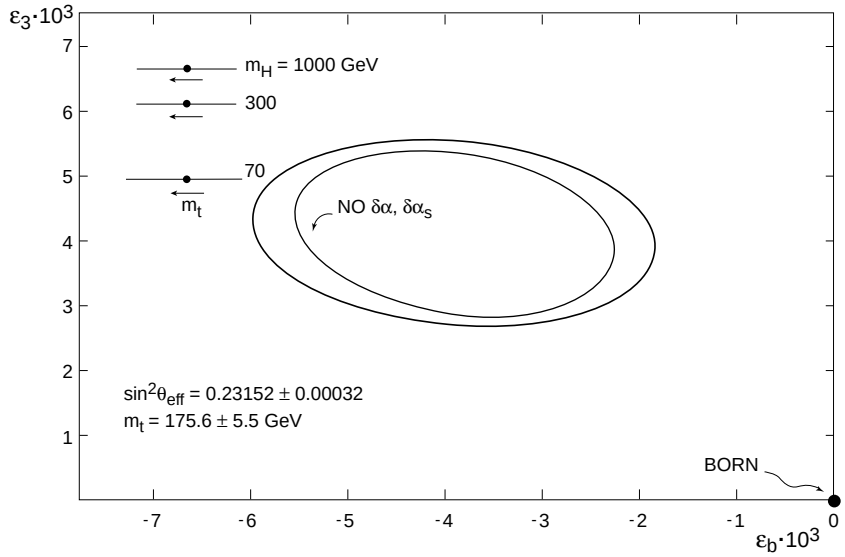

Fig. 40. – The same as in Fig. 39 in the ε_b-ε_3 plane (from ref. [154]; see also refs. [210, 211]). The effects of the errors on $\alpha(M_Z)$ and $\alpha_s(M_Z)$ are also shown.

the *top*-quark and the Higgs-boson masses can be inferred, according to a strategy that is different from what has been described in previous sections. Referring to the most recent data (with the TEVATRON result for m_t excluded from the analysis), one can see a preference of the precision data for a "light" Higgs boson and a m_t value somewhat lower than the CDF/D0 determination. These conclusions on m_t and m_H corroborate the results obtained from SM fits discussed in Sects. **4**˙2.1 and **4**˙2.2. Second, it is possible to observe a good agreement between the full SM predictions and the data. Noticeably, one can point out a strong evidence for pure weak radiative corrections, since the beautiful agreement between data and theory can not be simply explained in terms of an improved Born approximation based on tree-level SM plus QED and QCD corrections. This very important conclusion demonstrates by itself the constraining power of precision physics at LEP. The latter has been also emphasized by some authors that have studied the sensitivity of the data to a very peculiar subset of weak radiative corrections, namely the pure bosonic loops involving trilinear gauge-bosons and Higgs couplings [172]. As shown by these investigations, the LEP1/SLC data are so precise that they require the inclusion of such corrections in the SM calculation in order to precisely fit the data. Therefore, the present LEP1/SLC precision data feel the electroweak non-abelian couplings that are presently measured at LEP2 [184].

4˙3.3. Physics beyond the Standard Model. As already stressed, the main virtue of the ε parameterization is that they can be rather easily calculated in extensions of the SM, and therefore can be used to analyze models of new physics in the light of precision data. Typical examples studied in the literature are *technicolour models* [214], *models with an extended gauge group* [215,216] and the *Minimal Supersymmetric Standard Model* [217]. Also specific analyses within specific models of new physics beyond the SM have been considered in the literature, for instance concerning models with an extended

Higgs sector [218–221] or models with extra fermionic generations [222, 223]. The main conclusions of such analyses are summarized in the following.

Concerning *technicolour models*, it can be said that they tend to produce, in their typical realizations, corrections to the ε parameters (large and positive to ε_3, large and negative to ε_b) that are disfavored by the data [224]. In short, simple technicolour models are basically disfavored by LEP experiments [225], even if they can not be ruled out completely since particularly sophisticated versions with non trivial behaviour under the electroweak group could avoid their typical bad consequences [226].

As far as *models with an extended gauge group* are concerned, the case of the simplest models with an extra $U(1)$ (and with an associated new neutral vector boson) has been addressed in the literature [227]. For such a situation, two new parameters have to be introduced, the former being a mixing angle ξ in order to define the mixture of the standard and the new neutral vector bosons, the latter being the shift $\delta\rho_M$ induced at the tree-level in the ρ parameter by the above mixing. Considering the class of models based on E6 and for the left-right symmetric model, the main implication of precision data is that very strong constraints on ξ and $\delta\rho_M$ can be deduced. In particular, the amount of mixing allowed is very small, less than, say, 1%. It is worth observing that, in recent years, models containing an extra Z' boson with enhanced hadronic or almost vanishing leptonic couplings (hadrophilic or leptophobic Z') received particular attention as candidate models able to explain the simultaneous anomaly of R_b and R_c data (see for instance ref. [155]). At present, the R_b-R_c anomaly has substantially disappeared, but anyway these model have not been completely ruled out by the new data, and could be tested at LEP2 [228].

The *Minimal Supersymmetric Standard Model* (MSSM) deserves a special discussion since it is the most predictive framework beyond the SM. However, because of the very high number of free parameters, a convenient strategy when confronting theory and experiment is restricting to consider two limiting cases (the so-called "heavy" and "light" MSSM) rather than attempting a direct fit to the data. The "heavy" MSSM implies all supersymmetric particles to be sufficiently massive. In this limit, the MSSM predictions for electroweak data essentially coincide with the results of the SM with a light Higgs boson, say, lighter than 100 GeV [229]. Therefore, this particular realization of the MSSM can nicely accomodate the LEP data essentially in the same way as the SM does. In the "light" MSSM the masses of some of the superparticles are nearby their experimental lower limit. For such realization, the pattern of radiative corrections differs from that of the SM, with peculiar effects in vacuum polarization diagrams and $Z \to b\bar{b}$ vertex, that can be easily incorporated in the ε's [230]. These peculiar effects are reviewed in some detail in [231]. In particular, it is possible to find mechanisms able to explain a possible departure (if real) of R_b from the SM [232]. In conclusion, the MSSM agrees well with precision electroweak data, since it doesn't give rise, both in its "heavy" and "light" realizations, to effects that are inconsistent with the LEP measurements. This is due to the particular nature of the MSSM as new physics model that doesn't alter significantly the structure of the SM. This positive outcome of precision physics at LEP pointing towards supersymmetric extensions of the SM is corroborated by independent investigations of the MSSM with respect to the electroweak data performed in [160]. In these papers, instead of analyzing the MSSM implications on the data in terms of ε parameters, a more orthodox approach has been followed, namely a complete calculation of electroweak precision observables has been carried out, using one value for the Higgs-boson mass and $\tan\beta$, together with the set of SUSY soft breaking parameters fixing the chargino/neutralino and scalar fermion sectors. In this kind of analysis, an optimal

set of SUSY parameters can be extracted from a global fit to the data, showing how supersymmetry can consistently describe precision data without contradicting present limits from direct search on its mass spectrum (see Fig. 41).

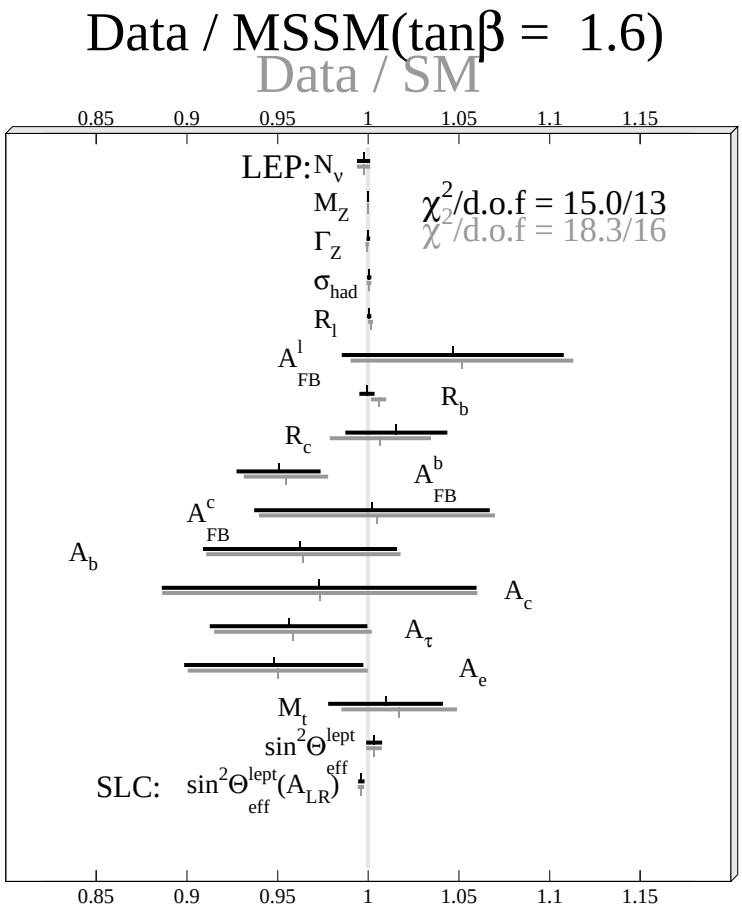

Fig. 41. – Experimental data normalized to the best fit results in the SM and MSSM (from ref. [160]).

Other specific models analyzed in the light of the LEP/SLC data concern the *extension of the Higgs-boson sector*. In the minimal SM the tree-level masses of the vector bosons are linked by means of the weak mixing angle through the relation $\rho = 1$, with

$$\rho = \frac{M_W^2}{M_Z^2 \cos^2 \vartheta_W}. \tag{152}$$

Since the Higgs-boson sector has not yet been tested with high accuracy, it is interesting to investigate a possible extension of the SM adopting an enlarged scalar sector. The simplest way to do this, by changing the tree-level expression of ρ, is to introduce, in addition to the minimal doublet representation, a Higgs-boson triplet with a vacuum expectation value different from zero in the neutral sector. In this case the masses of the vector bosons are no more related by the weak mixing angle, and the ρ parameter deviates from unity already at the tree level according to the following form:

$$\rho_{tree} = \frac{\sum_i v_i^2 (I_i^2 - I_{3i}^2 + I_i)}{\sum_i 2 v_i^2 I_{3i}^2}, \tag{153}$$

where $I_i(I_{3i})$ is the weak isospin (third component) of the $i-$th Higgs-boson multiplet, and v_i the respective vacuum expectation value. In addition to the standard Higgs boson, other Higgs particles belong to the physical spectrum. The scenarios arising in non minimal standard models with Higgs-boson triplets has been studied in refs. [218–220]. The calculation of the radiative corrections to precision observables within these non minimal models requires not only the evaluation of the extra loop diagrams involving the non standard Higgs bosons, but also an extension of the renormalization procedure. Due to the fact that the bare W- and Z-boson masses are not linked through the weak mixing angle, a fourth input data is necessary in order to perform the relative subtraction. In other words the ρ parameter is not calculable as in the minimal standard model but need to be fixed by a renormalization condition. The procedure has been discussed in ref. [51] within the $\overline{MS}$ scheme using the physical W-boson mass as the fourth data point, in addition to α, G_μ and M_Z. Recently, the radiative corrections to the full set of LEP1 electroweak observables have been calculated in a triplet model with a neutral Higgs boson and a pair of charged Higgs particles in addition to the standard Higgs boson [221]. The adopted renormalization framework is an extension of the on-shell scheme, where the fourth input data has been chosen to be the effective leptonic mixing angle at the Z^0 resonance. The interesting result of this study is that for a variation of the *top*-quark mass in the range $m_t = 175 \pm 6$ GeV, the predictions of the SM and of the triplet model are practically indistinguishable. As far as the Higgs-boson mass dependence is concerned, while the SM has a preference for a heavy Higgs boson from the observable Γ_Z and for a light Higgs boson from the mixing angle measurement, in the triplet model a light Higgs particle is compatible with all precision observables.

Models with *extra fermion generations* have been also investigated. As previously discussed, one of the achievements of the LEP experiments is the determination of the number of light neutrinos ($N_\nu = 2.993 \pm 0.011$) and hence of the number of fermionic generations. However, the theory does not exclude the presence of new sequential quark-lepton generations with heavy neutral leptons, whose production would be kinematically forbidden at LEP. The experimental lower bounds on the masses of the hypothetical new fermions available in the literature (including LEP1.5 data) are of about 60 GeV for the leptons and 100 GeV for the quarks [222]. In the literature, the indirect bounds obtained through the study of their effects on radiative corrections for LEP1 electroweak observables [222, 223] have been examined. A large mass splitting between the members of the doublets would spoil the agreement with the precision data, so the new heavy fermions should be almost degenerate in mass within a doublet. In order to reduce the number of parameters, a reasonable assumption is to work with quarks and leptons of equal masses. Within this scenario, the effect of one new generation can be compensated by increasing the fitted value of the *top*-quark mass. An analysis based on older data

sets shows that only at most two new sequential generations are allowed [222]. However, as a general *caveat*, it should be noticed that new experimental data, both from LEP2 and the TEVATRON, could modify this scenario. Considering the effects of electroweak vacuum stability and the absence of a Landau pole in the Higgs-boson potential allows to put upper bounds on the masses of the new fermions, depending on the scale at which new physics will appear. In the case of absence of new physics up to the grand unification scale, the upper bounds on the masses of the fourth generation are of the order of 100 GeV, a value viable for LEP2 direct searches [222].

As a last comment, it is worth pointing out that the present precision electroweak data coming from the LEP analysis can be used to derive constraints on the structure of a grand unified theory (GUT). In particular, within standard GUT's the evolution of the gauge couplings starting from the scale given by the Z-boson mass M_Z does not lead to the unambiguous identification of a grand unification scale. Viceversa, such a grand unification scale can be identified within the framework of supersymmetric GUT's [233]. This is at present considered as an indication of new physics beyond the SM, and in particular of supersymmetry [154].

5. – Physics at LEP2

As discussed in the Introduction, the ALEPH, DELPHI, L3 and OPAL experiments at LEP terminated in the fall 1995 their data taking at energies around the mass of the Z^0 resonance. After a short run at intermediate energies (the so-called LEP1.5 phase), the collider enters a new phase of operation far away the Z^0 peak, namely in the range $\sqrt{s} \simeq 161 - 192$ GeV. The energy upgrade of the LEP machine offers the possibility of exploring a new energy regime for electron-positron collisions, beyond the threshold of W-pair production (see Fig. 42). The precision measurements of Z-boson properties at LEP1/SLC can be therefore completed by the experiments at LEP2 with the precision determination of the W-boson properties. In addition to the precision physics of the W boson, experiments at LEP2 will continue to perform tests of the Standard Model (SM) in two-fermion production processes and in photonic final states, search for the Higgs boson, perform QCD studies as well as explore direct new physics signals [15]. Actually, as can be clearly seen from Fig. 42, there are at LEP2 many interesting processes with measurable cross sections, such as $e^+e^- \to f\bar{f}$, $e^+e^- \to \gamma\gamma$, $e^+e^- \to \nu\bar{\nu}\gamma$, $e^+e^- \to W^+W^-, ZZ$, the latter yielding four-fermion ($4f$) final states.

In the present section, the processes of main interest for precision studies of the electroweak theory at LEP2 are examined. The two-fermion production processes and radiative events are discussed, pointing out new physics aspects with respect to LEP1. The physics of the W boson in $4f$ production processes is then addressed, with particular emphasis on the status of theoretical predictions as well as first experimental results. The search for the SM Higgs boson in $4f$ final states is finally discussed.

5˙1. *Two-Fermion Processes.* – Although LEP2 was mainly conceived to measure precisely the properties of the W boson through the production of W pairs in e^+e^- collisions, the processes of quark and lepton pair production, still remaining among the most copious reactions at LEP2, is an important physics item. In this new energy regime, the two-fermion processes can be used to perform further tests of the SM, with enhanced sensitivity to the electroweak interference, as well as to obtain limits on possible extensions of the SM, such as the existence of new Z' bosons or effective $4f$ contact interactions [235]. However, the de-convoluted cross sections for these processes are

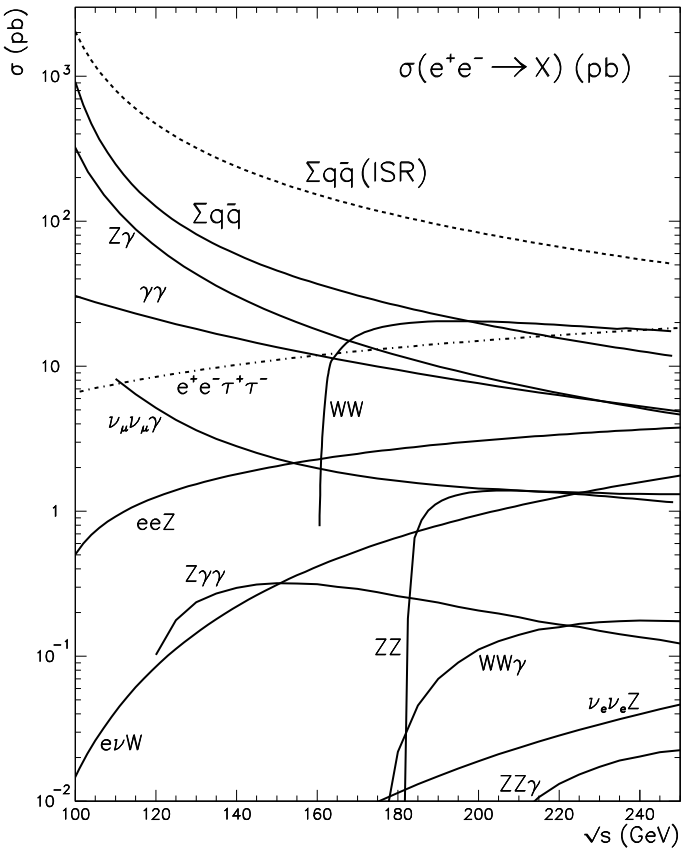

Fig. 42. – Standard Model cross sections at LEP (from [234]).

typically of the order of 10 pb in the LEP2 energy regime, *i.e.* three orders of magnitude smaller than the cross sections for the same processes at LEP1. Therefore, even when considering the highest final integrated luminosity expected at LEP2, *i.e.* 500 pb^{-1} [236], it will be possible to measure the two-fermion observables with a statistical error of the order of 1%, to be compared with the corresponding 0.1% of LEP1. Nonetheless, in order to meaningfully compare theory and experiment, precise predictions are still demanded and, therefore, radiative corrections need to be known with a good precision and incorporated in the theoretical calculations. To this aim, it is worth noticing that at LEP2 new aspects in the sector of radiative corrections to two-fermion processes do appear with respect to LEP1, noticeably [234]

- weak boxes (*i.e.* diagrams containing WW and ZZ internal lines) are at the level of a few per-cent of lepton and hadron cross sections, and hence no longer negligible as at LEP1;

- initial-state radiation (ISR) of hard photons is not inhibited as around the Z^0 peak, where, as discussed in Sect. **3**˙4, the Z-boson width Γ_Z acts a natural cut-off; consequently, hard-photon bremsstrahlung corrections become numerically relevant at LEP2.

The phenomenon of the so-called Z^0 *radiative return* constitutes the main manifestation of the relevance of hard-photon radiation in two-fermion production above the Z^0 peak. It corresponds to the emission of very energetic photons that reduce the two-fermion effective centre of mass (c.m.) energy back to the Z-boson mass, and considerably enhance the cross section. Actually, one can observe an increase of about a factor of four in the total rate of two-fermion events at LEP2, between the tree-level and the QED corrected predictions. This effect directly arises from the dependence of the two-fermion cross section on the c.m. energy, when going from LEP1 to LEP2. Actually, the Breit-Wigner behaviour for $\sqrt{s} \simeq M_Z$, followed by a fast $1/s$ decrease after it, makes very likely the production of a $f\bar{f}$ pair with invariant mass $m_{f\bar{f}}$ clustered around M_Z, accompanied by the emission of a real photon carrying away the residual energy. In fact, the photon energy spectrum shows a pronounced peak around the value $(1-M_Z^2/s)\,\sqrt{s}/2$, corresponding to those events (LEP1-like events) with an effective c.m. energy after ISR of $\sqrt{\hat{s}} \simeq M_Z$ (Z^0 *radiative return*) .

The above comments are referred to s-channel annihilation processes. As far as large-angle Bhabha scattering is concerned, it is worth noticing that already some GeV off-resonance the cross sections is dominated by t-channel photon exchange. Hence, large-angle Bhabha scattering at LEP2 is much more similar to small-angle than to large-angle Bhabha scattering at LEP1 (see ref. [18] for a detailed discussion).

5˙1.1. Weak corrections. As already discussed in Sect. **3**˙2, the one-loop pure weak corrections to $e^+e^- \to \gamma Z^0 \to f\bar{f}$ arise from those diagrams that involve corrections to the vector boson propagators, from the set of vertex corrections (with the exclusion of the virtual photon contributions that are accounted among the QED effects) and from the box diagrams containing the exchange of two *massive* gauge bosons. In fact, the box diagrams where at least one boson is a photon are classified as belonging to the QED corrections simply because they are IR divergent and need to be combined with the photonic initial-final state interference in order to get a meaningful result. Therefore, the genuine weak boxes are those with two W- and Z-boson propagators. Differently from the propagators and vertex corrections, they are ultra-violet finite in any gauge but the unitary one, where they actually give rise to UV infinities. Moreover, weak boxes introduce, in addition to s, a dependence on the scattering angle, that makes the parameterization of weak corrections in terms of "running" (s-dependent) effective couplings, successfully employed at LEP1, no longer viable at LEP2. In fact, since the box diagrams are negligibly small around the Z^0 pole, any dependence on the scattering angle can be neglected in the calculation of pure weak effects around the peak. Off resonance, *i.e.* in the LEP2 energy regime, the weak boxes become relevant corrections, due to the natural appearance of WW and ZZ thresholds. Therefore, they are actually included as relevant short-distance effects in the theoretical predictions for two-fermion physics above the Z^0 peak.

In order to make some quantitative statements on the effects of weak boxes on two-fermion observables, it is necessary to remember that the contribution of weak boxes is not gauge invariant by itself. It follows that a sensible evaluation of these corrections, as well as a comparison of their size as obtained from different computational tools

based on different theoretical framework, can not be carried out unless a gauge-invariant procedure of subtraction of weak boxes (the so-called *de-boxization*) is introduced. A possible procedure has been proposed in ref. [234]. Denoting the correction due to the WW box diagrams by $B_{WW}(\xi)$ as computed in a general R_ξ gauge, then $B_{WW}(\xi)$ can be split as

$$B_{WW}(\xi) \,=\, B_{WW}(1) + \left(\xi^2 - 1\right) \Delta(\xi). \tag{154}$$

In ref. [234], in order to get an estimate of the effect of weak boxes at LEP2, it was agreed to subtract from the full one-loop theoretical prediction $B_{WW}(\xi = 1)$. This contribution at LEP1 is of the order of 10^{-4} and its evaluation far from the peak can give an idea of the numerical effects introduced by the weak boxes at LEP2. The effect of weak boxes, as defined above, has been evaluated for the most relevant two-fermion processes ($e^+e^- \to \mu^+\mu^-, u\bar{u}, d\bar{d}, b\bar{b}$, hadrons) and for several c.m. energies. The main conclusion of this analysis, based on the predictions of different tools such as `TOPAZ0`, `ZFITTER` and `WOH` (see Sect. **3**˙5), is that the weak boxes introduce a significant relative correction of the order of a few per cent, especially around the WW threshold and at the highest LEP2 energies. In particular, for σ_μ the effect is positive, of the order of 1-2% at $\sqrt{s} = 161 - 175$ GeV and negative, of the order 1% at 205 GeV; for σ_{had} the correction is positive at $\sqrt{s} = 161$ GeV, of the order of 1%, negative and around 3% and 4% at 175 and 205 GeV, respectively. For the muon forward-backward asymmetry the effect of weak boxes is within 0.01.

5˙1.2. QED corrections. Because of the overwhelming effect due to ISR in the LEP2 energy regime discussed above, some contributions associated to the emission of hard photons that are irrelevant at LEP1 play a new rôle far above the Z^0 peak. Actually, the soft-photon dominance in the ISR mechanism emphasized in Sect. **3**˙4 for the energy region around the Z^0 resonance ceases to be valid at LEP2, and previously negligible hard-photon bremsstrahlung effects, both at the leading and next-to-leading level, show up. This implies the need for an upgrade in the treatment of QED corrections with respect to LEP1, since the numerical impact of the new corrections is typically at the 1% level and hence significant in view of the LEP2 experimental precision.

The first example of such effects due to hard-photon bremsstrahlung is given by the $\mathcal{O}(\alpha)$ NLO corrections arising from the emission of a hard *acollinear* photon by the initial state, because hard collinear photons are already taken into account by the leading logarithmic (LL) prescriptions (see Appendix A). Since these corrections are strongly affected by the imposed experimental cuts and can be very difficultly cast in a fully analytic form, one can evaluate their size by performing an exact $\mathcal{O}(\alpha)$ perturbative calculation, integrating it numerically and depurating the final result of the universal LL as well as of the non-leading (process dependent) soft+virtual corrections [237]. This procedure allows to isolate and quantify in a clean way the effect of hard-photon contributions in $\mathcal{O}(\alpha)$ ISR. The results of such an analysis can be found in ref. [237] for typical event selections (ES's) adopted by the LEP Collaborations, namely

- only a cut on the invariant mass of the event after ISR; this matches the ES adopted by recent analyses of hadron and lepton-pair production by the LEP Collaborations at LEP1.5 and LEP2 energies;
- fermion acceptance ($40^\circ \le \vartheta_- \le 140^\circ$) and acollinearity (acoll=$10^\circ, 25^\circ$) cuts in association with an invariant mass one.

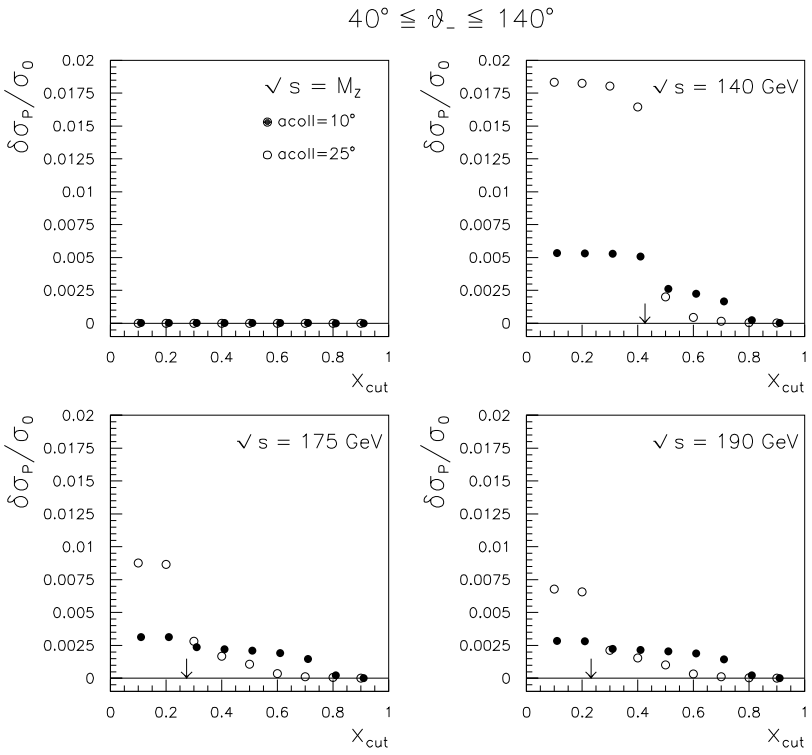

Fig. 43. – The theoretical error of the "Z^0-peak recipe" for the μ pair production cross section (relative deviation), as a function of the invariant mass cut x_{cut} defined by $s' > x_{cut}s$, s' being the invariant mass of the final-state fermion pair after ISR. The results correspond to two acollinearity cuts, for the same angular acceptance cut. The arrows point at $x_{cut} = M_Z^2/s$.

For the second ES, the results are shown in Figs. 43 and 44. They refer to four c.m. energies: $\sqrt{s} = M_Z$ (as a test case), 140, 175 and 190 GeV. In all the cases, the final state considered is $\mu^+\mu^-$.

Whenever a s' cut alone is imposed in the data analysis (that in practice coincides with what is done by the LEP Collaborations above the Z^0 peak), $\mathcal{O}(\alpha)$ non-leading hard-photon corrections are compatible with zero for hadronic and leptonic cross sections, and negligible at the 10^{-3} level for the lepton asymmetry. This applies both to loose and tight s' cuts, *i.e.* including or excluding the events with Z^0 radiative return. Therefore, for such typical ES's, those LEP1 calculations accounting for soft plus virtual NLO terms only (Z^0-peak recipe) can be safely extrapolated at higher energies without loss of accuracy. For more complicated ES's (see Figs. 43 and 44), including an acceptance and acollinearity cut, the theoretical error due to the neglect of the $\mathcal{O}(\alpha)$ non-leading hard-photon terms can grow up to about 2.5% for the cross section and to 1×10^{-2} for the forward-backward asymmetry. However, if the Z^0 radiative return is cut away, the above theoretical error is limited to 0.3% relative deviation for the cross section and 3×10^{-3} absolute deviation for the forward-backward asymmetry, that are acceptable in

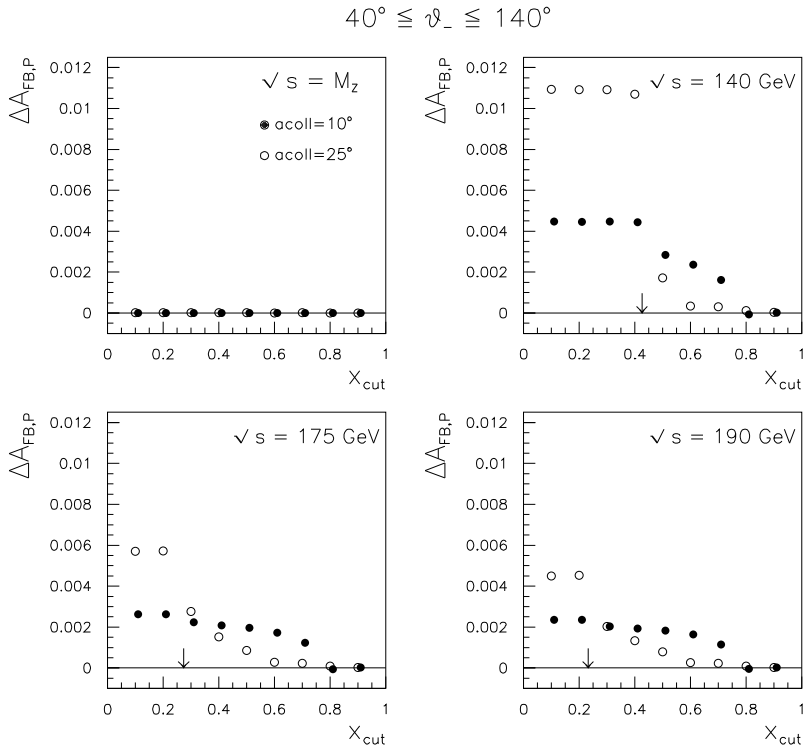

Fig. 44. – The same as in Fig. 43 for the forward-backward asymmetry (absolute deviation).

the light of the LEP2 experimental precision [237].

The second example of hard-photon contributions damped at LEP1 but no longer negligible at LEP2 comes from the IS second-order non-leading corrections and third-order LL contributions. The former arise from the configurations where a hard photon is radiated off in the direction of incoming electron or positron in association with a large-angle, acollinear additional hard photon, and provide corrections of the order of $\alpha^2 L$. The latter are due to the emission of three hard photons collinear to the colliding leptons, originating terms of the order of $\mathcal{O}(\beta^3)$. The $\mathcal{O}(\alpha^2 L)$ non-soft effects are exactly known from explicit perturbative calculation of the ISR spectrum [117]. They can be easily included in the radiator or flux function (see Appendix A) in such a way that the exact $\mathcal{O}(\alpha^2)$ calculation for an inclusive cross section is reproduced. The LL $\mathcal{O}(\beta^3)$ contributions, being universal photonic effects, can be kept under control employing one of the algorithms described in Appendix A. Referring in particular to the structure function (SF) method, these LL $\mathcal{O}(\beta^3)$ corrections are known for the electron SF [119, 238, 239] as well as the radiator [118, 120], both in factorized and additive form. It has to be noticed that the $\mathcal{O}(\alpha^2)$ non-leading non-soft corrections are in principle of the same order of magnitude as the third-order LL $\mathcal{O}(\beta^3)$ corrections. Therefore, a careful evaluation of the effects induced by higher-order hard-photon corrections in the LEP2 energy regime necessarily requires that both the contributions are simultaneously

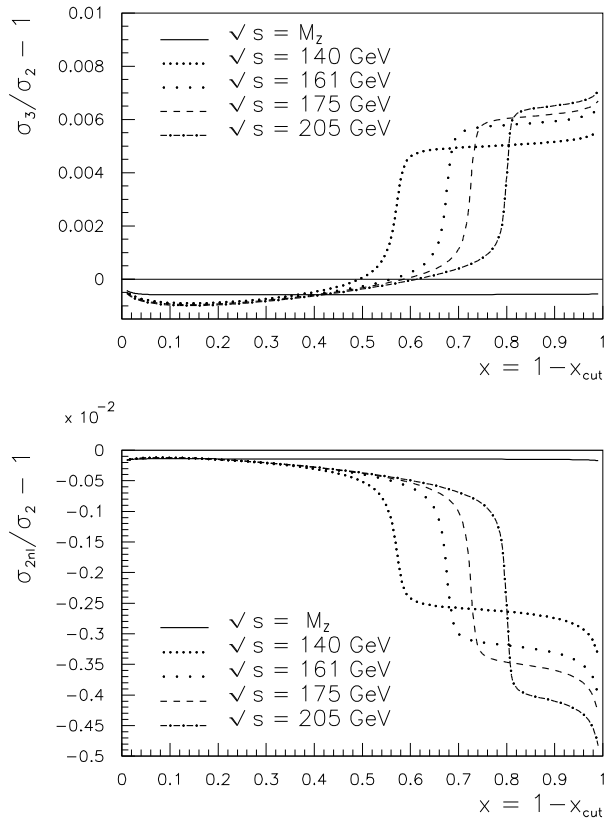

Fig. 45. – The effect of $\mathcal{O}(\beta^3)$ and $\mathcal{O}(\alpha^2 L)$ corrections on the $e^+e^- \to \mu^+\mu^-$ total cross section as a function of the s' cut (see ref. [120] for more details).

included in the theoretical predictions. The interplay between $\mathcal{O}(\alpha^2 L)$ and $\mathcal{O}(\beta^3)$ effects for the QED corrected muon-pair cross section, as a function of the s' cut defined as $s'/s \geq x_{cut}$, is shown in Fig. 45. The relative deviations with respect to the cross section computed by means of a standard additive radiator with up to $\mathcal{O}(\alpha^2)$ LL hard-photon corrections (σ_2) are shown for several c.m. energies. As can be seen, both the $\mathcal{O}(\beta^3)$ (upper window) and NL $\mathcal{O}(\alpha^2)$ (lower window) corrections amount to a contribution of several 0.1% when the Z^0 radiative return is included, but they tend to compensate one another, being of the same order of magnitude but of opposite sign. When the Z^0 radiative return is excluded, or close the Z^0 resonance, the NL $\mathcal{O}(\alpha^2)$ corrections are confined at the level of 0.01-0.02%, whereas the $\mathcal{O}(\beta^3)$ ones remain at the level of 0.05-0.1%. More precisely, the inclusion of the NL $\mathcal{O}(\alpha^2)$ plus $\mathcal{O}(\beta^3)$ corrections above the Z^0 peak causes a reduction of the QED corrected muon-pair cross section of about -0.1% when the Z^0 radiative return is excluded and an enhancement of about 0.25% when it is included. In the case of the hadronic cross section the effect of enhancement is around

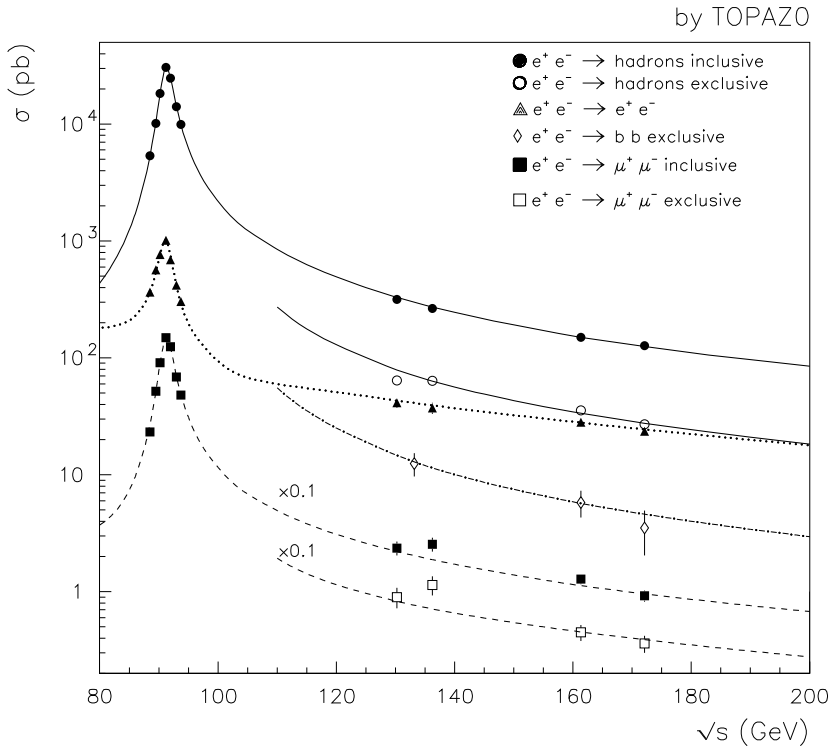

Fig. 46. – Data-theory comparison for two-fermion production cross sections at LEP. The experimental data can be found in [156] (on peak) and [240] ($\sqrt{s} > 130$ GeV). The theoretical prediction is performed by TOPAZ0 [111].

0.4%, *i.e.* comparable with the expected experimental precision for such an observable.

The theoretical predictions for cross sections and forward-backward asymmetries of two-fermion processes, as obtained by means of the code TOPAZ0 including all the weak and QED corrections discussed above, are compared with experimental data and shown as functions of the c.m. energy in Figs. 46 and 47, respectively.

5˙1.3. Radiative events. As already discussed in Sect. **4**, the study of single photon production in the process $e^+e^- \to \nu\bar{\nu}\gamma$ has been exploited at LEP1 as an alternative method for the determination of the invisible Z-boson width. At LEP2, the radiative processes, both with one and more final-state visible photons, still remain an important physics item, but within a different framework [234, 241]. For instance, they are used as QED or SM tests or, more generally, as tools to investigate physics beyond the SM. As a general feature, all these processes at LEP2 are affected by an error which is dominated by statistics and is of the order of some per cent. This in turn implies that a theoretical knowledge of the cross sections with a theoretical error of the order of one per cent is mandatory, thus requiring the inclusion of all the phenomenologically relevant radiative corrections.

The process $e^+e^- \to n\gamma$, $n \geq 2$, is well suited for testing QED. Actually, it is

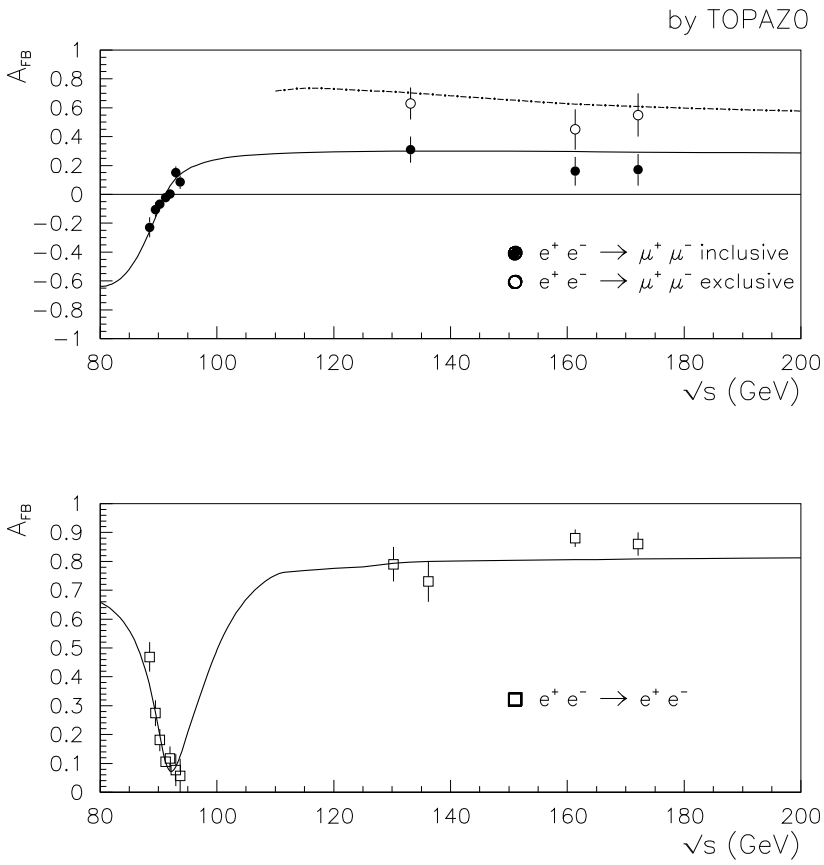

Fig. 47. – Data-theory comparison for the $e^+e^- \to \mu^+\mu^-$ and e^+e^- forward-backward asymmetries at LEP. The experimental data can be found in [156] (on peak) and [240] ($\sqrt{s} > 130$ GeV). The theoretical prediction is performed by TOPAZO [111].

marginally affected by weak or strong corrections, whose amount is below 1%. Since it provides a particularly clean signature, it can also be used to probe models predicting the existence of excited leptons or contact interactions. At present, the data-theory comparison confirms pure QED [242].

The production of single radiative events in the SM is dominated by the process $e^+e^- \to \nu\bar{\nu}\gamma$, with a sizeable background of radiative Bhabha events with the electrons lost. All these events manifest themselves as a single visible photon accompanied by missing transverse momentum ($\not{p}_\perp$). It is worth noticing that, at a difference from the LEP1 case where the radiative photon is essentially soft, at LEP2, due to the phenomenon of the Z^0 radiative return discussed above, the observable photon is essentially a very energetic one, and thus easily taggable (see Fig. 48). Standard computational tools employed by the LEP Collaborations for the evaluation of the SM cross sections are described in refs. [132], [244] and [243]. These events can also be used to probe processes beyond the SM, such as production of neutralino-pairs or excited neutrinos. Moreover,

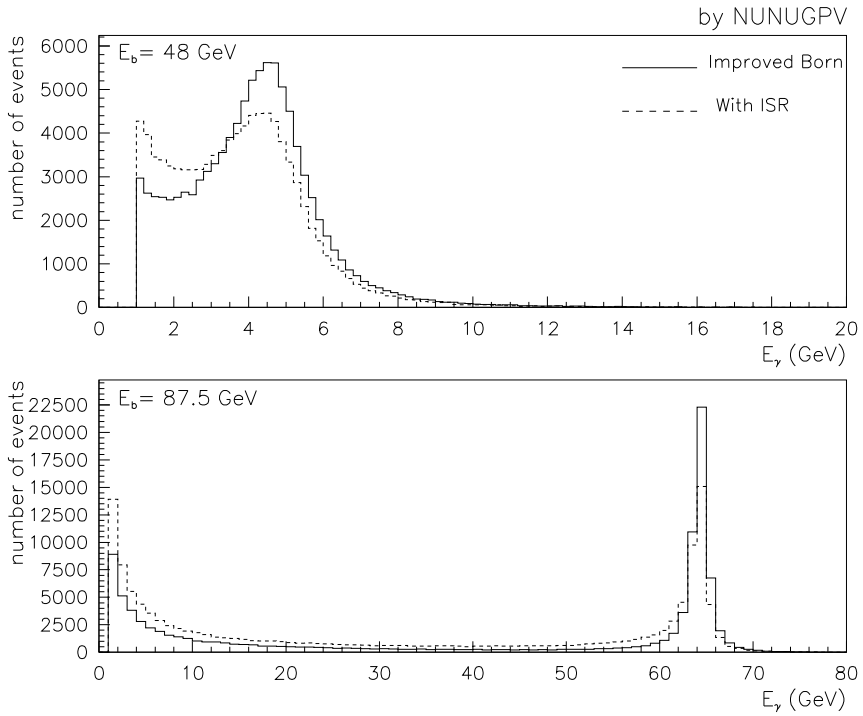

Fig. 48. – The energy spectrum of the observed photon at LEP1 and LEP2 energies. Numerical results by `NUNUGPV` [243].

they are in principle sensitive to $WW\gamma$ anomalous couplings (see Sect. **5**·3.2 for more details). Typical examples of new physics are the following:

- in the framework of the Minimal Supersymmetric Standard Model (MSSM), with R-parity conservation and the neutralino χ_1^0 as the lightest supersymmetric particle (LSP), the process of interest is $e^+e^- \to \chi_1^0\chi_1^0\gamma$ [245];
- in the framework of the so-called "no scale supergravity model" [246], the neutralino χ_1^0 should be visible through its radiative decay into a photon and a gravitino $\tilde{G}$, $\chi_1^0 \to \gamma\tilde{G}$, so that the process of interest is $e^+e^- \to \gamma\tilde{G}\tilde{G}$.

Unfortunately, both the processes are hardly detectable because of their too low rate. Actually, at present the data analyses do not point out any anomaly with respect to the SM predictions [247].

A radiative process that received particular attention during the last months is $e^+e^- \to \gamma\gamma + \not{p}_\perp$. Actually in the MSSM, such signatures could be produced by the process $e^+e^- \to \chi_2^0\chi_2^0 \to \gamma\gamma\chi_1^0\chi_1^0$, where χ_2^0 is the next-to-lightest neutralino decaying radiatively into $\chi_1^0\gamma$. In the framework of the "no scale supergravity model", instead, the process of interest is $e^+e^- \to \chi_1^0\chi_1^0 \to \gamma\gamma\tilde{G}\tilde{G}$. At present there is no evidence for physics beyond the SM, and the data are used to put constraints on the masses of the supersymmetric particles [247].

5˙2. *Four-Fermion Processes.* – As discussed in Sect. **5˙1**, two-fermion production processes certainly are an important physics item at LEP2, but the true novelty is represented by the processes involving the production of W-boson pairs (and their backgrounds), that at LEP2 energies are kinematically accessible with cross sections comparable to the ones typical of two-fermion production. The study of W-boson pair production can add information concerning two important items of the SM, namely the determination of the W-boson mass [248] and the structure of the triple gauge-boson couplings [249].

At LEP1, given the set of input parameters α, G_μ and M_Z (see Sects. **3** and **4** for more details) all the other observables can be derived within the SM. In particular, the W-boson mass M_W satisfies the relation (see eq. (61))

$$G_\mu = \frac{\alpha\pi}{\sqrt{2}M_W^2(1 - M_W^2/M_Z^2)}\frac{1}{1-\Delta r}, \tag{155}$$

which is essentially the SM prediction for the muon decay. In eq. (155), Δr represents the radiative corrections to the tree-level matrix element, and hence depends, in particular, on the *top*-quark and Higgs-boson masses, m_t and m_H. At LEP2, the W-boson mass is measured and therefore eq. (155) becomes a constraint that, *via* Δr, correlates m_t and m_H to one another. Of course, the more precise is the knowledge of the W-boson mass, the stronger is the resulting constraint, which can eventually shed light on the Higgs-boson mass.

Concerning the triple gauge-boson couplings, within the SM they have a specific form determined by the underlying $SU(2) \otimes U(1)$ symmetry. Any departure from such a specific form (anomalous couplings) is in general responsible of a bad high-energy behaviour of the cross sections, spoiling the renormalizability of the theory. As a matter of fact, at LEP2 energies an observable very sensitive to anomalous couplings is the angular distribution of the W bosons in W-pair production.

In order to exploit the experimental information as a stringent test of the SM, it is clear that one needs reliable theoretical calculations of the various W-pair production observables. It is also clear that the best knowledge is mandatory, *i.e.* the observables should be computed taking also into account all the relevant radiative corrections.

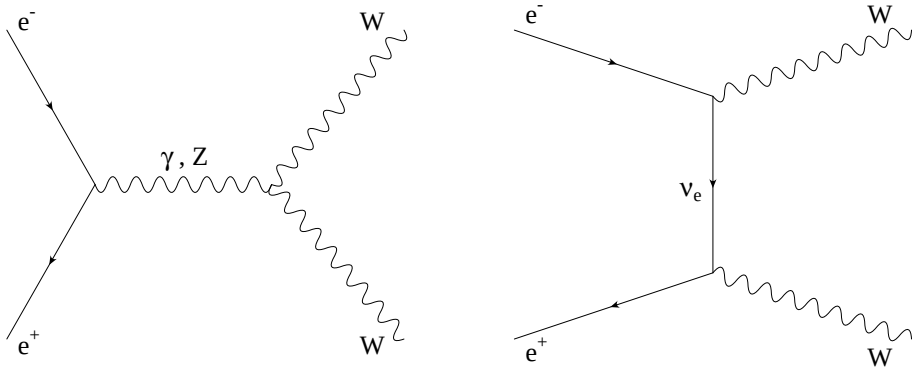

Fig. 49. – The tree-level Feynman diagrams for on-shell W-pair production.

A first step in this direction consists in calculating the cross section for W-pair production in the so called narrow-width (NW) approximation, *i.e.* assuming that the

W-boson width is zero and hence the W bosons are stable particles (see Fig. 49). A huge amount of work along this direction has been performed in the past [250–252], and today the process of on-shell W-pair production is known together with its full $\mathcal{O}(\alpha)$ radiative corrections.

On the other hand, the W bosons are, as well known, *unstable* particles, so that the effect of their finite width is in principle important, especially around the threshold region. Actually, whereas the cross section for the production of two real W bosons is exactly zero below $\sqrt{s} = 2M_W$, when the effect of the finite width is taken into account the cross section must become non-zero also below $\sqrt{s} = 2M_W$, due to the possibility of producing off-shell W's which subsequently decay (see Fig. 50). Moreover, the W bosons, being unstable, can be only intermediate states of the reactions, the true final states being *four-fermion* ($4f$) states. This in turn implies that, for a given $4f$ final state, besides the processes concerning the production and decay of a W-boson pair, one has to consider also those processes that lead to the same final state, but *via* different intermediate states (background processes).

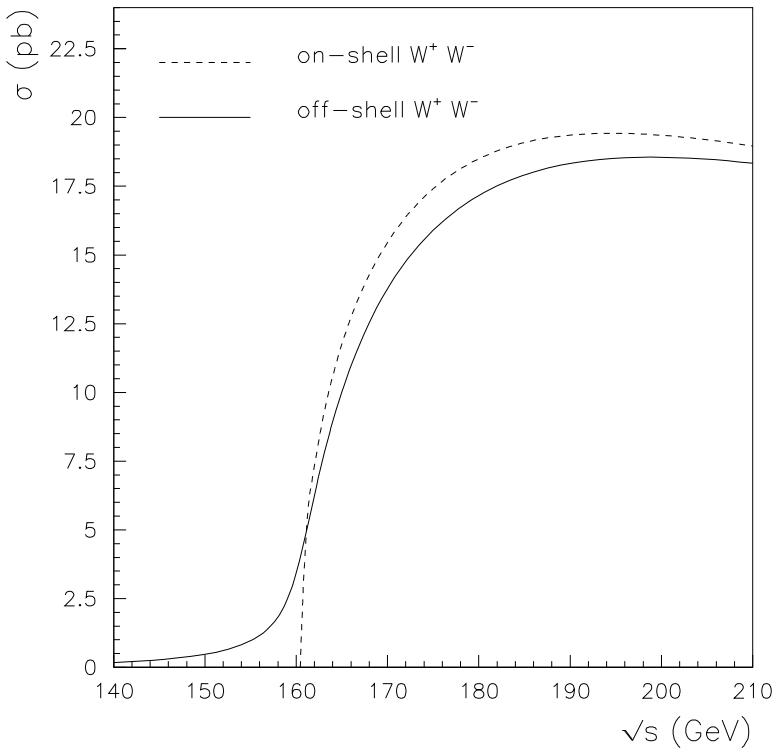

Fig. 50. – The effect of the finite W-boson width on the inclusive cross section.

The above comments point out the need of going beyond the NW approximation, both in order to obtain reliable cross sections and to study all the details concerning the W-boson decay products.

5˙2.1. Tree-level calculations. A first attempt in the direction of taking into account finite-width effects can be found in the approach described in ref. [253]. If one is interested in *inclusive* W-boson decays, then the total cross section can be approximatively factorized into two stages, namely off-shell W-boson pair production times their decay, as follows:

$$\sigma(s) = B_{f_1\bar{f}_2} B_{f_3\bar{f}_4} \int_0^s ds_1 \rho(s_1) \int_0^{(\sqrt{s}-\sqrt{s_1})^2} ds_2 \rho(s_2) \sigma_0(s, s_1, s_2). \tag{156}$$

In eq. (156) $\sigma_0(s, s_1, s_2)$ represents the total cross section for the production of two W bosons with squared masses s_1 and s_2, respectively (the Feynman diagrams of the production process at the tree level are still given in Fig. 49). Its explicit expression can be found in ref. [253]. $B_{f_a\bar{f}_b}$ is the branching ratio for the decay channel $W \to f_a\bar{f}_b$. $\rho(s_i)$ is the weight factor describing the inclusive decay of a W boson of squared mass s_i. It takes into account that the W bosons are produced off-shell and hence, rigorously speaking, they must be described by a propagator. The explicit expression of $\rho(s)$ is the following

$$\rho(s) = \frac{1}{\pi} \frac{\sqrt{s}\Gamma(s)}{(s - M_W^2)^2 + M_W^2 \Gamma(s)^2}, \tag{157}$$

where $\Gamma(s)$ is the total W-boson decay width. Equation (156) is a very simple and effective approximate description of the physics of W-pair production. Also, the main factorizable QED initial-state corrections to it have been considered in the literature and can be found in refs. [254–256]. On the other hand, its main limit is that it can provide at most double-differential spectra, namely the combined invariant mass distribution of the W bosons. If one is interested in the full description of the final-state products, a complete $4f$ calculation is mandatory.

A natural extension of eq. (156) to the description of a full $4f$ final state can be obtained by considering the diagrams of Fig. 51, where the W bosons are the intermediate states of the reaction and hence the full dynamical information on the final-state fermions is contained. The diagrams considered constitute the so called *CC03 class*, and describe the full $4f$ process in the so called double-resonant approximation. The complete calculation of the matrix elements corresponding to them, together with the appropriate four-body phase space, allows one to go beyond the "off-shell production times decay" approximation of eq. (156), and obtain the fully differential description of the process.

On the other hand, as already observed in Sect. **5**˙2, a given $4f$ final state can be obtained also *via* other sub-processes. For instance, if one considers a semi-leptonic channel, *i.e.* a channel in which one W-boson decays into hadrons and the other one into leptons, and restricts himself to those channels that do not have electrons in the final state, then the same final state as in Fig. 51 can also be generated by the diagrams of Fig. 52. These diagrams (background diagrams), together with the ones of Fig. 51, constitute the so called *CC11 class*, and are characterized by having a single W boson in the intermediate state, so that they are single-resonant. Of course, the full matrix element for such a final state is the sum of all the diagrams, and the squared matrix element includes also the interferences between double- and single-resonant diagrams.

In the presence of electrons in the final state, the situation is more involved. Actually, the full matrix element receives contributions also from additional t-channel diagrams, so that the total number of diagrams becomes 20 (the so called *CC20 class*).

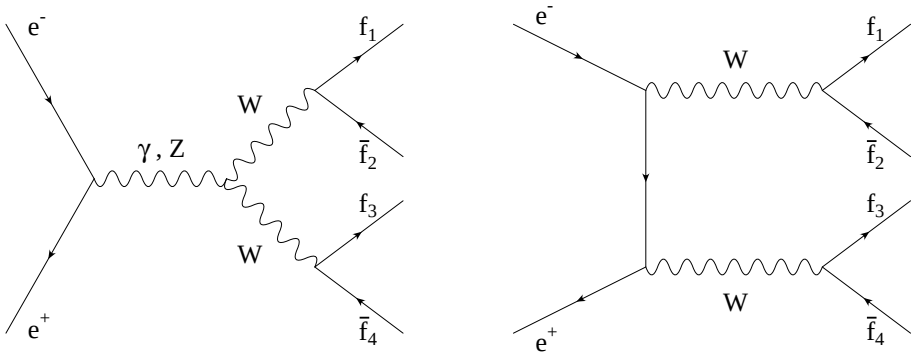

Fig. 51. – The tree-level Feynman diagrams for the CC03 class.

A full classification of the various Feynman diagrams contributing to a give $4f$ final state goes beyond the aims of the present paper. The interested reader is referred to refs. [234, 257, 258], and references therein, for a more detailed account. Here it is worth noticing that for particular final states, for instance fully hadronic final states, also neutral current (NC) and QCD backgrounds appear and become relevant.

The calculation of the scattering amplitudes for $2 \to 4$ processes is, already at the tree level, considerably more involved than the corresponding calculation for $2 \to 2$ processes, typical of LEP1/SLC physics. There are two main reasons for this, namely the fact that a single Feynman amplitude for $2 \to 4$ is algebraically more involved and the fact that, typically, for a given final state there are much more Feynman diagrams contributing. The calculational techniques adopted in the literature can be classified as follows:

- helicity-amplitude techniques: in this approach, the scattering amplitude for a given process, and for a given helicity pattern of the initial- and final-state fermions, is computed analytically as a complex number by exploiting the formal properties of the spin projection operators; the squared modulus of the amplitude is then computed numerically; the approach, in all its actual implementations (see refs. [259–262] and references therein), is particularly powerful for massless fermions, albeit also mass effects can be taken into account;

- automatic calculations: these approaches adopt both standard techniques for the evaluation of the squared matrix element [263] and the helicity amplitude formalism for the evaluation of the scattering amplitude [264], properly interfaced with software packages that render the calculation of cross sections almost automatic;

- numerical evaluation of the generating functional for the connected Green's functions: it is a new method, presented in ref. [265], in which the scattering amplitude is computed numerically by means of an iterative algorithm starting from the effective action of the theory and with no use of Feynman diagrams; it becomes strongly competitive with respect to standard techniques as the number of final-state particles becomes larger and larger.

5˙2.2. Gauge invariance. Being in the framework of a gauge theory, as is the case of the SM, means that the calculations of physical observables must be gauge invariant,

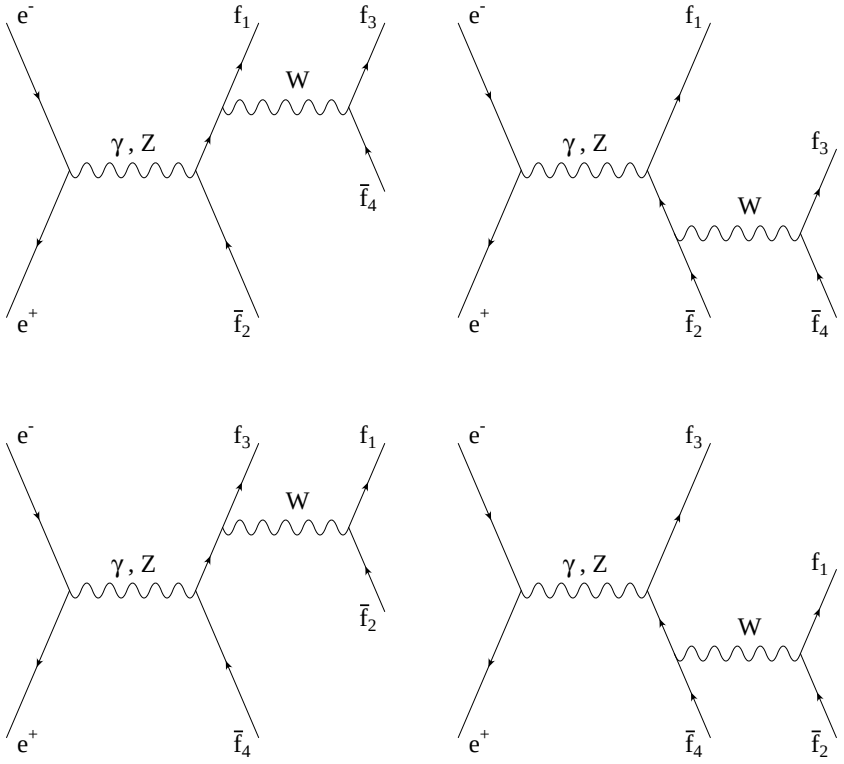

Fig. 52. – The additional eight tree-level Feynman diagrams for the CC11 class. Notice that in the semi-leptonic case ($e^+e^- \to u\bar{d}\mu^-\bar{\nu}_\mu$, for instance) the additional diagrams are seven; in the fully-leptonic case ($e^+e^- \to \tau^+\nu_\tau\mu^-\bar{\nu}_\mu$, for instance) the additional diagrams are six.

or at least the gauge violations have to be confined well below the required theoretical accuracy. In the case of $4f$ final states there are two sources of problems connected with gauge invariance in theoretical calculations (for a review see for instance ref. [266]).

The first one originates when the matrix element of the process is calculated considering only a subset of the Feynman diagrams contributing to the scattering amplitude. For example, in the case of W-boson production, the natural extension from the on-shell approximation to the more realistic off-shell production and subsequent decay would be the calculation of the three Feynman diagrams of the on-shell case with the two final-state fermionic currents attached to the virtual W-boson lines, *i.e.* the double-resonant diagrams of Fig. 51. In ref. [250] it has been shown that from the evaluation of the double-resonant diagrams in an axial gauge, gauge dependent terms arise, which exhibit a single pole structure in either of the two invariant masses and are cancelled when also the single-resonant diagrams (see Fig. 52) contributing to the process are evaluated. The single- and the non-resonant contributions are generally suppressed by a factor $\Gamma_W/M_W \simeq 2.5\%$ with respect to the double-resonant ones, but they need to be taken into account in view of the required theoretical accuracy.

Even when the calculation of all the tree-level diagrams contributing to a given $4f$ final state is performed, the problem of gauge invariance is not yet solved because of the

presence of singularities in the phase space due to the massive gauge boson propagators, which display poles at $p^2 = M^2$, p^2 being the invariant mass of the decay products of the unstable bosons. These singularities are cured by the introduction of the finite widths of the gauge bosons, which shift the poles away from the real axis. However, in field theory the widths arise from the imaginary parts of higher-order diagrams describing the gauge boson self-energies, resummed to all orders. So the tree-level amplitude is supplemented with only a subset of higher-order contributions and this can destroy the gauge invariance of the calculation.

A pragmatic approach, suitable for the construction of a lowest-order event generator, is the so called "fixed-width scheme", where the propagators $1/(p^2 - M^2)$ are systematically replaced with $1/(p^2 - M^2 + i\Gamma M)$ also for space-like momenta. This procedure has no physical motivation, because the propagator for space-like momenta does not develop any imaginary part. An improvement on this is the "running-width scheme", where the width is a function of p^2, equal to zero for space-like momenta, in agreement with the calculation of the imaginary part of the gauge boson self-energy.

Since the resonant diagrams are not gauge invariant by themselves, both of the above mentioned schemes violate gauge invariance, and their reliability needs to be checked by a truly gauge invariant scheme, even if it cannot be uniquely defined. In the literature several gauge restoration schemes have been studied. The simplest one is the "fudge-factor scheme" [267, 268], which amounts to calculate the matrix element without any width (so that the calculation is manifestly gauge invariant) and introduce an overall factor of the form $(p^2-M^2)/(p^2-M^2+i\Gamma M)$ for every singularity, in order to transform it in a resonance. The problem connected with this scheme is that when the double-resonant diagrams are not dominant, as is the case of charged current processes at energies below and at the W-pair production threshold, it can lead to large deviations [269].

Another possibility is the "pole scheme" [198, 270–272], where the complete amplitude is decomposed according to the pole structure in gauge invariant subsets of double-, single- and non-pole terms. Introducing the widths in the pole factors does respect gauge invariance. At present there is some debate about the correct way of implementing this scheme and about its validity in the vicinity of thresholds. Since the pole scheme is a gauge invariant decomposition of the amplitude according to its degree of resonance, it can be used as a starting point for the evaluation of higher-order corrections, as will be discussed in Sect. **5**˙2.3.

The most theoretically appealing solution to the gauge invariance problem is the "fermion loop scheme" [269, 273–275], where the minimal set of one-loop Feynman diagrams necessary for compensating the gauge violation caused by the self-energy graphs is included in the calculation. Since the lowest order decay widths of the gauge bosons are given by the imaginary parts of the fermion loops in the one-loop self-energies, according to this scheme the imaginary parts of all the other possible one-particle-irreducible fermionic one-loop corrections must be included. For the process $e^+e^- \to 4f$, after the resummation of the vector boson self-energies, the only left out contributions are given by the imaginary parts of the fermionic corrections to the triple gauge-boson vertex, which have been calculated in ref. [274] in the limit of massless fermions. The calculation has been extended in ref. [275] to take into account the complete fermionic one-loop corrections, including real and imaginary parts, and all contributions of the massive *top* quark.

Due to the complexity of the fermion loop scheme, the CPU time needed for the calculation of the cross section increases considerably with respect to the one performed within the fixed or running width scheme, based on a naive treatment of the bosonic

widths. For this reason, from a phenomenological point of view, it is important to quantify the amount of gauge violating effects in $4f$ processes of interest at LEP2. As a result of the detailed investigations pursued in refs. [274, 275], the violations connected with the gauge group $SU(2)$ are not relevant in the LEP2 energy range. They become important for energies reached at the next generation of linear colliders. The case of $U(1)_{e.m.}$ gauge invariance violation is different, since the effects are enhanced by a factor of $\mathcal{O}(s/m_e^2)$ in processes with an electron or positron in the final state, almost collinear to the incoming particle [268, 269, 273, 274]. This happens, for instance, for the CC20 process $e^+e^- \to e^-\bar{\nu}_e u\bar{d}$, which is particularly important for studying triple gauge-boson couplings. In ref. [274] it has been shown that the running width scheme for this process gives a totally wrong result when the minimum scattering angle of the electron is set to zero, unless it is improved with the fermionic corrections to the trilinear gauge boson coupling. On the other hand, the fixed width scheme, which does not violate the electromagnetic current conservation, gives reliable results. It is worth noticing that the results for the total cross section, obtained by means of different methods respecting current conservation, agree to $\mathcal{O}(\Gamma_W^2/M_W^2)$. In the limit $q^2 \to 0$, where q^2 represents the space-like momentum transfer of the electron through the photon, the fermion loop correction to the standard Yang-Mills vertex can be written in the following factorized form [274]:

$$C_{fl} = 1 + i\frac{\gamma_W(p_+^2)}{p_+^2 - p_-^2},$$

where

$$\gamma_W(q^2) = \frac{\Gamma_W}{M_W}q^2, \quad q^2 \geq 0,$$
$$\gamma_W(q^2) = 0, \quad q^2 \leq 0,$$

and $p_\pm$ are the squared momenta flowing in the $W^\pm$-boson propagators. This approximate factorized prescription can be easily implemented in a Monte Carlo event generator. However, the validity of the above formula is limited to the LEP2 energy range.

As a last comment, it is worth noticing that the problems connected with $U(1)_{e.m.}$ gauge invariance in the CC20 processes are rendered much more mild when a cut on the scattering angle of the outgoing electron is imposed. For a realistic cut of 10° the results obtained with the fixed width scheme are compatible with the ones obtained with the fermion loop corrections [274].

5˙2.3. Radiative corrections. As already discussed in Sect. **5**˙2, the main physical motivations of the LEP2 experiments are a precise determination of the W-boson mass and the study of the triple gauge-boson couplings. Since in the LEP2 energy range the integrated cross section is not very sensitive to the presence of anomalies in the Yang-Mill sector, the angular distributions are the best suited observables for the determination of the anomalous couplings. For this reasons the radiative corrections to both total and differential cross sections should be under control. Moreover, as will be illustrated in Sect. **5**˙3.1, one of the methods used for the W-boson mass measurement (the direct reconstruction method) relies upon the knowledge of the energy loss due to ISR defined as

$$< E_\gamma >= \frac{1}{\sigma_{tot}} \int dE_\gamma \frac{d\sigma}{dE_\gamma} E_\gamma, \tag{158}$$

which requires the best possible control of photonic radiative corrections. The other method (the threshold method) requires a good knowledge of the total cross section in the threshold region, *i.e.* a total cross section including all the relevant radiative corrections. However, it should also be kept in mind that, given the limited statistics of the LEP2 experiments with respect to LEP1, a theoretical relative accuracy of the order of 1% at the W-pair production threshold and of 0.5% at higher energy will be enough.

Before discussing various aspects of radiative corrections to $4f$ processes, it is worth recalling the rôle played by the W-boson mass at LEP2 with respect to the situation of LEP1. As already pointed out, in this last case it is an observable calculated by means of the input parameters α, G_μ and M_Z, and, with the inclusion of the radiative corrections to the μ decay, M_W shows a parametric dependence on m_t, m_H and α_s, as results from eq. (61). In the case of LEP2 it is more natural to consider M_W as a free parameter to be fitted by the experiments. As a consequence, eq. (61) can be solved with respect to m_{top} as a parametric function of α_s and M_H, to be compared with the direct measurement from the TEVATRON [8,276], allowing for a stringent determination of the Higgs-boson mass.

Turning now the attention to LEP2 processes, the ideal situation would be the knowledge of the complete set of $\mathcal{O}(\alpha)$ radiative corrections to processes with four fermions in the final state, but at present the calculation, due to its complexity, is not available. In fact, such a task would require the calculation of $\mathcal{O}(10^3 \div 10^4)$ one-loop diagrams. It is important to notice that, due to the presence of charged vector bosons in the Born amplitude, a separation between virtual photonic and pure weak corrections respecting the $SU(2)$ gauge invariance is not possible. Anyway a class of dominant corrections important for LEP2 physics can be singled out, and the effects of non-leading terms can be estimated relying upon the knowledge of the full one-loop electroweak corrections for the reaction $e^+e^- \to W^+W^-$, where the charged gauge bosons are considered in the on-shell limit [251, 252], including the bremsstrahlung process $e^+e^- \to W^+W^-\gamma$ [277]. Since the exact $\mathcal{O}(\alpha)$ calculation, already for on-shell W's, leads to complicated and lengthy expressions in terms of twelve s- and t-dependent effective couplings, the possibility of constructing an Improved Born Approximation in the LEP2 energy range has been studied [278], with the aim of providing simple and transparent formulae to be eventually implemented in Monte Carlo's for off-shell W-pair production.

Considering the realistic case of $4f$ production, in the following a brief account is given on the state-of-the-art about the three main classes of radiative corrections of interest for LEP2 physics: weak, QCD and QED corrections.

As already pointed out, at LEP2 the W-boson mass M_W should be a fitting parameter. By simply adding it to the three data points used as input parameters at LEP1 (see Sect. **3**˙2.2) leads to a four data points scheme, based on α, G_μ, M_Z and M_W, that is overcomplete, so that one of the typical LEP1 input parameters has to be replaced with M_W. Considering eq. (61) with $\Delta r = 0$, at least two tree-level schemes are possible:

$$s_W^2 = 1 - \frac{M_W^2}{M_Z^2},$$
$$g^2 = 4\sqrt{2} G_\mu M_W^2,$$

and

$$s_W^2 = \frac{\pi\alpha}{\sqrt{2} G_\mu M_W^2},$$

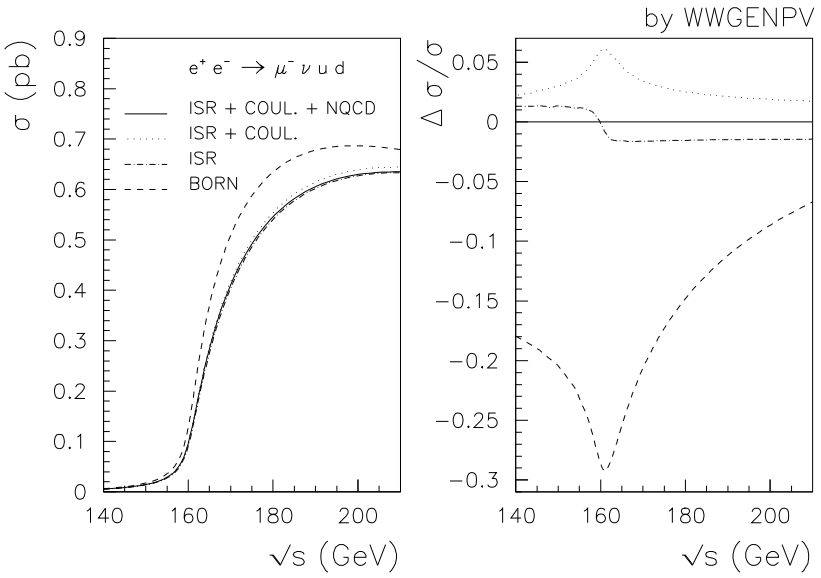

Fig. 53. – The contribution of various radiative corrections. The left window shows the cross section for the channel $e^+e^- \to \mu^-\bar{\nu_\mu}u\bar{d}$ at the tree level (dashed line) and including ISR (dash-dotted line), the coulombic correction (dotted line) and naive QCD corrections (continuous line). The right window shows the relative effect of each correction. $\Delta\sigma/\sigma$ is defined as $(\sigma_{ISR} - \sigma_{Born})/\sigma_{Born}$ for the dashed line (the relative effect of ISR), $(\sigma_{ISR+COUL.} - \sigma_{ISR})/\sigma_{ISR}$ for the dotted line (the relative effect of the Coulomb correction) and $(\sigma_{ISR+COUL.+NQCD} - \sigma_{ISR+COUL.})/\sigma_{ISR+COUL.}$ for the dash-dotted line (the relative effect of naive QCD corrections). Numerical results produced by `WWGENPV` [279].

$$g^2 = \frac{4\pi\alpha}{s_W^2}.$$

However, for practical calculations, the leading universal weak effects can be absorbed in the tree-level calculations by defining the input parameters in terms of G_μ and $\alpha(s)$. This choice, applied to the second scheme, is the one adopted in [258].

Going beyond this phenomenological attitude, it is necessary to talk about a complete one-loop calculation. By adopting the fermion loop scheme, all one-particle irreducible fermionic one-loop corrections are included, and a theoretically appealing strategy in this direction would be to calculate the remaining bosonic corrections, at least within a suitable approximation. The pole scheme [198,270,271] offers such a framework, provided that the c.m. energy is sufficiently far away from the threshold region (a few W-boson widths above). Actually, as stated in Sect. **5**˙2.2, this scheme is gauge invariant, contains the corrections for the production and decay of on-shell bosons as building blocks, and the number of Feynman diagrams to be evaluated is considerably reduced with respect to the complete set, because the potentially relevant corrections in the LEP2 energy region are given by the ones affecting the double-resonant diagrams. However, a simpler approximate procedure to take into account the leading bosonic corrections in the on-shell

W's limit has been recently suggested [280], which amounts to perform the substitution

$$G_\mu \to G_\mu/(1+\Delta y^{SC}_{bos}),$$

with $\Delta y^{SC}_{bos} = 11.1 \cdot 10^{-3}$. This replacement is equivalent to use the $SU(2)$ gauge coupling $g(M_W^2)$ at the high energy scale of M_W, defined by the theoretical value of the radiatively corrected leptonic W-boson width, $g^2(M_W^2) = 48\pi\Gamma_l^W/M_W$.(7) The essence of the approach is to use Γ_l^W instead of G_μ as input parameter, and it has been checked to work well in the case of on-shell W-pair production, providing results with an accuracy better than 1% with respect to the full one-loop results. Moreover, in ref. [280] it has been shown that strong cancellations occur between fermionic and bosonic corrections, at least at the level of on-shell W-pair production. Since the same behaviour can be reasonably expected also in the case of off-shell W-pair production [275], these results confirm that the fermionic loop contributions to $e^+e^- \to 4f$ need to be completed with some approximation of the bosonic corrections.

As far as the W-boson mass determination by the threshold method is concerned, it is worth mentioning a specific bosonic correction arising from the exchange of a relatively light Higgs boson between the slowly moving W bosons. Given the presently allowed range of variation for the Higgs-boson mass, it induces a theoretical uncertainty on the total cross section near the threshold of W-pair production. In the limit $m_H \ll M_W$ the leading behaviour in the on-shell case is given by [283]

$$\delta\sigma \simeq \frac{\alpha}{2s_W^2}\frac{M_W}{m_H}\sigma_{Born}.$$

In ref. [284] this correction has been computed for off-shell W-boson production neglecting the s-channel vertex contributions, due to the dominance of the ν exchange diagram at threshold. For an Higgs-boson mass of 60 GeV the correction amounts to about $0.8 - 0.9\%$ and decreases for higher Higgs-boson mass values (being less than 0.1% for $m_H = 300$ GeV). This effect translates into an uncertainty on the determination of M_W of 15 MeV from the LEP2 threshold run.

Concerning QCD corrections, when at least two quarks are present in the final state, *i.e.* in semileptonic and fully hadronic channels, also the strong radiative corrections to the $4f$ processes have to be considered. In the case of an inclusive set-up and in the CC03 approximation, the QCD corrections amount to use the QCD corrected values of the total and partial W-boson widths in the cross section. These have been calculated in the literature [285] and can be expressed in factorized form by the following replacements:

$$\Gamma_{Wu_id_j} \to \Gamma_{Wu_id_j}\left(1+\frac{\alpha_s}{\pi}\right),$$
$$\Gamma_W \to \Gamma_W\left(1+\frac{2\alpha_s}{3\pi}\right).$$

The impact of QCD corrections on the angular distribution of the decay products of a W boson and their application to the on-shell W-pair production has been discussed in ref. [286]. The QCD corrections for the inclusive set up and in the double-resonant

(7) The full one-loop electroweak and QCD corrections to the decay width of the W boson have been calculated in ref. [281]. An Improved Born Approximation absorbing the bulk of the radiative corrections can be obtained by writing the lowest order width in terms of G_μ and M_W [282].

approximations can be used as estimates of the corrections for more realistic cases. For this reason the above replacements are referred to in the literature as *naive* QCD corrections. The quality of the approximation when cuts on the jet directions are imposed has been discussed in ref. [287]. The effect of naive QCD corrections on the cross section of a typical $4f$ process is shown in Fig. 53.

Recently the exact $\mathcal{O}(\alpha_s)$ corrections to semileptonic and hadronic processes have been calculated [288] and compared with the naive approximation both in a fully inclusive situation and in the presence of ADLO-TH cuts [258]. The differences are below the foreseen experimental error at LEP2 for the semileptonic channels, while for fully hadronic final states the naive approach can give unreliable results. The analysis has been performed also at a c.m. energy of 500 GeV, typical of future e^+e^- linear colliders, where the naive approximation deteriorates at the percent level for NLC/TH cuts [289].

Concerning at last QED corrections, in principle they should consist of the virtual photonic corrections and the real-photon bremsstrahlung in order to have an infrared safe result. A separation between initial- and final-state radiation respecting the $U(1)$ electromagnetic gauge invariance, as in the case of LEP1 s-channel processes, is not possible because the ν-exchange diagram involves a non-conserved charge flow in the initial state. The problem is circumvented if the treatment of electromagnetic radiation is restricted at the LL level. The first theoretical calculations taking into account such effects in $4f$ productions can be found in refs. [290–296]. In this case the enhanced logarithmic terms coming from final-state radiation (FSR) cancel by virtue of the KLN theorem (when sufficiently inclusive cuts are considered) and the initial-state corrections reveal the presence of infra-red and collinear singularities, which are process-independent. Being phenomenologically relevant, these can be resummed to all orders by means of one of the methods described in Appendix A. Given the steep slope of the born cross section in the threshold region, the numerical effect of ISR is to reduce the cross section by several percent (see Fig. 53), depending on the c.m. energy [254]. By means of various procedures (for instance the variation of the scale in the LL theoretical predictions) it is possible to state that the overall accuracy of the LL QED corrections is of the order of 1%. Another possible way of estimating non-leading QED effects is the one followed in ref. [297], where a gauge invariant definition of ISR is given according to the current splitting technique. The electrically neutral neutrino of the t-channel diagram is split into two oppositely flowing charged leptons. One of them is attributed to the initial state to build a continuous charge flow, while the other one is attributed to the final state. In this way the $\mathcal{O}(\alpha)$ ISR form factor for s-channel processes used at LEP1 (see eq. (106)) is recovered, plus non-factorizing terms numerically small in the LEP2 energy range.

However, when aiming to study the impact of exclusive photon radiation on particular observables, such as the photon spectrum or the differential angular distributions of final-state particles in the presence of realistic experimental cuts, some improvements on the LL approximation have to be introduced. For example, in ref. [279] the transverse degrees of freedom of emitted photons have been introduced by means of the p_T dependent SF approach, in order to take into account the kinematical effects of the photonic radiation from all external charged particles. Alternatively, in ref. [298] the exclusive photonic contributions, including also multiple photon radiation from the W bosons, are implemented by means of a $\mathcal{O}(\alpha)$ YFS exponentiation. In this formulation the $\mathcal{O}(\alpha)$ corrections are implemented using the results for W-pair production in the on-shell limit.

In addition to the LL effects, a particularly sizeable photonic correction in the W-pair production region is the so-called *Coulomb singularity* (see Fig. 54). It originates from the electromagnetic interaction between the slowly moving W's. This effect is

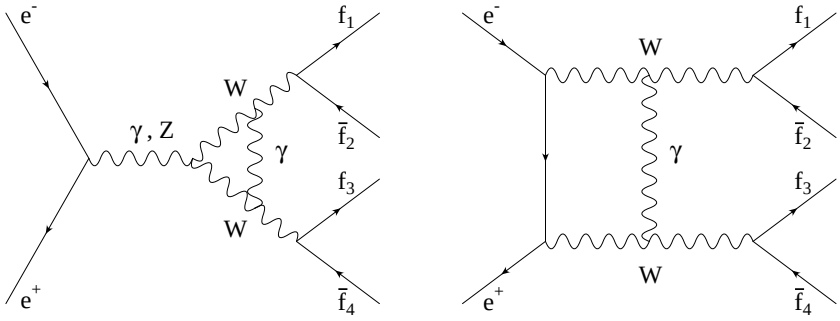

Fig. 54. – The Feynman diagrams for the Coulomb correction.

known since a long time [299] for stable particles to give a correction factor $\delta\sigma_{Coul}$ of the form

$$\delta\sigma_{Coul} = \frac{\pi\alpha}{2\beta}\sigma_{Born},$$

where $\beta = \sqrt{1 - M_W^2/E^2}$ represents the velocity of the W bosons. The off-shellness and the width of the W bosons modify radically the Coulomb interaction because they act as an effective cut off on the range of the electromagnetic interaction. Only for high enough energies, such that the typical interaction time between the W's is smaller than the W-boson lifetime, the effect derived for stable particles is substantially unchanged. In terms of Feynman diagrams the Coulomb singularity arises from three- and four-point scalar functions contained in the graphs with a photon line connecting the two virtual W bosons (see Fig. 54). Being the coefficients of these scalar functions gauge invariant, they can be worked out to give the following correction factor to the lowest order cross section resulting from the double-resonant diagrams [300]:

$$\delta\sigma_{Coul} = \sigma_{Born}^{CC03}\frac{\alpha\pi}{2\bar{\beta}}\left[1 - \frac{2}{\pi}\arctan\left(\frac{|\beta_M - \bar{\beta}|}{2\bar{\beta}\mathrm{Im}\beta_M}\right)\right],$$

with

$$\bar{\beta} = \frac{1}{s}\sqrt{s^2 - 2s(k_+^2 + k_-^2) + (k_+^2 - k_-^2)},$$
$$\beta_M = \sqrt{1 - \frac{4M^2}{s}}, \quad M^2 = M_W^2 - iM_W\Gamma_W - i\varepsilon.$$

where k_+, k_- are the four-momenta of the W^+ and W^-, respectively. By performing the on-shell limit on this formula the correction factor for stable particles is recovered. Higher-order effects due to the Coulomb correction are unimportant [300]. Numerically the Coulomb singularity amounts to a correction of the order of 6% at threshold and decreases smoothly to about 2% at $\sqrt{s} = 190$ GeV (see Fig. 53).

The QED corrections discussed above are phenomenologically relevant, gauge-invariant and include, besides the exponentiation of LL contributions, part of the full $\mathcal{O}(\alpha)$ electroweak corrections. The natural development is to consider the remaining non-leading $\mathcal{O}(\alpha)$ corrections. As stated previously, a step towards the calculation of the

bosonic contributions to the $\mathcal{O}(\alpha)$ radiative corrections to $4f$ processes can be performed within the pole scheme [198, 270, 271], even if this gives reliable results only a few Γ_W's above the W-pair production threshold. In the threshold scan the required theoretical accuracy is, on the other hand, more relaxed with respect to the high energy points. Given the dominance of the double-resonant diagrams in the LEP2 energy region, a good approximation is to consider the radiative corrections in the double pole approximation. These can be divided in factorizable and non-factorizable corrections (see Fig. 55 for an example of non-factorizable virtual QED corrections).

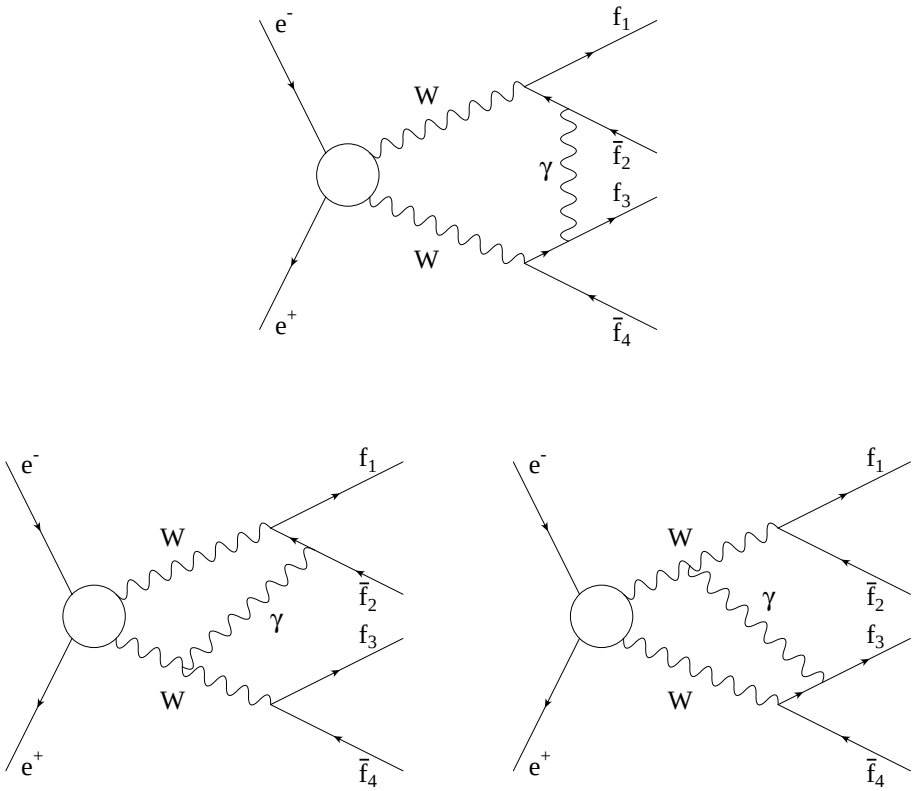

Fig. 55. – Examples of Feynman diagrams for non-factorizable virtual QED corrections.

The former contain manifestly two resonant W-boson propagators and can be distinguished between corrections to W-pair production and decay, while the latter do not. At present, the factorizable corrections to $e^+e^- \to 4f$ can be taken into account by using the known $\mathcal{O}(\alpha)$ corrections for on-shell W-pair production and decay. This is a first reasonable approximation to the full one-loop calculation, since the neglected terms are of the order of $\alpha\Gamma_W/\pi M_W$. This approach has been already followed in ref. [298]. Recently, the effects of non-factorizable QED diagrams in the soft-photon limit have been investigated [301–305]. As a result of this calculations, the non-factorizable corrections vanish in the case of initial-final state interference, and in all cases when the integrations over both invariant masses of the virtual W bosons are performed. Hence the W-boson production angle is insensitive to these corrections, so that the studies of anomalous triple

gauge-boson couplings at LEP2 are not affected by them. The case of the W-boson invariant mass distribution is different, since it receives a relative contribution of the order of 1%. The same corrections vanish for ZZ-mediated and ZH-mediated $4f$ processes.

5˙2.4. Computational tools. As done in Sects. **2**˙4 and **3**˙5, for small-angle Bhabha scattering and Z^0 physics, respectively, the basic features of the computer codes available for the calculation of observables of $4f$ production processes are briefly summarized. The aim of the discussion is to show how the theoretical results described in Sects. **5**˙2.1 and **5**˙2.3 are in practice implemented in computational tools used for the experimental analysis of W-pair production at LEP2. Since, as it will be discussed in Sect. **5**˙4, Higgs-boson physics at LEP requires the study of $4f$ final states, some of the programs developed for W-boson physics at LEP2 can provide also predictions for Higgs-boson production and decay. The goal of this discussion is to make an inventory of the theoretical approaches to the problem and of their realizations in the form of `FORTRAN` codes, rather then to give an exhaustive description of the programs. For a more detailed account of the programs, the reader is referred to refs. [258, 306, 307], and to the authors of the packages for the most recent developments.

The most of the $4f$ codes developed for LEP2 are Monte Carlo programs. Indeed, since the phase-space integration over the $4f$ final state involves seven dimensions, it can be more efficiently performed, especially in the presence of arbitrary kinematical cuts, by means of standard or adaptive Monte Carlo techniques. However, other numerical algorithms are available in the literature. For instance, semi-analytical programs, where a number of phase-space variables is integrated analytically, ending with two integrations over invariant masses (see eq. (156)) to be performed numerically, and deterministic tools have been developed. In particular, semi-analytical codes are useful as benchmark for the Monte Carlo's and for fitting purposes. Independent of the particular numerical algorithm employed, variance reduction techniques (such as importance sampling) are demanded and used in practice in order to take care of the peaking behaviour of the integrand.

Although different in many theoretical and technical aspects, most of the programs include the following common ingredients, necessary to match the LEP2 experimental precision (see the discussion in Sect. **5**˙2.3):

- the full or the numerically relevant set of Feynman diagrams for the processes $e^+e^- \to 4$ fermions;
- ISR in the collinear approximation, usually in the form of QED SF's;
- Coulomb correction;
- QCD corrections, in the naive realization, to the total and partial W-boson widths;
- possibility of anomalous couplings (see Sect. **5**˙3.2);
- interface to hadronization packages.

Some codes implement additionally QED FSR from fermionic legs. A few programs generate p_T-carrying photons, at the level of ISR and/or FSR, while others are able to calculate the matrix element for the radiative process $e^+e^- \to 4f + \gamma$. Finally, some programs include one or more of the gauge restoration mechanisms discussed in Sect. **5**˙2.2.

ALPHA [265] — This program is based upon an original theoretical algorithm recently proposed in the literature [265], and particularly powerful for the treatment of processes with a high number of final-state particles. Differently from all the other $4f$ codes, ALPHA computes automatically the tree-level $2 \to 4$ scattering amplitudes without making use of Feynman diagrams, but computing iteratively the saddle point of the path integral for given external momenta. All $4f$ final states can be treated. It can be used to predict the rate for the radiative process $e^+e^- \to 4f + \gamma$ [308].
CompHEP 3.0 [263] — It is a package of symbolical and numerical modules giving in output cross sections and distributions for processes with up to five particles in the final state, with a high level of automation. It uses the BASES&SPRING package for adaptive Monte Carlo integration and unweighted event generation. All $4f$ and 4 fermions + 1 photon final states can be treated. ISR is implemented using SF's in the collinear approximation.
ERATO [309] — It gives results for any $4f$ final state, using the "E-vector" formalism for the calculation of the $2 \to 4$ helicity amplitudes [259]. ISR in the collinear approximation and QCD corrections are allowed. A qualifying feature of ERATO is the incorporation of all CP conserving anomalous couplings. The fermion-loop scheme as gauge restoration mechanism is active. The program is a Monte Carlo that can run as an event generator and as an integrator. It has been interfaced to JETSET/HERWIG.
EXCALIBUR [310] — It is a Monte Carlo integrator that can give predictions for all possible $4f$ final states (excluding Higgs-boson exchange), with the possibility of selecting the contributions of subsets of diagrams and of particular spin configurations. The helicity amplitudes are computed using the Weyl-van der Waerden formalism [260]. ISR in the collinear approximation, Coulomb and QCD corrections, as well as anomalous couplings, are available.
GENTLE/4fan 3.0 [311] — It is a semi-analytical package designed to compute selected $4f$ production cross sections and invariant mass distributions for CC and NC mediated processes. SM Higgs-boson production in the NC case is included. All final states that do not contain identical particles, electrons or electron neutrinos can be studied. ISR in the collinear approximation is available both in the radiator and SF approach. Moreover, non-universal QED corrections to some classes of diagrams can be included. Coulomb and QCD corrections, as well as anomalous couplings, are implemented.
grc4f [312] — It is a Monte Carlo generator for all $4f$ final states automatically generated by the package GRACE [313]. All relevant radiative corrections and anomalous couplings are supplied. In particular, QED radiation is implemented by means of SF's for ISR, but a QED PS (QEDPS) [314] is also available both for ISR and FSR. Fermion masses can be kept nonzero everywhere. The numerical Monte Carlo integration and event generation is performed with the help of the package BASES&SPRING. Interface to hadronization is provided.
KORALW 1.03 [315] — It is a Monte Carlo that can treat any $4f$ final state *via* an interface to the GRACE library. All the phenomenologically relevant radiative corrections, anomalous couplings and interface to JETSET are provided. In particular, ISR is formulated according to the YFS exclusive exponentiation, thereby including the effect of transverse photon momenta, while FSR is treated within the SF approach. Recently, $\mathcal{O}(\alpha)$ non-leading QED corrections have been implemented [298] using the known results for on-shell W-pair production.
LEPWW [316] — This generator contains the CC03 and NC02 tree-level diagrams, supplemented with $\mathcal{O}(\alpha)$ ISR and FSR treated according to the package PHOTOS [317]. QCD corrections, anomalous couplings and interface to JETSET are provided. The program

aims at a 1-2% precision.

LPWW02 [318] — It is a Monte Carlo code containing the Feynman diagrams with two resonant W's and Z's, initial- and final-state radiation with SF's in the collinear approximation. Coulomb singularity and QCD corrections are incorporated. It is interfaced to JETSET.

PYTHIA/JETSET [319] — It is a general-purpose event generator for a multitude of processes in e^+e^-, ep and pp collisions. It is especially designed for detailed modelling of hadronic final states, rather than precision electroweak studies. It includes the CC03 diagrams for the Born matrix element and a hybrid SF+PS treatment of ISR. FSR is implemented according to a PS description. The Coulomb correction is available. Hadronization is built-in.

WOPPER 1.5 [320] — It is a Monte Carlo generator for unweighted $4f$ events. It includes the CC11 set of diagrams, ISR according to a PS algorithm, with finite p_T for photons generated according to the $1/(p \cdot k)$ pole. Coulomb and QCD corrections, anomalous couplings as well as interface to hadronization are provided.

WPHACT 1.0 [321] — This Monte Carlo program can compute all processes with four fermions in the final state. In particular, by virtue of the helicity formalism adopted that allows a semi-automatic calculation of the matrix elements [322, 323], finite b-quark mass effects are fully taken into account for NC processes. Higgs-boson production is included. ISR is included using SF in the collinear approximation. The Coulomb term and anomalous couplings are incorporated. Interface to hadronization is present.

WTO [324] — It is a deterministic code implementing the largest part of the $4f$ Feynman diagrams (including Higgs-boson signal) obtained with the helicity method described in [261]. ISR using SF's in the collinear approximation, anomalous couplings, QCD and Coulomb corrections are available. The fermion-loop scheme as gauge restoration mechanism is active. Some options for the estimate of the theoretical error are provided. Interface to hadronization is present.

WWF 2.2 [325] — This Monte Carlo generator is a kind of merger of an explicit $e^+e^- \to 4f+\gamma$ matrix element with SF's for the description of ISR beyond the LL approximation. However, non-leading corrections are implemented in an approximate way. The CC20 set of tree-level diagrams is included. FSR is implemented by using an explicit one-photon matrix element. All the other relevant radiative corrections, as well anomalous couplings and JETSET interface, are provided.

WWGENPV 2.1/HIGGSPV [279] — They are Monte Carlo generators computing the largest part of $4f$ tree-level matrix elements (including Higgs-boson production) derived according to the helicity formalism of ref. [261]. ISR and FSR are treated within the SF approach, including p_T/p_L effects. Coulomb and QCD corrections are implemented. Anomalous couplings and interface to JETSET are also available.

Before the start of the LEP2 operations, an extensive comparison of all the Monte Carlo and semi-analytical programs available for the analysis of $4f$ processes was carried out in the context of the working group "Event generators for WW physics" of the CERN workshop "Physics at LEP2" [258]. The predictions for both total cross sections and more exclusive observables of primary importance for the measurement of the properties of the W boson (such as W-boson production angle, invariant masses, radiative energy loss etc.) were compared in detail. "Tuned" comparisons generally showed very satisfactory agreement between the codes (at the level of 0.1%), pointing out a correct implementation of the advertised features and a high technical precision. Other highlights of the study can be summarized as follows

- the contribution of background processes is in general not negligible and therefore dedicated $4f$ codes are more suitable for precision measurements of the W-boson properties than general-purpose programs;
- for several observables, the effect of photon p_T is important on both ISR and FSR;
- the available estimates of the present theoretical error show that it is not much smaller than the expected experimental uncertainty; as a consequence, a more reliable estimate of the complete one-loop corrections to $e^+e^- \to 4f$ could give some relevant piece of information.

5˙3. *The W-boson Mass and Anomalous Couplings.* – As discussed in Sect. **5˙2**, the basic aims of the study of W-pair production in $4f$ final states at LEP2 are the precise direct measurement of the mass of the W boson, M_W, and the detection of possible anomalies in the γWW and ZWW vertices (*anomalous couplings*). All the decay channels of W-pair production are used in the experimental analysis: the hadronic channel $WW \to q\bar{q}q\bar{q}$ (45.6% decay fraction), the semi-leptonic channel $WW \to l\nu q\bar{q}$ (43.8%) and the leptonic channel $WW \to l\nu l\nu$ (10.6%).

5˙3.1. The W-boson mass. Two different methods are employed to measure the mass of the W boson at LEP2 [248]:

- the threshold method;
- the direct reconstruction method.

The former determination exploits the strong sensitivity of the W^+W^- production cross section to the W-boson mass near the nominal threshold; in the latter method, the Breit-Wigner resonant shape of the invariant mass distribution of the $W^{\pm}$-boson decay products is directly reconstructed, thus yielding M_W. The statistically most precise determination comes from the direct reconstruction method, since most of the LEP2 data is and will be collected at energies well above the threshold. Furthermore, very different systematic errors affect the two strategies, that therefore can be considered as complementary methods able to provide an internal cross-check on the W-boson mass measurement at LEP2.

As can be seen from Fig. 50, the cross section for W-pair production increases very rapidly near the nominal kinematic threshold at $\sqrt{s} = 2M_W$, although the finite W-boson width and ISR significantly smear out the sharp rise of the (unphysical) cross section for producing two on-shell W's (see Fig. 53). This means that for a given $\sqrt{s}$ near threshold the W-pair production cross section is very sensitive to the W-boson mass, so that a measurement of the cross section in this energy region directly yields a measurement of M_W. In the threshold determination, the error on the W-boson mass due to signal statistics is given by

$$\Delta M_W = \sqrt{\sigma_{WW}} \left| \frac{dM_W}{d\sigma_{WW}} \right| \frac{1}{\sqrt{\varepsilon_{WW} L}}, \tag{159}$$

where σ_{WW} is the total W-pair production cross section, ε_{WW} is the overall signal efficiency and L is the integrated luminosity. By studying the sensitivity factor given by $\sqrt{\sigma_{WW}}\,|dM_W/d\sigma_{WW}|$ as a function of $\sqrt{s} - 2M_W$, one finds that there is a minimum located at

$$\sqrt{s} \simeq 2M_W + 0.5 \text{ GeV}, \tag{160}$$

corresponding to around 161 GeV as the c.m. energy providing the optimal sensitivity to M_W (see Fig. 56). Since the statistical uncertainty is the most relevant source of error for the threshold method, the optimal strategy for data taking consists therefore in operating at $\sqrt{s} \simeq 161$ GeV in order to minimize the statistical error. The systematic errors on M_W in the threshold method are due to the uncertainties in the W-pair production cross section: the luminosity error, unknown corrections to the theoretical cross section, as those discussed in Sect. **5**˙2.3, the uncertainty in the beam energy, the background subtraction and others. However, as already stressed, the overall error in the threshold measurement is largely dominated by the limited statistics. The present LEP average for M_W from the WW production cross section at $\sqrt{s} \simeq 161$ GeV is [8]

$$M_W = 80.40 \pm 0.22 \text{GeV}\,. \tag{161}$$

The direct reconstruction method consists in reconstructing the peak in the invariant mass distributions of the W-boson decay products, by using either the semi-leptonic decay mode ($WW \to l\nu q\bar{q}$) or the hadronic one ($WW \to q\bar{q}q\bar{q}$). The measurements are carried out at energies above the threshold ($\sqrt{s} > 170$ GeV) in order to reduce the statistical error thanks to the larger WW cross section. The accuracy of the jet energy measurement is too poor to allow a precision measurement of M_W. Therefore, kinematic fit techniques, using the constraints of energy and momentum conservation, together with the equality of the two W-boson masses in an event, are used by the LEP Collaborations to improve the mass resolution [248]. This implies that a good knowledge of the c.m. energy is essential. As already pointed out, systematics affecting this method are largely independent of those present in the threshold method. In particular, the $q\bar{q}q\bar{q}$ channel turns out to be more problematic than the $l\nu q\bar{q}$ one: indeed, besides a larger background contamination, the phenomena of *colour reconnection* and *Bose-Einstein correlations* (see below) introduce additional systematic uncertainties that are absent in the semi-leptonic channel. Systematic errors that are common to both channels are

- error from the LEP beam energy;
- errors from the theoretical description (ISR, background, $4f$ diagrams and fragmentation);
- errors from the detector.

In order to estimate the uncertainties due to $4f$ diagrams and ISR, the theoretical ingredients discussed in Sects. **5**˙2.1 and **5**˙2.3, and the corresponding computational tools based on them, are very useful tools. Indeed, the effect of $4f$ subprocesses other than the ones belonging to the CC03 class, induces an uncertainty of 20 MeV and 25 MeV on M_W for the $q\bar{q}q\bar{q}$ and $l\nu q\bar{q}$ channel, respectively, and is evaluated by using MC samples generated with one or more of the $4f$ generators described in Sect. **5**˙2.4. Moreover, precision calculations of the radiative energy loss (see eq. (158)) in $4f$ production at LEP2 are mandatory. Actually, the relatively large average energy ($< E_\gamma > \simeq 1.1, 2.1, 3.2$ GeV at $\sqrt{s} = 175, 190, 205$ GeV, respectively) carried away by the radiated photons leads to a significant mass-shift if it is not taken into account in rescaling or constraining the energies of the final-state W-boson decay products to the beam energy. Indeed, the average mass-shift caused by ISR is of the order of $< E_\gamma > M_W/\sqrt{s}$, *i.e.* about 500 MeV at $\sqrt{s} = 175$ GeV. However, since a fit to the mass distribution gives more weight to the peak, the actual mass shift at $\sqrt{s} = 175$ GeV is about 200 MeV, anyway important in view of the envisaged experimental precision on M_W. Since, as discussed in Sect. **5**˙2.3,

the exact treatment of $\mathcal{O}(\alpha)$ corrections to off-shell W-pair production is not yet available, the theoretical predictions for $< E_\gamma >$, including the presently under control LL and Coulomb corrections, are affected by an intrinsic uncertainty, that translates into an error of 10-15 MeV on the W-boson mass. This theoretical uncertainty is due to non-leading photonic terms, for instance associated with the radiation of photons off the intermediate W bosons, and should be reduced soon in the light of the recent progress in the calculation of non-leading QED corrections discussed in Sect. **5**˙2.3.

Colour reconnection and *Bose-Einstein effects* [248], that are systematics specific to the $q\bar{q}q\bar{q}$ channel, are interconnection phenomena that may obscure the separate identities of the two W bosons, so that the $4f$ final state may no longer be considered as consisting of two separate W-boson decays. Indeed, in the LEP2 energy regime the average distance between the W^+ and W^- decay vertices is smaller than 0.1 fm, *i.e.* less than a typical hadronic size. Therefore the fragmentation of the W^+ and the W^- may not be independent and may seriously affect the mass reconstruction. The colour-reconnection problem arises from the fact that the W-boson pair, decaying into quark-antiquark pairs $q\bar{q}$ and $Q\bar{Q}$, respectively, can either fragment into two strings stretched between $q\bar{q}$ and $Q\bar{Q}$, or into two strings stretched between $q\bar{Q}$ and $Q\bar{q}$. Owing to the colour charges, the probability and the properties of the two possible configurations are very different. Of the two phases characterizing the fragmentation of the initial quark-antiquark pairs into hadrons, *i.e.* perturbative parton cascade and non-perturbative hadronization, the perturbative QCD interconnection effects have been shown not to be very important [326, 327], whereas the influence of non-perturbative fragmentation can be only estimated by comparing different models. The interesting aspect is that quite different approaches give uncertainties of the same order, *i.e.* about 100 MeV, conservatively. Also Bose-Einstein correlations are due to the overlapping of the W^+ and W^- hadronization regions: consequently, low-momentum bosons coming from different W's can experience coherence effects. Their influence on the W-boson mass-shift can be estimated by using theoretical models. However, it is worth noticing that experimental studies at LEP2 show no evidence yet for Bose-Einstein correlations and that recent theoretical investigations suggest that they may not be a serious systematic (see for instance [328]). The present experimental attitude consists in trying to measure interconnection effects in data through detailed comparison of $q\bar{q}q\bar{q}$ and $l\nu q\bar{q}$ channels.

The present LEP average for M_W from the direct reconstruction method at $\sqrt{s} =$ 172 GeV is [8]

$$M_W \;=\; 80.53 \pm 0.18 \text{ GeV}\,. \tag{162}$$

It is worth noticing that good consistency between experiments and between $q\bar{q}q\bar{q}$ and $l\nu q\bar{q}$ channels is observed.

By combining the $\sqrt{s} = 161$ GeV (threshold) and the $\sqrt{s} = 172$ GeV (direct reconstruction) results, the present M_W value from LEP2 is [8]

$$M_W \;=\; 80.48 \pm 0.14 \text{ GeV}\,. \tag{163}$$

The LEP2 result for M_W can be combined with the measurement by CDF/D0 at the TEVATRON, in order to compile a world average. The W-boson mass measurements at the TEVATRON are based on fits to the transverse mass distribution of $l\nu$ produced in the process $q\bar{q} \to W \to l\nu (l = e, \mu)$. By combining the CDF/D0 results with the UA2 measurement, the average M_W from hadron machines is [8]

$$M_W \;=\; 80.41 \pm 0.09 \text{ GeV}\,. \tag{164}$$

The present world average M_W from LEP2 and $p\bar{p}$ colliders is [8]

$$M_W = 80.43 \pm 0.08 \text{ GeV}. \tag{165}$$

By the end of LEP2 and TEVATRON run 2, both experiments expect to achieve an error on M_W of around 0.03-0.04 GeV, comparable with the present error from indirect determination by means of precision data.

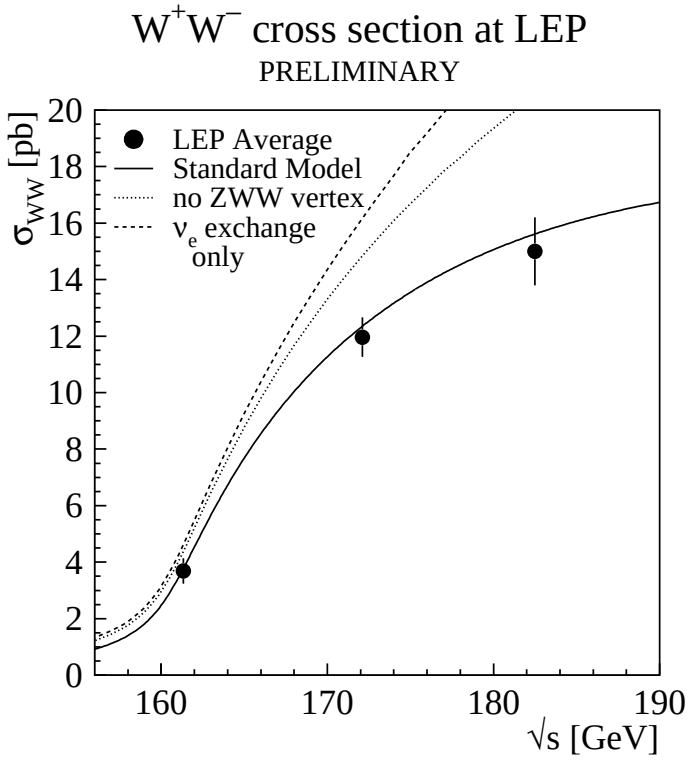

Fig. 56. – The W-pair production cross section (from [8]).

5˙3.2. Anomalous couplings. In addition to the W-boson mass, the second important piece of information that W-pair production at LEP2 can provide is the structure of the triple gauge-boson couplings (TGC). Contrary to LEP1 physics, where TGC only enter through loop corrections to two-fermion production, at LEP2 these couplings are responsible of the behaviour of the tree-level W-pair cross section. Since the specific form for the TGC in the SM is a consequence of the Yang-Mills character of the theory, the study of W-pair production at LEP2 allows to test directly the non-abelian nature of the $SU(2) \times U(1)$ gauge theory. Indeed, in spite of the precision tests of the electroweak interaction at LEP1 and SLC, the non-abelian sector of the SM remains poorly measured to date, even if the very existence of non-abelian coupling can be considered experimentally proved by the recent LEP2 data (see Fig. 56).

WWZ and $WW\gamma$ couplings different from the form predicted by the SM are called *anomalous couplings*. The latter will in general lead to a bad high-energy behaviour of

cross sections violating unitarity. However, since at LEP2 the c.m. energy is too low to point out such effects, the presence of anomalous couplings can be eventually established through the study of the angular distributions of the W bosons and their decay products. As for the W-boson mass measurement, the control of radiative corrections and background contributions is necessarily required, since they induce deviations from the tree-level angular distributions.

Possible anomalies in the WWV ($V = Z$ or γ) vertex can be parameterized in terms of a purely phenomenological effective Lagrangian [329, 330]

$$\begin{aligned} i\mathcal{L}_{eff}^{WWV} \;=\; & g_{WWV}\Big[g_1^V V^\mu \left(W^-_{\mu\nu}W^{+\nu} - W^+_{\mu\nu}W^{-\nu}\right) + k_V W^+_\mu W^-_\nu V^{\mu\nu} + \\ & \frac{\lambda_V}{M_W^2} V^{\mu\nu} W^{+\rho}_\nu W^-_{\rho\mu} + i g_5^V \varepsilon_{\mu\nu\rho\sigma}\left((\partial^\rho W^{-,\mu})W^{+,\nu} - W^{-,\mu}(\partial^\rho W^{+,\nu})\right) V^\sigma + \\ & i g_4^V W^-_\mu W^+_\nu (\partial^\mu V^\nu + \partial^\nu V^\mu) - \frac{\tilde{k}_V}{2} W^-_\mu W^+_\nu \varepsilon^{\mu\nu\rho\sigma} V_{\rho\sigma} - \\ & \frac{\tilde{\lambda}_V}{2M_W^2} W^-_{\rho\mu} W^{+\mu}_\nu \varepsilon^{\nu\rho\alpha\beta} V_{\alpha\beta}\Big], \end{aligned} \tag{166}$$

that provides the most general Lorentz invariant WWV vertex, observable in processes where the vector bosons couple to effectively massless fermions. The definitions in eq. (166) read as follows

$$\begin{aligned} & g_{WW\gamma} = e \qquad && g_{WWZ} = e\cot\vartheta_W \\ & W_{\mu\nu} = \partial_\mu W_\nu - \partial_\nu W_\mu \qquad && V_{\mu\nu} = \partial_\mu V_\nu - \partial_\nu V_\mu. \end{aligned} \tag{167}$$

Therefore, 2×7 independent parameters are needed to describe the most general Lorentz invariant WWV vertex. Within the SM and at the tree level the couplings in eq. (166) are given by $g_1^Z = g_1^\gamma = k_Z = k_\gamma = 1$, with all other couplings vanishing. It is worth noticing that g_1^V, k_V and λ_V conserve C and P separately, while g_5^V violates C and P but conserves CP. Furthermore $g_V^4, \tilde{k}_V$ and $\tilde{\lambda}_V$ parameterize a possible CP violation in the bosonic sector. In particular, the C and P conserving parameters in $\mathcal{L}_{eff}^{WW\gamma}$ can be linked to the static e.m. moments of the W^+ boson as follows [331]

$$\begin{aligned} & \text{charge} \quad Q_W = e g_1^\gamma\,, \\ & \text{magnetic dipole moment} \quad \mu_W = \frac{e}{2M_W}(g_1^\gamma + k_\gamma + \lambda_\gamma)\,, \\ & \text{electric quadrupole moment} \quad q_W = -\frac{e}{M_W^2}(k_\gamma - \lambda_\gamma)\,. \end{aligned} \tag{168}$$

In practice it is impossible to set limits on all the above couplings, so that a number of assumptions have to be made in order to reduce the number of parameters. In the literature, two different theoretical strategies are followed. On the one side, the number of parameters can be reduced by advocating symmetry arguments [330, 332]. On the other hand, the dimensional analysis of the operators involved in the parameterization allows to establish a hierarchy of the operators themselves according to a scaling law of the kind $(E/\Lambda)^{d-4}$, where E is the energy of interest, Λ is the typical energy scale of non-standard physics and d is the dimension of the operators. The latter procedure allows to single out a reduced set of parameters able to produce phenomenologically relevant effects at the energy scale of interest [333].

For instance, if C, P and electromagnetic gauge invariance are imposed, the number of parameters reduces to five, namely $\lambda_\gamma, \lambda_Z, k_\gamma, k_Z$ and g_1^Z. Furthermore, since the effective Lagrangian of eq. (166) contains as a particular case the triple gauge-bosons Lagrangian of the electroweak theory, it is possible and convenient to introduce deviations from the SM predictions for the five parameters as

$$\Delta g_1^Z = g_1^Z - 1, \quad \Delta k_{\gamma,Z} = k_{\gamma,Z} - 1, \quad \lambda_\gamma, \quad \lambda_Z \,. \tag{169}$$

A set of parameters widely used by the LEP Collaborations is given by the following three combinations, which do not affect the tree-level gauge boson propagators and are not yet constrained by low energy and Z^0 peak data [249]

$$\begin{aligned} &\Delta k_\gamma - \Delta g_1^Z \cos^2\vartheta_W = \alpha_{B\phi}, \\ &\Delta g_1^Z \cos^2\vartheta_W = \alpha_{W\phi}, \\ &\lambda_Z = \lambda_\gamma = \alpha_W, \end{aligned} \tag{170}$$

with the constraint $\Delta k_Z = \Delta g_1^Z - \Delta k_\gamma \tan^2\vartheta_W$. The above combinations are all zero according to the SM.

The experimental strategy followed at LEP2 for the determination of anomalous couplings relies upon the measurement, in $4f$ production processes, of the differential cross sections $d^n\sigma = d^n\sigma(\Theta, \vartheta_\pm^*, \varphi_\pm^*; \alpha)$ with $n = 1, 3, 5$, where Θ is the polar production angle of the W^- boson, $\vartheta_\pm^*$ and $\varphi_\pm^*$ are the $W^\pm$ decay angles in W-boson rest frames. Among the W-pair decay channels, the strongest information comes from the semi-leptonic channel because it allows unambiguous charge assignment. Also single W-boson and single γ production processes, that are sensitive to the non-abelian $WW\gamma$ coupling are studied by the LEP Collaborations, even if they are less powerful than the $WW \to 4f$ reactions. Present combined results from the four LEP experiments are [8]

$$\begin{aligned} &\alpha_{W\phi} = 0.02^{+0.16}_{-0.15} && -0.28 < \alpha_{W\phi} < 0.33 \quad (95\%\,\text{CL limit}) \\ &\alpha_W \;\; = 0.15^{+0.27}_{-0.27} && -0.37 < \alpha_W \;\; < 0.68 \quad (95\%\,\text{CL limit}) \\ &\alpha_{B\phi} = 0.45^{+0.56}_{-0.67} && -0.81 < \alpha_{B\phi} < 1.50 \quad (95\%\,\text{CL limit}) \end{aligned} \tag{171}$$

Therefore no discrepancy with the SM is seen in the data. Moreover, an important result of the anomalous couplings analysis is that the existence of the ZWW vertex is firmly established, namely $g_{WWZ} = 0$ is excluded at $> 95\%$ CL (see Fig. 56).

5˙4. *Higgs-boson Searches.* – As shown in Sect. **4**˙2.2, the electroweak precision data can be conveniently used to obtain indirect determinations of the Higgs-boson mass through radiative corrections to the physical observables. Although the weak dependence of the theoretical predictions on the Higgs-boson mass as well as the their intrinsic uncertainties prevent to derive stringent predictions for m_H, there is a slight preference in the precision measurements for a relatively light SM Higgs boson, with an upper limit $m_H < 420\,\text{GeV}$ @ 95% CL [7]. Future more precise direct measurements of the *top*-quark mass at the TEVATRON and of the W-boson mass at LEP2 and the TEVATRON, associated with recent progress in the calculation of two-loop electroweak graphs, should improve the present constraints on the mass of this yet elusive particle. Indeed, the search for the Higgs boson certainly constitutes one of the main tasks of present-day experiments in high-energy physics. The discovery of this neutral scalar particle would establish the validity of the electroweak theory in its standard formulation, and shed light on the mechanism of electroweak symmetry breaking and mass generation.

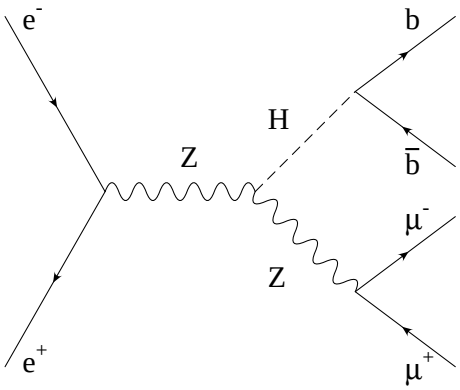

Fig. 57. – Tree-level Feynman diagram for Higgs-boson production in the channel $e^+e^- \to \mu^+\mu^- b\bar{b}$ (Higgs-strahlung).

By searching directly for the SM Higgs boson, the LEP experiments have set a lower bound on the Higgs-boson mass, namely $m_H > 77\,\text{GeV}$ @ 95% CL (four LEP experiments combined) [182, 183]. This lower limit comes from negative searches of Higgs-boson production in electron-positron collisions around and above the Z^0 peak. The dominant production mechanism for the SM Higgs boson in the LEP energy range is the s-channel Higgs-strahlung process $e^+e^- \to ZH$, where the intial states annihilate into a virtual Z^0 boson that converts into a Z^0 and a Higgs boson. Other production mechanisms, *i.e.* the fusion processes, where the Higgs boson is formed in WW, ZZ t-channel collisions, with the W, Z's radiated off the incoming electron and positrons, have smaller cross section at LEP energies. However, it is worth keeping in mind that for $\nu_e\bar{\nu}_e$ and e^+e^- in the final state, the two amplitudes for the Higgs-strahlung and fusion process both contribute and interfere.

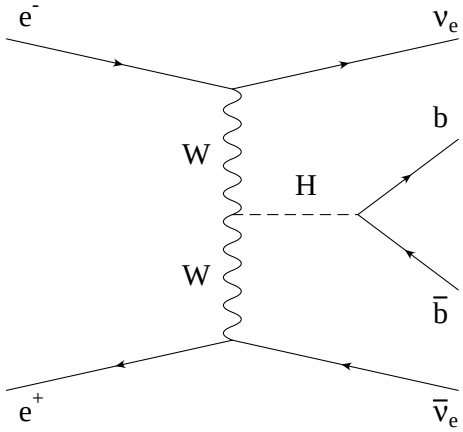

Fig. 58. – Tree-level Higgs-boson production *via* WW fusion.

In view of the LEP2 physics potential, the reachable Higgs-boson mass limit is

roughly given by $m_H \simeq \sqrt{s} - 100$ GeV. Even assuming the highest c.m. energy in the LEP2 operation ($\sqrt{s} = 205$ GeV), the discovery potential of the LEP2 experiments will not exceed a Higgs-boson mass of around 100 GeV. For a SM Higgs boson with a mass in the range between 77 (present lower limit) and 100 GeV, the dominant decay mode is by far $H \to b\bar{b}$. Branching ratios for the decays $H \to \tau^+\tau^-, c\bar{c}, gg$ are suppressed by an order of magnitude or more. The corresponding total decay width is predicted in the electroweak theory to be very narrow, *i.e.* less than a few MeV for m_H less than 100 GeV. As a consequence of the fact that the Higgs boson predominantly decays into $b\bar{b}$ pairs when $m_H < 100$ GeV, the observed final states in Higgs-boson searches at LEP consists of four fermions. In the case of the Higgs-boson signal these $4f$ final states are mainly achieved through the Higgs-strahlung process $e^+e^- \to ZH$, with the subsequent decays $Z \to f\bar{f}$ and $H \to b\bar{b}$. In general, whenever excluding Higgs-boson decay channels other than $H \to b\bar{b}$ (such as $H \to \tau^+\tau^-$ that is actually considered in Higgs-boson searches at LEP), the interesting final states for the physics of the Higgs particle at LEP are $b\bar{b}\mu^+\mu^-, b\bar{b}e^+e^-$ (leptonic channels), $b\bar{b}\nu\bar{\nu}$ (missing energy channel) and $b\bar{b}q\bar{q}$ (four-jet channel). Therefore, Higgs-boson physics at LEP2 requires, as for W-pair production, the calculation of $2 \to 4$ fermions scattering amplitudes, including signal and backgrounds in the SM. The Feynman diagram for the Higgs-boson signal in the channel $e^+e^- \to \mu^+\mu^- b\bar{b}$ is depicted in Fig. 57. The additional Higgs-boson production mechanism in the case of $\nu_e\bar{\nu}_e b\bar{b}$ final state can be found in Fig. 58; an analogous diagram with ZZ fusion is present for the $e^+e^- b\bar{b}$ final state. For the channel $\mu^+\mu^- b\bar{b}$, that provides the cleanest event signature, background events are generated, among others, by double vector-boson production $e^+e^- \to ZZ, Z\gamma$ and $\gamma\gamma$ with the virtual Z^0 and γ decaying to $\mu^+\mu^-$ and $b\bar{b}$ pairs (see Fig. 59). Actually, just to give an idea of the degree of complexity of the full calculation of $2 \to 4$ amplitudes for Higgs-boson physics, 25 diagrams are present in the $\mu^+\mu^- b\bar{b}$ channel, 50 diagrams in $e^+e^- b\bar{b}$ and 68 in the $b\bar{b}b\bar{b}$ channel (unitary gauge). Full $4f$ calculations for Higgs-boson searches are certainly less demanded with respect to the case of precision studies of W^+W^- production. Indeed, given the small Higgs-boson production cross sections (of the order of tens of fb, two-three orders of magnitude smaller than the $e^+e^- \to W^+W^-$ cross section) and the low statistics, precise predictions are not strictly necessary for discovery physics. However, the theoretical and technical expertise developed for $4f$ production in W-boson physics and described in the previous sections allows to apply the corresponding "machinery" to a comprehensive analysis of Higgs-boson production as well. The main motivations for complete $4f$ calculations for Higgs-boson physics at LEP is that no approximations are introduced in the tree-level matrix element, differential distributions for the final-state products are directly available and the background can be precisely evaluated. Therefore, a full calculation allows to test the degree of validity of the usual approximation of computing production cross section $\times$ branching ratios and of summing squared amplitudes incoherently, thus quantifying off-shellness and interference effects. Furthermore, once the Higgs boson is discovered, complete $4f$ calculations and relative generators could be of great help in the extraction of the Higgs-boson properties (mass, spin, parity, etc.) that require a good control of exclusive distributions.

Complete $4f$ calculations for Higgs-boson physics at LEP have been carried out in the last few years by several groups [258, 306, 334–338]. The typical calculation strategy consists in computing all tree-level diagrams for a given channel and including the best available set of radiative corrections, *i.e.* running electroweak couplings, initial-state QED radiation, naive QCD final-state corrections and running heavy-quark masses. This framework is implemented, although with some minor differences, in $4f$ programs such as

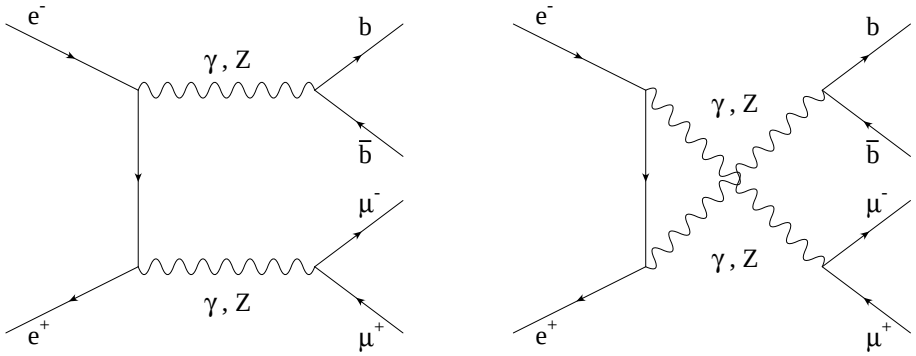

Fig. 59. – Tree-level Feynman diagrams for the main background processes in the channel $e^+e^- \to \mu^+\mu^- b\bar{b}$.

compHEP, GENTLE/4fan, HIGGSPV, HZGEN [335], WPHACT and WTO, that have been described in Sect. **5**˙2.4. The programs compHEP, GENTLE/4fan, HZGEN and WPHACT can evaluate matrix elements taking into account the finite b quark mass, while HIGGSPV and WTO consider massless final-state fermions. WPHACT includes also the contribution of SUSY neutral Higgs-boson production. Some of the codes provide unweighted events with the four-momenta of all final-state particles, that can be used to process the event through the detector and to apply cuts for data analysis. The above $4f$ generators are described in more detail in [306], where also reference to other programs for Higgs-boson physics at LEP, such as PHYTIA and HZHA, based on production times decay approximation and with an incomplete treatment of the SM amplitudes, can be found. In ref. [306] some comparisons between the predictions of different programs are shown for a sample of $4f$ final states, with the conclusions that the agreement between the dedicated $4f$ generators is systematically at the level of 1% or better, pointing out the high technical precision achieved, and that there are situations, such as the $b\bar{b}\nu_e\bar{\nu}_e$ final state, where the difference between $4f$ codes and standard computational tools for Higgs-boson searches at LEP, such as HZHA, not including the full set of SM diagrams, can reach 20-40%, depending on the c.m. energy and the Higgs-boson mass value. Thanks to the availability of complete $4f$ calculations, some topics previously not investigated but of interest for Higgs-boson searches, such as the amount of signal-background interference and the effect of finite b-quark mass corrections, received the due attention. In the case of massless final-state fermions, the interference between signal and background diagrams is exactly vanishing, because massless fermions are coupled to spin-vectors in γ, Z decays and to spin-scalar in Higgs-boson decay, so that the two amplitudes do not interfere as a consequence of the different helicity pattern. If the mass of the b quark is kept different from zero in the full matrix element, then a finite interference does develop. However, it was found that this effect never exceeds the percent level. Indeed, since for $m_H < 100$ GeV the Higgs-boson width is of the order of a few MeV, it can be expected *a priori* that the non-vanishing signal-background interference is highly suppressed at LEP, as demonstrated by explicit calculations. Therefore, signal-background interference may be neglected in Higgs-boson search experiments at LEP. Other conclusions that comes from these analyses is that ISR is large, varying between 10-20% on the total cross section, and must be included in Higgs-boson event generators, especially in the light of the distortions induced on exclu-

sive distributions that are relevant for the determination of the properties of the Higgs particle.

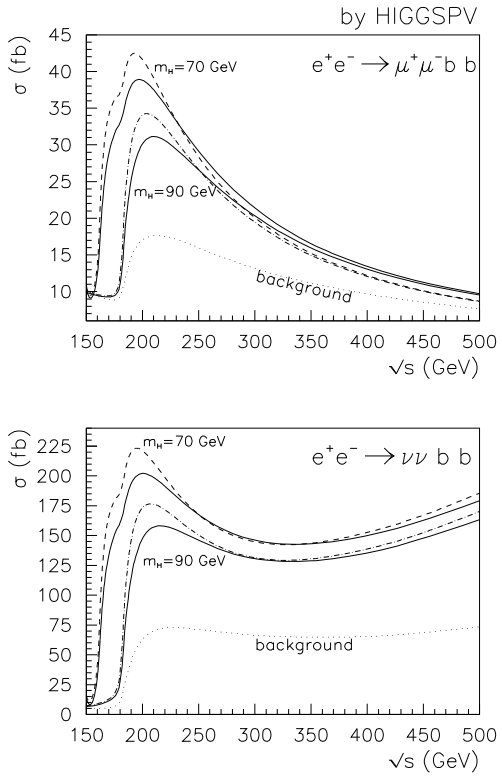

Fig. 60. – The cross section for Higgs-boson production in the channels $e^+e^- \to b\bar{b}\mu^+\mu^-$ and $e^+e^- \to b\bar{b}\nu\bar{\nu}$. The dotted and dash-dotted lines show tree-level predictions; the solid lines include ISR. The background cross section is also shown. Numerical results by `HIGGSPV` [279].

The predictions obtained with the help of the $4f$ generator `HIGGSPV` for the Higgs-boson production cross section in the channels $e^+e^- \to b\bar{b}\mu^+\mu^-$ and $e^+e^- \to b\bar{b}\nu\bar{\nu}$ can be seen in Fig. 60, for two representative values of the Higgs-boson mass. The effect of backgrounds and ISR are shown as a function of the c.m. energy up to 0.5 TeV. It is worth observing that in the LEP2 energy range the size of the total cross sections in both channels can give by itself clear evidence of Higgs-boson production. In the case of the $b\bar{b}\nu\bar{\nu}$ final state the rise with the c.m. energy of the cross section is due to the logarithmic enhancement introduced by the t-channel WW fusion processes that are absent in the $b\bar{b}\mu^+\mu^-$ final state. As said above, in order to extract information on the quantum numbers assignment of the Higgs particle, the angular distributions are known to be the most sensitive observables. An example of such quantities is given in Fig. 61, showing the distribution, obtained by means of `HIGGSPV`, of the b-quark scattering angle in the laboratory frame, at $\sqrt{s} = 192$ GeV and for three Higgs-boson mass values

and background alone ($e^+e^- \to b\bar{b}\nu\bar{\nu}$ channel). As can be seen, in the presence of the Higgs-boson signal as dominant contribution to the $b\bar{b}\nu\bar{\nu}$ cross section, a clearly isotropic spin zero behaviour is present, whereas it disappears whenever considering the background only. Since this differential distribution can be meaningfully and more extensively analyzed by means of complete $4f$ calculations, the above example should clarify the usefulness of dedicated precision tools for the measurement of the Higgs-boson properties.

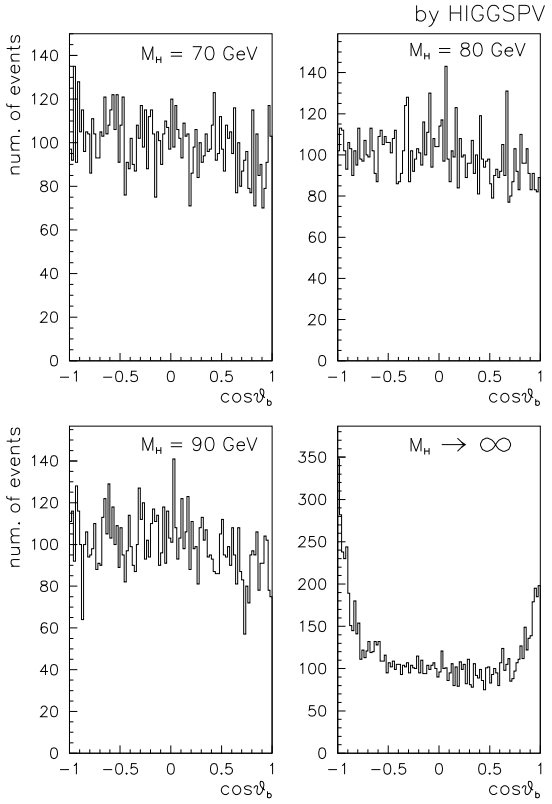

Fig. 61. – The b-quark scattering angle distribution in the laboratory frame at $\sqrt{s} = 192$ GeV for the process $e^+e^- \to b\bar{b}\nu\bar{\nu}$. Numerical results by `HIGGSPV` [279].

To conclude the discussion on Higgs-boson searches in electron-positron collisions, it is worth noticing that, if LEP does not discover the Higgs boson and its mass lies in the intermediate range ($140\,\mathrm{GeV} < m_H < 2M_Z$), the search for the Higgs particle at future e^+e^- colliders will require the analysis of six-fermion production processes, due to the decay chain $H \to W^+W^- \to 4f$. Also in this case, in view of the expected experimental precision and particularly for a precise determination of the Higgs-boson properties, complete six-fermion calculations of Higgs-boson production and relative computational tools should be desirable. Actually, the first results along this direction very recently appeared in the literature [339, 340].

6. – Conclusions

Since 1989 the four experiments ALEPH, DELPHI, L3 and OPAL at LEP and the SLD Collaboration at SLC collected a large amount of precision data by studying the processes of two-fermion production in electron-positron collisions at centre of mass energies close to the mass of the Z^0 boson. About 16 millions of Z^0 events have been recorded. The LEP phase around the Z^0 resonance (LEP1) was terminated in 1995, while SLC is continuing in data taking on the Z^0 peak. During 1996, the LEP energy was increased in order to allow the production of W-boson pairs for the first time in high-energy e^+e^- collisions. The LEP2 phase is in progress and will continue until 1999. Meanwhile, almost final results of the analysis of the LEP1/SLC precision data have become available, although the data analyses, including the final LEP energy calibrations, are not yet finished.

Looking at the high accuracy reached by the most recent measurements of the electroweak observables, the program of *precision physics at LEP/SLC* can be considered as a complete success, thanks to a combined experimental and theoretical effort. Actually, besides the very successful performance of the LEP machine and important experimental/technological achievements, the effort undertaken on the theoretical side in precision calculations for Z^0 physics significantly contributed to the progress of precision tests of the Standard Model (SM).

A key ingredient of the striking success of precision physics at LEP/SLC is undoubtedly the high precision determination of the machine luminosity. This has been possible thanks to the experimental achievements on luminometers, and to the high-precision calculations of the small-angle Bhabha process, today accurate at the level of 0.1%.

The extremely accurate theoretical predictions for observables of e^+e^- collisions into two-fermion final states at large scattering angles provided the necessary theoretical background for the precise determination of the electroweak parameters performed by the high-precision experiments.

Concerning the comparison between theory and experiment, the electroweak precision data confirm the validity of the SM with an impressive accuracy. The standard theoretical framework is able to accomodate all experimental facts, providing predictions in agreement with precision measurements. Just to mention some of the major achievements, the number of light neutrino species has been unambiguously determined to be equal to 3; the Z-boson mass is at present known with a relative precision of 2×10^{-5}, comparable with the precision of the muon decay constant G_μ; lepton universality has been tested with an unprecedented precision; the stringent constraints on the neutral current couplings allow the determination of the weak effective mixing angle with an absolute error at the level of 3×10^{-4}; the W-boson mass is indirectly determined with a relative error below 0.1%.

By virtue of their high accuracy, the precision measurements show a clear evidence of pure weak radiative corrections and they can be used to infer valuable information about the fundamental parameters of the SM. Actually, the measurements are sensitive, *via* the virtual effects of radiative corrections, to the *top*-quark mass m_t, the Higgs-boson mass m_H and the strong coupling constant α_s. The indirect constraints obtained from precision data on the mass of the particles not energetically accessible clearly illustrate the rôle of quantum loops in raising *precision physics* to the level of *discovery physics*.

From all the available data (excluding the direct determination of m_t and M_W from

the TEVATRON and LEP2) the best current estimate of the *top*-quark mass is [7, 8]

$$m_t = 157^{+10}_{-9} \text{ GeV}.$$

This indirect determination is in beautiful agreement with the measurement of the *top*-quark mass from direct production at the TEVATRON [168], $m_t = 175.6 \pm 5.5$ GeV, illustrating the constraining power of the precision measurements.

The value of $\alpha_s(M_Z)$ derived from a fit to all electroweak data is [7, 8]

$$\alpha_s(M_Z) = 0.120 \pm 0.003,$$

in very good agreement with the world average and of similar precision. This indirect determination, when associated with the α_s measurements from other processes and at different energy scales, significantly proves the running of α_s as predicted by the non-abelian structure of QCD.

The Higgs-boson is the still missing block of the SM. Although the constraints inferred on the mass of the Higgs boson from precision data are not conclusive, as a consequence of the weak logarithmic dependence of radiative corrections on m_H, electroweak measurements imply an indicative mass window, thus providing valuable information in view of the planned searches at the LHC and future e^+e^- colliders. A fit to all data gives [7, 8]

$$\begin{aligned} &m_H = 115^{+116}_{-66} \text{ GeV}, \\ &m_H < 420 \text{ GeV} \quad (95\% \text{ CL}), \end{aligned}$$

where also the theoretical uncertainty due to missing higher-order corrections is taken into account in the one-sided 95% CL upper limit. A general *caveat* is in order here. The upper limit quoted above depends heavily on the presence of the left-right asymmetry from SLC in the data set. Therefore, the only reliable conclusion is that a very heavy Higgs boson, that would be rather problematic for future direct searches, is excluded by precision data. Future improved measurements of the W-boson mass at LEP2 and the TEVATRON and of the *top*-quark mass at the TEVATRON, together with recent progress in the calculation of higher-order radiative corrections, are expected to sharpen the existing constraints on m_H.

The first experimental results of LEP2 are available. As in the LEP1 case, the theoretical tools, noticeably the accurate predictions concerning reactions of the kind $e^+e^- \to$ 4-fermion final states, provide the necessary theoretical scheme for the data-theory comparison. The recent LEP2 measurements of the W pair production cross section already show clear evidence for the existence of the gauge bosons self-interactions, thus testing a crucial prediction of the non-abelian structure of the theory. Future measurements of the W-boson mass are expected to reach an accuracy comparable with the one obtained in the direct determination performed at the TEVATRON and the indirect determination at LEP1/SLC as calculated *via* radiative corrections.

Looking beyond the SM, the possible scenarios of new physics are strongly constrained by the delicate agreement between the SM and the precision data. Since no significant anomalies are present, the natural candidates are represented by models that do not modify the structure of the SM significantly. For this reason, theories with fundamental Higgs particles, such as supersymmetry, are generally considered more favourite than models implying composite Higgs bosons and new strong interactions. Given the large value of the *top*-quark mass, a fundamental Higgs-boson with a relatively low mass,

as inferred by precision electroweak data, can be nicely accommodated in a supersymmetric theory (such as the Minimal Supersymmetric Standard Model) broken at some high energy scale. Supersymmetry provides also a viable scenario to realize the unification of the coupling constants in a grand unified theory (GUT). Actually, the determination of $\sin^2\vartheta_{eff}$ and $\alpha_s(M_Z)$ as obtained from precision data is compatible with gauge coupling unification at a large energy scale, provided the mass spectrum of the GUT includes supersymmetric particles.

Although new elementary particles have not been directly discovered by experiments at LEP and SLC, it can be said that *precision physics* provided important pieces of information to our present knowledge in particle physics and contributed significantly to obtain hints on how new physics beyond the SM is realized in Nature.

* * *

The authors are indebted with several colleagues for having provided figures that appear in the present paper, in particular with G. Altarelli for Figs. 39 and 40, S. Ambrosanio for Fig. 42, W. Hollik for Fig. 41, B. Pietrzyk for Figs. 35, 67, 68 and 69, G. Quast for Figs. 1, 33, 36 and 37, and D. Ward for Figs. 27, 28, 34 and 56. The authors are also grateful to F. Teubert for useful discussions concerning the propagation of the luminosity error to Z-boson parameters.

The present paper has been written after almost a decade of intense activity on precision physics at LEP. During these years, the authors had the occasion to collaborate with several colleagues: they wish to warmly thank all of them for all the stimulating discussions, and the collaborative environment found. Without these interactions, most probably this paper would never be written.

Last, but not least, the authors gratefully acknowledge the Italian Physical Society (SIF) for having provided the opportunity of writing the present review paper.

A. – Universal Photonic Corrections

A common set of radiative corrections to s-channel annihilation and t-channel scattering processes is represented by QED radiative corrections. In the so called leading logarithmic (LL) approximation, they are dominated by long-distance contributions, and hence are process independent. Going beyond the LL approximation, it is necessary to take into account process-dependent corrections, which are no more universal and can be computed by means of standard diagrammatic techniques. In the following, an overview of the most popular algorithms developed for the computation of QED corrections in the LL approximation, namely the Structure Function (SF) method, the Parton Shower (PS) method and Yennie-Frautschi-Suura (YFS) exclusive exponentiation, will be given.([8]) Just for definiteness, only s-channel processes will be considered, the generalization to t-channel processes being almost straightforward. It is worth noticing that for two of these methods, namely the SF method and YFS exclusive exponentiation, proper procedures for matching the all-orders LL results with finite-order exact diagrammatic results have been developed.

([8]) It is worth noticing that at least two additional frameworks for the computation of QED corrections in the LL approximation have been also developed, namely the Coherent States approach [341] and the Unitary Method [342]. The interested reader is referred to the original literature.

A˙1. *The Structure Function Method.* – Let us consider the annihilation process $e^-e^+ \to X$, where X is some given final state, and let $\sigma_0(s)$ be its lowest order cross section, possibly including all the short-distance process dependent corrections, as those discussed in Sect. **3**. Initial-state (IS) QED radiative corrections can be described according to the following picture. Before arriving at the annihilation point, the incoming electron (positron) of four-momentum $p_{-(+)}$ radiates real and virtual photons (bremsstrahlung). These photons, due to the dynamical features of QED, are mainly radiated along the direction of motion of the radiating particles, and their effect is mainly to reduce the original four-momentum of the incoming electron (positron) to $x_{1(2)}p_{-(+)}$. After this "pre-emission", the "hard" subprocess $e^-(x_1p_-)e^+(x_2p_+) \to X$ takes place, at a reduced centre of mass energy squared $\hat{s} = x_1x_2s$. The resulting cross section, corrected for IS QED radiation, can be represented as follows [343]:

$$\sigma(s) = \int_0^1 dx_1 dx_2 D(x_1, s) D(x_2, s) \sigma_0(x_1 x_2 s) \Theta(\text{cuts}), \tag{172}$$

where $D(x, s)$ are the electron structure functions, representing the probability that an incoming electron (positron) radiates a collinear photon, retaining a fraction x of its original momentum, and Θ(cuts) represent the rejection algorithm implemented in order to take care of experimental cuts (see Fig. 62 for a graphical representation).

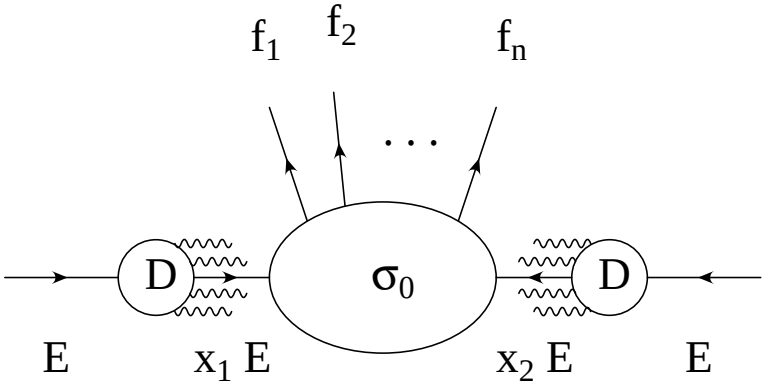

Fig. 62. – Graphical representation of eq. (172).

Equation (172) takes into account only IS photonic radiation, for the sake of simplicity. It has however to be noticed that in the literature more accurate LL results can be found, taking into account also kinematical effects due to IS radiation and/or the effect of final-state radiation for the small-angle Bhabha process [21, 122].

Actually, when considering photonic radiation only the non-singlet part of the SF is of interest. If the running of the QED coupling constant $\alpha(s)$ is neglected (which corresponds to neglecting the corrections due to additional pair production, that can be taken into account properly by means of dedicated formulae [121]), the non-singlet part of the SF is the solution of the following Renormalization Group (RG) equation:

$$s\frac{\partial}{\partial s} D(x, s) = \frac{\alpha}{2\pi} \int_x^1 \frac{dz}{z} P_+(z) D\left(\frac{x}{z}, s\right), \tag{173}$$

where $P_+(z)$ is the so called Altarelli-Parisi (AP) splitting function [344], given by

$$P_+(z) = P(z) - \delta(1-z)\int_0^1 dx P(x),$$

$$P(z) = \frac{1+z^2}{1-z}. \tag{174}$$

Equation (173) can be also transformed into an integral equation, subject to the boundary condition $D(x, m_e^2) = \delta(1-x)$:

$$D(x,s) = \delta(1-x) + \frac{\alpha}{2\pi}\int_{m_e^2}^{s}\frac{dQ^2}{Q^2}\int_x^1 \frac{dz}{z}P_+(z)D\left(\frac{x}{z}, Q^2\right). \tag{175}$$

Equation (175) can be solved exactly by making use of numerical methods. One of these is the so called inverse Mellin transform method, which is briefly described in the following. The Mellin transformation is defined as

$$F(n) = \int_0^1 dx x^{n-1} f(x), \tag{176}$$

$$f(x) = \int_{\gamma-i\infty}^{\gamma+i\infty}\frac{dn}{2\pi i}x^{-n}F(n). \tag{177}$$

By taking the Mellin transform of eq. (172), switching to the differential form of the evolution equation and solving for the Mellin moments, one finds

$$D(n,s) = \exp\left[\frac{\eta}{4}C(n)\right], \tag{178}$$

where $C(n)$ are the Mellin moments of the AP splitting function

$$C(n) = \int_0^1 dz z^{n-1}P_+(z) \tag{179}$$

and

$$\eta = \frac{2\alpha}{\pi}\ln\left(\frac{s}{m_e^2}\right). \tag{180}$$

By computing the moments of eq. (179), inserting them into (178), and performing numerically the anti-transformation given by (177), the exact numerical solution of (175) is obtained. There is only a technical remark at this point: the integrand of the anti-transformation is strongly oscillating in the asymptotic region, so that a proper regularization procedure must be adopted in order to obtain numerical convergence.

For practical purposes, it is also of great interest to obtain approximate analytical representations of the solution of the evolution equation. A first analytical solution can be obtained in the so called *soft photon approximation*, *i.e.* in the limit $x \simeq 1$. In such a limit, the dominant contribution to eq. (177) comes from the large n region, so that one can approximate the moments of the AP splitting function by means of their asymptotic expansion, namely

$$C(n) \simeq \frac{3}{2} - 2\gamma_E - 2\ln n + O\left(\frac{1}{n}\right), \tag{181}$$

γ_E being the Euler constant. By inserting eq. (181) into eq. (178) and computing the anti-transformation one obtains

$$D_{GL}(x,s) = \frac{\exp\left[\frac{1}{2}\eta\left(\frac{3}{4}-\gamma_E\right)\right]}{\Gamma\left(1+\frac{1}{2}\eta\right)}\frac{1}{2}\eta(1-x)^{\frac{1}{2}\eta-1}, \tag{182}$$

Γ being the Euler gamma-function. The solution shown in eq. (182) is known as the *Gribov-Lipatov* (GL) approximation [345]. Its main feature is that it exponentiates at all perturbative orders the large logarithmic contributions of the kind $\eta\ln(1-x)$. Its main drawback is that it is valid only in the soft limit, *i.e.* it does not take into account properly hard-photon effects.

The evolution equation (175) can also be solved iteratively. At the n-th step of the iteration, one obtains the $\mathcal{O}(\alpha^n)$ contribution to the structure function. The iterative solution of the evolution equation is, in some sense, complementary to the exponentiated GL solution. Actually, on the one hand the GL solution is exponentiated at all perturbative orders, whereas the iterative solution must be truncated at a given finite perturbative order. On the other hand, the GL solution is valid in the limit $x \simeq 1$, whereas any given iterative contribution can be computed exactly.

In order to go beyond the soft-photon approximation, the following general strategy has been adopted. Given an iterative solution up to a given perturbative order, for each perturbative contribution it is possible to isolate the part which is contained in the GL solution. Then, by combining the GL solution with the iterative one, in which that part has been eliminated in order to avoid double counting, one can build a *hybrid* solution of the evolution equation, which exploits all the positive features of the two kinds of solutions and does not present anymore the limitations intrinsic to each of them. As a matter of fact, in the literature it is possible to find two classes of hybrid solutions, namely the additive and factorized ones. The additive solutions have the following general structure: they are built by simply adding to the GL solution the finite order terms computed by means of the iterative solutions. The factorized solutions, on the contrary, are obtained by multiplying the GL solution by finite order terms, in such a way that, order by order, the iterative contributions are exactly recovered. In the following, the third order exponentiated additive and factorized solutions are reported. The additive one reads [239]:

$$\begin{aligned}
D_A(x,s) &= \sum_{i=0}^{3} d_A^{(i)}(x,s),\\
d_A^{(0)}(x,s) &= D_{GL}(x,s),\\
d_A^{(1)}(x,s) &= -\frac{1}{4}\eta(1+x),\\
d_A^{(2)}(x,s) &= \frac{1}{32}\eta^2\left[(1+x)\left(-4\ln(1-x)+3\ln x\right)-4\frac{\ln x}{1-x}-5-x\right],\\
d_A^{(3)}(x,s) &= \frac{1}{384}\eta^3\left\{(1+x)\left[18\zeta(2)-6\mathrm{Li}_2(x)-12\ln^2(1-x)\right]\right.\\
&\quad+\frac{1}{1-x}\left[-\frac{3}{2}(1+8x+3x^2)\ln x-6(x+5)(1-x)\ln(1-x)\right.\\
&\quad\left.\left.-12(1+x^2)\ln x\ln(1-x)+\frac{1}{2}(1+7x^2)\ln^2 x\right.\right.
\end{aligned}$$

$$-\frac{1}{4}(39-24x-15x^2)\Big]\Big\}, \tag{183}$$

where ζ is the Riemann ζ-function. The factorized one reads [119, 238]:

$$\begin{aligned}
&D_F(x,s) = D_{GL}(x,s)\sum_{i=0}^{2} d_F^{(i)},\\
&d_F^{(0)} = \frac{1}{2}(1+x^2),\\
&d_F^{(1)} = \frac{1}{4}\frac{\eta}{2}\left[-\frac{1}{2}(1+3x^2)\ln x-(1-x)^2\right],\\
&d_F^{(2)} = \frac{1}{8}\left(\frac{\eta}{2}\right)^2\Big[(1-x)^2+\frac{1}{2}(3x^2-4x+1)\ln x\\
&+\frac{1}{12}(1+7x^2)\ln^2 x+(1-x^2)\mathrm{Li}_2(1-x)\Big].
\end{aligned} \tag{184}$$

It is worth noting that also higher order solutions are known, numerically and/or analytically, for both the classes of solution. However, LEP phenomenology is not sensitive to hard photonic terms beyond the third order.

If only cuts on the invariant mass of the event after ISR are considered, eq. (172) can be simplified by performing explicitly one of the integrations. Actually, for $s' \geq x_0 s$, it can be shown that the QED corrected cross section can be written as

$$\sigma(s) = \int_0^{1-x_0} dx H(x,s)\sigma_0\left((1-x)s\right), \tag{185}$$

where $H(x,s)$ is the so called *radiator*, or *flux function*, defined as

$$H(x,s) = \int_{1-x}^{1}\frac{dz}{z}D(z,s)D\left(\frac{1-x}{z},s\right). \tag{186}$$

By defining

$$K(x,s) = H(1-x,s) \tag{187}$$

and taking the Mellin moments of eq. (187), the following identity can be shown:

$$K(n,s) = \int_0^1 dx x^{n-1}K(x,s) = D^2(n,s) = \exp\left[\frac{\eta}{2}C(n)\right], \tag{188}$$

where $C(n)$ are the Mellin moments of the AP splitting function, given by eq. (181). In virtue of eq. (188), the following identity holds:

$$H_\eta(x,s) = D_{2\eta}(1-x,s). \tag{189}$$

It is worth noticing that in QED there are some non-leading corrections that behave much like the leading logarithmic ones. Actually, it can be verified by inspection that after the substitution

$$\eta \to \beta = \frac{2\alpha}{\pi}\left[\ln\left(\frac{s}{m_e^2}\right)-1\right] \tag{190}$$

the $\mathcal{O}(\alpha)$ distribution of the invariant mass of the event after ISR as extracted from eq. (185) reproduces exactly the standard diagrammatic calculation.

Moreover, it has to be noticed that it is possible to match the all-orders LL results of the SF method with exact finite-order diagrammatic results. For the Z^0 line shape, the match has been performed in the soft-photon approximation up to $\mathcal{O}(\alpha^2)$, according to the procedure described in Sect. **3**˙4. Also a more general procedure for implementing the matching beyond the soft-photon approximation, and hence taking into account hard-photon effects, is known and can be found in ref. [23].

A˙2. *The Parton Shower Method.* – The Parton Shower method is substantially a method for providing a Monte Carlo iterative solution of the evolution equation, at the same time generating the four-momenta of the electron and photon at a given step of the iteration. It has been studied within the context of QCD (see for instance refs. [346] and [347]) and subsequently developed also for QED (see refs. [348], [349], [350] and references therein). In order to implement the algorithm, it is first necessary to assume the existence of an upper limit for x, in such a way that the AP splitting is regularized as follows:

$$P_+(z) = \theta(x_+ - z)P(z) - \delta(1-z)\int_0^{x_+} dx P(x). \tag{191}$$

Of course, in the limit $x_+ \to 1$ eq. (191) recovers the usual definition of the AP splitting function given in eq. (174). By inserting the modified AP vertex into eq. (173), one obtains

$$s\frac{\partial}{\partial s}D(x,s) = \frac{\alpha}{2\pi}\int_x^{x_+}\frac{dz}{z}P(z)D\left(\frac{x}{z},s\right) - \frac{\alpha}{2\pi}D(x,s)\int_x^{x_+}dzP(z). \tag{192}$$

Separating now the variables and introducing the Sudakov form factor

$$\Pi(s_1,s_2) = \exp\left[-\frac{\alpha}{2\pi}\int_{s_2}^{s_1}\frac{ds'}{s'}\int_0^{x_+}dzP(z)\right], \tag{193}$$

which is the probability that the electron evolves from virtuality $-s_2$ to $-s_1$ without emitting photons of energy fraction larger than $1-x_+$, eq. (192) can be recast into integral form as follows:

$$D(x,s) = \Pi(s,m_e^2)D(x,m_e^2) + \frac{\alpha}{2\pi}\int_{m_e^2}^{s}\frac{ds'}{s'}\Pi(s,s')\int_x^{x_+}\frac{dz}{z}P(z)D\left(\frac{x}{z},s'\right). \tag{194}$$

The formal iterative solution of eq. (194) can be represented by the following infinite series:

$$\begin{aligned} D(x,s) = & \sum_{n=0}^{\infty}\prod_{i=1}^{n}\left\{\int_{m_e^2}^{s_{i-1}}\frac{ds_i}{s_i}\Pi(s_{i-1},s_i)\frac{\alpha}{2\pi}\int_{x/(z_1\cdots z_{i-1})}^{x_+}\frac{dz_i}{z_i}P(z_i)\right\} \\ & \Pi(s_n,m_e^2)D\left(\frac{x}{z_1\cdots z_n},m_e^2\right). \end{aligned} \tag{195}$$

The particular form of (195) allows to use a Monte Carlo method for building the solution iteratively. The algorithm is standard, and can be described as follows:

1 – set $Q^2 = m_e^2$, and fix $x = 1$ according to the boundary condition $D(x,m_e^2) = \delta(1-x)$;

2 – generate a random number ξ in the interval $[0,1]$;

3 – if $\xi < \Pi(s, Q^2)$ stop the evolution; otherwise

4 – compute Q'^2 as a solution of the equation $\xi = \Pi(Q'^2, Q^2)$;

5 – generate a random number z according to the probability density $P(z)$ in the interval $[0, x_+]$;

6 – substitute $x \to xz$ and $Q^2 \to Q'^2$; go to 2.

An important feature of this algorithm is that it can be used to generate exclusive events containing the complete information on the four-momenta of the particles. This fact is well known for the QCD analog of the algorithm, and relies upon the kinematical rules of the so called *jet calculus*. For the case under consideration, in which at the i-th step of the iteration a virtual parent electron branches into a virtual electron plus a real photon, the space-like kinematics apply. In particular, one has

$$e(p) \to e(p') + \gamma(q), \tag{196}$$

where $p^2 = -K^2$, $p'^2 = -K'^2$ and $q^2 = 0$. Assuming that the parent electron moves along the z axis, the four-momenta of the particles can be parameterized as follows:

$$\begin{aligned} p &= (E, \vec{0}, p_z), \\ p' &= (E', \vec{p}_\perp, z p_z), \\ q &= (E_\gamma, -\vec{p}_\perp, (1-z) p_z). \end{aligned} \tag{197}$$

From the kinematics of eq. (197), in the limit $p_z \to \infty$, the following relations can be derived:

$$\begin{aligned} E &\simeq p_z - \frac{K^2}{2p_z}, \\ E' &\simeq z p_z + \frac{p_\perp^2}{2 z p_z} - \frac{K'^2}{2 z p_z}, \\ E_\gamma &\simeq (1-z) p_z + \frac{p_\perp^2}{2(1-z) p_z}, \end{aligned} \tag{198}$$

from which, by imposing energy conservation, one obtains

$$-K^2 = -\frac{K'^2}{z} + \frac{p_\perp^2}{z(1-z)}. \tag{199}$$

Given K^2, K'^2 and z, eq. (199) allows one to compute the absolute value of the transverse momentum at the branching.

A˙3. *YFS Exponentiation.* – The Yennie-Frautschi-Suura exponentiation procedure is essentially a technique for summing up all the infra-red (IR) singularities present in any given process accompanied by photonic radiation [351]. It is inherently exclusive, *i.e.* all the summations of the IR-singular contributions are done before any phase-space integration over the virtual- or real-photon four-momenta are performed [352]. In the following, the general idea underlying the procedure will be shortly described (see for instance [353] for a more detailed analysis).

Let us consider the process $e^+(p_1)e^-(p_2) \to f_1(q_1) \cdots f_n(q_n)$, where $f_1(q_1) \cdots f_n(q_n)$ represents a given arbitrary final state, and let $\mathcal{M}_0$ be its matrix element. By using

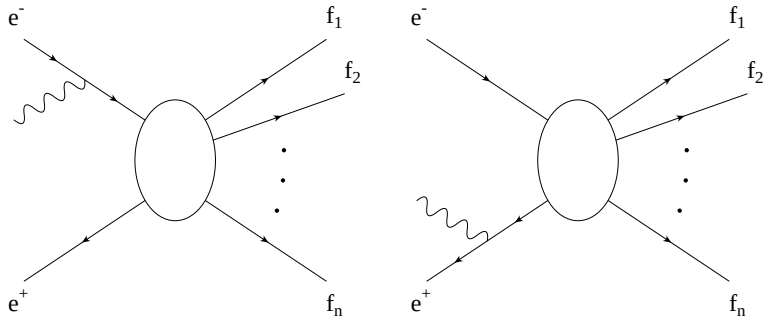

Fig. 63. – The Feynman diagrams for the initial-state $\mathcal{O}(\alpha)$ bremsstrahlung correction.

standard Feynman-diagram techniques, it is possible to show that the same process, when accompanied by l additional real photons radiated by the initial-state particles, and under the assumption that the l additional photons are soft, *i.e.* their energy is much smaller that any energy scale involved in the process, can be described by the factorized matrix element built up by the lowest order one, $\mathcal{M}_0$, times the product of l eikonal currents, namely

$$\mathcal{M} \simeq \mathcal{M}_0 \prod_{i=1}^{l} \left[e \left(\frac{\varepsilon_i(k_i) \cdot p_2}{k_i \cdot p_2} - \frac{\varepsilon_i(k_i) \cdot p_1}{k_i \cdot p_1} \right) \right], \tag{200}$$

where e is the electron charge, k_i are the momenta of the photons and $\varepsilon_i(k_i)$ their polarization vectors (see Fig. 63 for a representation of the Feynman diagrams relative to the initial-state $\mathcal{O}(\alpha)$ bremsstrahlung correction). By taking the square of the matrix element in eq. (200), multiplying for the proper flux factor and the Lorentz-invariant phase space volume element, neglecting the four-momenta of the radiated photons in the overall energy-momentum conservation, summing over the final state photons polarizations and combining properly all the factors, the cross section for the process $e^+(p_1)e^-(p_2) \to f_1(q_1) \cdots f_n(q_n) + l$ real photons can be written as

$$d\sigma_r^{(l)} = d\sigma_0 \frac{1}{l!} \prod_{i=1}^{l} \left[k_i dk_i d\cos\vartheta_i d\varphi_i \frac{1}{2(2\pi)^3} \sum_{\varepsilon_i} e^2 \left(\frac{\varepsilon_i(k_i) \cdot p_2}{k_i \cdot p_2} - \frac{\varepsilon_i(k_i) \cdot p_1}{k_i \cdot p_1} \right)^2 \right]. \tag{201}$$

By summing now on the number of final-state photons, one obtains the cross section for the original process accompanied by an arbitrary number of real photons, namely

$$\begin{aligned} d\sigma_r^{(\infty)} &= \sum_{l=0}^{\infty} d\sigma_r^{(l)} \\ &= d\sigma_0 \exp \left[kdkd\cos\vartheta d\varphi \frac{1}{2(2\pi)^3} \sum_{\varepsilon} e^2 \left(\frac{\varepsilon(k) \cdot p_2}{k \cdot p_2} - \frac{\varepsilon(k) \cdot p_1}{k \cdot p_1} \right)^2 \right]. \end{aligned} \tag{202}$$

Equation (202), being limited to real radiation only, is IR divergent once the phase space integrations are performed down to zero photonic energy. This problem, as well known, finds its solution in the matching between real and virtual photonic radiation. At any

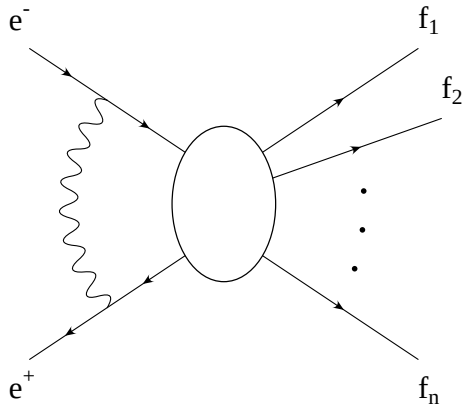

Fig. 64. – The Feynman diagram for the photonic vertex-like correction.

rate, eq. (202) already shows the key feature of exclusive exponentiation, *i.e.* summing up all the perturbative contributions before performing any phase space integration.

In order to get meaningful radiative corrections, besides initial-state real photon corrections it is necessary to consider also initial-state virtual photon corrections, *i.e.* the corrections due to additional internal photon lines connecting the initial-state electron and positron (see Fig. 64). For a vertex-type amplitude, the result can be written as

$$\mathcal{M}_{V_1} = -i\frac{e^2}{(2\pi)^4}\int d^4k \quad \frac{1}{k^2+i\varepsilon}\bar{v}(p_1)\gamma^\mu\frac{-(\not{p}_1+\not{k})+m}{2p_1\cdot k+k^2+i\varepsilon} \times \Gamma\frac{(\not{p}_2+\not{k})+m}{2p_2\cdot k+k^2+i\varepsilon}\gamma_\mu u(p_2), \tag{203}$$

where Γ stands for the Dirac structure competing to the lowest order process, in such a way that $\mathcal{M}_0 = \bar{v}(p_1)\Gamma u(p_2)$. The soft-photon part of the amplitude can be extracted by taking $k^\mu \simeq 0$ in all the numerators. In this approximation, the amplitude of eq. (203) becomes

$$\begin{aligned}&\mathcal{M}_{V_1} = \mathcal{M}_0 \times V\\ &V = \frac{2i\alpha}{(2\pi)^3}\int d^4k\frac{1}{k^2+i\varepsilon}\frac{4p_1\cdot p_2}{(2p_1\cdot k+k^2+i\varepsilon)(2p_2\cdot k+k^2+i\varepsilon)}.\end{aligned} \tag{204}$$

Some comments are in order here. First, as in the real case, the IR virtual correction factorizes off the lowest order matrix element, so that it is universal, *i.e.* independent of the details of the lowest order process under consideration. Moreover, it is also free of ultraviolet (UV) infinities; this, of course, does not mean that the UV behaviour of the complete amplitude is irrelevant, but that the IR part can be treated independently of renormalization problems. Last, as in the real case, it is divergent in the IR portion of the phase space.

The correction given by n soft virtual photons can be seen to factorize with an additional $1/n!$ factor [351], namely

$$\mathcal{M}_{V_n} = \mathcal{M}_0 \times \frac{1}{n!}V^n, \tag{205}$$

so that by summing over all the additional soft virtual photons one obtains

$$\mathcal{M}_V = \mathcal{M}_0 \times \exp[V]. \tag{206}$$

As already noticed, both the real and virtual factors are IR divergent. In order to obtain meaningful expressions, one has to adopt some regularization procedure. One possible regularization procedure is to give the photon a (small) mass λ and modifying eqs. (201) and (204) accordingly. Once all the expressions are properly regularized, one can write down the YFS master formula, which takes into account real and virtual photonic corrections to the lowest order process. In virtue of the factorization properties discussed above, the master formula can be obtained from eq. (202) with the substitution $d\sigma_0 \to d\sigma_0 |\exp(V)|^2$, *i.e.*

$$d\sigma = d\sigma_0 |\exp(V)|^2 \exp\left[kdkd\cos\vartheta d\varphi \frac{1}{2(2\pi)^3} \sum_\varepsilon e^2 \left(\frac{\varepsilon(k)\cdot p_2}{k\cdot p_2} - \frac{\varepsilon(k)\cdot p_1}{k\cdot p_1} \right)^2 \right]. \tag{207}$$

As a last step, it is possible to perform analytically the IR cancellation between virtual and very soft real photons. Actually, since very soft real photons do not affect the kinematics of the process, the real photon exponent can be split into a contribution coming from photons with energy less than a cutoff k_{min} plus a contribution coming from photons with energy above the same cutoff. The first contribution can be integrated over all its phase space and then combined with the virtual exponent. The physical meaning of this procedure is to sum over all the degenerate final states: in fact, a very soft real photon produces a signature that is indistinguishable from the signature typical of the elastic event. After this step it is possible to remove the regularizing photon mass by taking the limit $\lambda \to 0$, so that eq. (207) becomes

$$d\sigma = d\sigma_0 \exp(Y) \exp\left[kdkd\Theta(k-k_{min}) \cos\vartheta d\varphi \frac{1}{2(2\pi)^3} \sum_\varepsilon e^2 \left(\frac{\varepsilon(k)\cdot p_2}{k\cdot p_2} - \frac{\varepsilon(k)\cdot p_1}{k\cdot p_1} \right)^2 \right], \tag{208}$$

where Y is given by

$$Y = 2V + \int kdkd\Theta(k_{min}-k) \cos\vartheta d\varphi \frac{1}{2(2\pi)^3} \sum_\varepsilon e^2 \left(\frac{\varepsilon(k)\cdot p_2}{k\cdot p_2} - \frac{\varepsilon(k)\cdot p_1}{k\cdot p_1} \right)^2. \tag{209}$$

The explicit form of Y can be derived by performing all the details of the calculation, and reads

$$\begin{aligned} Y &= \beta \ln \frac{k_{min}}{E} + \delta_{YFS}, \\ \delta_{YFS} &= \frac{1}{4}\beta + \frac{\alpha}{\pi}\left(\frac{\pi^2}{3} - \frac{1}{2} \right), \\ \beta &= \frac{2\alpha}{\pi}\left[\ln\left(\frac{s}{m_e^2} \right) - 1 \right]. \end{aligned} \tag{210}$$

As in the SF method, the method of YFS exclusive exponentiation has been refined in order to take into account all-orders corrections on top of finite-order exact results (see for instance ref. [28] and references therein).

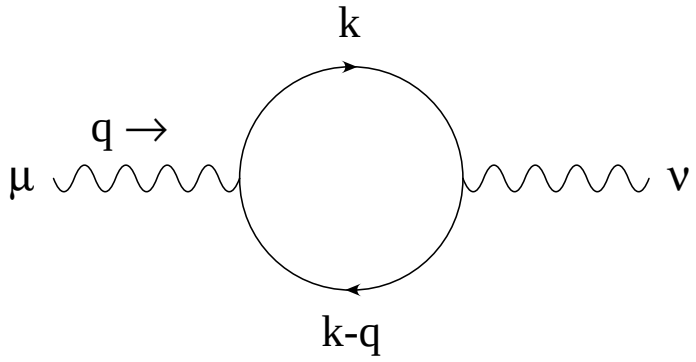

Fig. 65. – The fermionic vacuum polarization Feynman graph.

B. – Vacuum Polarization Corrections

The input parameter adopted for the analysis of the precision electroweak data collected at LEP are the QED coupling constant at zero momentum transfer α, the Fermi constant G_μ and the Z-boson mass M_Z. Given these input parameters, all the other unknown (or poorly known) parameters, such as the *top*-quark mass, the Higgs-boson mass and the QCD coupling constant α_s, are determined by means of best fits.

Actually, the QED coupling constant α is known with great precision at zero momentum transfer from measurements such as the electron/muon $g-2$, the Lamb shift, the muonium hyperfine splitting, the neutron compton wavelength, the quantum Hall and the Josephson effects [354, 355]; but for precision physics at LEP it must be evolved up to the Z-boson mass scale, so that the relevant parameter is rather the running QED coupling constant $\alpha(s)$. As is well known, the running of α is largely dominated by the contribution of fermionic vacuum polarization diagrams, which represent by themselves a gauge-invariant and universal subset of radiative corrections for two-fermion production processes (see Fig. 65). The bosonic contribution to vacuum polarization is, on the contrary, gauge-dependent. Its contribution is small, at least around the Z^0 resonance, and can be taken into account together with other gauge- and process-dependent radiative corrections at a given perturbative order. From now on, only the fermionic contribution to vacuum polarization will be discussed.

The QED running coupling constant is given by

$$\alpha(s) = \frac{\alpha(0)}{1-\Delta\alpha(s)},$$

$$\Delta\alpha(s) = -4\pi\alpha(0)\mathrm{Re}\left[\Pi_\gamma(s)-\Pi_\gamma(0)\right], \tag{211}$$

where $\Pi(q^2)$ is the two-point electromagnetic correlator, given by

$$(q^\mu q^\nu - q^2 g^{\mu\nu})\Pi_\gamma(q^2) = i\int d^4x e^{iq\cdot x}\langle 0|T(j^\mu(x)j^\nu(0))|0\rangle. \tag{212}$$

The vacuum polarization contribution can be naturally split into the contributions coming from the leptons, the *light* hadrons and the *top* quark according to the following relation:

$$\Delta\alpha(s) = \Delta\alpha_l(s) + \Delta\alpha_h^{(5)}(s) + \Delta\alpha_t(s). \tag{213}$$

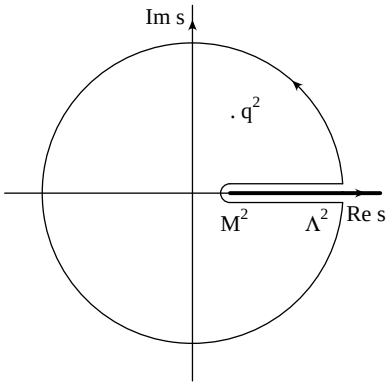

Fig. 66. – The integration contour $\mathcal{C}$ to be used for the integral of eq. (217) in order to obtain the dispersion relation of eq. (218).

The contributions from leptons and *top*-quark loops can be safely computed by means of ordinary perturbation theory. In particular, the leptonic contributions can be very well approximated by the expression of the loop-integrals for $m_l^2 << s$, and read

$$\Delta\alpha_l(s) = \frac{\alpha(0)}{3\pi}\sum_l \left(\ln\frac{s}{m_l^2} - \frac{5}{3}\right). \tag{214}$$

On the other hand, the *top*-quark contribution, due to the decoupling properties of QED, can be represented by

$$\Delta\alpha_t(s) = -\frac{\alpha(0)}{3\pi}\frac{4}{15}\frac{s}{m_t^2}. \tag{215}$$

In particular, eqs. (214) and (215), when evaluated at $s = M_Z^2$ give the values

$$\begin{aligned} &\Delta\alpha_l(M_Z^2) = 0.03142, \\ &\Delta\alpha_t(M_Z^2) = -0.6\times 10^{-4}. \end{aligned} \tag{216}$$

For the *light*-quark contributions, on the contrary, the perturbative expression of eq. (214) cannot be used. In fact, due to the ambiguities inherent in the definition of the *light*-quark masses, the answer provided by eq. (214) is affected by very large uncertainties, proportional to $\delta m_q/m_q$. Moreover, one can *a priori* expect very large non-perturbative QCD corrections in the region of the hadronic resonances. The standard procedure adopted in order to circumvent this problem is to exploit the analyticity properties of the vacuum polarization amplitudes by making use of dispersion relations (DR) techniques (see for instance [357]).

Given a complex-valued function F of complex argument s, if F is olomorphic in a region $\mathcal{R}$ and on its boundary $\mathcal{C}$, the value of F at any point q^2 inside $\mathcal{R}$ can be computed, according to the Cauchy's integral representation, as a contour integral:

$$F(q^2) = \frac{1}{2\pi i}\oint_{\mathcal{C}} ds\frac{F(s)}{s-q^2}. \tag{217}$$

Under the assumption that

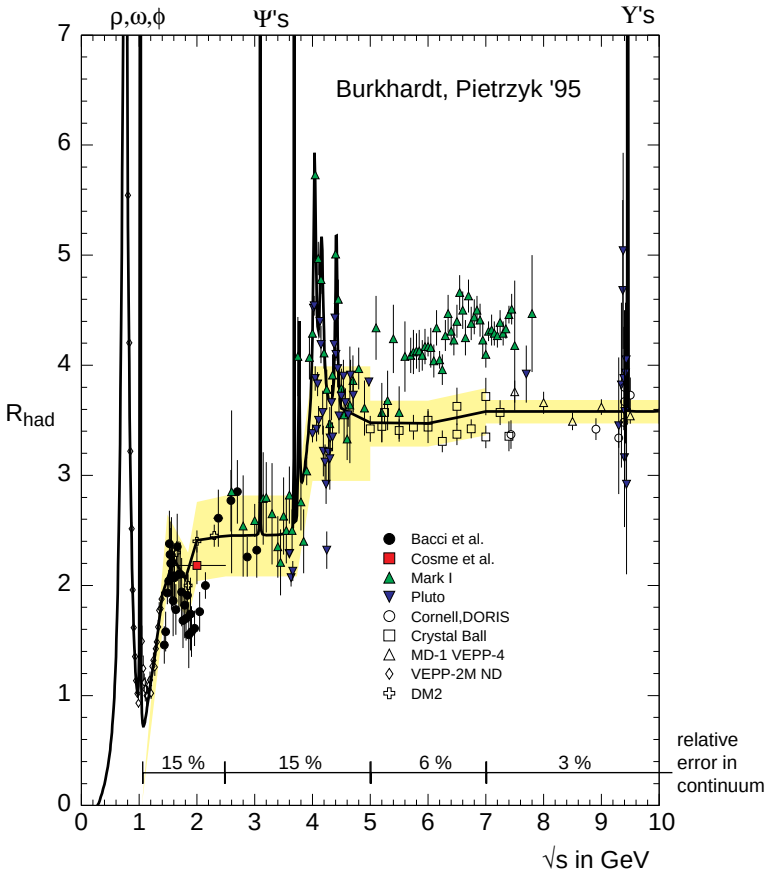

Fig. 67. – The total cross section for the process $e^+e^- \to hadrons$, normalized to the total cross section for the process $e^+e^- \to \mu^+\mu^-$ at low centre of mass energy (from [356]).

- $F(s)$ is real for real s, up to a threshold M^2,
- $F(s)$ has a branch cut for real $s > M^2$,
- $F(s)$ is olomorphic except along the branch cut,

and taking as integration contour the one shown in Fig. 66, one can derive the following once-subtracted DR

$$F(q^2) = F(q_0^2) + \frac{q^2 - q_0^2}{\pi} \int_{M^2}^{\infty} \frac{ds}{s - q_0^2} \frac{\mathrm{Im}F(s)}{s - q^2 - i\varepsilon}. \tag{218}$$

Equation (218) allows one to compute the value of F at any point q^2 with the only knowledge of the imaginary part of F along the branch cut. The optical theorem provides the link between the absorptive part of the hadronic vacuum polarization amplitude and the total cross section for the reaction $e^+e^- \to$ hadrons, namely

$$\sigma(s) = \frac{16\pi^2\alpha^2(s)}{s} \mathrm{Im}\Pi_\gamma(s). \tag{219}$$

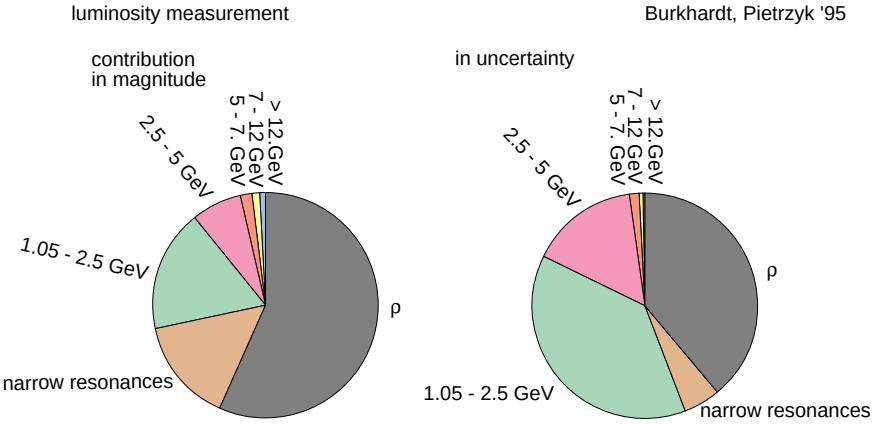

Fig. 68. – The relative contributions to $\Delta\alpha(t = -1.424\ \mathrm{GeV}^2)$ in magnitude and uncertainty (from [356]).

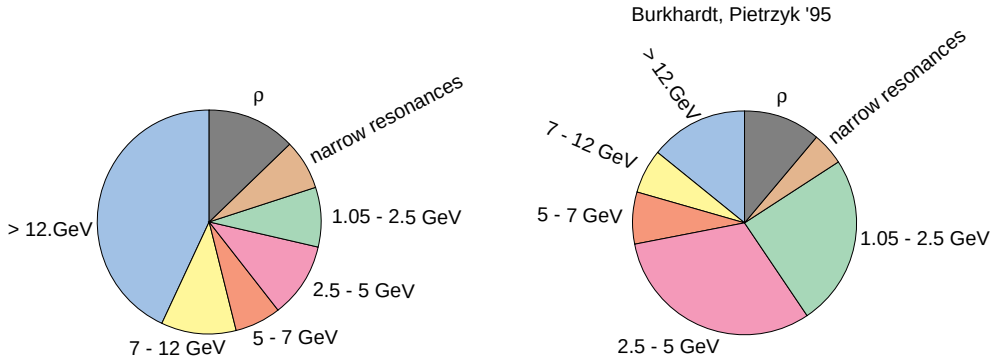

Fig. 69. – The relative contributions to $\Delta\alpha(s = M_Z^2)$ in magnitude and uncertainty (from [356]).

Hence, from the experimental data for $e^+e^- \to$ hadrons (see Fig. 67) one can compute the hadronic contribution of the hadronic vacuum polarization as follows:

$$\Delta\alpha_h^{(5)}(s) = -\frac{s}{4\pi^2\alpha}\mathrm{Re}\int_{4m_\pi^2}^{\infty} ds' \frac{\sigma_h(s')}{s' - s - i\varepsilon}. \tag{220}$$

Several determinations of the hadronic contribution to the running of the QED coupling constant α have been performed [356, 358–367]. The differences between the various determinations can be traced back to the procedures adopted for fitting the data, treating the experimental errors and performing the numerical integrations. The differences are also determined by the different thresholds chosen to start the application of perturbative QCD at large s, and to the value used for $\alpha_s(M_Z)$. Figures 68 and 69 show the relative contributions to $\Delta\alpha$ in magnitude and uncertainty at a scale typical of the luminosity measurement (Fig. 68) and at the Z^0 peak (Fig. 69). In Fig. 70 several determinations of $\Delta\alpha(M_Z)$ and $\alpha^{-1}(M_Z)$ are shown, together with the value used by

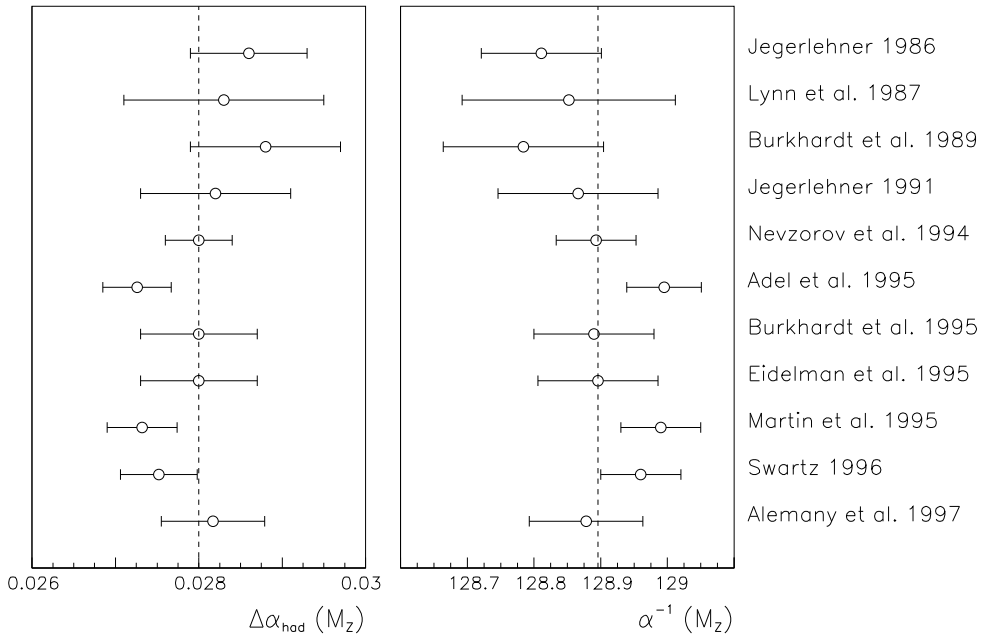

Fig. 70. – The determinations of $\Delta\alpha_h^{(5)}(M_Z)$ and $\alpha^{-1}(M_Z)$. The dashed vertical line selects the value used by the LEP Collaborations.

the LEP Collaborations.([9])

For practical purposes, the running of the QED coupling constant for large time-like momenta can be computed by means of the following effective formula, in terms of fermion masses and effective *light*-quark masses:

$$\Delta\alpha(s) = \frac{\alpha(0)}{3\pi}\sum_f Q_f^2 N_{cf}\left(\ln\frac{s}{m_f^2} - \frac{5}{3}\right). \tag{221}$$

In eq. (221), the sum is extended to all *light* fermions (charged leptons and *light* quarks), Q_f is the fermion charge in units of the electron charge and N_{cf} is 1 for leptons and 3 for quarks. The effective *light*-quark masses $m_d = m_u = 47$ MeV, $m_s = 150$ MeV, $m_c = 1.55$ GeV and $m_b = 4.7$ GeV insure that the hadronic vacuum polarization contribution of refs. [356, 364] is reproduced.

C. – One-loop Integrals and Dimensional Regularization

The evaluation of one-loop diagrams generally leads to the problem of ultraviolet divergences, so that a regularization procedure has to be adopted in order to deal with well

([9]) Two new determinations of $\alpha(M_Z)$ have recently appeared [368, 369] giving $\alpha^{-1}(M_Z) = 128.923 \pm 0.036$ and $\alpha^{-1}(M_Z) = 128.98 \pm 0.06$, respectively. After the completion of this work, a further analysis of $\alpha(M_Z)$ has been performed in [370], yelding the result $\alpha^{-1}(M_Z) = 128.928 \pm 0.023$.

defined objects before implementing a renormalization program. As said in Sect. **3**˙2.1 the method commonly used in the case of gauge theories is the dimensional regularization [45–47], where the singularities arise as poles of the form $1/(4-n)$, n being the number of space time dimensions where the integrals are convergent. In the literature a general method has been developed [48], which allows to write every loop diagram in terms of certain combinations of scalar form factors [49]. In this appendix some technical details concerning this procedure are provided for the simple case of the two-point form factors. In the evaluation of a self-energy diagram the following integrals are encountered:

$$B_0; B_\mu; B_{\mu\nu}(p^2, m_1, m_2) = \frac{1}{i\pi^2}\int d^n q \frac{1; q_\mu; q_{\mu\nu}}{(q^2+m_1^2)((q+p)^2+m_2^2)}. \tag{222}$$

The vector and tensor integrals can be decomposed into Lorentz covariants and scalar coefficients:

$$B_\mu(p^2, m_1, m_2) = p_\mu B_1(p^2.m_1, m_2), \tag{223}$$

$$B_{\mu\nu}(p^2, m_1, m_2) = p_\mu p_\nu B_{21}(p^2, m_1, m_2) + \delta_{\mu\nu} B_{22}(p^2, m_1, m_2). \tag{224}$$

The functions B_1, B_{21} and B_{22} are algebraically related to the two-point scalar integral B_0 and to the one-point scalar integral $A(m)$, defined by

$$A(m) = \frac{1}{i\pi^2}\int d^n q \frac{1}{q^2+m^2}. \tag{225}$$

The expression for B_1 can be obtained multiplying eq. (223) by p_μ and taking into account of the identity

$$q\cdot p = \frac{1}{2}\left[(q+p)^2 + m_2^2 - (q^2+m_1^2) - p^2 - m_2^2 + m_1^2\right]. \tag{226}$$

It follows that

$$B_1 = \frac{1}{2p^2}\left[A(m_1) - A(m_2) - (p^2 + m_2^2 - m_1^2)B_0\right], \tag{227}$$

where the arguments have been omitted for simplicity of notation. The expressions for B_{21} and B_{22} are analogously obtained multiplying eq. (224) by $p_\mu p_\nu$ and $\delta_{\mu\nu}$:

$$B_{22} = \frac{1}{3}\left\{-m_1^2 B_0 + \frac{1}{2}[A(m_2) - (m_1^2 + m_2^2 + \frac{1}{3}p^2) - (m_1^2 - m_2^2 - p^2)B_1]\right\}, \tag{228}$$

$$B_{21} = \frac{1}{3p^2}\left[A(m_2) + 2(m_1^2 - m_2^2 - p^2)B_1 + \frac{1}{2}(m_1^2 + m_2^2 + \frac{1}{3}p^2) + m_1^2 B_0\right]. \tag{229}$$

In so doing only the basic scalar integrals $A(m)$ and $B_0(p^2, m_1, m_2)$ need to be calculated.

Let us consider the one-point integral $A(m)$ in four dimensions:

$$A(m) = \frac{1}{i\pi^2}\int_0^\infty dq_0 \int d^3 q \frac{1}{q^2 + m^2 - i\varepsilon}. \tag{230}$$

In the complex q_0 plane the integrand has poles for

$$q_0 = \pm\left(\sqrt{|q|^2 + m^2} - i\varepsilon\right). \tag{231}$$

The introduction of the Wick rotation allows to transform the Minkowski space in a Euclidean space and perform the integration by means of polar coordinates.

Working in Euclidean space in the case of n dimensions, a set of generalized polar coordinates can be introduced [47, 371]

$$\int d^n q = \int_0^\infty \omega^{n-1} d\omega \int_0^{2\pi} d\vartheta_1 \int_0^\pi \sin\vartheta_2 d\vartheta_2 \ldots \int_0^\pi \sin^{n-2}\vartheta_{n-1} d\vartheta_{n-1}. \tag{232}$$

Since the integrand of $A(m)$ depends only on q^2, the angular integrations are easily performed by means of the relation

$$\int_0^\pi \sin^m \vartheta d\vartheta = \sqrt{\pi}\frac{\Gamma\left(\frac{m+1}{2}\right)}{\Gamma\left(\frac{m+2}{2}\right)}, \tag{233}$$

yielding

$$A(m) = \frac{2\pi^{\frac{n}{2}-2}}{\Gamma\left(\frac{n}{2}\right)} \int_0^\infty \omega^{n-1} d\omega \frac{1}{\omega^2 + m^2} \tag{234}$$

$$= \frac{2\pi^{\frac{n}{2}-2}}{\Gamma\left(\frac{n}{2}\right)} \cdot \frac{1}{2} \cdot \frac{\Gamma\left(\frac{n}{2}\right)\Gamma\left(1-\frac{n}{2}\right)}{\Gamma(1) m^{2\left(1-\frac{n}{2}\right)}} \tag{235}$$

$$= \frac{\pi^{\frac{n}{2}-2}}{m^{2-n}} \Gamma\left(1-\frac{n}{2}\right), \tag{236}$$

where $\Gamma(x)$ is the Euler Γ function with the property $x\Gamma(x) = \Gamma(x+1)$. Since the physical results are recovered for n approaching 4, it is convenient to introduce the notation $n = 4 - \varepsilon$, and expand the expression of $A(m)$ around $\varepsilon = 0$:

$$A(m) = m^2 \pi^{-\frac{\varepsilon}{2}} m^{-\varepsilon} \frac{\Gamma\left(\frac{\varepsilon}{2}\right)}{-1 + \frac{\varepsilon}{2}} \tag{237}$$

$$\simeq m^2 \left(-\Delta + \ln m^2 - 1\right), \tag{238}$$

where

$$\Delta = \frac{2}{4-n} - \gamma - \ln\pi \tag{239}$$

contains the ultraviolet divergence, and the expansion of the Γ function around the zero of its argument has been used

$$\Gamma(x) = \frac{1}{x} - \gamma + \mathcal{O}(x), \tag{240}$$

with γ indicating the Euler constant.

The calculation of the two-point scalar integral B_0 is more involved than $A(m)$ because of the presence of two factors in the denominator. As a first step it is necessary to use the Feynman parameterization to combine the denominators:

$$\frac{1}{ab} = \int_0^1 dx \frac{1}{[ax + b(1-x)]^2}, \tag{241}$$

where

$$b = q^2 + m_1^2,$$
$$a = (q+p)^2 + m_2^2.$$

With a shift in the integration variable $q \to q + xp$ the term linear in the integration variable disappears, yielding

$$B_0(p^2, m_1, m_2) = \frac{1}{i\pi^2} \int_0^1 dx \int d^n q \frac{1}{(q^2 + \chi - i\varepsilon)^2}, \tag{242}$$

with $\chi = -p^2 x^2 + (p^2 + m_2^2 - m_1^2)x + m_1^2$. The angular integration is now straightforward and the last integral is again worked out in terms of the Γ function:

$$B_0(p^2, m_1, m_2) = \frac{\pi^{\frac{n}{2}-2}}{\chi^{2-\frac{n}{2}}} \frac{\Gamma\left(2 - \frac{n}{2}\right)}{\Gamma(2)}. \tag{243}$$

By means of an expansion of n around 4 as for the case of the one-point scalar integral, the expression for B_0 reads:

$$B_0(p^2, m_1, m_2) = \Delta - \int_0^1 dx \ln \chi. \tag{244}$$

For arbitrary values of momentum and masses the integral in eq. (244) can be worked out by means of the method outlined in ref. [50]. The integration becomes straightforward for particular values of the arguments. For example, to obtain the asymptotic expressions of the fermionic self-energies written in Sect. **3**˙2.1, the following asymptotic expressions for the B_0 scalar function are useful:

$$\begin{aligned}
&B_0(p^2, m, m)_{|p^2| \gg m^2} \simeq \Delta - \ln(-p^2) + 2 + i\pi, \\
&B_0(p^2, m, m)_{|p^2| \ll m^2} \simeq \Delta - \ln m^2 - \frac{p^2}{6m^2} + \frac{p^4}{60m^4}, \\
&B_0(p^2, 0, m)_{|p^2| \gg m^2} \simeq \Delta - \ln(-p^2) + 2 + i\pi, \\
&B_0(p^2, 0, m)_{|p^2| \ll m^2} \simeq \Delta - \ln m^2 + 1 - \frac{p^2}{2m^2}.
\end{aligned}$$

Concerning the vertex correction diagrams, the following three-point integrals are encountered:

$$C_0; C_\mu; C_{\mu\nu}(p_1, p_2, m_1, m_2, m_3) = \frac{1}{i\pi^2} \int d^n q \frac{1; q_\mu; q_{\mu\nu}}{(1)(2)(3)}, \tag{245}$$

where

$$\begin{aligned}
(1) &= q^2 + m_1^2, \\
(2) &= (q + p_1)^2 + m_2^2, \\
(3) &= (q + p_1 + p_2)^2 + m_3^2.
\end{aligned}$$

The vector and tensor integrals can be decomposed into Lorentz covariants and scalar coefficients in the following way:

$$\begin{aligned}
C_\mu &= p_1^\mu C_{11} + p_2^\mu C_{12}, \\
C_{\mu\nu} &= p_1^\mu p_1^\nu C_{21} + p_2^\mu p_2^\nu C_{22} + (p_1^\mu p_2^\nu + p_2^\mu p_1^\nu) C_{23} + \delta_{\mu\nu} C_{24},
\end{aligned}$$

where the arguments in the functions C_{ij} have been neglected for simplicity of notations. According to the procedure illustrated in ref. [48], the three-point scalar form factors can be expressed as linear combinations of two-point functions and of the fundamental three-point scalar integral C_0. It is worth noticing that only the function C_{24} contains the UV divergences, while the other form factors are UV finite.

REFERENCES

[1] S.L. Glashow, *Nucl. Phys. A*, **22**, (1961) 579; S. Weinberg, *Phys. Rev. Lett.*, **19**, (1967) 1264; A. Salam, in *Elementary Particle Theory*, edited by N. Svartholm, (Almquist and Wiksell, Stockolm, 1968), p. 367.

[2] M. Gell-Mann, *Acta Phys. Austriaca Suppl.*, **IX**, (1972) 733; H. Fritzsch, M. Gell-Mann and H. Luetwyler, *Phys. Lett. B*, **47**, (1973) 365; D.J. Gross and F. Wilczek, *Phys. Rev. Lett.*, **30**, (1973) 1343, *Phys. Rev. D*, **8**, (1973) 3633; H.D. Politzer, *Phys. Rev. Lett.*, **30**, (1973) 1346.

[3] P.W. Higgs, *Phys. Lett.*, **12**, (1964) 132; *Phys. Rev. Lett.*, **13**, (1964) 508, *Phys. Rev.*, **145**, (1966) 1156; F. Englert and R. Brout, *Phys. Rev. Lett.*, **13**, (1964) 321.

[4] F.J. Hasert *et al.*, *Phys. Lett. B*, **46**, (1973) 121, **46**, (1973), 138.

[5] G. Arnison *et al.* (UA1 coll.), *Phys. Lett. B*, **122**, (1983) 103, **126**, (1983), 398, **129**, (1983), 273; M. Banner *et al.* (UA2 coll.), *Phys. Lett. B*, **122**, (1983) 476; P. Bagnaia *et al.* (UA2 coll.), *Phys. Lett. B*, **129**, (1983) 130.

[6] See, for instance, F.A. Berends and A. Böhm, in *High Energy Electron-Positron Physics*, edited by A. Ali and P. Söding, (World Scientific, Singapore, 1988).

[7] G. Quast, talk given at the International Conference on High Energy Physics, Jerusalem, 19-26 August, 1997.

[8] D. Ward, plenary talk given at the International Europhysics Conference on High Energy Physics, Jerusalem, 19-26 August, 1997, `hep-ph/9711515`.

[9] H. Burkhardt and J. Steinberger, *Annual Rev. of Nucl. and Part. Science*, **41**, (1991) 55; D. Schaile, *Fortschr. Phys.*, **42**, (1994) 429; J. Mnich, *Phys. Rep.*, **271**, (1996) 181.

[10] M. Böhm, W. Hollik and H. Spiesberger, *Fortschr. Phys.*, **34**, (1986) 687; M.E. Peskin, in *Physics at the 100 GeV mass scale*, edited by E.C. Brennan, SLAC, 1990, p. 71; W. Hollik, *Fortschr. Phys.*, **38**, (1990) 165; F. Jegerlehner, *Progress in Part. and Nucl. Phys.*, **27**, (1991) 1; W.J. Marciano, *Annual Rev. of Nucl. and Part. Science*, **41**, (1991) 469; B.A. Kniehl, *Phys. Rep*, **240**, (1994) 211; A. Sirlin, *Comments Nucl. and Part. Phys.*, **21**, (1994) 287; W. Hollik, *Acta Phys. Pol. B*, **27**, (1996) 3685 and `hep-ph/9602380`; M.I. Vysotskii, V.A. Novikov, L.B. Okun and A.N. Rozanov, *Phys. Usp.*, **39**, (1996) 503.

[11] *Physics at LEP*, edited by J. Ellis and R. Peccei, CERN Report 86-02, Vols. 1 and 2 (CERN, Geneva) 1986.

[12] *Polarization at LEP*, edited by G. Alexander *et al.*, CERN Report 88-06, Vols. 1 and 2 (CERN, Geneva) 1988.

[13] *Z Physics at LEP 1*, edited by G. Altarelli, R. Kleiss and C. Verzegnassi, CERN Report 89-08, Vols. 1 and 2 (CERN, Geneva) 1989.

[14] *Reports of the Working Group on Precision Calculations for the Z Resonance*, edited by D. Bardin, W. Hollik and G. Passarino, CERN Report 95-03, (CERN, Geneva) 1995.

[15] *Physics at LEP2*, edited by G. Altarelli, T. Sjöstrand and F. Zwirner, CERN Report 96-01, Vols. 1 and 2 (CERN, Geneva) 1996.

[16] D. Abbaneo *et al.*, CERN-PPE/97-154.

[17] M. Caffo, E. Remiddi *et al.*, *Bhabha Scattering* in [13], Vol. 1, p. 171.

[18] S. Jadach, O. Nicrosini *et al.*, *Event Generators for Bhabha Scattering* in [15], Vol. 2, p. 229.

[19] G.M. Dallavalle, *Acta Phys. Pol. B*, **28**, (1997) 901.

[20] F. Bloch and A. Nordsieck, *Phys. Rev.*, **52**, (1937) 54;
T. Kinoshita, *J. Math. Phys.*, **3**, (1962) 650;
T.D. Lee and M. Nauenberg, *Phys. Rev. B*, **133**, (1964) 1549.
[21] M. Cacciari, G. Montagna, O. Nicrosini and F. Piccinini, in [14], p. 389.
[22] M. Cacciari, G. Montagna, O. Nicrosini and F. Piccinini, *Comput. Phys. Commun.*, **90**, (1995) 301.
[23] G. Montagna, O. Nicrosini and F. Piccinini, *Phys. Lett. B*, **385**, (1996) 348.
[24] S. Jadach, M. Skrzypek and B.F.L. Ward, *Phys. Rev. D*, **55**, (1997) 1206.
[25] W. Beenakker, M. Martinez and B. Pietrzyk, in [14], pag. 399.
[26] S. Jadach, W. Płaczek and B.F.L. Ward, *Phys. Lett. B*, **353**, (1995) 349.
[27] M. Caffo, H. Czyż and E. Remiddi, in [14], p. 361.
[28] S. Jadach, E. Richter-Wąs, B.F.L. Ward and Z. Wąs, *Phys. Lett. B*, **353**, (1995) 362, *Comput. Phys. Commun.*, **70**, (1992) 305.
[29] S. Jadach, W. Płaczek, E. Richter-Wąs, B.F.L. Ward and Z. Wąs, *Comput. Phys. Commun.*, **102**, (1997) 229.
[30] A. Arbuzov *et al.*, *Nucl. Phys. Proc. Suppl.*, **51C**, (1996) 154, *Nucl. Phys. B*, **485**, (1997) 457, *Phys. Lett. B*, **394**, (1997) 218.
[31] F.A. Berends and R. Kleiss, *Nucl. Phys. B*, **228**, (1983) 537.
[32] M. Greco, G. Montagna, O. Nicrosini and F. Piccinini, *Phys. Lett. B*, **318**, (1993) 635; G. Montagna, O. Nicrosini and F. Piccinini, *Comput. Phys. Commun.*, **78**, (1993) 155; erratum, **79**, (1994), 351.
[33] M. Cacciari, A. Deandrea, G. Montagna, O. Nicrosini and L. Trentadue, *Phys. Lett. B*, **268**, (1991) 441, **271**, (1991), 431.
[34] A. Arbuzov *et al.*, *Phys. Lett. B*, **383**, (1996) 238.
[35] S. Jadach, M. Melles, B.F.L. Ward and S.A. Yost, *Nucl. Phys. Proc. Suppl.*, **51C**, (1996) 164.
[36] S. Jadach and B.F.L. Ward, *Phys. Lett. B*, **389**, (1996) 129.
[37] S. Jadach, M. Melles, B.F.L. Ward and S.A. Yost, *Phys. Lett. B*, **377**, (1996) 168.
[38] S. Jadach *et al.*, in *Proceedings of the 28th International Conference on High Energy Physics*, edited by Z. Ajduk and A.K. Wroblewski, (World Scientific, Singapore, 1997), Vol. II, p. 1072.
[39] B.F.L. Ward *et al.*, *Acta Phys. Pol. B*, **28**, (1997) 925.
[40] S. Jadach, B.F.L. Ward and S.A. Yost, *Phys. Rev. D*, **47**, (1993) 2682.
[41] R. Barbieri, J.A. Mignaco and E. Remiddi, *Nuovo Cimento*, **11A**, (1972) 824, 865.
[42] E.A. Kuraev and V. Fadin, *Sov. J. Nucl. Phys.*, **41**, (1985) 466.
[43] M. Greco, *Rivista del Nuovo Cimento Vol.*, **11, N. 5**, (1988) 1.
[44] G. 't Hooft, *Nucl. Phys. B*, **33**, (1971) 173; *Nucl. Phys. B*, **35**, (1971) 167.
[45] C. Bollini and J. Giambiagi, *Nuovo Cim. B*, **12**, (1972) 20.
[46] J. Ashmore, *Nuovo Cim. Lett.*, **4**, (1972) 289.
[47] G. 't Hooft and M. Veltman, *Nucl. Phys. B*, **44**, (1972) 189.
[48] G. Passarino and M. Veltman, *Nucl. Phys. B*, **160**, (1979) 151.
[49] G. 't Hooft and M. Veltman, *Nucl. Phys. B*, **153**, (1979) 365.
[50] M. Green and M. Veltman, *Nucl. Phys. B*, **169**, (1980) 137.
[51] G. Passarino, *Nucl. Phys. B*, **361**, (1991) 351.
[52] T. Appelquist and J. Carazzone, *Phys. Rev. D*, **11**, (1975) 2856.

[53] A. Akhundov, D. Bardin and T. Riemann, *Nucl. Phys. B*, **276**, (1986) 1; W. Beenakker and W. Hollik, *Z. Phys. C*, **40**, (1988) 1; J. Bernabéu, A. Pich and A. Santamaria, *Phys. Lett. B*, **200**, (1988) 569, *Nucl. Phys. B*, **363**, (1991) 326; B.W. Lynn and R.G. Stuart, *Phys. Lett. B*, **252**, (1990) 676.
[54] M. Veltman, *Phys. Lett. B*, **91**, (1980) 95.
[55] F. Antonelli, M. Consoli and G. Corbò, *Phys. Lett. B*, **91**, (1980) 90.
[56] F. Antonelli, M. Consoli, G. Corbò and O. Pellegrino, *Nucl. Phys. B*, **183**, (1981) 195.
[57] D.A. Ross and J.C. Taylor, *Nucl. Phys. B*, **51**, (1973) 25; G. Passarino and M. Veltman, *Nucl. Phys. B*, **160**, (1979) 151; A. Sirlin, *Phys. Rev. D*, **22**, (1980) 971; W.J. Marciano and A. Sirlin, *Phys. Rev. D*, **22**, (1980) 2695; D. Bardin, P.Ch. Christova and O.M. Fedorenko, *Nucl. Phys. B*, **175**, (1980) 235, *Nucl. Phys. B*, **197**, (1982) 1; D. Bardin, M.S. Bilenky, G.V. Mitselmakher, T. Riemann and M. Sachwitz, *Z. Phys. C*, **44**, (1989) 493; J. Fleischer and F. Jegerlehner, *Phys. Rev. D*, **23**, (1981) 2001; K.I. Aoki, Z. Hioki, R. Kawabe, M. Konuma and T. Muta, *Suppl. Prog. Theor. Phys.*, **73**, (1982) 1; M. Consoli, S. LoPresti and L. Maiani, *Nucl. Phys. B*, **223**, (1983) 474; M. Böhm, W. Hollik and H. Spiesberger, *Fortschr. Phys.*, **34**, (1986) 687; W. Hollik, *Fortschr. Phys.*, **38**, (1990) 165.
[58] G. 't Hooft, *Nucl. Phys. B*, **61**, (1973) 455, *Nucl. Phys. B*, **62**, (1973) 444; W.J. Marciano and A. Sirlin, *Phys. Rev. Lett.*, **46**, (1981) 163; A. Sirlin, *Phys. Lett. B*, **232**, (1989) 123; G. Degrassi, S. Fanchiotti and A. Sirlin, *Nucl. Phys. B*, **351**, (1991) 49; G. Degrassi and A. Sirlin, *Nucl. Phys. B*, **352**, (1991) 342; G. Passarino and M. Veltman, *Phys. Lett. B*, **237**, (1990) 537.
[59] F. Jegerlehner, *Z. Phys. C*, **32**, (1986) 425; W. Hollik and H.J. Timme, *Z. Phys. C*, **33**, (1986) 125; G. Passarino and R. Pittau, *Phys. Lett. B*, **228**, (1989) 89; G. Passarino, *Nucl. Phys. B*, **361**, (1991) 351; V.A. Novikov, L.B. Okun and M.I. Vysotsky, *Nucl. Phys. B*, **397**, (1993) 35.
[60] D.C. Kennedy and B.W. Lynn, *Nucl. Phys. B*, **322**, (1989) 1; M. Kuroda, G. Moultaka and D. Schildknecht, *Nucl. Phys. B*, **350**, (1991) 25.
[61] A. Sirlin, *Phys. Rev. D*, **22**, (1980) 971; W.J. Marciano and A. Sirlin, *Phys. Rev. D*, **22**, (1980) 2695.
[62] D. Ross and M. Veltman, *Nucl. Phys. B*, **95**, (1975) 135.
[63] M. Veltman, *Nucl. Phys. B*, **123**, (1977) 89.
[64] M.S. Chanowitz, M.A. Furman and I. Hinchliffe, *Phys. Lett. B*, **78**, (1978) 285.
[65] M. Veltman, *Acta. Phys. Pol. B*, **8**, (1977) 475.
[66] M. Consoli, W. Hollik and F. Jegerlehner, *Electroweak radiative corrections for Z physics* in [13], p. 7.
[67] G. Burgers and F. Jegerlehner, *Δr, or the relation between the electroweak couplings and the weak vector boson masses* in [13], p. 55.
[68] A. Sirlin, *Phys. Rev. D*, **29**, (1984) 89.
[69] G. Degrassi, S. Fanchiotti and A. Sirlin, *Nucl. Phys. B*, **351**, (1991) 49.
[70] G. Degrassi and A. Sirlin, *Nucl. Phys. B*, **352**, (1991) 342.
[71] A. Sirlin, *Phys. Lett. B*, **232**, (1989) 123.
[72] W. Hollik and H.J. Timme, *Z. Phys. C*, **33**, (1986) 125.
[73] G. Passarino and R. Pittau, *Phys. Lett. B*, **228**, (1989) 89.
[74] D.C. Kennedy and B.W. Lynn, *Nucl. Phys. B*, **322**, (1989) 1.

[75] F.M. Renard and C. Verzegnassi, *Phys. Rev. D*, **52**, (1995) 1369; **53**, (1996), 1290.

[76] D. Bardin *et al.*, *Electroweak Working Group Report* in [14], p. 7, hep-ph/9709229.

[77] M. Cacciari, G. Montagna, O. Nicrosini and G. Passarino, *Phys. Lett. B*, **279**, (1992) 384; M. Cacciari, G. Montagna, O. Nicrosini, G. Passarino and R. Pittau, *Phys. Lett. B*, **286**, (1992) 387; F. Piccinini and R. Pittau, *Phys. Lett. B*, **293**, (1992) 237.

[78] G. Montagna, O. Nicrosini, G. Passarino, F. Piccinini and R. Pittau, *Nucl. Phys. B*, **401**, (1993) 3.

[79] W.J. Marciano, *Phys. Rev. D*, **20**, (1979) 274; F. Antonelli and L. Maiani, *Nucl. Phys. B*, **186**, (1981) 269.

[80] M. Consoli, W. Hollik and F. Jegerlehner, *Phys. Lett. B*, **227**, (1989) 167.

[81] J.J. van der Bij and F. Hoogeven, *Nucl. Phys. B*, **283**, (1987) 477.

[82] R. Barbieri, M. Beccaria, P. Ciafaloni, G. Curci and A. Viceré, *Phys. Lett. B*, **288**, (1992) 95, erratum **312**, (1993), 511, *Nucl. Phys. B*, **409**, (1993) 105.

[83] J. Fleischer, F. Jegerlehner and O.V. Tarasov, *Phys. Lett. B*, **319**, (1993) 249, *Phys. Rev. D*, **51**, (1995) 3820; G. Degrassi, S. Fanchiotti and P. Gambino, *Int. J. Mod. Phys. A*, **10**, (1995) 1337.

[84] A. Denner, W. Hollik and B. Lampe, *Z. Phys. C*, **60**, (1993) 193.

[85] J.J. van der Bij and M. Veltman, *Nucl. Phys. B*, **231**, (1984) 205; J.J. van der Bij, *Nucl. Phys. B*, **248**, (1984) 141.

[86] R. Barbieri, P. Ciafaloni and A. Strumia, *Phys. Lett. B*, **317**, (1993) 381.

[87] G. Degrassi, S. Fanchiotti, F. Feruglio, P. Gambino and A. Vicini, in [14], p. 163, *Phys. Lett. B*, **350**, (1995) 75.

[88] G. Degrassi, P. Gambino and A. Vicini, *Phys. Lett. B*, **383**, (1996) 219.

[89] G. Degrassi, P. Gambino and A. Sirlin, *Phys. Lett. B*, **394**, (1997) 188.

[90] S. Bauberger and G. Weiglein, *Nucl. Instrum. Meth. A*, **389**, (1997) 318, hep-ph/9707510, hep-ph/9712227.

[91] G. Weiglein, *Acta Phys. Polon. B*, **28**, (1997) 1381.

[92] K.G. Chetyrkin, J.H. Kühn and A. Kwiatkowski, in [14] p. 175; *Phys. Rep.*, **277**, (1996) 189.

[93] A. Djouadi and C. Verzegnassi, *Phys. Lett. B*, **195**, (1987) 265; A. Djouadi, *Nuovo Cim. A*, **100**, (1988) 357; B.A. Kniehl, J.H. Kühn and R.G. Stuart, *Phys. Lett. B*, **214**, (1988) 621; D. Bardin and A.V. Chizhov, Dubna preprint E2-89-525 (1989); B.A. Kniehl, *Nucl. Phys. B*, **347**, (1990) 86; F. Halzen and B.A. Kniehl, *Nucl. Phys. B*, **353**, (1991) 567; B.A. Kniehl and A. Sirlin, *Nucl. Phys. B*, **371**, (1992) 141, *Phys. Rev D*, **47**, (1993) 883; S. Fanchiotti, B.A. Kniehl and A. Sirlin, *Phys. Rev D*, **48**, (1993) 307; A. Djouadi and P. Gambino, *Phys. Rev. D*, **49**, (1994) 3499; N.A. Nekrasov, V.A. Novikov, L.B. Okun and M.I. Vysotsky, *Yad. Fiz.*, **57**, (1994) 883.

[94] L. Avdeev, J. Fleischer, S.M. Mikhailov and O.V. Tarasov, *Phys. Lett. B*, **336**, (1994) 560, erratum **349**, (1995), 597; K.G. Chetyrkin, J.H. Kühn and M. Steinhauser, *Phys. Lett. B*, **351**, (1995) 331, *Phys. Rev. Lett.*, **75**, (1995) 3394.

[95] A. Djouadi *et al.*, *Phys. Rev. Lett.*, **78**, (1997) 3626.

[96] J. Fleischer, F. Jegerlehner, P. Rączka and O.V. Tarasov, *Phys. Lett. B*, **293**, (1992) 437; G. Buchalla and A.J. Buras, *Nucl. Phys. B*, **398**, (1993) 285; G. Degrassi, *Nucl. Phys. B*, **407**, (1993) 271; K.G. Chetyrkin, A. Kwiatkowski and M. Steinhauser, *Mod. Phys. Lett. A*, **8**, (1993) 2785.
[97] A. Kwiatkowski and M. Steinhauser, *Phys. Lett. B*, **344**, (1995) 359; S. Peris and A. Santamaria, *Nucl. Phys. B*, **445**, (1995) 252.
[98] R. Harlander, T. Seidensticker and M. Steinhauser, `hep-ph/9712228`.
[99] A.L. Kataev, *Phys. Lett. B*, **287**, (1992) 209.
[100] K.G. Chetyrkin, A.L. Kataev and F.V. Tkachov, *Phys. Lett. B*, **85**, (1979) 277; M. Dine and J. Sapirstein, *Phys. Rev. Lett.*, **43**, (1979) 668; W. Celmaster and R. Gonsalves, *Phys. Rev. Lett.*, **44**, (1980) 560.
[101] S.G. Gorishny, A.L. Kataev and S.A. Larin, *Phys. Lett. B*, **259**, (1991) 144; L.R. Surguladze and M.A. Samuel, *Phys. Rev. Lett.*, **66**, (1991) 560.
[102] B.A. Kniehl, *Phys. Lett. B*, **237**, (1990) 127; A.H. Hoang, M. Jeżabek, J.H. Kühn and T. Teubner, *Phys. Lett. B*, **338**, (1994) 330.
[103] B.A. Kniehl and J.H. Kühn, *Phys. Lett. B*, **224**, (1990) 229, *Nucl. Phys. B*, **329**, (1990) 547; K.G. Chetyrkin and J.H. Kühn, *Phys. Lett. B*, **248**, (1990) 359; K.G. Chetyrkin, J.H. Kühn and A. Kwiatkowski, *Phys. Lett. B*, **282**, (1992) 221; K.G. Chetyrkin and A. Kwiatkowski, *Phys. Lett. B*, **305**, (1993) 285, **319**, (1993), 307, *Z. Phys. C*, **59**, (1993) 525; K.G. Chetyrkin, *Phys. Lett. B*, **307**, (1993) 169; K.G. Chetyrkin and J.H. Kühn, *Phys. Lett. B*, **308**, (1993) 127; K.G. Chetyrkin and O.V. Tarasov, *Phys. Lett. B*, **327**, (1994) 114; S.A. Larin, T. van Ritbergen and J.A.M. Vermaseren, *Phys. Lett. B*, **320**, (1994) 159.
[104] L.R. Surguladze and M.A. Samuel, *Rev. Mod. Phys.*, **68**, (1996) 259.
[105] S.A. Larin, T. van Ritbergen and J.A.M. Vermaseren, in [14] p. 265.
[106] A. Czarnecki and J.H. Kühn, *Phys. Rev. Lett.*, **77**, (1996) 3955.
[107] A. Djouadi, J.H. Kühn and P.M. Zerwas, *Z. Phys. C*, **46**, (1990) 411; G. Altarelli and B. Lampe, *Nucl. Phys. B*, **391**, (1993) 3; A. Djouadi, B. Lampe and P.M. Zerwas, *Z. Phys. C*, **67**, (1995) 123.
[108] J.H. Kühn, P. Zerwas *et al.*, in [13], Vol. 1, p. 267.
[109] K.G. Chetyrkin, B.A. Kniehl and M. Steinhauser, *Phys. Rev. Lett.*, **79**, (1997) 2184.
[110] T. van Ritbergen, J.A.M. Vermaseren and S.A. Larin, *Phys. Lett. B*, **400**, (1997) 379.
[111] G. Montagna, O. Nicrosini, G. Passarino, F. Piccinini and R. Pittau, *Nucl. Phys. B*, **401**, (1993) 3, *Comput. Phys. Commun.*, **76**, (1993) 328; G. Montagna, O. Nicrosini, G. Passarino and F. Piccinini, *Comput. Phys. Commun.*, **93**, (1996) 120.
[112] O. Nicrosini and L. Trentadue, *Phys. Lett. B*, **196**, (1987) 551.
[113] F.A. Berends *et al.*, *Z line shape* in [13], p. 89.
[114] G. Montagna, O. Nicrosini and L. Trentadue, *Phys. Lett. B*, **231**, (1989) 492.
[115] M. Böhm, W. Hollik *et al.*, *Forward-backward asymmetries* in [13], p. 203.
[116] G. Burgers, *Phys. Lett. B*, **164**, (1985) 167.
[117] F.A. Berends, G. Burgers and W.L. van Neerven, *Nucl. Phys. B*, **297**, (1988) 429.
[118] S. Jadach, M. Skrzypek and B.F.L. Ward, *Phys. Lett. B*, **257**, (1991) 173.
[119] M. Skrzypek, *Acta Phys. Pol. B*, **23**, (1992) 135.

[120] G. Montagna, O. Nicrosini and F. Piccinini, *Phys. Lett. B*, **406**, (1997) 243.
[121] B.A. Kniehl, M. Krawczyk, J.H. Kühn and R.G. Stuart, *Phys. Lett. B*, **209**, (1988) 337; S. Jadach, M. Skrzypek and M. Martinez, *Phys. Lett. B*, **280**, (1992) 129.
[122] G. Montagna, O. Nicrosini and F. Piccinini, *Phys. Rev. D*, **48**, (1993) 1021.
[123] A. Arbuzov, D. Bardin and A. Leike, *Mod. Phys. Lett. A*, **7**, (1992) 2029, erratum, **9**, (1994), 1515.
[124] G. Montagna, O. Nicrosini and G. Passarino, *Phys. Lett. B*, **309**, (1993) 436.
[125] R. Kleiss, *Nucl. Phys. B*, **376**, (1992) 145.
[126] O. Nicrosini and L. Trentadue, *Z. Phys. C*, **39**, (1988) 479.
[127] M. Caffo, R. Gatto and E. Remiddi, *Phys. Lett. B*, **139**, (1984) 439, *Nucl. Phys. B*, **252**, (1985) 378; J. Fleisher and F. Jegerlehner, *Z. Phys. C*, **26**, (1985) 629; M. Cacciari, G. Montagna and O. Nicrosini, *Phys. Lett. B*, **274**, (1992) 473.
[128] W. Hollik, *Fortschr. Phys.*, **38**, (1990) 165.
[129] F.A. Berends, R. Kleiss and S. Jadach, *Nucl. Phys. B*, **202**, (1982) 63.
[130] G. Marchesini *et al.*, *Comput. Phys. Commun.*, **67**, (1992) 465.
[131] T. Sjöstrand, *Comput. Phys. Commun.*, **82**, (1994) 74 and Lund University report LU TP 95-20 (1995).
[132] S. Jadach, B.F.L. Ward and Z. Wąs, *Comput. Phys. Commun.*, **79**, (1994) 503.
[133] J.H. Field and T. Riemann, *Comput. Phys. Commun.*, **94**, (1996) 53.
[134] S. Jadach, W. Płaczek and B.F.L. Ward, *Phys. Lett. B*, **390**, (1997) 298.
[135] H. Anlauf *et al.*, *Comput. Phys. Commun.*, **79**, (1994) 466 and version 2.2 in `hep-ex/9512006`.
[136] G. Burgers, W. Hollik and M. Martinez, unpublished.
[137] M. Martinez *et al.*, *Z. Phys. C*, **49**, (1991) 645.
[138] D. Bardin *et al.*, *Z. Phys. C*, **44**, (1989) 493, *Phys. Lett. B*, **255**, (1991) 290, *Nucl. Phys. B*, **351**, (1991) 1 and CERN preprint CERN-TH.6443/92 (1992), `hep-ph/9412201`.
[139] V.A. Novikov, L.B. Okun and M.I. Vysotsky, *Nucl. Phys. B*, **397**, (1993) 35, *Phys. Lett. B*, **320**, (1994) 388, **324**, (1994), 89; V.A. Novikov, L.B. Okun, A.N. Rozanov, M.I. Vysotsky and V. Yurov, *Phys. Lett. B*, **331**, (1994) 433; V.A. Novikov, L.B. Okun, A.N. Rozanov and M.I. Vysotsky, *Mod. Phys. Lett. A*, **9**, (1994) 2641.
[140] W. Hollik, unpublished.
[141] D. Bardin, W. Hollik and T. Riemann, *Z. Phys. C*, **49**, (1991) 485.
[142] W. Beenakker, F.A. Berends and S.C. van der Mark, *Nucl. Phys. B*, **349**, (1991) 323.
[143] G. Passarino, *Nucl. Phys. Proc. Suppl. B*, **37**, (1994) 32 and *Precision Calculations for the Z*, talk given at 27th International Conference on High Energy Physics, Glasgow, 20-27th July 1994.
[144] D. Bardin, in *Proceedings of International Europhysics Conference on High Energy Physics*, edited by J. Lemonne, C. Vander Velde, F. Verbeure, World Scientific, 1996, p. 1011.
[145] G. Degrassi, P. Gambino and M. Passera, `hep-ph/9708311`.
[146] G. Montagna, O. Nicrosini, G. Passarino and F. Piccinini, `TOPAZ0` version 4.0.

[147] See, for instance, M. Martinez, *Nucl. Phys. Proc. Suppl.*, **51C**, (1996) 49; M. Pepe Altarelli, *Acta Phys. Pol. B*, **28**, (1997) 653.

[148] A. Borrelli, M. Consoli, L. Maiani and R. Sisto, *Nucl. Phys. B*, **333**, (1990) 357.

[149] W. Beenakker, F.A. Berends and S.C. van der Marck, *Z. Phys. C*, **46**, (1990) 687.

[150] S. Jadach, Z. Wąs *et al.*, in [13], Vol. 1, p. 235.

[151] R.E. Frey, talk given at "Beyond the Standard Model V", Balholm, Norway, 1997, `hep-ex/9710016`.

[152] A. Blondel, in *Proceedings of the 28th International Conference on High Energy Physics*, edited by Z. Ajduk and A.K. Wroblewski, (World Scientific, Singapore, 1997), Vol. I, p. 205.

[153] L. Trentadue *et al.*, *Neutrino Counting* in [13], p. 129.

[154] G. Altarelli, talk given at the XVIII International Symposium on Lepton Photon Interactions, July 28 - August 1, 1997, Hamburg, CERN-TH.97-278, `hep-ph/9710434`.

[155] G. Altarelli, N. Di Bartolomeo, F. Feruglio, M.L. Mangano and R. Gatto, *Phys. Lett. B*, **375**, (1996) 292; P. Chiappetta, J. Layssac, F.M. Renard and C. Verzegnassi, *Phys. Rev. D*, **54**, (1996) 789; M.L. Mangano, G. Altarelli, N. Di Bartolomeo, F. Feruglio and R. Gatto, in *Proceedings of the 28th International Conference on High Energy Physics*, edited by Z. Ajduk and A.K. Wroblewski, (World Scientific, Singapore, 1997), Vol. II, p. 1332.

[156] OPAL Collab., P.D. Acton *et al.*, *Z. Phys. C*, **58**, (1993) 219.

[157] K. Hagiwara, D. Haidt, and S. Matsumoto, KEK-TH-512, DESY 96-192, `hep-ph/9706331`.

[158] S. Dittmaier and D. Schildknecht, *Phys. Lett. B*, **391**, (1997) 420.

[159] W. Hollik, *Acta Phys. Pol. B*, **27**, (1996) 1581, **27**, (1996), 3685.

[160] W. de Boer, A. Dabelstein, W. Hollik, W. Mösle and U. Schwickerath, *Z. Phys. C*, **75**, (1997) 627; updated in U. Schwickerath, XVI Int. Workshop on Weak Interactions and Neutrinos, Capri, 1997 (to appear in the proceedings).

[161] A. Gurtu, *Phys. Lett. B*, **385**, (1996) 415.

[162] G. Passarino, *Acta Phys. Pol. B*, **28**, (1997) 635.

[163] J. Ellis, G.L. Fogli and E. Lisi, *Phys. Lett. B*, **389**, (1996) 321, *Z. Phys. C*, **69**, (1996) 627.

[164] S. Dittmaier, D. Schildknecht and G. Weiglein, *Phys. Lett. B*, **386**, (1996) 247.

[165] P. Chankowski and S. Pokorski, *Acta Phys. Pol. B*, **27**, (1996) 1719.

[166] G. Montagna, O. Nicrosini and G. Passarino, *Phys. Lett. B*, **303**, (1993) 170.

[167] F. Abe *et al.* (CDF coll.), *Phys. Rev. D*, **50**, (1994) 2966; *Phys. Rev. Lett.*, **74**, (1995) 2626; S. Abachi *et al.* (D0 coll.), *Phys. Rev. Lett.*, **74**, (1995) 2632.

[168] J. Konigsberg, talk given at the International Europhysics Conference on High Energy Physics, Jerusalem, 19-26 August, 1997; M. Strovink, talk given at the International Europhysics Conference on High Energy Physics, Jerusalem, 19-26 August, 1997; J. Cochran, talk given at the XVII International Conference on Physics in Collision, Bristol, June 25-27, 1997.

[169] E. Laenen, J. Smith and W. van Neerven, *Nucl. Phys. B*, **369**, (1992) 543, *Phys. Lett. B*, **321**, (1994) 254; E. Berger and H. Contopanagos, *Phys. Lett. B*, **361**, (1995) 115, *Phys. Rev. D*, **54**, (1996) 3085; S. Catani, M. Mangano, P. Nason and L. Trentadue, *Nucl. Phys. B*, **478**, (1996) 273, *Phys. Lett. B*, **378**, (1996) 329.

[170] M.S. Chanowitz, LBNL-40877, `hep-ph/9710308`.

[171] J.L. Rosner, `hep-ph/9704331`.

[172] S. Dittmaier, D. Schildknecht and G. Weiglein, *Nucl. Phys. B*, **465**, (1996) 3.

[173] Z. Hioki, *Acta Phys. Pol. B*, **27**, (1996) 2573.

[174] S. Dittmaier, D. Schildknecht and M. Kuroda, *Nucl. Phys. B*, **448**, (1995) 3.

[175] S. Dittmaier, C. Grosse Knetter and D. Schildknecht, *Z. Phys. C*, **67**, (1995) 109.

[176] M. Consoli and Z. Hioki, *Mod. Phys. Lett. A*, **10**, (1995) 845, *Mod. Phys. Lett. A*, **10**, (1995) 2245.

[177] S. Dittmaier, D. Schildknecht, K. Kolodziej and M. Kuroda, *Nucl. Phys. B*, **426**, (1994) 249, erratum **446**, (1995), 334.

[178] J. Ellis, G.L. Fogli and E. Lisi, *Phys. Lett. B*, **333**, (1994) 118.

[179] G. Montagna, O. Nicrosini, G. Passarino and F. Piccinini, *Phys. Lett. B*, **335**, (1994) 484.

[180] V.A. Novikov, L.B. Okun, A.N. Rozanov, M.I. Vysotsky and V.P. Yurov, *Phys. Lett. B*, **331**, (1994) 433.

[181] V.A. Novikov, L.B. Okun, A.N. Rozanov and M.I. Vysotsky, *Mod. Phys. Lett. A*, **9**, (1994) 2641.

[182] W. Murray, talk given at the International Europhysics Conference on High Energy Physics, Jerusalem, 19-26 August, 1997.

[183] P. Janot, plenary talk given at the International Europhysics Conference on High Energy Physics, Jerusalem, 19-26 August, 1997.

[184] D. Schildknecht, `hep-ph/9711314`.

[185] B. Pietrzyk, *Acta Phys. Pol. B*, **28**, (1997) 673.

[186] T. Hebbeker, *Phys. Rep.*, **217**, (1992) 69; S. Bethke and J. Pilcher, *Ann. Rev. Nucl. Part. Science*, **42**, (1992) 251.

[187] M. Schemelling, in *Proceedings of the 28th International Conference on High Energy Physics*, edited by Z. Ajduk and A.K. Wroblewski, (World Scientific, Singapore, 1997), Vol. I, p. 91.

[188] P.N. Burrows, *Acta Phys. Pol. B*, **28**, (1997) 701 and talk given at the XVII International Conference on Physics in Collision, Bristol, June 25-27, 1997, `hep-ex/9709010`.

[189] W.J. Stirling, DTP/97/80, `hep-ph/9709429`.

[190] S. Bethke, talk given at the High Energy Conference on Quantum Chromodynamics (QCD'97), 3-9 July 1997, Montpellier, `hep-exp/9710030`.

[191] S. Catani, talk given at the XVIII International Symposium on Lepton Photon Interactions, July 28 - August 1, 1997, Hamburg, `hep-ph/9712442`.

[192] W. de Boer, R. Ehret and S. Schael, proceedings of the Workshop on QCD at LEP, Aachen, 1994; PITHA 94/33 (1994).

[193] T. Hebbeker, M. Martinez, G. Passarino and G. Quast, *Phys. Lett. B*, **331**, (1994) 165; J. Chýla and A.L. Kataev, in [14], p. 313; P.A. Raczka and A. Szymacha, *Phys. Rev. D*, **54**, (1996) 3073; D.E. Soper and L.R. Surguladze, *Phys. Rev. D*, **54**, (1996) 4566.
[194] G.F. Chew, in *The analytic S-matrix: a basis for nuclear democracy*, (Benjamin, New York, 1966).
[195] R.J. Eden, P.V. Landshoff, D.I. Olive and J.C. Polkinghorne, in *The analytic S-matrix*, (Cambridge U.P., Cambridge, 1966).
[196] A. Böhm, in *Quantum Mechanics - Foundations and Applications*, (Springer, New York, 1994).
[197] A. Martin, *Phys. Lett. B*, **156**, (1985) 411.
[198] R.G. Stuart, *Phys. Lett. B*, **262**, (1991) 113.
[199] R.G. Stuart, *Phys. Lett. B*, **272**, (1991) 353.
[200] R.G. Stuart, *Phys. Rev. D*, **56**, (1997) 1515.
[201] M. Levy, *Nuovo Cimento*, **13**, (1959) 115.
[202] R.E. Peierls, in *Proc. 1954 Glasgow Conf. on Nuclear and Meson Physics* (Pergamon, New York, 1955), p. 296.
[203] M. Consoli and A. Sirlin, in [11], Vol. 1, p. 63.
[204] A. Leike, T. Riemann and J. Rose, *Phys. Lett. B*, **273**, (91) 513.
[205] T. Riemann, talk given at 21st International Colloquium on Group Theoretical Methods in Physics, Goslar, Germany, 15-20th July 1996, `hep-ph/9709208`.
[206] T. Riemann, *Phys. Lett. B*, **293**, (1992) 451.
[207] D. Bardin, A. Leike, T. Riemann and M. Sachwitz, *Phys. Lett. B*, **206**, (1988) 539.
[208] F.A. Berends, G. Burgers, W. Hollik and W. van Neerven, *Phys. Lett. B*, **203**, (1988) 177.
[209] S. Willenbrock and G. Valencia, *Phys. Lett. B*, **259**, (1991) 373.
[210] G. Altarelli, R. Barbieri and S. Jadach, *Nucl. Phys. B*, **369**, (1992) 3; G. Altarelli, R. Barbieri and F. Caravaglios, *Nucl. Phys. B*, **405**, (1993) 3, *Phys. Lett. B*, **314**, (1993) 357.
[211] G. Altarelli, R. Barbieri and F. Caravaglios, `hep-ph/9712368`.
[212] M.E. Peskin and T. Takeuchi, *Phys. Rev. Lett.*, **65**, (1990) 964; *Phys. Rev. D*, **46**, (1991) 381.
[213] B.W. Lynn, M.E. Peskin and R.G. Stuart, in [11], Vol. 1, p. 90; B. Holdom and J. Terning, *Phys. Lett. B*, **247**, (1990) 88; G. Altarelli and R. Barbieri, *Phys. Lett. B*, **253**, (1990) 161; D.C. Kennedy and P. Langacker, *Phys. Rev. Lett.*, **65**, (1990) 2967; E. Gates and J. Terning, *Phys. Rev. Lett.*, **67**, (1991) 1840; A. Dobado, D. Espriu and M.J. Herrero, *Phys. Lett. B*, **255**, (1991) 405; B. Holdom, *Phys. Lett. B*, **259**, (1991) 329; M. Golden and L. Randall, *Nucl. Phys. B*, **361**, (1991) 3; M. Dugan and L. Randall, *Phys. Lett. B*, **264**, (1991) 154; E. Ma and P. Roy, *Phys. Rev. Lett.*, **68**, (1992) 2879; G. Bhattacharyya, S. Banerjee and P. Roy, *Phys. Rev. D*, **45**, (1992) 729, erratum **46**, (1992), 3215; J. Layssac, F.M. Renard and C. Verzegnassi, *Phys. Rev. D*, **49**, (1994) 3650, C. Burgess, S. Godfrey, H. Konig, D. London and I. Maksymyk, *Phys. Lett. B*, **326**, (1994) 276, *Phys. Rev. D*, **49**, (1994) 6115.
[214] S. Weinberg, *Phys. Rev. D*, **13**, (1976) 974, *Phys. Rev. D*, **19**, (1979) 1277; L. Susskind, *Phys. Rev. D*, **20**, (1979) 2619; E. Farhi and L. Susskind, *Phys. Rep.*, **74**, (1981) 277.

[215] G.F. Giudice, M.L. Mangano, G. Ridolfi, R. Rúckl *et al.*, in [15], Vol. 1, p. 463, and references therein.
[216] P. Chiappetta, C. Verzegnassi *et al.*, in [15], Vol. 1, p. 577, and references therein.
[217] H.P. Nilles, *Phys. Rep. C*, **110**, (1984) 1; H.E. Haber and G.L. Kane, *Phys. Rep. C*, **117**, (1985) 75; R. Barbieri, *Riv. Nuovo Cim.*, **11**, (1988) 1.
[218] G. Passarino, *Phys. Lett. B*, **231**, (1989) 458.
[219] G. Passarino, *Phys. Lett. B*, **247**, (1990) 587.
[220] B.W. Lynn and E. Nardi, *Nucl. Phys. B*, **381**, (1992) 467.
[221] T. Blank and W. Hollik, `hep-ph/9703392`.
[222] V. Novikov, `hep-ph/9606318`.
[223] T. Inami, T. Kawakami and C.S. Lim, *Mod. Phys. Lett. A*, **10**, (1995) 1471; V. Novikov, L. Okun, A. Rozanov and M. Vysotsky, *Mod. Phys. Lett. A*, **10**, (1995) 1915; erratum **11**, (1996), 687; A. Masiero, F. Feruglio, S. Rigolin and R. Strocchi, *Phys. Lett. B*, **355**, (1995) 329.
[224] R. Casalbuoni, S. De Curtis, D. Dominici, F. Feruglio and R. Gatto, *Phys. Lett. B*, **258**, (1991) 161; C. Roiesnel and T.N. Truong, *Phys. Lett. B*, **256**, (1991) 439, erratum **270**, (1991), 128, erratum **272**, (1991), 455; R.N. Cahn and M. Suzuki, *Phys. Rev. D*, **44**, (1991) 3641; T. Appelquist and G. Triantaphyllou, *Phys. Lett. B*, **278**, (1992) 345; J. Ellis, G.L. Fogli and E. Lisi, *Phys. Lett. B*, **285**, (1992) 238; R.S. Chivukula, S.B. Selipsky and E.H. Simmons, *Phys. Rev. Lett.*, **69**, (1992) 575.
[225] J. Ellis, G.L. Fogli and E. Lisi, *Phys. Lett. B*, **343**, (1995) 282.
[226] R.S. Chivukula, E. Gates, E.H. Simmons and J. Terning, *Phys. Lett. B*, **311**, (1993) 157; R.S. Chivukula, E.H. Simmons and J. Terning, *Phys. Lett. B*, **331**, (1994) 383, *Phys. Rev. D*, **53**, (1996) 5258.
[227] G. Altarelli *et al.*, *Phys. Lett. B*, **318**, (1993) 139.
[228] G. Montagna, F. Piccinini, J. Layssac, F.M. Renard and C. Verzegnassi, *Z. Phys. C*, **75**, (1997) 641.
[229] R. Barbieri, F. Caravaglios and M. Frigeni, *Phys. Lett. B*, **279**, (1992) 169.
[230] L. Alvarez-Gaumé, J. Polchinski and M. Wise, *Nucl. Phys. B*, **221**, (1983) 495; R. Barbieri and L. Maiani, *Nucl. Phys. B*, **224**, (1983) 32; W. Hollik, *Mod. Phys. Lett. A*, **5**, (1990) 1909; A. Djouadi, G. Girardi, W. Hollik, F.M. Renard and C. Verzegnassi, *Nucl. Phys. B*, **349**, (1991) 48; M. Boulware and D. Finnell, *Phys. Rev. D*, **44**, (1991) 2054; P. Chankowski *et al.*, *Nucl. Phys. B*, **417**, (1994) 101; D. Garcia and J. Solà, *Mod. Phys. Lett. A*, **9**, (1994) 211, *Phys. Lett. B*, **354**, (1995) 335.
[231] G. Altarelli, *Acta Phys. Pol. B*, **28**, (1997) 991.
[232] G. Altarelli, R. Barbieri and F. Caravaglios, *Phys. Lett. B*, **314**, (1993) 357; C.S. Li, B.Q. Hu, J.M. Yang and Z.Y. Fang, *J. Phys. G*, **19**, (1993) 13; J.D. Wells, C. Kolda and G.L. Kane, *Phys. Lett. B*, **338**, (1994) 219; G.L. Kane, R.G. Stuart and J.D. Wells, *Phys. Lett. B*, **354**, (1995) 350; X. Wang, J.L. Lopez and D.V. Nanopoulos, *Phys. Rev. D*, **52**, (1995) 4116; D. Garcia, R. Jiménez and J. Solà, *Phys. Lett. B*, **347**, (1995) 309, **347**, (1995), 321; D. Garcia and J. Solà, *Phys. Lett. B*, **357**, (1995) 349; E. Ma and D. Ng, *Phys. Rev. D*, **53**, (1996) 255; M. Drees, R.M. Godbole, M. Guchait, S. Raychaudhuri and D.P. Roy, *Phys. Rev. D*, **54**, (1996) 5598; P. Chankowski and S. Pokorski, *Nucl. Phys. B*, **475**, (1996) 3; Y. Yamada, K. Hagiwara and S. Matsumoto, *Prog. Theor. Phys. Suppl.*, **123**, (1996) 195; J. Ellis,

J.L. Lopez and D.V. Nanopoulos, *Phys. Lett. B*, **372**, (1996) 95; P. Bamert, C.P. Burgess, J.M. Cline, D. London and E. Nardi, *Phys. Rev. D*, **54**, (1996) 4275; A. Brignole, F. Feruglio and F. Zwirner, *Z. Phys. C*, **71**, (1997) 679.

[233] J. Ellis, S. Kelley and D.V. Nanopoulos, *Phys. Lett. B*, **249**, (1990) 441; U. Amaldi, W. de Boer and H. Fürstenau, *Phys. Lett. B*, **290**, (1991) 447; P. Langacker and M. Luo, *Phys. Rev. D*, **44**, (1991) 817; F. Anselmo, L. Cifarelli, A. Peterman and A. Zichichi, *Nuovo Cimento A*, **104**, (1991) 1817; P. Langacker and N. Polonsky, *Phys. Rev. D*, **47**, (1993) 4028, **52**, (1995), 3081.

[234] F. Boudjema, B. Mele *et al.*, *Standard Model processes* in [15], Vol. 1, p. 207.

[235] P. Ward, talk given at the International Europhysics Conference on High Energy Physics, Jerusalem, 1997.

[236] S. Myers and C. Wyss, in [15], Vol. 1, p. 23.

[237] G. Montagna, O. Nicrosini and F. Piccinini, *Z. Phys. C*, **76**, (1997) 45.

[238] M. Skrzypek and S. Jadach, *Z. Phys. C*, **49**, (1991) 577.

[239] M. Cacciari, A. Deandrea, G. Montagna and O. Nicrosini, *Europhys. Lett.*, **17**, (1992) 123.

[240] OPAL Collab., K. Ackerstaff *et al.*, CERN-PPE/97-10.

[241] G. Montagna, O. Nicrosini, F. Piccinini and L. Trentadue, *Nucl. Phys. B*, **452**, (1995) 161.

[242] V. Choutko, talk given at the International Europhysics Conference on High Energy Physics, Jerusalem, 19-26 August, 1997.

[243] G. Montagna, O. Nicrosini and F. Piccinini, *Comput. Phys. Commun.*, **98**, (1996) 206.

[244] R. Miquel, C. Mana and M. Martinez, *Z. Phys. C*, **48**, (1990) 309.

[245] S. Ambrosanio, B. Mele, G. Montagna, O. Nicrosini and F. Piccinini, *Nucl. Phys. B*, **478**, (1996) 46.

[246] J.L. Lopez, D.V. Nanopoulous and A. Zichichi, *Phys. Rev. D*, **55**, (1997) 5813.

[247] M. Chemarin, talk given at the International Europhysics Conference on High Energy Physics, Jerusalem, 1997.

[248] Z. Kunszt, W.J. Stirling *et al.*, *Determination of the mass of W boson* in [15], Vol. 1, p. 141.

[249] G. Gounaris, J.-L. Kneur, D. Zeppenfeld *et al.*, *Triple gauge boson couplings* in [15], Vol. 1, p. 525.

[250] W. Beenakker and A. Denner, *Int. J. Mod. Phys. A*, **9**, (1994) 4837.

[251] M. Böhm *et al.*, *Nucl. Phys. B*, **304**, (1988) 463; W. Beenakker, K. Kolodziej and T. Sack, *Phys. Lett. B*, **258**, (1991) 469; W. Beenakker, F.A. Berends and T. Sack, *Nucl. Phys. B*, **367**, (1991) 287.

[252] J. Fleischer, F. Jegerlehner and M. Zrałek, *Z. Phys. C*, **42**, (1989) 409; K. Kolodziej and M. Zrałek, *Phys. Rev.*, **43**, (1991) 3619; J. Fleischer, F. Jegerlehner and K. Kolodziej, *Phys. Rev. D*, **47**, (1993) 830.

[253] T. Muta, R. Najima and S. Wakaizumi, *Mod. Phys. Lett. A*, **1**, (1986) 203; G. Barbiellini *et al.*, in [11], Vol. 2, p. 1.

[254] M. Cacciari, A. Deandrea, G. Montagna and O. Nicrosini, *Z. Phys. C*, **52**, (1991) 421.

[255] V.S. Fadin, V.A. Khoze, A.D. Martin and W.J. Stirling, *Phys. Lett. B*, **363**, (1995) 112.

[256] V.A. Khoze and W.J. Stirling, *Phys. Lett. B*, **356**, (1995) 373.

[257] F.A. Berends, W. Beenakker *et al.*, *WW cross-sections and distributions* in [15], Vol. 1, p. 79.
[258] D. Bardin, R. Kleiss *et al.*, *Event generators for WW physics* in [15], Vol. 2, p. 3.
[259] E.N. Argyres and C.G. Papadopoulos, *Phys. Lett. B*, **263**, (1991) 298; C.G. Papadopoulos, *Phys. Lett. B*, **352**, (1995) 144.
[260] F.A. Berends and W.T. Giele, *Nucl. Phys. B*, **294**, (1987) 700.
[261] G. Passarino, *Phys. Rev. D*, **28**, (1983) 2867, *Nucl. Phys. B*, **237**, (1984) 249.
[262] A. Ballestrero and E. Maina, *Phys. Lett. B*, **350**, (1995) 225.
[263] E. Boos *et al.*, hep-ph/9503280.
[264] H. Tanaka, *Comput. Phys. Commun.*, **58**, (1990) 153; H. Tanaka, T. Kaneko and Y. Shimizu, *Comput. Phys. Commun.*, **64**, (1991) 149.
[265] F. Caravaglios and M. Moretti, *Phys. Lett. B*, **358**, (1995) 332.
[266] W. Beenakker, in *Proceedings of the 28th International Conference on High Energy Physics*, edited by Z. Ajduk and A.K. Wroblewski, (World Scientific, Singapore, 1997), Vol. II, p. 1113; *Acta Phys. Pol. B*, **28**, (1997) 679.
[267] U. Baur, J.A.M. Vermaseren and D. Zeppenfeld, *Nucl. Phys. B*, **375**, (1992) 3.
[268] Y. Kurihara, D. Perret-Gallix and Y. Shimizu, *Phys. Lett. B*, **349**, (1995) 367.
[269] U. Baur and D. Zeppenfeld, *Phys. Rev. Lett.*, **75**, (1995) 1002.
[270] M. Veltman, *Physica*, **29**, (1963) 186.
[271] A. Aeppli, G.J. van Oldenborgh and D. Wyler, *Nucl. Phys. B*, **428**, (1994) 126.
[272] R.G. Stuart, hep-ph/9603351, hep-ph/9706431, hep-ph/9706550.
[273] C.G. Papadopoulos, *Phys. Lett. B*, **352**, (1995) 144.
[274] E.N. Argyres *et al.*, *Phys. Lett. B*, **358**, (1995) 339.
[275] W. Beenakker *et al.*, *Nucl. Phys. B*, **500**, (1997) 255.
[276] L. Taylor, talk given at the XVII International Conference on Physics in Collision, Bristol, June 25-27, 1997, hep-ex/9712016.
[277] V. Barger, T. Han and R.J.N. Phillips, *Phys. Rev. D*, **39**, (1989) 146; H. Tanaka, T. Kaneko and Y. Shimizu, *Comput. Phys. Commun.*, **64**, (1991) 149; E.N. Argyres *et al.*, *Phys. Lett. B*, **259**, (1991) 195.
[278] M. Böhm, A. Denner and S. Dittmaier, *Nucl. Phys. B*, **376**, (1992) 29, erratum **391**, (1993), 483.
[279] G. Montagna, O. Nicrosini and F. Piccinini, version 1.0, *Comput. Phys. Commun.*, **90**, (1995) 141; D.G. Charlton, G. Montagna, O. Nicrosini and F. Piccinini, version 2.0, *Comput. Phys. Commun.*, **99**, (1997) 355; D.G. Charlton, G. Montagna, O. Nicrosini, M. Osmo and F. Piccinini, version 2.1, FNT/T 97/18.
[280] M. Kuroda, I. Kuss and D. Schildknecht, *Phys. Lett. B*, **409**, (1997) 405.
[281] W.J. Marciano and D. Wyler, *Z. Phys. C*, **3**, (1979) 181; D. Albert *et al.*, *Nucl. Phys. B*, **166**, (1980) 460; K. Inoue *et al.*, *Prog. Theo. Phys.*, **64**, (1980) 1008; T.H. Chang, K.J.F. Gaemers and W.L. van Neerven, *Nucl. Phys. B*, **202**, (1982) 407; F. Jegerlehner, *Z. Phys. C*, **32**, (1986) 425 and in Proc. of the 11th International School of Theoretical Physics *Testing of the Standard Model*, Szczyrk-Bila (Poland) 1987, edited by M. Zrałek and R. Manka (World Scientific, Singapore, 1988), p. 127; D. Bardin, S. Riemann and T. Riemann, *Z. Phys. C*, **32**, (1986) 121; A. Denner and T. Sack, *Z. Phys. C*, **46**, (1990) 653.

[282] A. Denner, *Fortschr. Phys.*, **41**, (1993) 307.
[283] S. Dittmaier, *Acta Phys. Pol. B*, **28**, (1997) 619.
[284] W. Beenakker and G.J. van Oldenborgh, *Phys. Lett. B*, **381**, (1996) 248.
[285] D. Albert, W.J. Marciano, D. Wyler and Z. Parsa, *Nucl. Phys. B*, **166**, (1980) 460.
[286] K.J. Abraham and B. Lampe, *Nucl. Phys. B*, **478**, (1996) 507.
[287] E. Maina and M. Pizzio, *Phys. Lett. B*, **369**, (1996) 341.
[288] E. Maina, R. Pittau and M. Pizzio, *Phys. Lett. B*, **393**, (1997) 445, hep-ph/9709454, hep-ph/9710375.
[289] E. Accomando *et al.*, in *Physics with e^+e^- Linear Colliders*, hep-ph/9705442.
[290] F.A. Berends, R. Pittau and R. Kleiss, *Nucl. Phys. B*, **424**, (1994) 308.
[291] F.A. Berends, R. Pittau and R. Kleiss, *Nucl. Phys. B*, **426**, (1994) 344.
[292] G. Montagna, O. Nicrosini, G. Passarino and F. Piccinini, *Phys. Lett. B*, **348**, (1995) 178.
[293] M. Skrzypek, S. Jadach, M. Martinez, W. Płaczek and Z. Wąs, *Phys. Lett. B*, **372**, (1996) 298.
[294] S. Jadach, W. Płaczek, M. Skrzypek and B.F. L. Ward, *Phys. Rev. D*, **54**, (1996) 5434.
[295] D. Bardin, D. Lehner and T. Riemann, *Nucl. Phys. B*, **477**, (1996) 27.
[296] D. Bardin and T. Riemann, *Nucl. Phys. B*, **462**, (1996) 3.
[297] D. Bardin, M. Bilenky, A. Olshevsky and T. Riemann, *Phys. Lett. B*, **308**, (1993) 403, erratum **357**, (1995), 725.
[298] S. Jadach, W. Płaczek, M. Skrzypek, B.F.L. Ward and Z. Wąs, hep-ph/9705429.
[299] A. Sommerfeld, *Atombau und Spektrallinien* (Vieweg, Braunschweig, 1939), Bd. 2; A.D. Sakharov, *JETP*, **18**, (1948) 631.
[300] V.S. Fadin, V.A. Khoze and A.D. Martin, *Phys. Lett. B*, **311**, (1993) 311; V.S. Fadin, V.A. Khoze, A.D. Martin and A. Chapovsky, *Phys. Rev. D*, **52**, (1995) 1377; D. Bardin, W. Beenakker and A. Denner, *Phys. Lett. B*, **317**, (1993) 213.
[301] V.S. Fadin, V.A. Khoze and A.D. Martin, *Phys. Rev. D*, **49**, (1994) 2247.
[302] K. Melnikov and O. Yakovlev, *Phys. Lett. B*, **324**, (1994) 217.
[303] K. Melnikov and O. Yakovlev, *Nucl. Phys. B*, **471**, (1996) 90.
[304] W. Beenakker, F.A. Berends and A.P. Chapovsky, *Phys. Lett. B*, **411**, (1997) 203; *Nucl. Phys. B*, **508**, (1997) 17.
[305] S. Dittmaier, talk given at the International Europhysics Conference on High Energy Physics, Jerusalem, 19-26 August, 1997; A. Denner, S. Dittmaier and M. Roth, hep-ph/9710521.
[306] M.L. Mangano, G. Ridolfi *et al.*, *Event generators for discovery physics* in [15], Vol. 2, p. 299.
[307] T. Ohl, *Acta Phys. Pol. B*, **28**, (1997) 847.
[308] F. Caravaglios and M. Moretti, *Z. Phys. C*, **74**, (1997) 291.
[309] C.G. Papadopoulos, *Comput. Phys. Commun.*, **101**, (1997) 183.
[310] F.A. Berends, R. Kleiss and R. Pittau, *Comp. Phys. Commun.*, **85**, (1995) 437.
[311] D. Bardin *et al.*, *Comp. Phys. Commun.*, **104**, (1997) 161.
[312] J. Fujimoto *et al.*, *Comput. Phys. Commun.*, **100**, (1997) 128.
[313] Minami-Tateya collaboration, in *GRACE manual version 1.0*, KEK Report 92-19, 1993.

[314] Y. Kurihara, J. Fujimoto, T. Munehisa and Y. Shimizu, *Progr. Theor. Phys.*, **96**, (1996) 1223.
[315] M. Skrzypek, S. Jadach, W. Płaczek and Z. Wąs, *Comput. Phys. Commun.*, **94**, (1996) 216.
[316] F.C. Erné, unpublished.
[317] E. Barberio, B. van Ejik and Z. Wąs, *Comput. Phys. Commun.*, **79**, (1994) 291.
[318] R. Miquel and M. Schmitt, *Z. Phys. C*, **71**, (1996) 251.
[319] T. Sjöstrand, *Comput. Phys. Commun.*, **82**, (1994) 74.
[320] H. Anlauf *et al.*, *Comput. Phys. Commun.*, **79**, (1994) 487, *Nucl. Phys. Proc. Suppl.*, **37B**, (1994) 81; H. Anlauf, P. Manakos, T. Ohl and H.D. Dahmen, IKDA-96-15 (1996), `hep-ph/9605457`.
[321] E. Accomando and A. Ballestrero, *Comput. Phys. Commun.*, **99**, (1997) 270.
[322] A. Ballestrero and E. Maina, *Phys. Lett. B*, **350**, (1995) 225.
[323] A. Ballestrero, `PHACT 1.0` - Program for Helicity Amplitudes Calculations with Tau matrices.
[324] G. Passarino, *Comput. Phys. Commun.*, **97**, (1996) 261.
[325] G.J. van Oldenborg, *Comput. Phys. Commun.*, **83**, (1994) 14.
[326] T. Sjöstrand and V.A. Khoze, *Z. Phys. C*, **62**, (1994) 281, *Phys. Rev. Lett.*, **72**, (1994) 28.
[327] E. Accomando, A. Ballestrero and E. Maina, *Phys. Lett. B*, **362**, (1995) 141.
[328] S. Jadach and K. Zalewski, *Acta Phys. Pol. B*, **28**, (1997) 1363; K. Fiałkowki and R. Wit, *Acta Phys. Pol. B*, **28**, (1997) 2039; J. Häkkinen and M. Ringnér, `hep-ph/9711212`; B.R. Webber, *J. Phys. G*, **24**, (1998) 287.
[329] K. Gaemers and G.J. Gounaris, *Z. Phys. C*, **1**, (1979) 259.
[330] K. Hagiwara, K. Hikasa, R.D. Peccei and D. Zeppenfeld, *Nucl. Phys. B*, **282**, (1987) 253.
[331] H. Aronson, *Phys. Rev.*, **186**, (1969) 1434.
[332] M. Bilenky, J.-L. Kneur, F.M. Renard and D. Schildknecht, *Nucl. Phys. B*, **409**, (1993) 22.
[333] C.P. Burgess and D. London, *Phys. Rev. Lett.*, **69**, (1992) 3428, *Phys. Rev. D*, **48**, (1993) 4337; G.J. Gounaris and F.M. Renard, *Z. Phys. C*, **59**, (1993) 375; F. Boudjema, in *Physics and Experiments with Linear e^+e^- Colliders*, edited by F.A. Harris *et al.*, (World Scientific, Singapore, 1993), Vol. II, p. 712.
[334] M. Carena, P.M. Zerwas *et al.*, *Higgs physics* in [15], Vol. 1, p. 351.
[335] D. Apostolakis, P. Ditsas and S. Katsanevas, *Z. Phys. C*, **76**, (1997) 201.
[336] G. Passarino, *Nucl. Phys. B*, **488**, (1997) 3.
[337] D. Bardin, A. Leike and T. Riemann, *Phys. Lett. B*, **353**, (1995) 513.
[338] G. Montagna, O. Nicrosini and F. Piccinini, *Phys. Lett. B*, **348**, (1995) 496.
[339] G. Montagna, M. Moretti, O. Nicrosini and F. Piccinini, `hep-ph/9705333`, to appear in European Phys. J. C (Z. Phys. C).
[340] E. Accomando, A. Ballestrero and M. Pizzio, `hep-ph/9709277`.
[341] V. Chung, *Phys. Rev. B*, **140**, (1965) 1110; M. Greco and G. Rossi, *Il Nuovo Cimento Vol.* , **LA N. 1**, (1967) 168; M. Greco, G. Pancheri and Y. Srivastava, *Nucl. Phys. B*, **101**, (1975) 234; **171**, (1980), 118; see also [43].
[342] H.D. Dahmen *et al.*, *Z. Phys. C*, **50**, (1991) 75.

[343] E.A. Kuraev and V. Fadin, *Sov. J. Nucl. Phys.*, **41**, (1985) 466; G. Altarelli and G. Martinelli, in [11], Vol. 1, p.47; O. Nicrosini and L. Trentadue, *Phys. Lett. B*, **196**, (1987) 551; O. Nicrosini and L. Trentadue, *Z. Phys. C*, **39**, (1988) 479; F.A. Berends, G. Burgers and W.L. van Neerven, *Nucl. Phys. B*, **297**, (1988) 429; F.A. Berends *et al.*, in [13], Vol. 1, p. 89; W. Beenakker, F.A. Berends and W.L. van Neerven, in *Radiative Corrections for e^+e^- Collisions*, edited by J.H. Kühn, (Springer, Berlin Heidelberg) 1989 p. 3; O. Nicrosini and L. Trentadue, ibidem, p. 25; O. Nicrosini and L. Trentadue, in *QED Structure Functions (Ann Arbor, MI, 1989)*, edited by G. Bonvicini, AIP Conf. Proc. No. 201 (AIP, New York, 1990), p. 12; O. Nicrosini, ibidem, p. 73.
[344] G. Altarelli and G. Parisi, *Nucl. Phys. B*, **126**, (1977) 298.
[345] V.N. Gribov and L.N. Lipatov, *Sov. J. Nucl. Phys.*, **15**, (1972) 438, 675.
[346] R. Odorico, *Nucl. Phys. B*, **172**, (1980) 157.
[347] G. Marchesini and B.R. Webber, *Nucl. Phys. B*, **238**, (1984) 1.
[348] K. Kato and T. Munehisa, *Phys. Rev. D*, **39**, (1989) 156.
[349] J. Fujimoto, Y. Shimizu and T. Munehisa, *Prog. Theo. Phys.*, **90**, (1993) 177; **91**, (1994), 333.
[350] T. Munehisa *et al.*, KEK-CP-034, KEK preprint 95-114, 1995.
[351] D.R. Yennie, S. Frautschi and H. Suura, *Ann. Phys. (NY)*, **13**, (1961) 379.
[352] S. Jadach and B.F.L. Ward, in *Proceedings of the Workshop on Radiative corrections*, Brighton, 1989, p. 325.
[353] Z. Wąs, in *Proceedings of the 1993 European School of High Energy Physics*, Zakopane, Poland (1993), edited by N. Ellis and M.B. Gavela,, CERN 94-04.
[354] *Quantum Electrodynamics*, edited by T. Kinoshita, World Scientific, Singapore, 1990.
[355] T. Kinoshita, *History of Original Ideas and Basic Discoveries in Particle Physics*, edited by H. Newman and T. Ypsilantis, Plenum Press, New York, 1995.
[356] H. Burkhardt and B. Pietrzyk, *Phys. Lett. B*, **356**, (1995) 398.
[357] B.A. Kniehl, *Acta Phys. Polon. B*, **27**, (1996) 3631.
[358] F. Jegerlehner, *Z. Phys. C*, **32**, (1986) 195.
[359] B.W. Lynn, G. Penso and C. Verzegnassi, *Phys. Rev. D*, **35**, (1987) 42.
[360] H. Burkhardt, F. Jegerlehner, G. Penso and C. Verzegnassi, *Z. Phys. C*, **43**, (1989) 497.
[361] F. Jegerlehner, *Prog. Part. Nucl. Phys.*, **27**, (1991) 32.
[362] R.D. Nevzorov and A.V. Novikov, preprint FTUV/94-27, MAD/PH/855, 1994.
[363] K. Adel and F.J. Yndurain, hep-ph/9509378.
[364] S. Eidelman and F. Jegerlehner, *Z. Phys. C*, **67**, (1995) 585.
[365] A.D. Martin and D. Zeppenfeld, *Phys. Lett. B*, **345**, (1995) 558.
[366] M.L. Swartz, *Phys. Rev. D*, **53**, (1996) 5268.
[367] R. Alemany, M. Davier and A. Höcker, preprint LAL 97-02, `hep-ph/9703220`.
[368] M. Davier and A. Höcker, `hep-ph/9711308`.
[369] N.V. Krasnikov and R. Rodenberg, `hep-ph/9711367`.
[370] J.H. Kühn and M. Steinhauser, `hep-ph/9802241`.
[371] M. Veltman, *Diagrammatica*, edited by P. Goddard and J. Yeomans, Cambridge University Press, Cambridge, 1994.